APPENDIX D

THREE-DIMENSIONAL FINITE ELEMENT MODEL DEVELOPMENT AND VALIDATION

Many pavement researchers have resorted to three-dimensional (3-D) finite element models as the best method of solving complicated structural analysis problems. Two-dimensional (2-D) finite element models have inherent limitations related to plate theory assumptions; thus, many interesting problems cannot be realistically modelled by 2-D finite element programs. Thanks to the development of finite element techniques and computer capabilities and speeds, well-developed versatile 3-D finite element packages are capable of modelling numerous complex mechanisms in engineering problems within tolerable computer run times. A realistic "simulated pavement system" may then be built in a computer model instead of in the field.

None of the available 3-D finite element programs is designed specifically for pavement analysis. The SAP finite element program for structural mechanics was used to model dowel-concrete interactions by Tabatabaie. [36] A study of stress-dependent foundations was performed with a 3-D model using GEOSYS, which was primarily designed for geotechnical problems. [37] In the 1990s, ABAQUS has gained popularity in simulating pavement problems concerning nonlinear subgrades, dynamic loading [38], and Falling Weight Deflectometer tests [39].

This appendix presents a brief overview of ABAQUS, a sensitivity study of feasible element types in ABAQUS, a description of the development of a 3-D concrete pavement model with ABAQUS, and a variety of analyses conducted to validate the 3-D concrete pavement model (3DPAVE) by comparison with measured field data from the AASHO Road Test and other experiments.

OVERVIEW OF ABAQUS

ABAQUS has been widely used for stress/strain, fatigue, flow and thermal analysis in many fields, such as structures, geotechnical engineering, hydrosystems, and materials. It is available in most research computer systems. Since it was not developed specifically for pavement analysis, preparation of an input file requires understanding of the organization of ABAQUS as well as the conventions of finite element model building.

The ABAQUS components used in 3DPAVE are ABAQUS/Standard, a general-purpose finite element program, and ABAQUS/Post, an interactive postprocessing program. The complete AQABUS system contains additional components, including one intended explicitly for dynamic analyses using a supercomputer.

Model Input

The first problem in using ABAQUS to analyze pavements is how to generate the desired pavement section in the computer. The pavement geometry may be input in one of two ways. The first way is to write an input file containing several commands for node and element definition and generation. For example:

NODE:	Defines node coordinates,
NGEN:	Generates nodes between two end nodes,
NFILL:	Generates nodes by filling nodes in the area bounded by two sets of nodes,
NCOPY:	Generates nodes by shifting or mirroring a set of defined nodes,
ELEMENT:	Defines elements with given node numbers, and
ELGEN:	Generates elements with defined master element.

With combinations of these commands, a complicated multilayer pavement model can be defined in few lines of commands. This model input method has two drawbacks. First, users must number nodes with care to meet the requirements of subsequent automatic element-generating commands. The input order of node numbers of elements also has to be exactly followed to ensure the elements are correctly defined. Second, the input model cannot be visualized until the input file is run and completed.

The second way to input the pavement geometry is with the popular graphical assistant software, PATRAN, which generates the model, displays the mesh on the screen simultaneously, as illustrated in Figure D-1, and writes the model data to an input file. Users are able to check, without running ABAQUS, if the pavement is correctly modelled and also if the model is properly meshed. Another advantage of using PATRAN is that node numbers and element numbers are automatically assigned by PATRAN. This eliminates the error of inconsistent numbering by users. Once the correct model is shown on screen, the user knows that a correct ABAQUS input file has been generated by PATRAN.

However, two drawbacks are associated with this input generation process. First, the generated input model define nodes with nodal coordinates instead of the keyword command listed for the first method. It therefore takes much more computer memory than the other input file does. Second, some elements cannot be generated by PATRAN because either the elements are not supported in PATRAN, or the geometry of element cannot be defined graphically. For example, the INTERFACE element between layers is needed to defined two nodes with the same coordinates. However, PATRAN does not allow the same point to be assigned to two node numbers. A preprocessing program must be developed to modify input models generated by PATRAN.

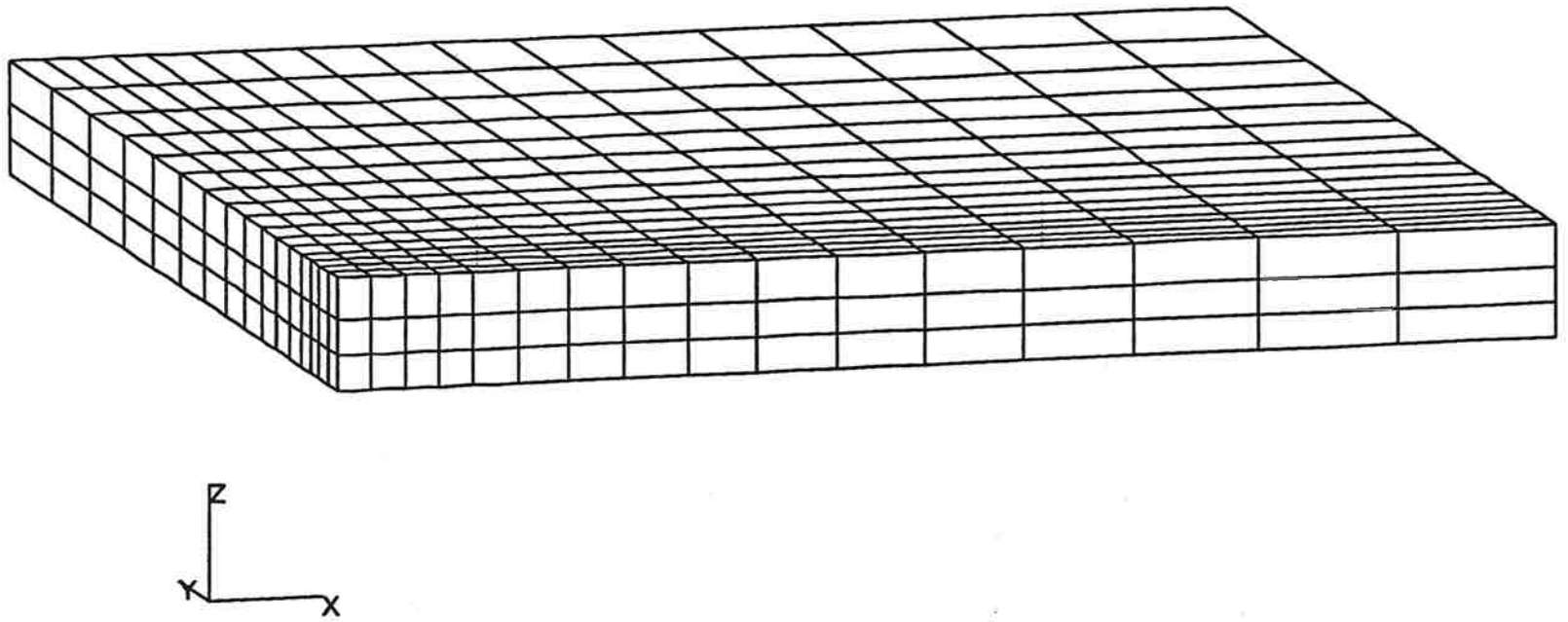

Figure D-1. Example of mesh generated by PATRAN.

The input data are organized around a few natural concepts and conventions, such as property definition, kinematic constraints, material definitions, etc. [5]
A problem is described by a *data deck* which contains model data and history data, as illustrated in Figure D-2. The data deck is a file, created either directly by the user or using PATRAN, for input to ABAQUS. Model data define a finite element model: the coordinates of nodes, elements, element properties, material properties, and so on. History data define what happens to the model: the sequence of events or loadings for which the model's response is sought. This history could be a composed of a sequence of steps in which the analysis procedure type, control parameters, loading and output requests are included. Two types of cards are used: keyword cards and data cards. Keyword cards begin with a "*" followed by the keyword and options, if any. Any data associated with this keyword follow on data cards after the keyword card. Comments are indicated by "**" at the beginning of the input card.

Element Library

The ABAQUS element library provides 250 types of elements for various purposes and degrees of accuracy. They include solid stress/displacement elements, infinite elements (suitable for elastic solid subgrade modelling, for example), heat transfer elements, coupled temperature-displacement solid elements, solid elements incorporating pore pressure, acoustic elements, elements with electric potential, etc.

Materials Library

The ABAQUS material library is intended to provide comprehensive coverage of both linear and nonlinear, isotropic and anisotropic material models and a broad range of possible material behaviors. Some of the material options are:

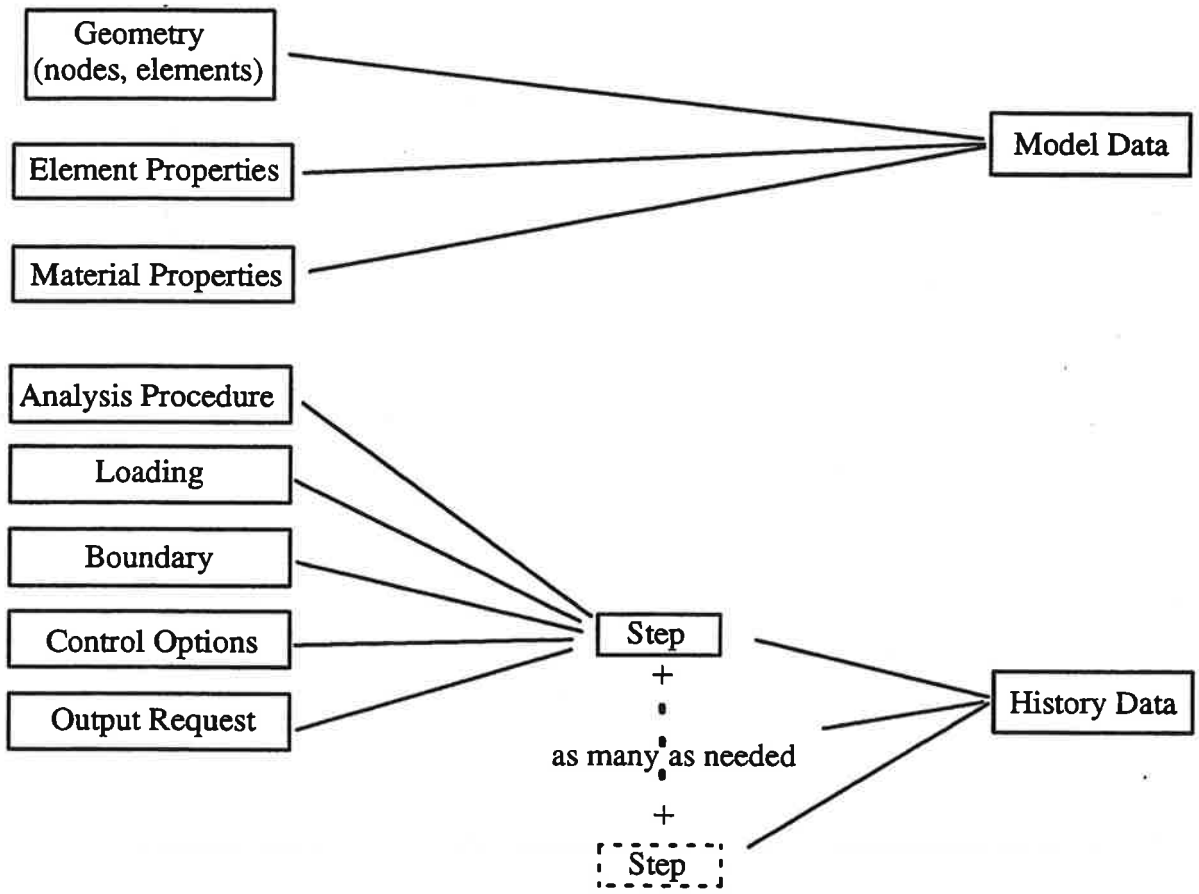

Figure D-2. Components of data deck in ABAQUS.

- Damping
- Permeability
- Moisture swelling
- Porous elastic
- Concrete behavior
- Plastic
- Cycled plastic
- Friction
- Expansion
- Porous bulk moduli
- Elastic
- No compression
- Clay plasticity
- Rate dependent
- Swelling
- Surface contact
- Conductivity
- Absorption
- Hyperelastic
- No tension
- Jointed material
- Creep
- Viscoelasticity
- Gap conductance

User subroutines provide an extremely powerful and flexible tool for analysis. Many additional subroutines are available to define material behaviors and material properties for users' special purposes which are not available in the materials library.

Analysis Procedures

To analyze different loading histories and responses, many analysis procedures are available, such as:

- Static
- Dynamic
- Geostatic
- Heat transfer
- Soils: effective stress analysis for porous media
- Visco: transient, static, stress/displacement analysis with time-dependent material response.

Postprocessing

Many convenient features for output interpretation are provided as postprocessing options. Time history plots and tables, variable-variable plots, displaced shape, and contours may be produced automatically if these options are specified in the input file. The interactive postprocessing program offers more advanced features for postprocessing. In addition, ABAQUS output may be viewed using PATRAN.

FEASIBILITY STUDY OF ELEMENT TYPES

An appropriate element is essential to a good pavement model. It must be capable of simulating pavement behavior realistically and efficiently. Furthermore, ABAQUS provides a wide variety of elements which are potentially suitable for plate-type problems. A study of element performance is necessary to choose the most appropriate element to build 3-D model for pavement analysis.

The accuracy of finite element analysis is very sensitive to mesh fineness. The mesh must be sufficiently fine, especially in the vicinity of the load, to achieve an acceptable level of accuracy. Different types of elements may require different degrees of mesh fineness to achieve the same accuracy.

2-D Elements

In the first stage of this development process, a 2-D model was developed in order to gain experience in correctly building a model in ABAQUS. This experience facilitated the more complicated 3-D modeling in the next stage of the process. The ABAQUS 2-D pavement model was compared with ILLI-SLAB and Westergaard's solutions, which are both based on plate theory.

ABAQUS provides a wide variety of shell elements which are suitable for both shell and plate problems. A brief comparison of the characteristics of shell elements which are appropriate for pavement models is given in Table D-1. The type of 2-D element used in ILLI-SLAB and also in FINITE, a popular general-purpose finite element code, is included in the table to demonstrate the embedded difference in formulation among these finite element analysis models. Notice that the element type used in ILLI-SLAB is very similar to the triangular element in ABAQUS except in element shape. The rectangular shell elements in ABAQUS provide additional degrees of freedom for consideration of transverse shear, a capability which is generally considered unnecessary for "thin plate" modelling. A "thin plate" is defined as one with a length-to-thickness ratio greater than about 20. (Note that what in the structural analysis literature is called a "thin plate" is often called in the pavement literature a "medium-thick plate" but the definition is the same). Transverse shear may become a significant factor when the loaded area is small or when the slab does not satisfy the thin plate definition.

An example was run in ABAQUS using selected 2-D elements and the results were compared with results from ILLI-SLAB and FINITE runs. The results are shown in Tables D-2 and D-3. ILLI-SLAB and FINITE match excellently for both deflection and maximum stresses a coarse mesh. This is expected because both programs use the same type of element. Of the 2-D elements employed in ABAQUS, the 8-node rectangular element S8R5 yielded stresses which agreed well with ILLI-SLAB regardless of mesh fineness. The 4-node rectangular element S4R5 did not agree well with the ILLI-SLAB result when a coarse mesh was used; it converged to the ILLI-SLAB result when a fine mesh was used. The triangular element, which has properties similar to the 4-node rectangular element RPB12 used in ILLI-SLAB, gave results close to those obtained from ILLI-SLAB even with a coarse mesh.

Table D-1. Characteristics of shell elements in ABAQUS.

	FINITE & ILLI–SLAB	ABAQUS Shell Elements							
Name	RPB12	STRI3	STRI35	STRI65	S4R	S4R5	S8R	S8R5	S9R5
Shape	Rectangular	Triangular			Rectangular				
Nodes	4	3	3	6	4	4	8	8	9
D.O.F.	3	6	5	5	6	5	6	5	5
Reduced integration	No	No			Yes				
Restriction	Thin Only	Thin Plate Only							
Transverse Shear	No	No			Yes				

Table D-2. Comparison of maximum tensile stress, psi [1 psi = 6.89 kPa].

	S4R5	S8R5	ILLI–SLAB	FINITE	STRI3	STRI35
1×1	235.2	298.9	297.8	299.3	291.7	294.1
2×2	268.8	283.7	284.2	–	–	–
3×3	274.6	281.1	–	–	–	–
4×4	277.5	280.3	280.7	–	–	–

Table D-3. Comparison of maximum deflection, mils [1 mil = 25.4 μm].

	S4R5	S8R5	ILLI–SLAB	FINITE	STRI3	STRI35
1×1	9.234	9.322	9.050	9.042	8.980	8.980
2×2	9.297	9.322	9.036	–	–	–
3×3	9.311	9.322	–	–	–	–
4×4	9.315	9.322	9.039	–	–	–

Inputs:

Slab size = 25 ft [7.6 m] square

Slab thickness = 6 in [152 mm]

PCC E = 4 million psi [27560 MPa]

μ = 0.15

Loaded area = 10.468 in [265.89 mm] square

P = 9000 pounds [40 kN]

k = 200 psi/in [54 kPa/mm]

Interior Loading

Figure D-3 shows the convergence to Westergaard's solution with different elements and various meshes. Although the S8R5 element performs almost exactly the same as ILLI-SLAB, it is less efficient than ILLI-SLAB because S8R5 is a quadratic element which requires almost three times as many nodes as the RPB12 element. However, in some cases in which pavement slabs are too thick to be modelled appropriately as thin plates (i.e., length-to-thickness ratio of 20 or more), S8R5 will yield better results than ILLI-SLAB. ABAQUS also provides a linear triangular element, STRI35, which is efficient in modelling thin plates. However, a triangular element is not as convenient as a rectangular element for modelling rectangular pavement slabs.

3-D Elements

The objectives of this portion of the study were to select the most appropriate element for a 3-D pavement model and to identify the mesh fineness and other criteria for achieving acceptable accuracy. The 3-D solution ought to agree with the 2-D solution for slabs which satisfy the thin plate definition. The 3-D solution also should agree with Westergaard's equations, within the range of load sizes for which Westergaard's equations are applicable, for slabs which satisfy the thin plate definition.

Three sets of analyses were conducted in the 3-D element feasibility study. A plate resting on Winkler foundation was run and compared with Westergaard's interior and edge loading equations. Another set of comparisons dealt with a simply supported rectangular plate with a large distributed load. The results were compared with an analytical solution to investigate the mesh effect. It should be pointed out that both analytical solutions only serve as benchmarks, rather than exact solutions,

Westergaard's solution :

σ_{max} = 281.4 psi

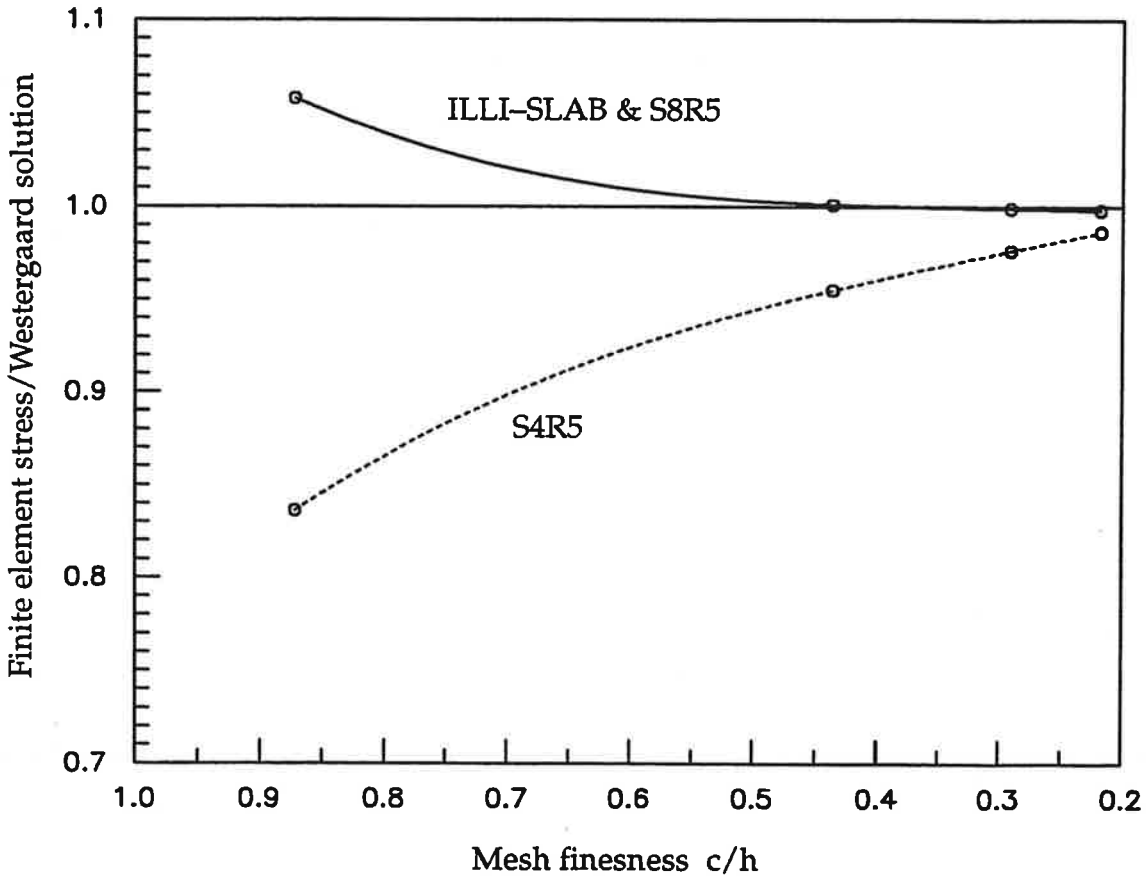

where c = the finest mesh size

Figure D-3. Mesh fineness and element type comparison.

because these equations are all based on plate theory which ignores plate compressibility and shear deformation.

Element Selection

The candidate brick elements considered are shown in Figure D-4. The first one selected was C3D8, which is a linear interpolation element with a node at each corner of a brick. The support is modeled with the "FOUNDATION" option which requires users to input a spring coefficient with "FL^{-3}" dimension (e.g., k value).

After several runs with various mesh designs, it was concluded that the C3D8 linear element does not compare well with Westergaard's solution. Even when a single pavement layer was meshed up to 4 layers of brick elements with aspect ratio 1:1:1, the results did not show significant improvement. Therefore, the C3D8 element was ruled out in later comparisons.

According to the "ABAQUS Example Problems Manual," quadratic elements perform very well even with a coarse mesh. There are many types of quadratic elements provided in the ABAQUS element library. According to finite element theory [41, 42, 43], some 3-D elements may *lock* when the major deformation mode is bending, which usually happens in transversely loaded plate problems. Reduced integration elements should be used to remedy this problem. Hybrid elements are also available in ABAQUS, but are intended for use with incompressible material behavior (i.e., Poisson's ratio = 0.5) which is not the case for concrete. Thus, only two quadratic elements, C3D20 and C3D20R elements (the latter with reduced integration) were considered further in this study.

The same example as that used in the 2-D element study was run with several 3-D models made of C3D20, C3D20R and different meshes, as shown in Figure D-5. The results are summarized in Table D-4 and Table D-5.

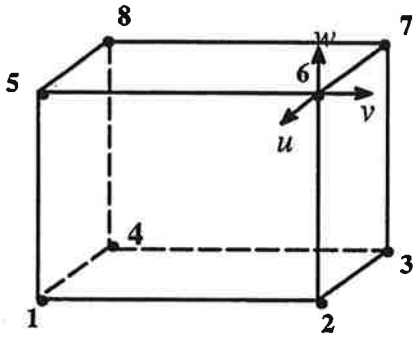

(a) C3D8 series element

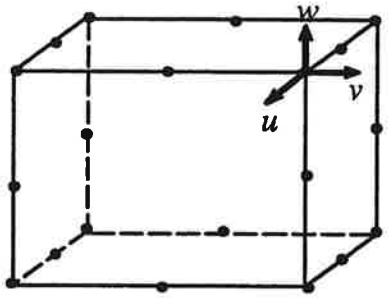

(b) C3D20 series element

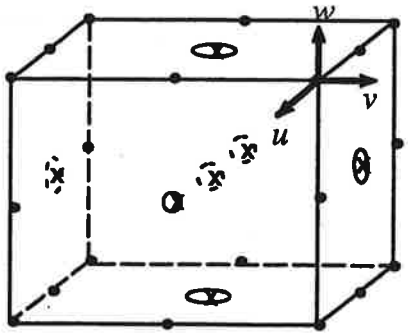

(c) C3D27 series element

Figure D-4. Major brick elements in ABAQUS.

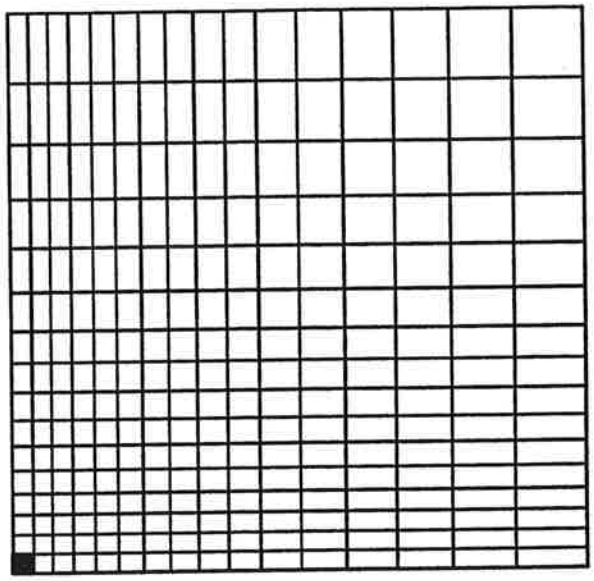

(a) 1 x 1 mesh

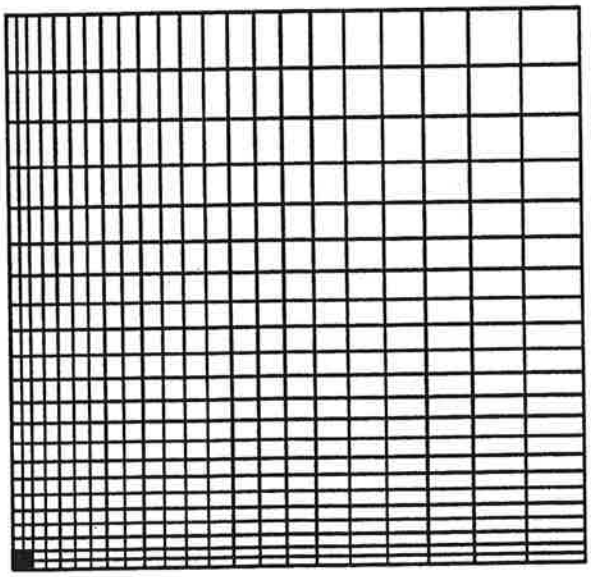

(b) 2 x 2 mesh

Figure D-5. Finite element meshes used for interior loading in case 1. (Note: one quadrant of grid is shown; symmetry is used to reduce run time).

Table D-4. Deflections at center of load, mils [1 mil = 25.4 μm].

		C3D20	C3D20R
1 x 1	δ_{top}	9.272	9.273
	δ_{bottom}	9.214	9.221
	ε_{zz}	9.667	8.667
2 x 2	δ_{top}	9.276	9.273
	δ_{bottom}	9.211	9.215
	ε_{zz}	10.83	9.667

Table D-5. Stresses at center of load, psi [1 psi = 6.89 kPa].

		C3D20	C3D20R
1 x 1	σ_{top}	–305.8	–308.3
	σ_{bottom}	289.0	299.7
	τ	49.09	43.62
2 x 2	σ_{top}	–292.6	–289.3
	σ_{bottom}	277.9	283.6
	τ	49.54	41.46

C3D20R converged to Westergaard's analytical solution better than the C3D20 element did in a finer mesh. As for deflection, the two elements gave almost the same results for various meshes. The calculated vertical compressibility of the concrete slab in these examples was about 5×10^{-5} inch [1.3×10^{-3} mm], or $\varepsilon_{zz} = 0.01$, which is less than 0.7 percent of deflection. This justifies one of the hypotheses for thin plate theory that transverse compressibility (ε_{zz}) of the plate is negligible in some cases.

However, the vertical shear stresses are very significant compared to the maximum stresses, about 15 percent of the maximum tensile stresses. This shows that the assumption of neglecting transverse shear in thin plate theory is not appropriate in some cases. In this example, some points were noticed:

- High shear stresses only occur in the vicinity of the loaded area. Most of the plate has no significant transverse stresses. Westergaard mentioned this problem and developed an equation based on "special theory" to take the shear deformation near a small loaded area into account.
- Load size plays a key role in this situation. Although the length-to-thickness ratio of this plate is 50, which satisfies the thin plate criterion, a small load may still violate plate theory in the neighborhood of the loaded area. When the load is distributed over a large area, transverse shear should be negligible as assumed in thin plate theory.

Performance of 3-D Elements Versus 2-D Elements

Another interesting issue in developing a 3-D model is how 3-D results compare with 2-D results. As mentioned before, 2-D and 3-D results are not

expected to match in all cases because some plate responses are neglected in 2-D model formulation. Agreement of 2-D and 3-D models can only be expected when the following conditions are all satisfied:

1. The plate is thin enough,
2. The loaded area is large enough,
3. The finite element meshes meet requirements for accuracy,
4. The problem is restricted to the type for which 2-D models apply.

Interior Loading Case. To compare the elements for various mesh finenesses and loading sizes, a series of runs was made using different elements and changing the loading area, from 9 to 72 inches [229 to 1829 mm] square, at the interior of a slab of constant size 20 feet square, as shown in Figure D-6. The slab modulus of elasticity was 4 million psi [27560 MPa], the slab thickness 6 inches [152 mm], the slab Poisson's ratio 0.15, and the k value 200 psi/in [54 kPa/mm]. The load magnitude was 9,720 pounds [43.25 kN]. The interior stresses and deflections computed using Westergaard's equations, ILLI-SLAB and FINITE (2-D models), 2-D elements in ABAQUS (STR13, S4R, and S8R) and the 3-D brick element in ABAQUS (C3D20R) are given in Tables D-6 and D-7, and plotted in Figures D-7 and D-8.

Westergaard's interior stress equation predicts lower stresses than the finite element results at small load sizes and predicts higher stresses than the finite element results at large load sizes. The latter trend supports the statement by Timoshenko [8] that Westergaard's equations apply only when the loaded area is small in comparison with ℓ. However, the transverse shear effect may become significant when the loaded area approaches a point load. Consequently, Westergaard's interior stress equation agrees with the 3-D model within an intermediate range of load area size.

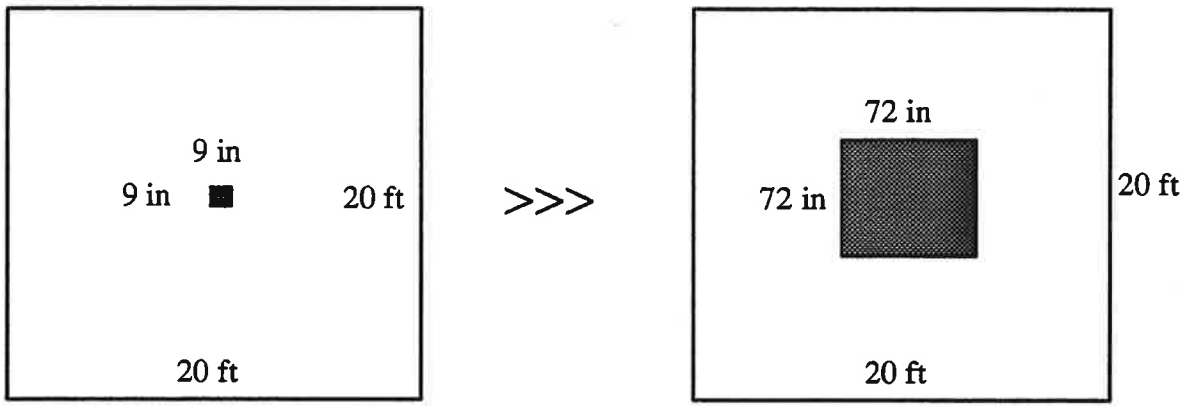

1 in = 25.4 mm, 1 ft = 304.8 mm

Figure D-6. Change of load size in interior loading of case 2.

Table D-6. Maximum interior stress comparison, psi [1 psi = 6.89 kPa].

	ILLI-SLAB	FINITE	ABAQUS (STRI3)	ABAQUS (S4R)	ABAQUS (S8R)	ABAQUS (C3D27R)	Westergaard
9*9	345.129	345.141	339.5	275.8	344.8	346.1	324.79
18*18	228.168	228.176	228.0	212.2	227.3	227.5	223.56
27*27	168.186	168.204	168.4	161.6	167.5	167.7	166.61
36*36	128.584	128.601	128.7	125.1	128.0	128.2	128.39
45*45	99.597	99.975	100.1	97.92	99.47	99.61	100.99
54*54	78.321	78.350	78.42	77.07	77.92	78.04	80.92
63*63	61.582	61.602	61.65	60.78	61.25	61.34	66.29
72*72	48.426	48.449	48.48	47.91	48.15	48.23	55.98

Table D-7. Maximum interior deflection comparison, mils [1 mil = 25.4 μm].

	ILLI-SLAB	FINITE	ABAQUS (STRI3)	ABAQUS (S4R)	ABAQUS (S8R)	ABAQUS (C3D27R)	Westergaard
9*9	9.86	9.847	9.779	10.132	10.186	10.144	9.807
18*18	9.43	9.417	9.370	9.600	9.642	9.600	9.370
27*27	8.892	8.880	8.848	9.012	9.042	9.014	8.867
36*36	8.300	8.288	8.263	8.386	8.408	8.389	8.296
45*45	7.686	7.673	7.655	7.752	7.764	7.751	7.718
54*54	7.070	7.058	7.044	7.119	7.127	7.119	7.164
63*63	6.471	6.459	6.449	6.507	6.512	6.507	6.659
72*72	5.897	5.885	5.876	5.923	5.926	5.923	6.224

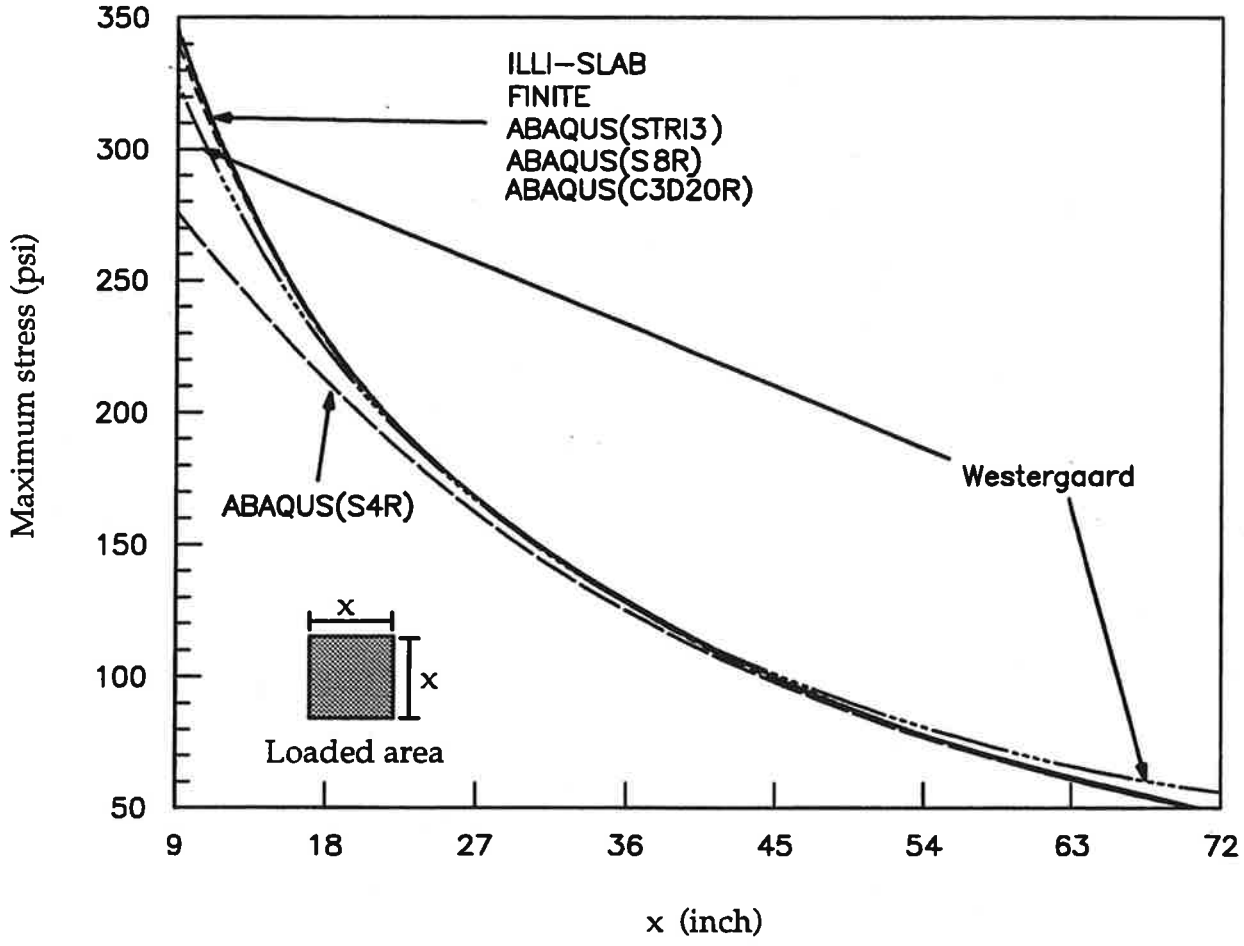

1 in = 25.4 mm, 1 psi = 6.89 kPa

Figure D-7. Westergaard, 2-D, and 3-D finite element interior stress results.

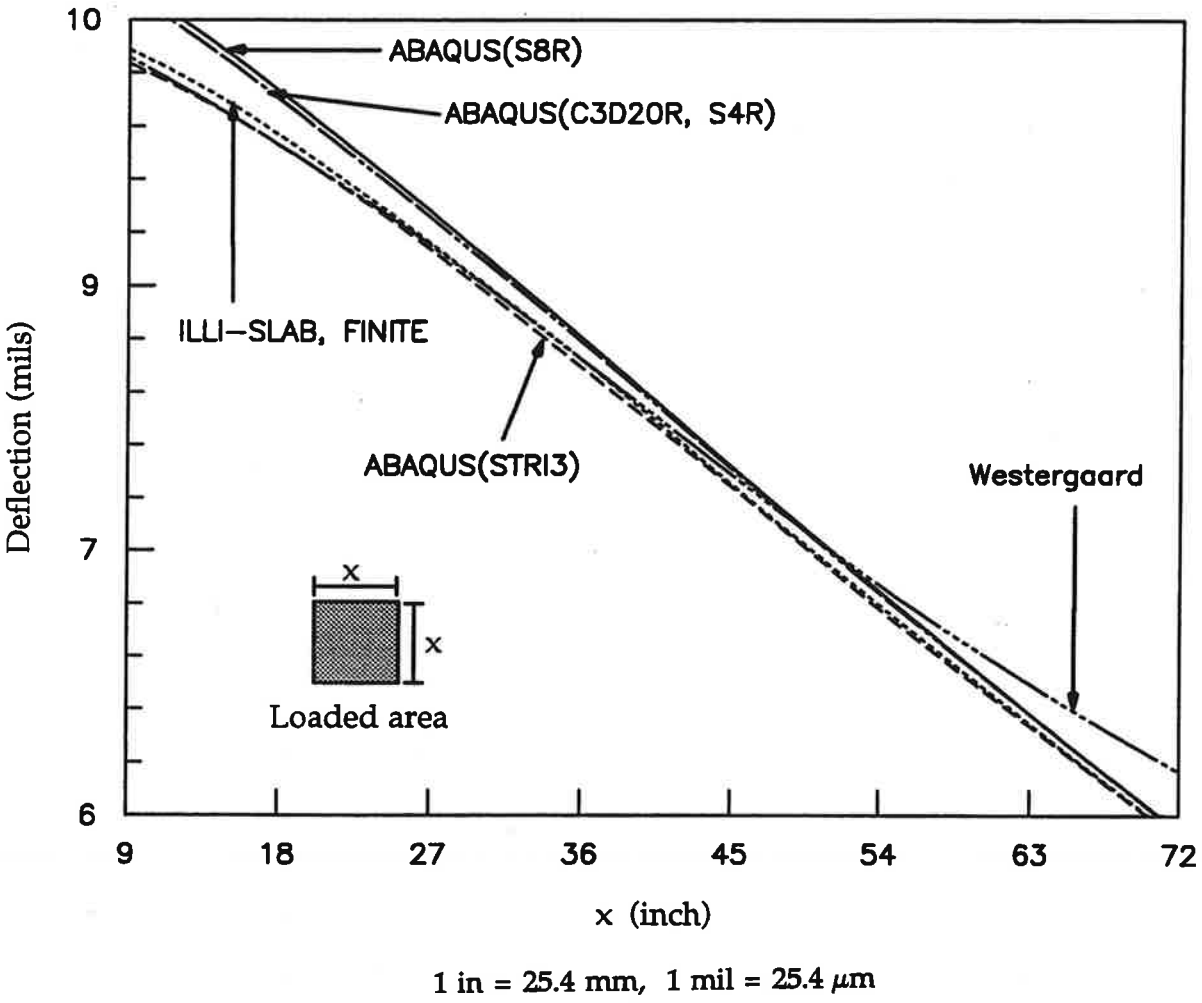

1 in = 25.4 mm, 1 mil = 25.4 μm

Figure D-8. Westergaard, 2-D, and 3-D finite element interior deflection results.

Detailed research by Ioannides on load size effects on 2-D finite element results has shown the same conclusion. [9]

Interior stress results are similar for nearly all of the 2-D and 3-D element types over a wide range of load sizes, as shown in Figure D-7. The exception is the ABAQUS 2-D S4R element which was expected to agree more closely with the 3-D results than the other elements because it takes into account transverse shear.

Interior deflections for all element types converge as the load size increases, but Westergaard's deflection solution diverges from the finite element solutions as the load size increases, as shown in Figure D-8. In the range of small load sizes, the finite element deflection results form two groups: one group consists of the ABAQUS element types which consider transverse shear, and the other group consists of the ILLI-SLAB, FINITE, and ABAQUS STR13 elements which ignore transverse shear.

These results indicate that 2-D elements are capable of good agreement with 3-D results for interior stress over a wide range of load sizes, but a discrepancy exists over a wide range of load sizes between the interior deflections computed using 2-D elements and those computed using 3-D elements.

Edge Loading Case. Another set of sensitivity runs was conducted for edge loading, using load sizes from 9 to 36 inches [229 to 914 mm] square, and all of the other parameters the same except for the slab size, which was a constant 10 by 20 ft [3 by 6 m], as shown in Figure D-9. The edge stresses and deflections computed using Westergaard's equations, ILLI-SLAB and FINITE (2-D models), 2-D elements in ABAQUS (STR13, S4R, and S8R) and the 3-D brick element in ABAQUS (C3D20R) are given in Tables D-8 and D-9 and plotted in Figures D-10 and D-11.

The edge stress results shown in Figure D-10 indicate that Westergaard's edge solution agrees excellently with the 3-D finite element solution until the load size becomes larger than about 20 inches [508 mm] square. The RPB12 element (used in

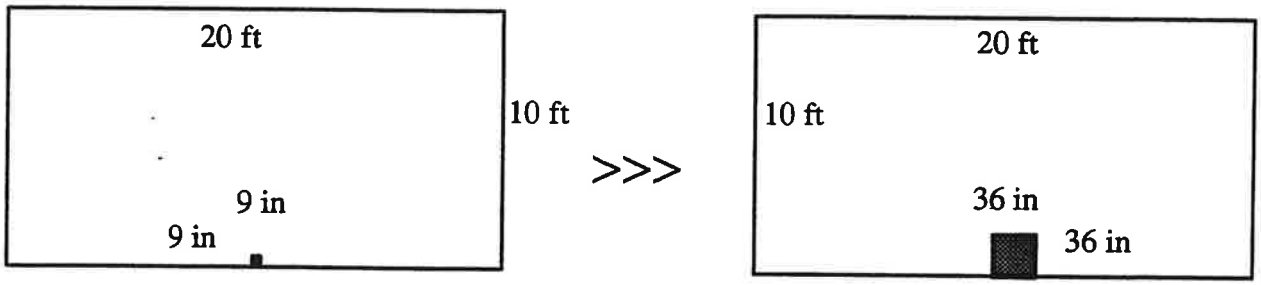

1 in = 25.4 mm, 1 ft = 304.8 mm

Figure D-9. Change of load size in edge loading of case 2.

Table D-8. Maximum edge stress comparison, psi [1 psi = 6.89 kPa].

	ILLI–SLAB	FINITE	ABAQUS (STRI3)	ABAQUS (S8R)	ABAQUS (C3D27R)	Westergaard
9*9	653.153	652.906	608.6	612.9	624.2	623.719
18*18	403.944	403.792	384.6	385.9	390.0	390.232
27*27	277.712	277.620	269.7	267.7	269.9	263.143
36*36	198.735	198.672	195.6	192.7	194.0	179.615

Table D-9. Maximum edge deflection comparison, mils [1 mil = 25.4 μm].

9*9	29.580	29.454	29.500	30.551	30.481	28.754
18*18	25.009	24.904	24.954	25.585	25.527	22.852
27*27	20.995	20.907	20.97[illegible]	21.357	21.325	16.951
36*36	17.546	17.471	17.528	17.777	17.760	11.049

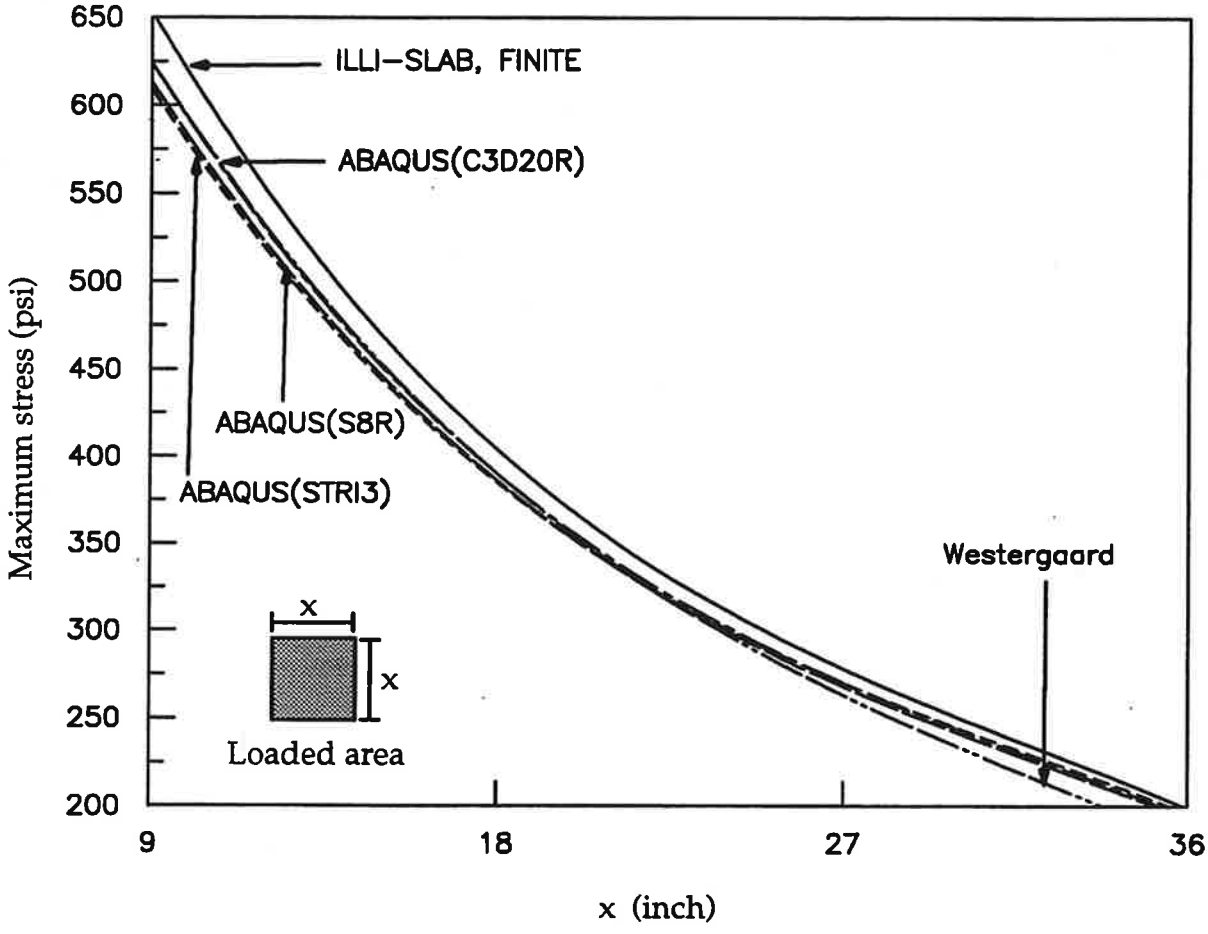

1 in = 25.4 mm, 1 psi = 6.89 kPa

Figure D-10. Westergaard, 2-D, and 3-D finite element edge stress results.

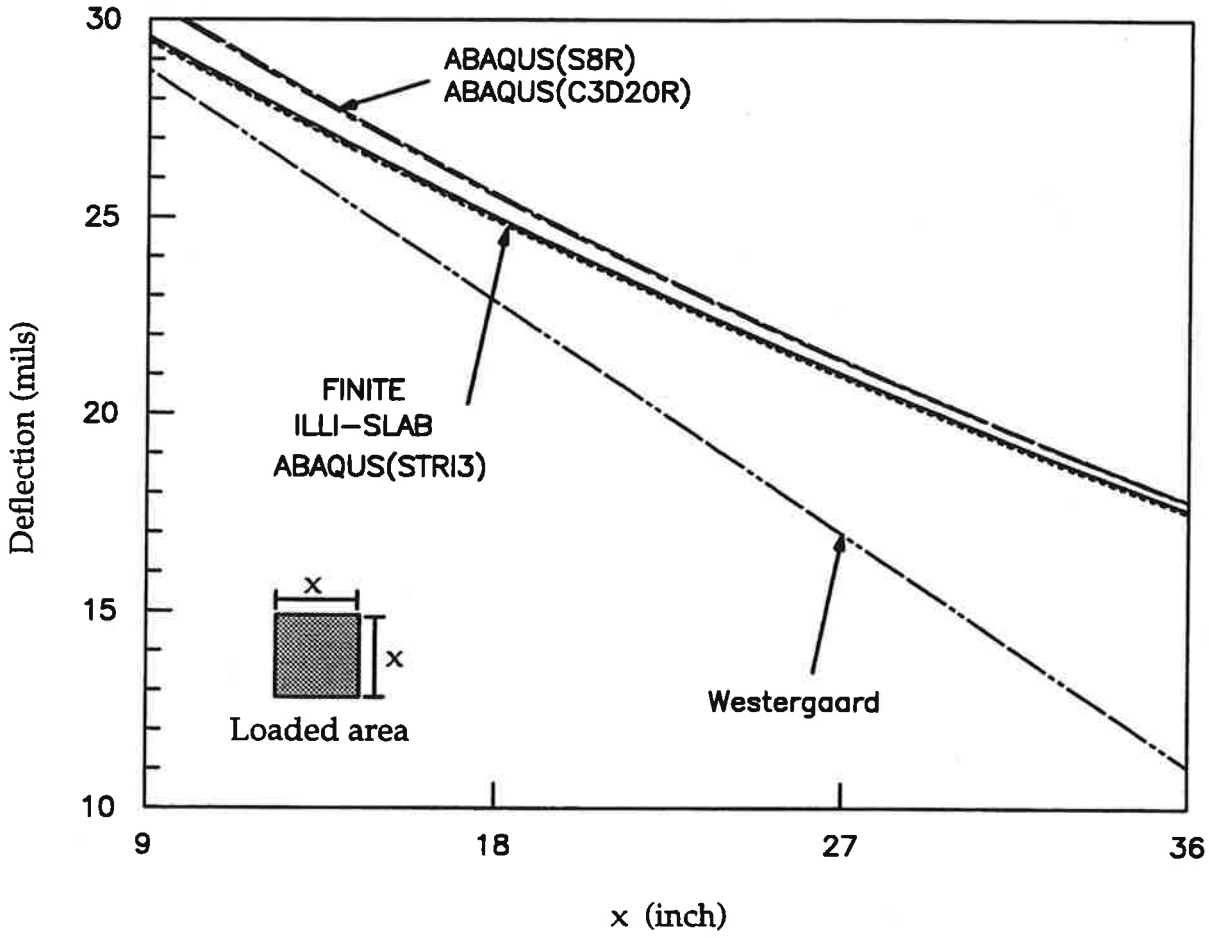

1 in = 25.4 mm, 1 mil = 25.4 μm

Figure D-11. Westergaard, 2-D, and 3-D finite element edge deflection results.

ILLI-SLAB and FINITE) predicts somewhat higher edge stresses than do the shell and solid elements in ABAQUS. (Note that the ILLI-SLAB and FINITE edge stress results are nearly identical so their lines coincide in Figure D-10.) This discrepancy narrows as the load size becomes larger. Thus, it might be explained by the transverse shear effect in edge loading being slightly more significant than in the interior loading situation. Further investigation of this is needed. Although STRI3 is a thin shell element, like RPB12, the geometry and different formulation, e.g., using 6 degrees of freedom rather than 3 degrees of freedom in RPB12, might explain the gap between the STRI3 and ILLI-SLAB edge stress curves. However, the gap is less than 5 percent even under very concentrated loading.

Westergaard's edge deflection solution diverges dramatically from all of the finite element solutions as the load size increases, as shown in Figure D-11. The edge deflections computed with ABAQUS using the 2-D S8R element and the 3-D C3D20R element are higher than the edge deflections computed with ILLI-SLAB, FINITE, and the STR13 element over the full range of load sizes examined. The gap narrows with increasing load size.

The edge loading results using the 3-D model agree with the 2-D model results for slabs which could be considered thin plates, that is, having length-to-thickness ratio of 20 or less. However, in analysis of thicker and smaller slabs which did not satisfy the definition of a thin plate, discrepancies between the 3-D and 2-D results became more significant. The edge loading comparison may be summarized as follows:

- The performance of various element types in edge loading is similar to that in interior loading.

- Thin plate elements produce either higher or lower stresses than solid elements. Transverse shear effects might be responsible for these discrepancies.
- Westergaard's edge stress and deflection solutions are best suited for small loads.
- Good agreement between the 3-D and 2-D models is achieved for edge deflection and stress results when the slab is a thin plate, i.e., when the length-to-thickness ratio is more than 20. Below this limit progressively greater discrepancies exist.

Element Proportions

In finite element analysis, a balance must be achieved between accuracy of results and efficiency of computation. The mesh must be sufficiently fine to yield results with an acceptable level of accuracy. However, computer storage space and CPU time increase with mesh fineness. In 3-D analysis with solid elements, not only the horizontal fineness of the mesh but also its vertical fineness may be important to the accuracy of results. An examination of the sensitivity of solid element size was conducted to assess its significance. Instead of placing a plate on a foundation, a simply supported plate under interior loading is considered, because the responses of a simply supported plate are more sensitive to changes in the analysis parameters than a plate resting on a foundation. The load was applied over a large area to eliminate the effect of transverse shear caused by concentrated loading. The theoretical solution of this case is given below:

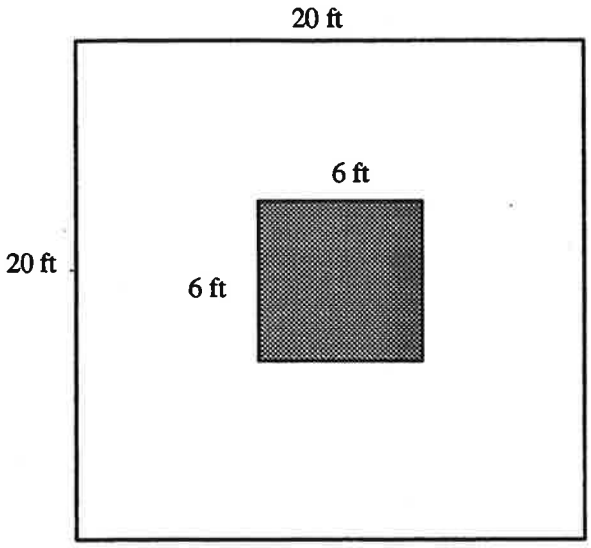

P = 3600 lb [16 kN]

E = 30 million psi [206700 MPa]

μ = 0.3

h = 6 in [152 mm]

Theoretical solution:

σ_{max} = 102.3 psi [704.8 kPa]

[1 ft = 0.305 m]

Compared to the exact solution derived by thin plate theory, the maximum stress calculated with the solid element model yielded less than 2 percent discrepancy even with the coarse mesh (2a/h=2). The mesh becomes more plate-like as this ratio increases. Therefore, the model will lose accuracy if it is meshed with a plate-like solid. For highway pavements, the 2a/h ratio rarely exceeds one under normal truck wheel loads if the model is meshed no larger than the load size. Hence, the mesh fineness will generally be satisfactory from the standpoint of accuracy if the element aspect ratio 2a/h is less than 2. For larger loaded areas it may be necessary to divide the loaded area into multiple elements.

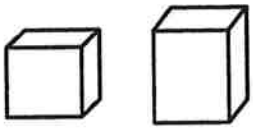

Good

Not recommended

MOTIVATION FOR 3-D MODEL DEVELOPMENT

The above comparison of 2-D and 3-D element types demonstrates that it is possible, with careful element selection and mesh definition, to achieve very good agreement between 2-D and 3-D models, for the limited range of problems which 2-D models are able to solve. The performance comparison is necessarily limited to those types of problems. The motivation for developing 3DPAVE was that many aspects of concrete pavement behavior cannot be realistically modelled in two dimensions. Among the aspects which were considered very important to this research study are the following:

- **Curling or warping of a slab off of a base layer:** In 2-D models the slab and base always have the same curvature, and though the layers may be unbonded horizontally, the slab and base can never be any distance apart at any node.
- **Direct modelling of nonlinear and/or unequal temperature or moisture gradients in the slab and base:** A 2-D element is by its nature incapable of modelling a nonlinear gradient. The 2-D models such as ILLI-SLAB are also incapable of modelling unequal gradients in the slab and base. Although ILLI-SLAB allows different slab and base gradients as input, the program converts these into a single linear gradient through the full slab and base thickness. Some 2-D methods represent a nonlinear gradient by an equivalent linear gradient, or add the stresses due to linear and nonlinear components of the total nonlinear gradient. A direct and more realistic analysis of the effects of nonlinear gradients through the slab and/or base requires a 3-D model.
- **Widened base, widened lane, and mismatched joints and cracks:** In 2-D models the horizontal boundaries of the slab and base must coincide. 3-D modelling permits analysis of more realistic geometries in which the slab and base have mismatched edges, joints, and cracks.

- **Friction coefficients and horizontal and vertical bond strengths:** These interface characteristics can be directly and realistically modelled in 3-D. In 2-D models, layer interfaces can only be bonded or unbonded.
- **Thicker pavement and base cross-sections:** Transverse shear stress is significant for thicker cross-sections, but cannot be considered in analytical solutions (e.g., Westergaard) based on "medium-thick" plate theory, nor in most of the available 2-D pavement analysis programs (the only exception is the little-used and little-verified ILLI-LAYER program by Korovesis [14]).
- **Layer compressibilities:** 3-D modelling permits direct definition of the compressibility of the slab and base layers. In 2-D plate models all layers above the subgrade are incompressible.

In addition to these capabilities, a 3-D model developed within a powerful and versatile finite-element package such as ABAQUS provides the potential to directly and relatively easily model a wide variety of other pavement behaviors which would be of interest to other research efforts. Just a few of these are:

- Dynamic loading,
- Viscoelastic behavior,
- Temperature-dependent properties,
- No tension in unbound materials,
- Explicit modelling of steel reinforcement (for JRCP and CRCP),
- Variable joint width and its effect on variable load transfer in dowelled or undowelled joints,
- Stress-dependent response of unbound materials, and
- Concrete behavior beyond the elastic range, including inelastic response, cracking failure, and behavior after cracking.

DEVELOPMENT OF THE 3DPAVE MODEL

Since ABAQUS is a general-purpose finite element program, not specifically for pavement analysis, extra efforts are needed to model pavement system characteristics with those general purpose options and parameters provided by ABAQUS. Therefore, the 3DPAVE model was developed step by step as shown in Figure D-12. The reason for beginning with 2-D shell element modelling is that ABAQUS is very versatile, so experience is very important in correctly assembling the commands and options needed in the pavement model. The 2-D model was then upgraded systematically to a 3-D model. Each step in the development process involves many challenges involving model input, element properties, execution problems, results checking, etc. Brief descriptions of the model-building steps are presented in this section.

3-D Solid Element (Brick Element)

Solid elements are rarely used for simple problems in plate models because 2-D plate elements usually give satisfactory results with greater computational economy. Furthermore, the difficulties of modelling thin plates or shells with solid elements prevent the use of solid elements in solving plate problems. However, as discussed previously, solid elements are more appropriate for investigate the complicated interactions among environmental factors and pavement layers which are not necessarily treated appropriately by 2-D plate elements. As long as the mesh is properly designed, more realistic results are expected from the 3-D model.

Based on the element study presented earlier, C3D20R was selected as the standard element for this model. However, the C3D20R element had difficulty converging to a solution when contact problems were modelled. Since it is important to be able to model the mechanisms of contact and loss of contact when a slab curls

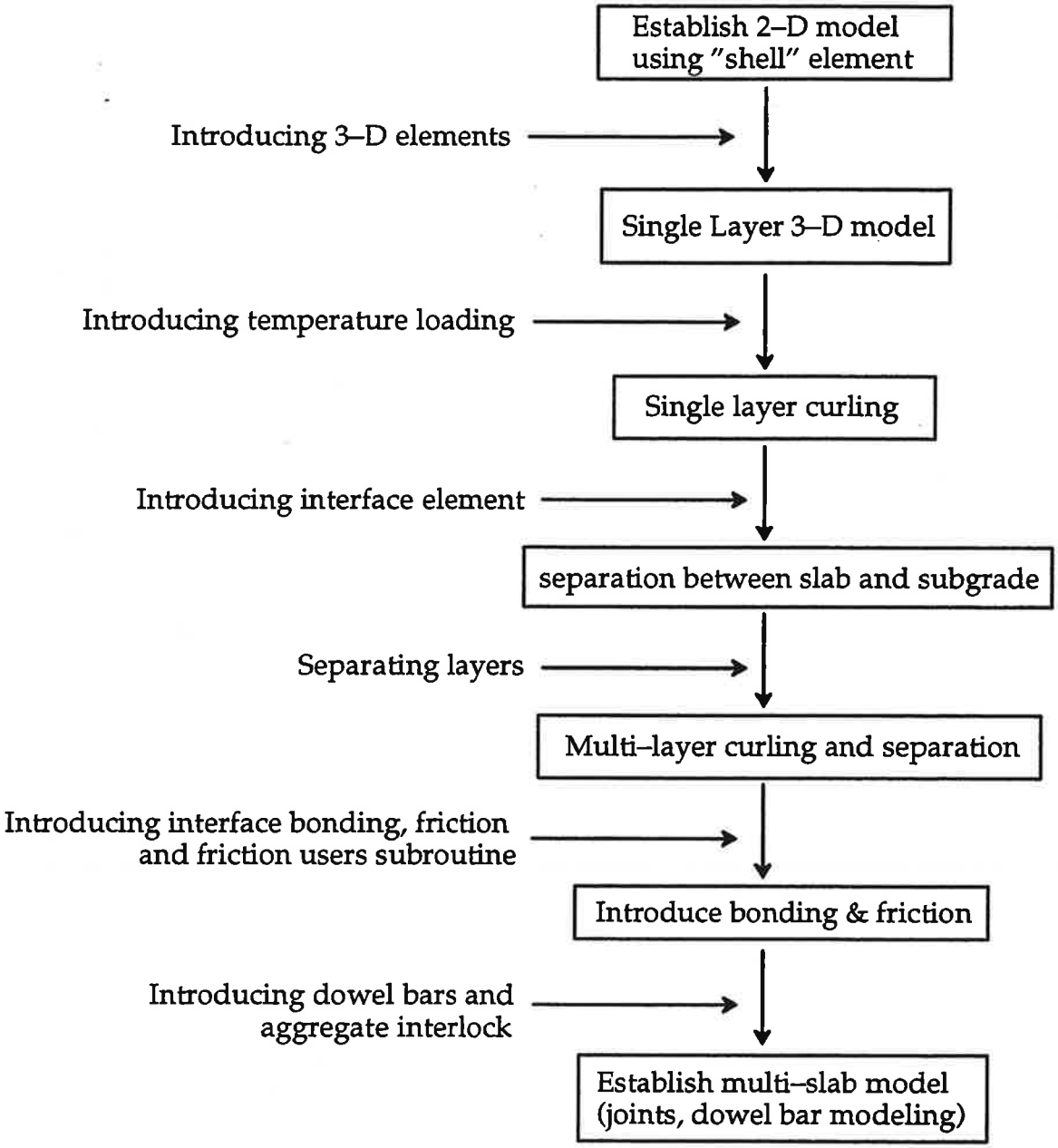

Figure D-12. Steps in development of 3-D model.

on top of a stiff base, the C3D27R element shown in Figure D-13 was used in place of the C3D20R element. C3D27R is a *variable node element*, similar to C3D20R but with extra nodes on faces which are contact surfaces.

C3D20R and C3D27R are quadratic elements, meaning that they have nodes at the middle of each edge in addition to nodes at the corners. This makes it possible to model a bilinear temperature gradient through the slab, using the nodes at the top, middle, and bottom of the element as shown as Figure D-14. More nonlinear temperature distributions may be modelled with multiple layers of C3D27R elements. However, modelling a slab with multiple layers instead of a single layer increases the computer run time dramatically. Thus, unless the stress distribution through slab depth is a major concern, a single-layer mesh is considered adequate for calculation of curling stresses at the top and bottom of the slab.

Interface Element

To investigate the effects of separation between layers, interface friction, and bonding, the interface should be modelled. ABAQUS provides many interface elements for surface contact problems. The INTER9 element shown in Figure D-15 is an interface element which can be used with the C3D27R element. Detailed interface responses, e.g., vertical contact stress or separation, and horizontal stress or slip, may be calculated when this element is used in model. Further studies of complex behavior under loading, such as crack growth, are also available in the options associated with this element.

The interface element can be either no thickness, which is the case when two layers are in contact, or can have a thickness equal to the distance between two layers of nodes to simulate an initial gap. Analyses involving separations between layers, such as curling problems, require several iterations to converge to a solution.

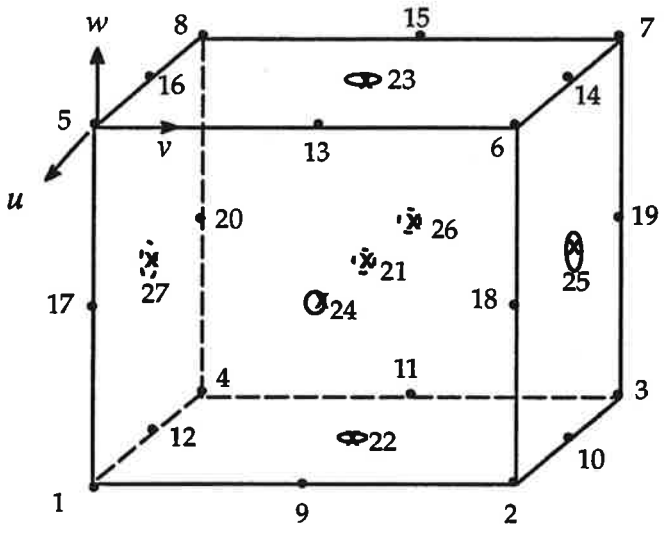

Figure D-13. C3D27R element.

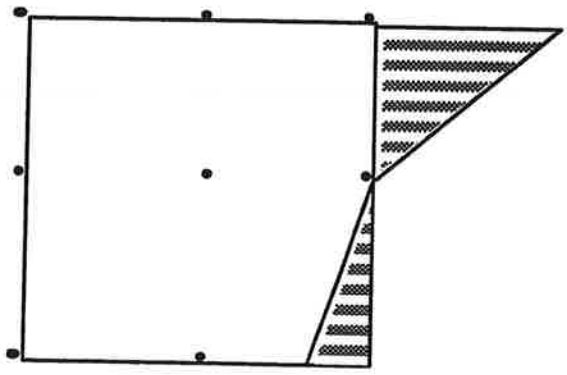

Figure D-14. Nonlinear temperature distribution with C3D27R element.

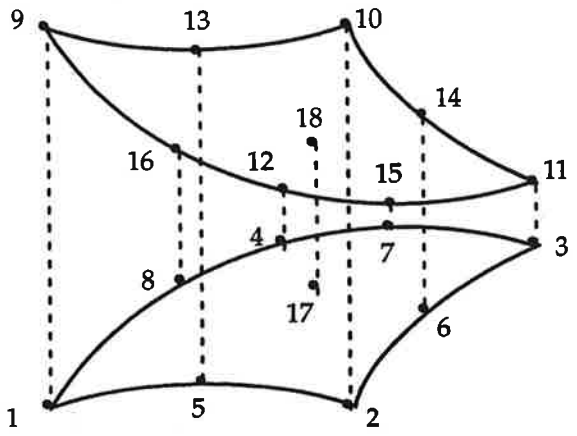

Figure D-15. INTER9 interface element.

Some curling analyses in ABAQUS required up to 24 iterations to achieve convergence. It is reported in the finite element literature that meshes made of the popular 20-node brick elements introduce a particular convergence difficulty for modeling contact problems, because of the 8-node interpolation used on the 20-node element. The C3D27R and INTER9 elements adopted for use in this model overcome this difficulty. [40]

Subgrade Modelling

Dense liquid foundations and elastic solid foundations can easily be modelled in ABAQUS. For a dense liquid foundation, a keyword *FOUNDATION* is available for all solid, shell, and membrane elements to provide spring support under elements. The keyword and its parameters are listed below.

FOUNDATION

elset name, support face, k value

where elset name = the name of the element set resting upon the foundation

support face = the supported face number of the solid element

k value = coefficient of subgrade reaction

However, introducing interface elements between the slab and subgrade hinders the use of the dense liquid foundation because FOUNDATION is not compatible with interface elements. Hence, when the FOUNDATION option is used, another element should be used below the interface element so that the dense liquid foundation can be modelled under the interface element (Figure D-16). The stiffness and thickness of the extra membrane layer is minimal to eliminate its effect on slab stresses. To investigate the error caused by this membrane layer, the results from two models were compared with no curling; one model with brick elements directly resting on the foundation, and another model with the membrane layer between the slab and the foundation, as shown in Figure D-16. The differences in maximum stresses and deflections were all less than 0.05 percent.

To model the subgrade as an elastic solid foundation, layers of brick elements may be used to a certain depth at which the foundation deflection is assumed to be negligible, as illustrated in Figure D-17a. This model has two drawbacks: (1) it requires the determination of the depth to which deflection is expected, and (2) it takes much more computer storage space and execution time to complete one run because of the number of elements. An alternative which addresses both of these drawbacks is to use infinite elements, a new feature in ABAQUS. A model using infinite subgrade elements is illustrated in Figure D-17b.

Bonding and Friction

In ABAQUS version 5.2, new options named "DEBONDING" and "BOND SURFACE" have been added for advanced modelling of contact problems. Users may specify debonding criteria or debonding mechanisms as parameters of the keyword "DEBONDING." Separation between layers may also be modelled with "DEBONDING." Unfortunately, two fatal problems with these new options were

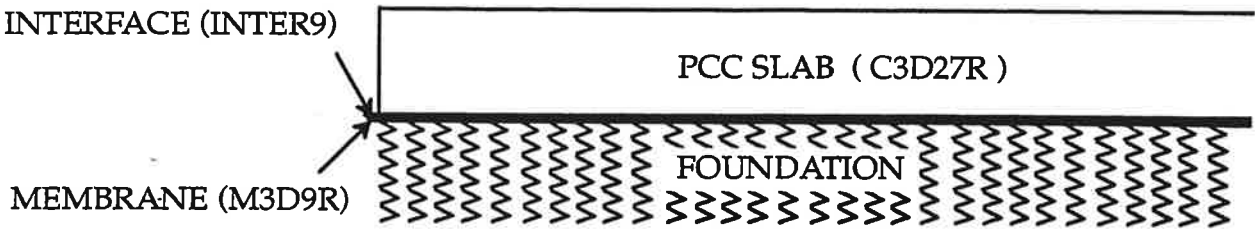

Figure D-16. Model of slab resting on Winkler foundation.

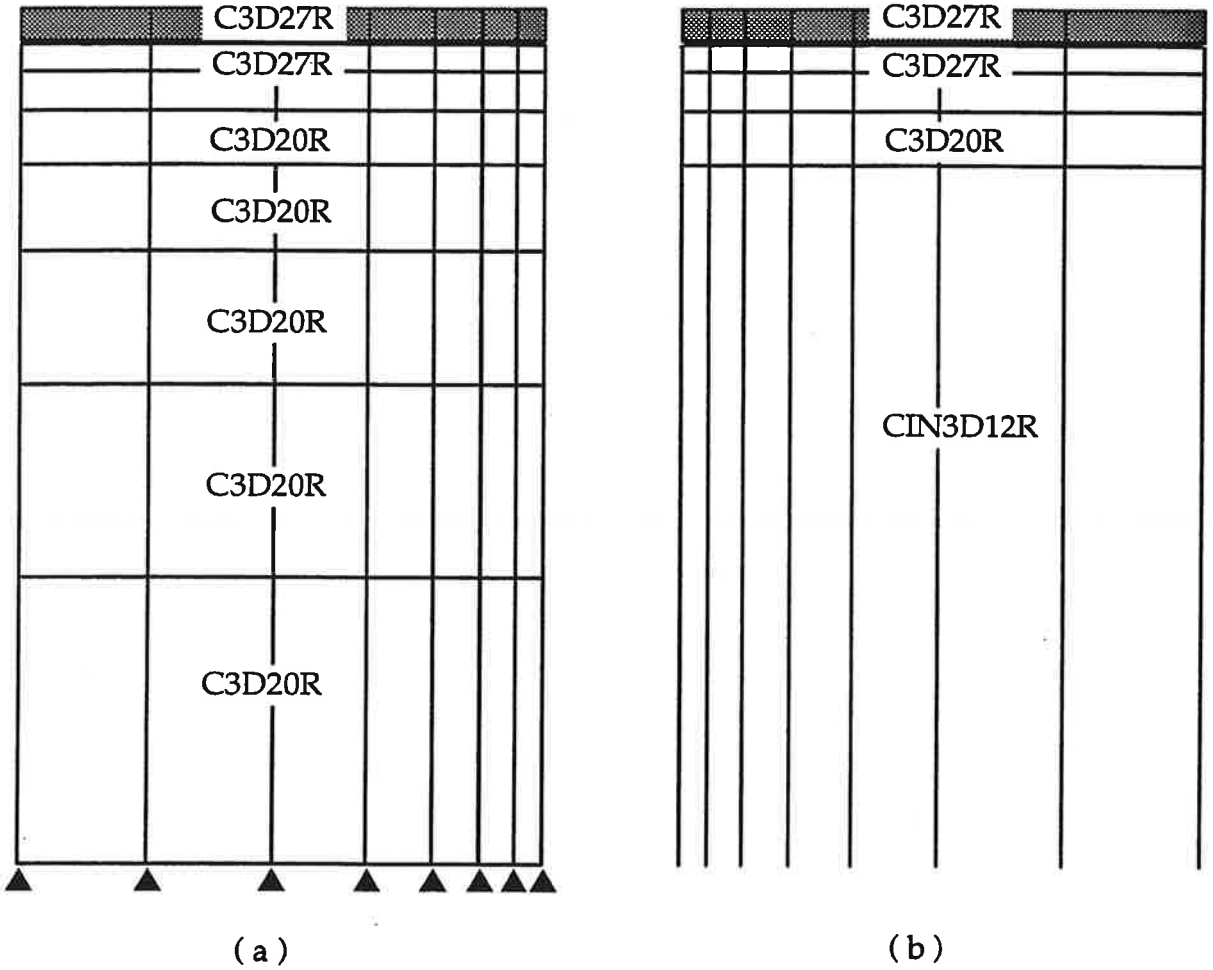

Figure D-17. Model of slab resting on elastic solid foundation.

found during the model development. First, the "BOND SURFACE" only addresses vertical bonding between layers. This means that horizontal slip is still allowed. This renders the "BOND SURFACE" option ineffective for pavement modelling because of the significance of modelling horizontal slip. Second, the inclusion of the "DEBONDING" option causes a fatal execution error in some cases. This has been confirmed by the ABAQUS developers as the result of bugs in the 5.2 version. Due to the difficulties involved with the bonding and debonding options, alternative methods were developed to consider vertical and horizontal interface stresses.

Vertical Bonding:

SURFACE CONTACT, NO SEPARATION

This card makes two layers fully bonded without vertical separation.

SURFACE CONTACT

bonding stress

The vertical bond will break when the vertical interface stress exceeds the specified bonding stress.

If two layers remain vertically bonded, the output file will report the vertical stresses at each node. If separation occurs, the vertical interface stress is zero and the gap size will be reported in the output file.

Friction (Horizontal Bonding):

ABAQUS provides a variety of parameters to model interface friction. The standard friction model in ABAQUS is classical Coulomb friction with an optional limit on the shear stress (Figure D-18). Some relative motion (elastic slip) is permitted when the interface is still sticking (Figure D-19). Permitting a large

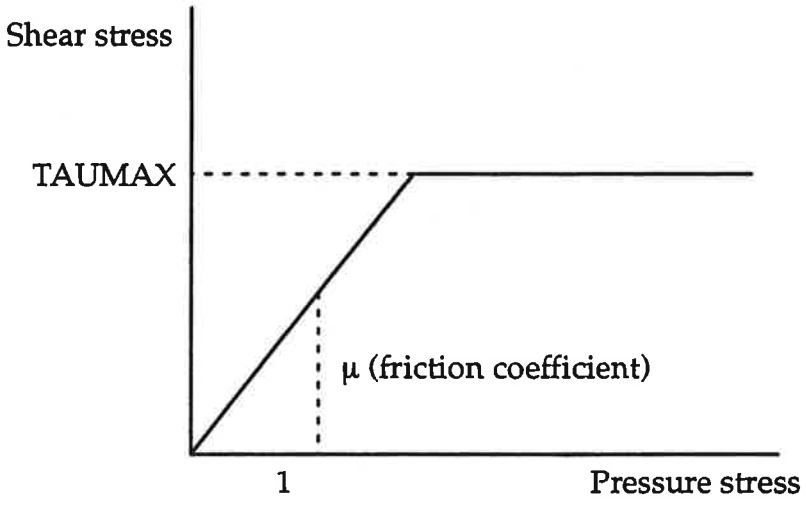

Figure D-18. Friction model in ABAQUS.

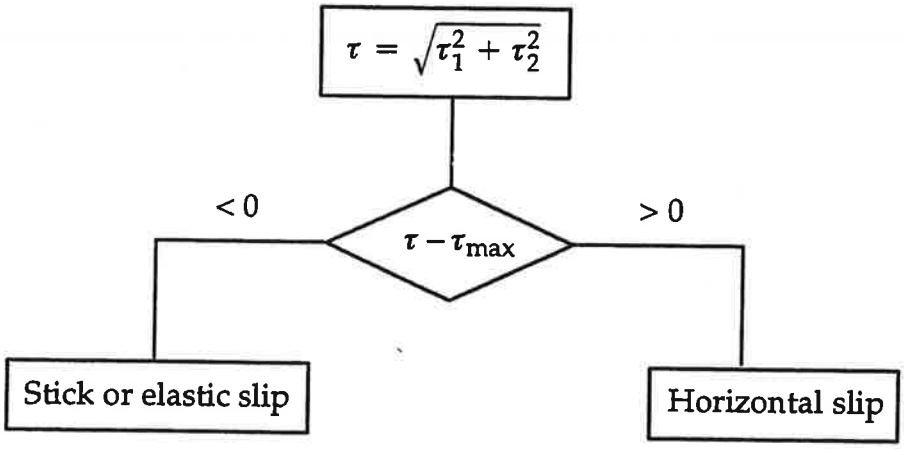

Figure D-19. Implementation of friction in ABAQUS.

amount of relative motion during sticking makes convergence of the solution more rapid at the expense of local solution accuracy. Permitting only a small amount of relative sliding motion better simulates behavior in which no slip is permitted in the sticking state, but requires more iterations to converge.

FRICTION, ROUGH

This card is intended to accompany SURFACE CONTACT, NO SEPARATION to simulate fully bonded layers. This is equivalent to a friction coefficient μ approaching infinity.

FRICTION, TAUMAX = *bonding stress,* [SLIP TOLERANCE = *number*], or [LAGRANGE]

friction coefficient

A variable degree of bonding may be modelled by specifying the ultimate bonding stress which can be carried by the bond in the field. After a load is applied, some regions may remain bonded, whereas bond breaks at those nodes whose calculated interfacial shear stresses exceeds TAUMAX.

By changing the value of TAUMAX and/or the vertical bonding stress in SURFACE CONTACT, various degrees of bonding are simulated. If "LAGRANGE" is included, no elastic slip is allowed.

The situation with no bonding but accounting for friction at the interface may be achieved by specifying a realistic friction coefficient. The last situation is fully unbonded and no friction considered. This case may be modelled in two ways. One is by excluding the SURFACE CONTACT and FRICTION options. The other is to specify the friction coefficient and vertical bond strength as zero:

FRICTION

0.

SURFACE CONTACT

0

Advanced friction mechanisms may be specified with the user subroutine FRIC provided in ABAQUS. For example, friction coefficients before and after slip occurs may be different. Simulating the change of friction coefficient requires the subroutine FRIC. However, correct use of the capabilities of FRIC requires considerable expertise and in-depth knowledge of friction theory.

Dowel Bars and Aggregate Interlock

Dowel bars are modelled in 3DPAVE with beam elements, as shown in Figure Figure D-20. Unlike the dowel models available in 2-D programs, the use of beam elements in ABAQUS eliminates the need to assign bending stiffness and shear stiffness values to the dowels elements. Instead, only physical properties, i.e., steel stiffness, bar diameter, and dowel spacing are needed. A comparison with ILLI-SLAB was made using the following example:

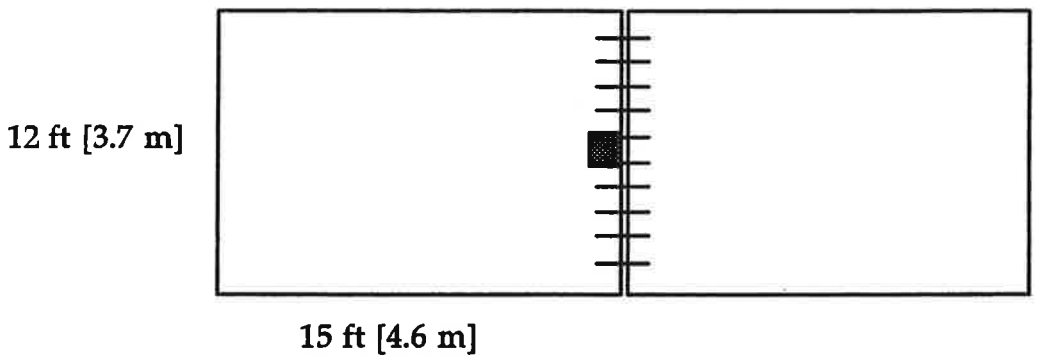

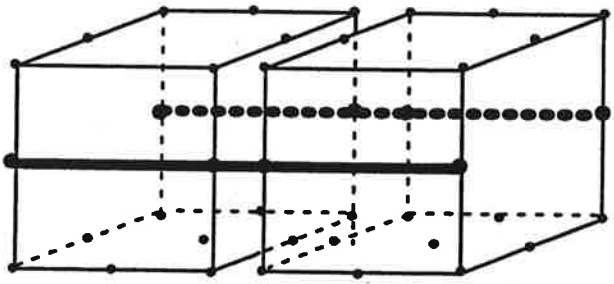

(a)

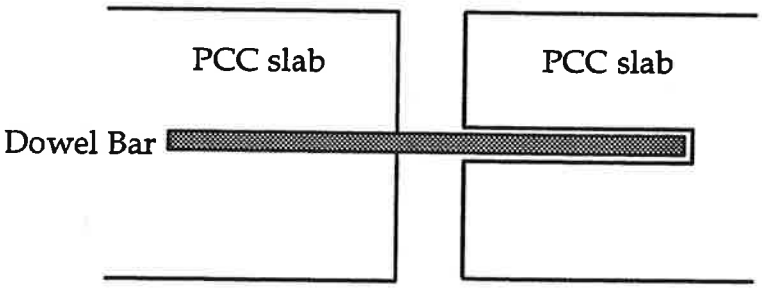

(b)

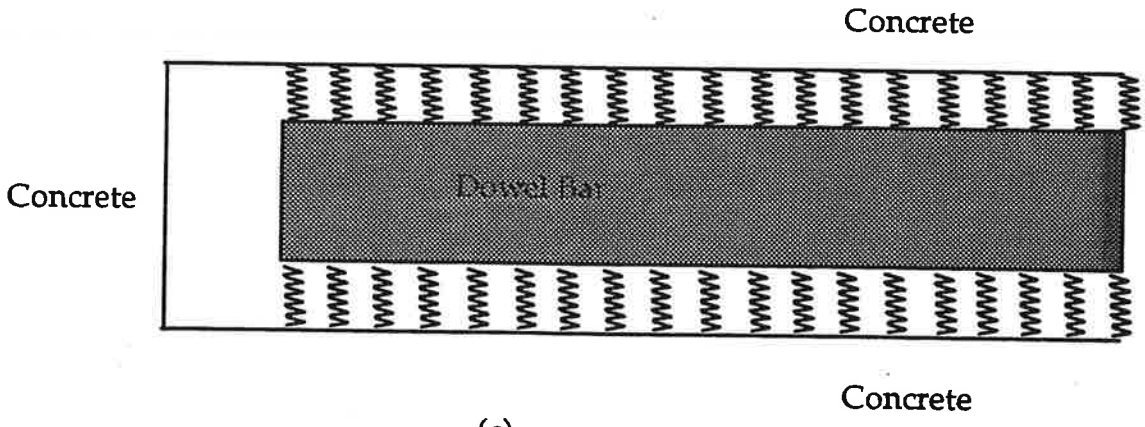

(c)

Figure D-20. Dowel bar model.

Slab thickness = 10 inches [254 mm]

Concrete modulus = 5.9 million psi [40651 MPa]

Poisson's ratio = 0.15

Subgrade k = 200 psi/in [54 kPa/mm]

Dowels: E = 30 million psi [206700 MPa]

μ = 0.3

spacing = 7.2 inches [183 mm]

diameter = 1.0 inch [25 mm]

As shown in Figure D-21, dowel bars modelled with beam elements in the 3-D model give the same results as ILLI-SLAB gives with a high dowel-concrete interaction (DCI) factor. This also confirms that, since no dowel looseness is allowed in the current version of 3-D model, the 3-D model tends to have excellent load transfer. A displaced shape of the jointed slabs generated from the ABAQUS postprocessor is shown in Figure D-22.

Dowel bars in this model may slip relative to the slab by using the option "SLIDER," one of the "multi-point constraints" (MPC). This simulates the dowel behavior in the field (Figure D-20b) better than other programs. Although it is possible using ABAQUS to consider the interaction of dowel bars and concrete (Figure D-20c), the analyses done for this study did not require detailed investigation of this ABAQUS feature.

Aggregate interlock is modelled in a straightforward manner by formulating the joints connecting slabs by shear springs. The JOINT and SPRING options used together provide a flexible model for various interlock stiffnesses, and even considering moment transfer (Figure D-23). Finding the spring stiffness which represent the load transfer provided by aggregate interlock has been a subject of

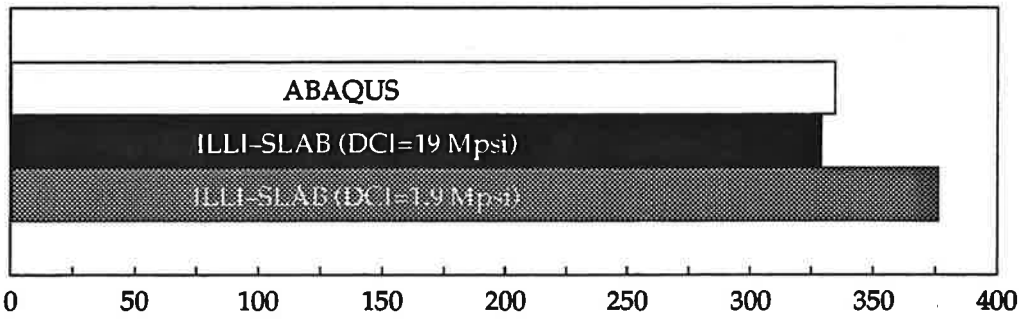

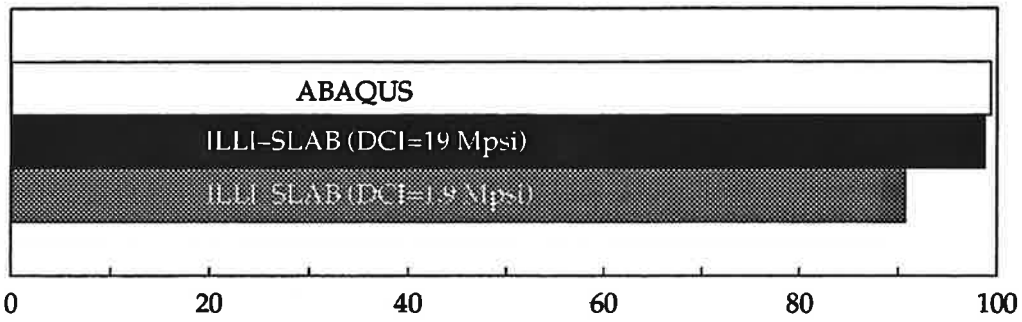

[1 psi = 6.89 kPa, 1 million psi = 6890 MPa]

Figure D-21. Dowel model comparison between ABAQUS and ILLI-SLAB.

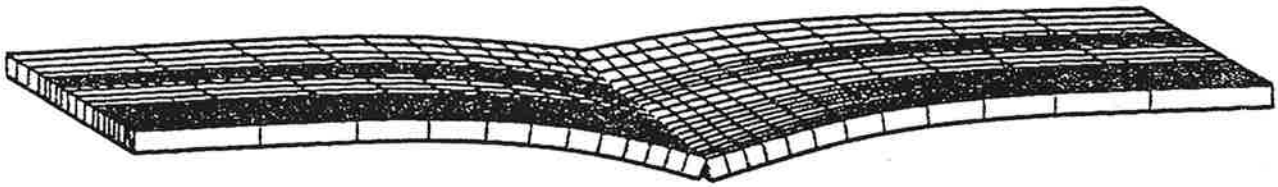

Figure D-22. 3-D displaced shape of jointed slabs modelled by ABAQUS.

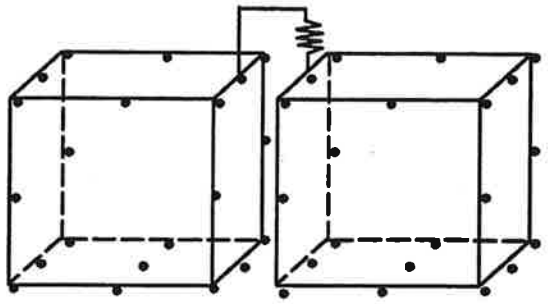

(a)

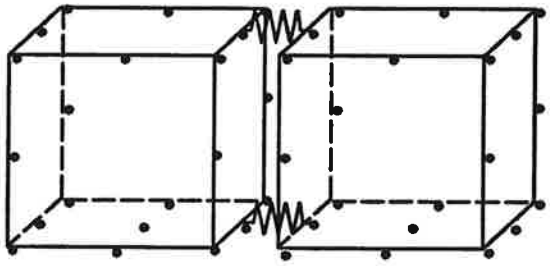

(b)

Figure D-23. Aggregate interlock model.

research [44]. It appears that moment transfer is not significant in aggregate interlock. A simple case was examined using both ABAQUS and the ILLI-SLAB 2-D program with the same shear interlock stiffness. Very close results were obtained in load transfer efficiency and maximum slab stresses.

A schematic illustration of the single slab 3DPAVE model is shown in Figure D-24. Examples of complete input files and notes for 3DPAVE are presented in Reference 45.

VALIDATION OF 3DPAVE

Validation of the new model was the next and most important step of its development. As mentioned before, most 2-D models and theoretical solutions are limited by their inherent assumptions. 3DPAVE was developed to overcome these shortcomings. Thus, validation of the model was done by comparison with full-scale field test data.

AASHO Road Test

The comparison between 3DPAVE and AASHO Road Test measurements is made with the data measured on the main loops. The main loop test was set up to measure the edge deflections and strains under moving truck loads. These data are valuable because the measured location was fixed at the midslab edge, whereas Loop 1 measurements were located at various positions and only the maximum strain data reported. The strain measurement position and axle load position with respect to the slab dimensions for the main loop tests are illustrated in Figure D-25.

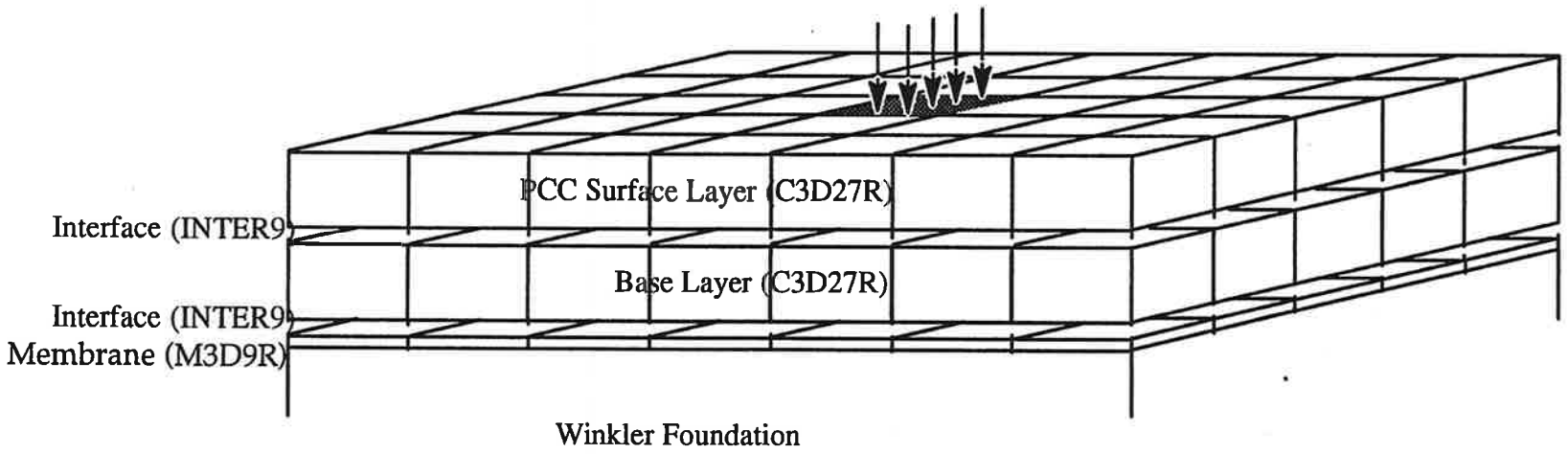

Figure D-24. 3-D single slab model in ABAQUS.

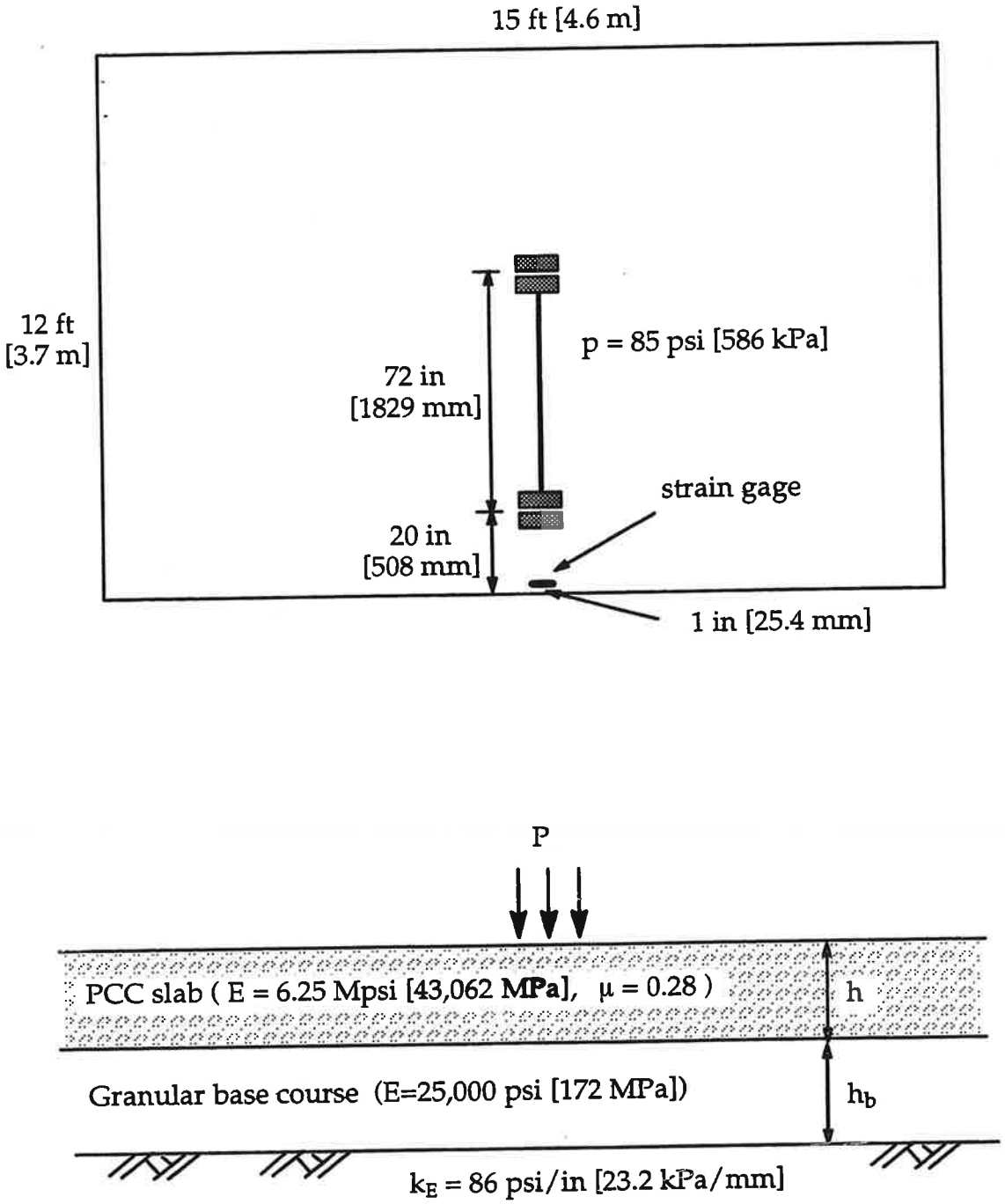

Figure D-25. Configuration of main loop test setup at AASHO Road Test.

Stress Validation. According to the AASHO Road Test vehicle specifications [46], air pressure in the tires was maintained to insure that the contact pressure was uniform for all test vehicles and axle loads. Thus, in the 3DPAVE model validation runs, contact pressure was held constant and load size was varied with varying axle load magnitudes. Finite element meshes were adjusted to match the tire prints which changed as axle loadings changed. Also, meshes were refined when the plate thickness was less than the smallest element width, as shown in Figure D-26.

The primary subgrade k value test conducted at the AASHO Road Test was the "elastic k" which was obtained from measurements of the elastic deformation of the subgrade (not including permanent deformation) under a 30-in-diameter [762 mm] plate after a 15-second loading. The mean elastic k value for springtime conditions was 86 psi/in [23 kPa/mm]. [17] However, it is reasonable to expect that a higher k value is required to match the deflections and stresses measured on the main loops under wheel loads moving at 30 mph [48 km/hr]. Initial modelling of single-axle loads on the main loop slabs with a range of input k values indicated that the best match of the stresses computed by 3DPAVE and the stresses computed from the field-measured strains was achieved at a k value of about 170 psi/in [46 kPa/mm], which is about double the measured plate load k_E. An example of the results of several runs at two k values, 120 and 170 psi/in [32 and 46 kPa/mm] is shown in Figure D-27. Subsequent modelling with the full range of single-axle and tandem-axle load magnitudes applied to the main loops showed that a k value of 170 psi/in [46 kPa/mm] achieved excellent agreement between the 3DPAVE stresses and the stresses corresponding to the field-measured strains over the full range of main loop slab thicknesses, as summarized in Table D-10 and shown in Figure D-28.

K Value versus Traffic Speed. At the AASHO Road Test, deflections and strains were measured for a range of truck speeds from creep speed to 60 mph

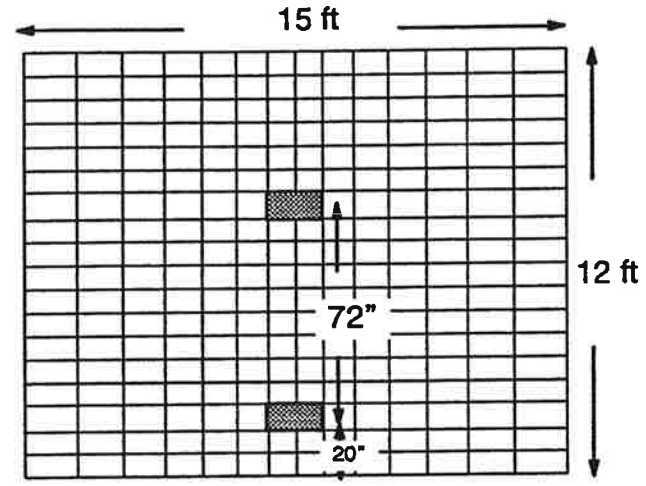

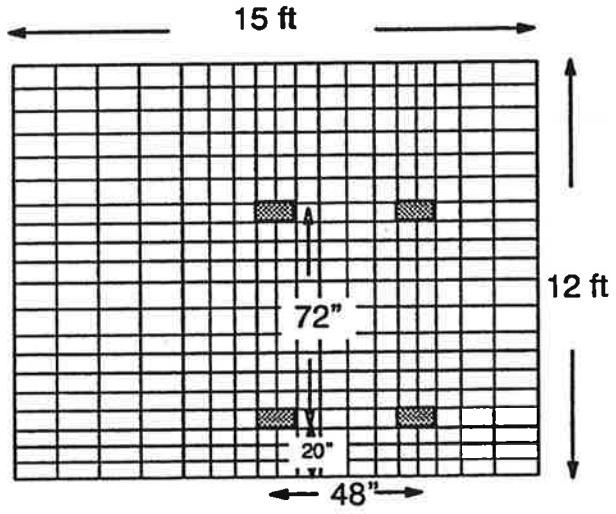

Figure D-26. 3DPAVE meshes for AASHO Road Test single and tandem axles.

Axle Load (kips)	Thickness (inch)	AASHO (psi/kip)	3DPAVE (k=120) (psi/kip)	3DPAVE(k=170) (psi/kip)
30.00	6.50	12.73	13.86	12.39
30.00	8.00	9.76	10.87	9.82
30.00	9.50	7.84	8.70	8.00
30.00	11.0	6.50	7.02	6.57

1 kip = 4.4 kN, 1 inch = 25.4 mm,
1 psi/kip = 1.566 kPa/kN, 1 psi/in = 0.27 kPa/mm

$E = 6.25 \times 10^6$ psi [43,062 MPa]
$\mu = 0.28$
Slab = 12 ft x 15 ft [3.7 m x 4.6 m]
Speed = 30 mph [48 km/hour]
p = 85 psi [585.7 kPa]

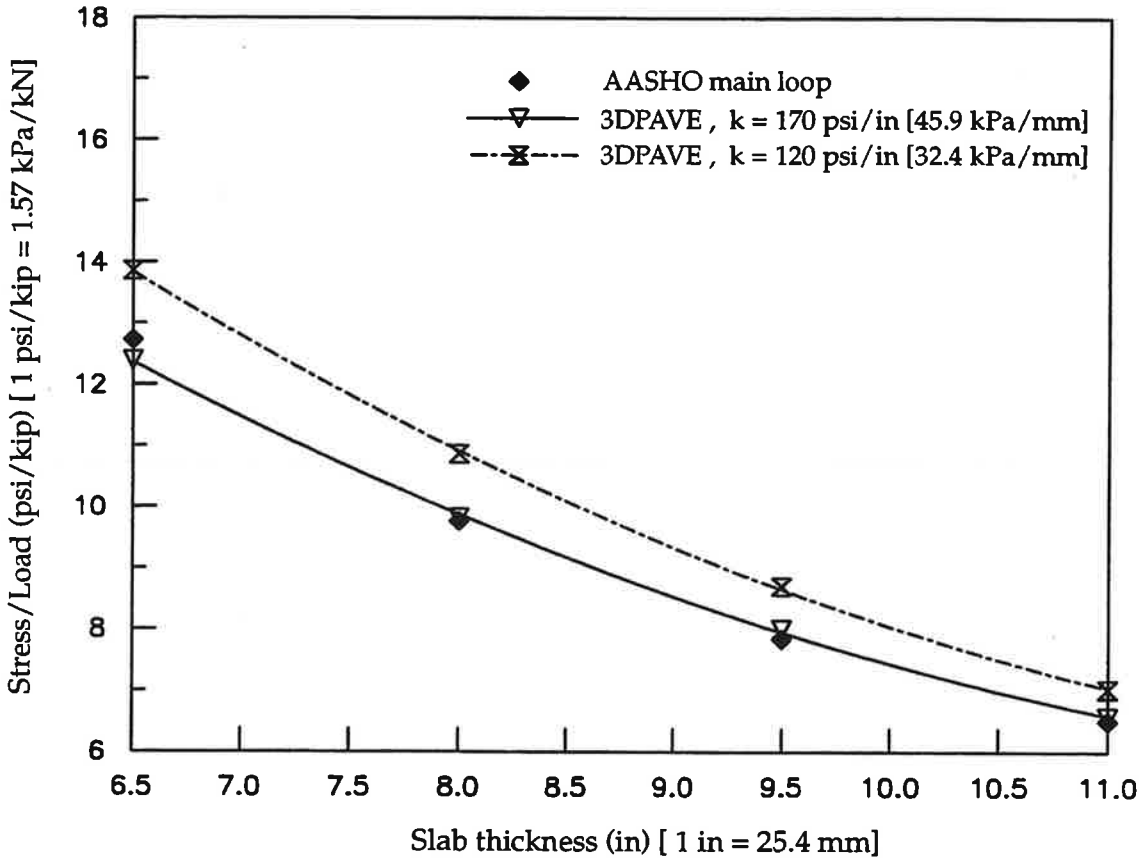

Figure D-27. Moving truck edge stress comparisons for AASHO Road Test.

Table D-10. Stress comparison between AASHO Road Test and 3DPAVE.

Single–Axle

Axle Load (kips)	Thickness (inch)	Measured (psi)	Equation* (psi)	3DPAVE (psi)
12.00	6.50	153.00	152.73	157.10
18.00	6.50	229.00	229.09	230.60
22.40	6.50	285.00	285.09	283.20
22.40	8.00	219.00	218.64	223.70
22.40	9.50		175.50	182.10
30.00	6.50	382.00	381.82	371.70
30.00	8.00	293.00	292.83	294.60
30.00	9.50	235.00	235.09	240.20
30.00	11.0		194.90	197.10

Tandem Axle

Axle Load (kips)	Thickness (inch)	Measured (psi)	Equation** (psi)	3DPAVE (psi)
32.00	6.50	168.00	167.85	165.10
32.00	8.00	141.00	140.63	139.50
40.00	6.50	210.00	209.82	204.20
40.00	8.00	176.00	175.79	172.80
40.00	9.50	152.00	151.84	145.60
48.00	6.50	252.00	251.78	248.20
48.00	8.00	211.00	210.94	210.20
48.00	9.50	182.00	182.20	177.40
48.00	11.00	161.00	160.80	149.10

1 kip = 4.45 kN, 1 inch = 25.4 mm, 1 psi = 6.89 kPa

* Edge stresses, single axle loading : $\tilde{\sigma} = \frac{139.2\ P}{10^{0.0031t}\ h^{1.278}}$

** Edge stresses, tandem axle loading : $\tilde{\sigma} = \frac{25.86\ P}{10^{0.0035t}\ h^{0.8523}}$

where $\tilde{\sigma}$ = predicted stress, psi [1 psi = 6.89 kPa]

P = axle load of the test vehicle, kips

t = temperature difference between top and bottom of slab, °F

h = thickness of the concrete slabs, inch

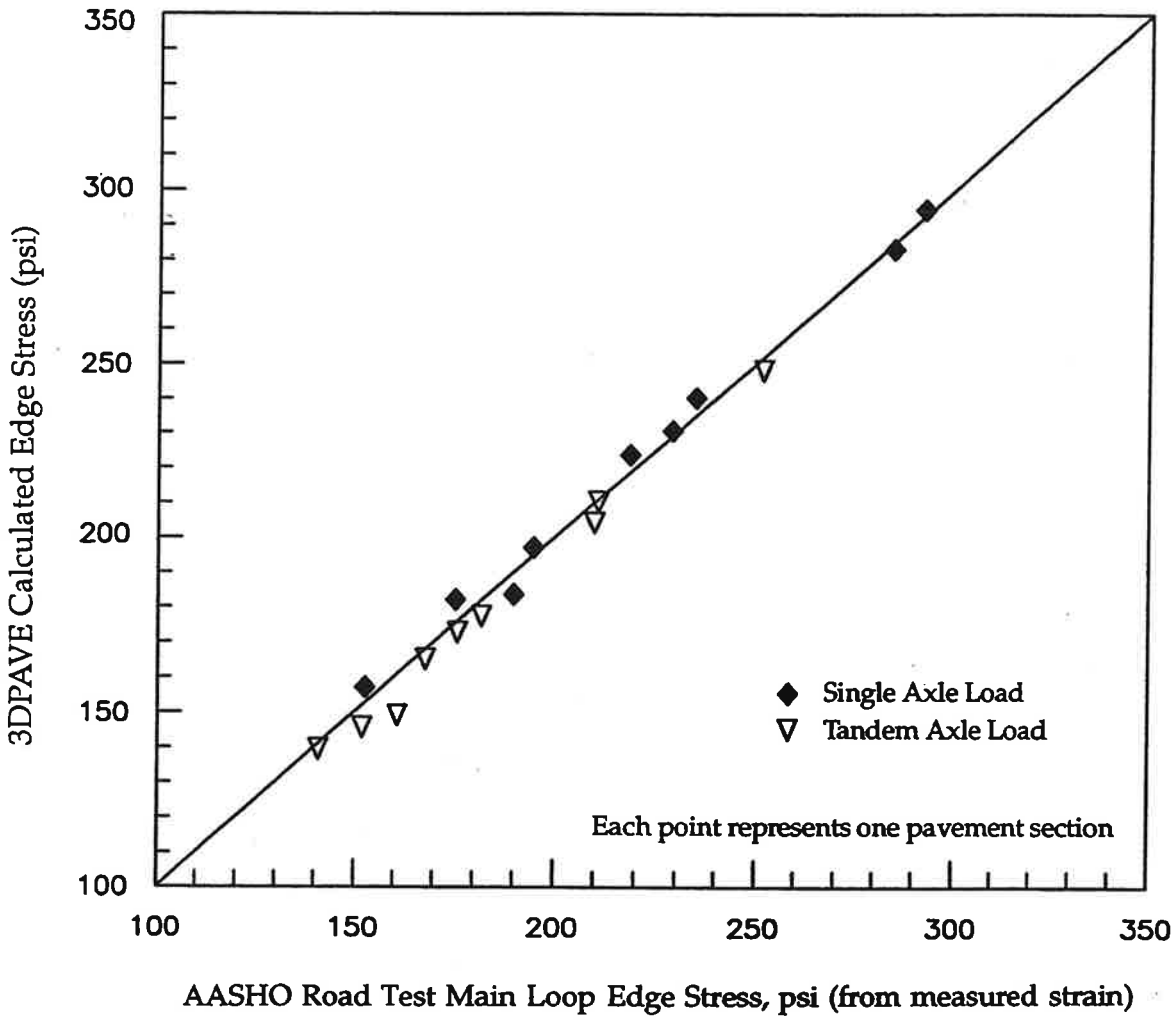

PCC E = 6.25 million psi [43063 MPa]
PCC μ = 0.28
k = 170 psi/in [46 kPa/mm]
Speed = 30 mph [48 km/hr]
Axle load range = 12 to 48 kips [53 to 214 kN]
Slab thickness range = 6.5 to 11 inches [165 to 279 mm]
1 psi = 6.89 kPa
3DPAVE/AASHO stress ratio range is from 0.93 to 1.03
Mean 3DPAVE/AASHO stress ratio is 1.00
R^2 = 0.99
n = 18

Figure D-28. 3DPAVE stress versus AASHO Road Test stress from measured strain.

[97 km/hr]. The Road Test investigators developed empirical equations relating deflections and strain to vehicle speed. [17] These relationships make it possible to estimate the variation of k value with speed. According to Reference 17, the reduction factor for deflection and strain measured on the main loops for any speed between 2 and 60 mph [3.2 and 97 km/hr] may be obtained from the following equation or from Figure D-29:

$$R = 100 \left(1 - 1.012 * 10^{-0.0026 v} \right) \qquad \text{(D-1)}$$

where R = reduction factor from 2 mph [3.22 km/hr]

v = speed, mph [1 mph = 1.61 km/hr]

Since the main loop tests were conducted at a speed of 30 mph [48 km/hr], the strains and deflections measured at that speed may be used in the above equation to estimate the deflections and strains at 2 mph [3.2 km/hr]:

$$\sigma_2 = \frac{\sigma_{30}}{1.012 \times 10^{-0.0026 \times 30}} \quad \text{and} \quad \delta_2 = \frac{\delta_{30}}{1.012 \times 10^{-0.0026 \times 30}} \qquad \text{(D-2)}$$

where σ_2, δ_2 = stress and deflection at 2 mph [3.2 km/hr]

σ_{30}, δ_{30} = stress and deflection at 30 mph [48 km/hr]

These results were used to develop a relationship for the AASHO Road Test main loop experiment between k value and speed. 3DPAVE was run to analyze the axle loads on the main loop slabs using a range of k values, and the stresses and deflections obtained from 3DPAVE were used to calculate reduction factors from the creep speed deflections and strains, as shown below:

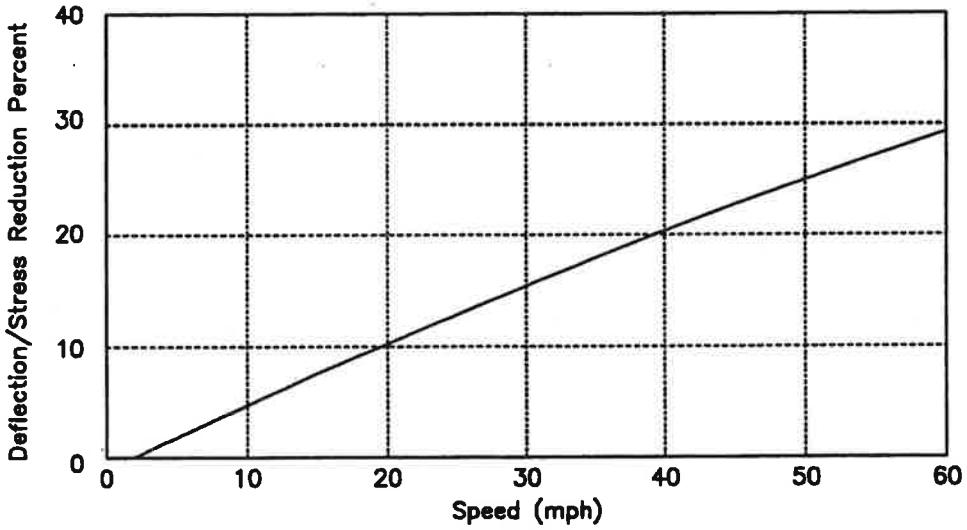

[1 mph = 1.61 km/hr]

Figure D-29. Percent reduction in edge strain with increase in vehicle speed. [17]

$$R = 100 \times \frac{\sigma_2 - \sigma_k}{\sigma_2} \quad \text{or} \quad R = 100 \times \frac{\delta_2 - \delta_k}{\delta_2} \qquad \text{(D-3)}$$

where σ_k, δ_k = stress and deflection computed for input k value

The reduction factors calculated were used to determine the speed corresponding to each input k value. For example, the verification results presented earlier show that a k value 170 psi/in [46 kPa/mm] represents the subgrade modulus of the main loop test under 30-mph loads. It is straightforward to estimate the stress at a vehicle speed of 2 mph by substituting σ_{30} = 182.1 psi [1255 kPa], from Table D-10, into Equation D-2.

$$\sigma_2 = \frac{\sigma_{30}}{1.012 \times 10^{-0.0026 \times 30}} = \frac{182.1}{1.012 \times 10^{-0.0026 \times 30}} = 215.3$$

A 3DPAVE run was made with k = 240 psi/in [65 kPa/mm]. The stress reduction factor was then calculated with Equation D-3 and the calculated stress.

$$R = 100 \times \frac{\sigma_2 - \sigma_k}{\sigma_2} = 100 \times \frac{215.3 - 166.0}{215.3} = 22.9\%$$

The speed, v, corresponding to k = 240 psi/in [65 kPa/mm] can be calculated by equating 22.9 percent to Equation D-1:

$$22.9\% = 100\ (1 - 1.012 \times 10^{-0.0026 \times v})$$
$$v = 45.4 \text{ mph}$$

The results of correlating k values with various speeds is shown in Figure D-30. The estimated k value for creep speed traffic is about 75 psi/in. This value is close to the elastic k value of 86 psi/in obtained by plate load tests on the subgrade.

Crack Initiation Location AASHO Road Test

Crack development locations were recorded at the AASHO Road Test, as shown in Figures D-31 and D-32. Cracks in thin slab sections (3.5 and 5 inches [89 and 127 mm]) were first observed along the direction of the wheel path; then developing toward the midslab edge. In thick slabs (6.5 to 12.5 in), cracks most often developed from the edge at midslab.

To verify crack initiation in thin and thick slabs with the 3-D model, two pavements with slab thicknesses of 4 and 12 inches [102 and 305 mm] were modelled with loads applied at the joint, at various distances up to 60 inches [1524 mm] from the joint, and at midslab, as shown in Figure D-33. Examination of the principal stress contours from 3DPAVE (Figure D-34) confirms that the critical stresses in thin slabs occur at the bottom of the slabs beneath the wheel loads; thus, the regions along the wheel path suffered the most severe fatigue damage and developed longitudinal cracks. Joint loading produced the highest stresses in thin slabs among the load positions analyzed. This explains why the cracks in the thin slabs initiated from the transverse joints.

In contrast to the thin slabs, the critical loading position for the thicker slabs (6.5 inches [165 mm] and greater) is midslab loading. The highest stress is located at the longitudinal edge (see Figure D-35) where the first cracks occurred, resulting in transverse cracks.

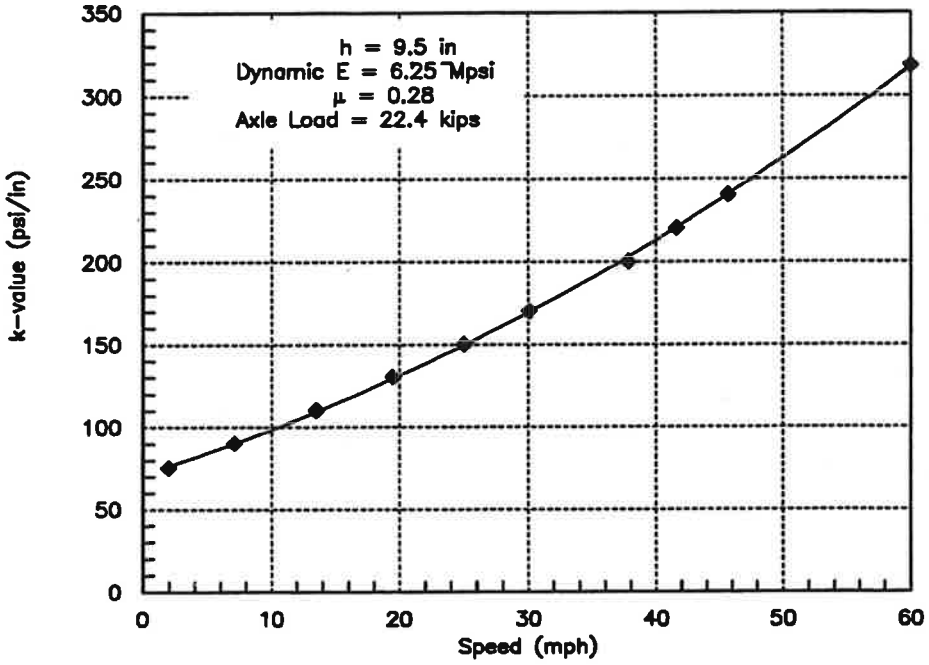

[1 psi/in = 0.27 kPa/mm, 1 mph = 1.61 km/hr, 1 in = 25.4 mm,

1 million psi = 6890 MPa, 1 kip = 4.45 kN]

Figure D-30. Speed versus k value matching stress, AASHO Road Test.

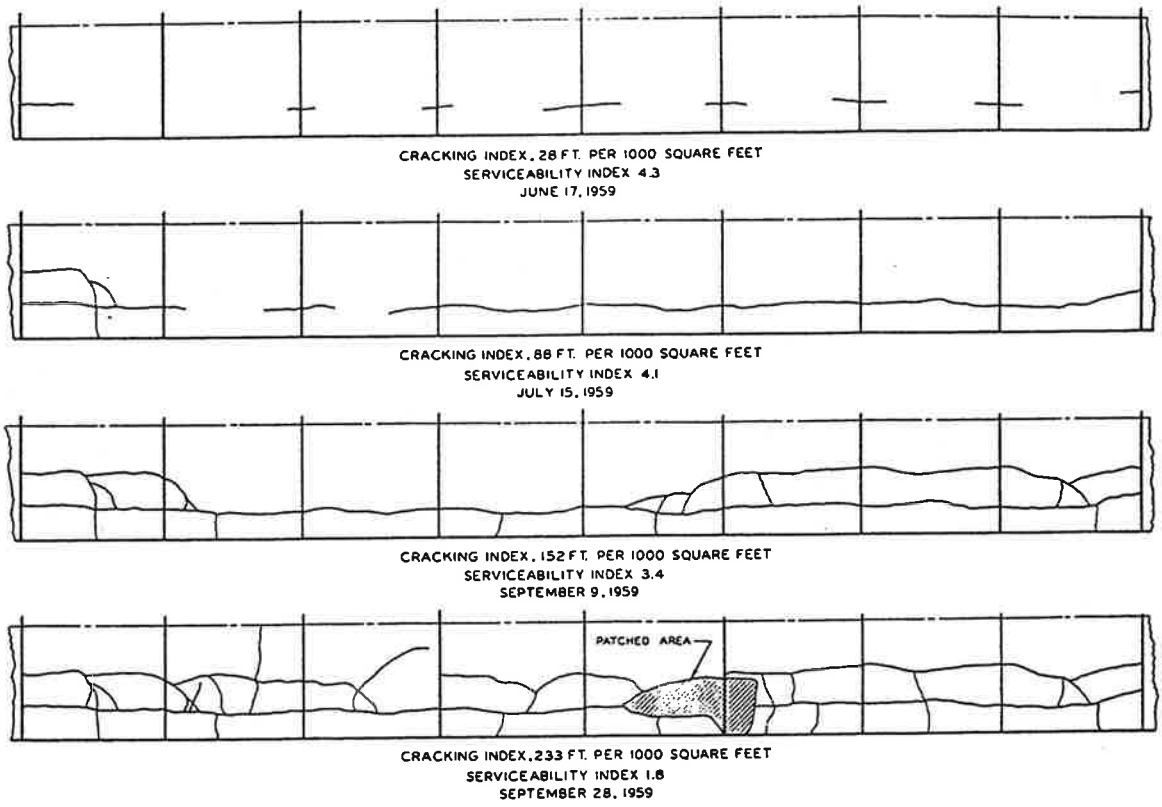

Figure D-31. Crack progression in 3.5-in [89 mm] unreinforced slabs at AASHO Road Test. [17]

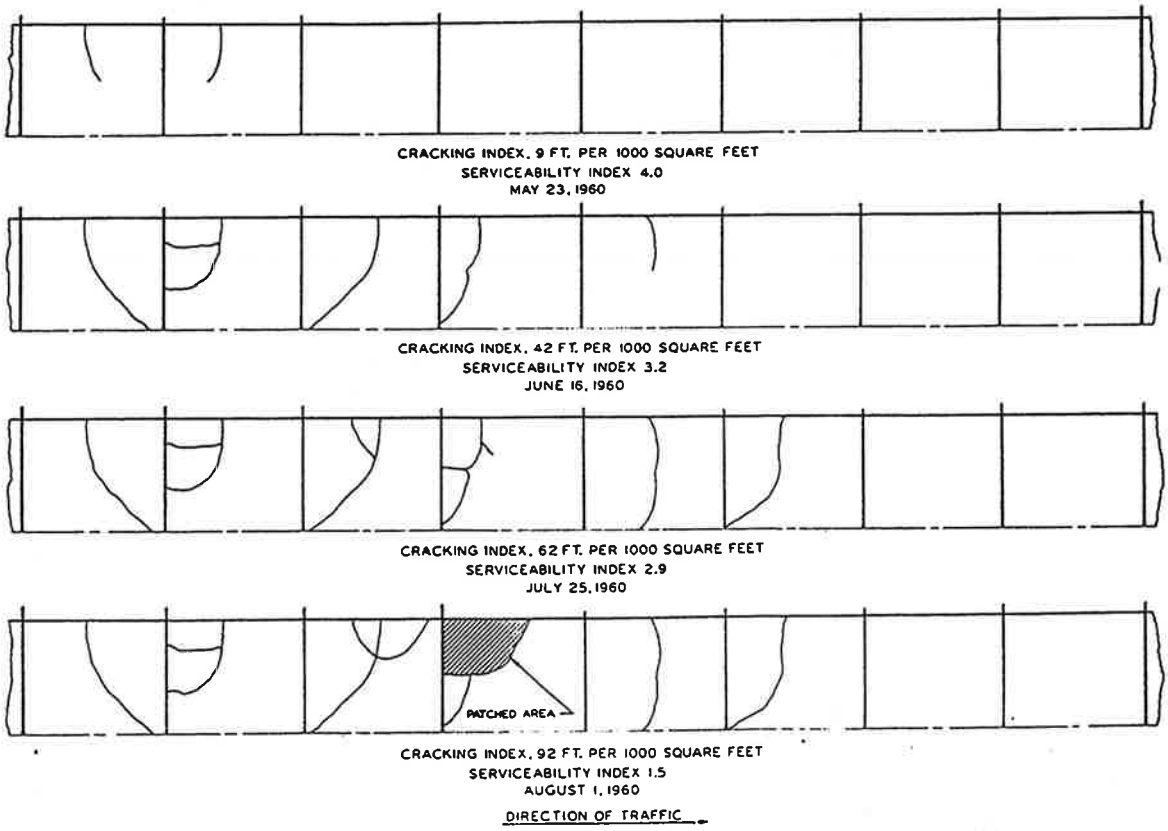

Figure D-32. Crack progression in 8-in [203 mm] unreinforced slabs at AASHO Road Test. [17]

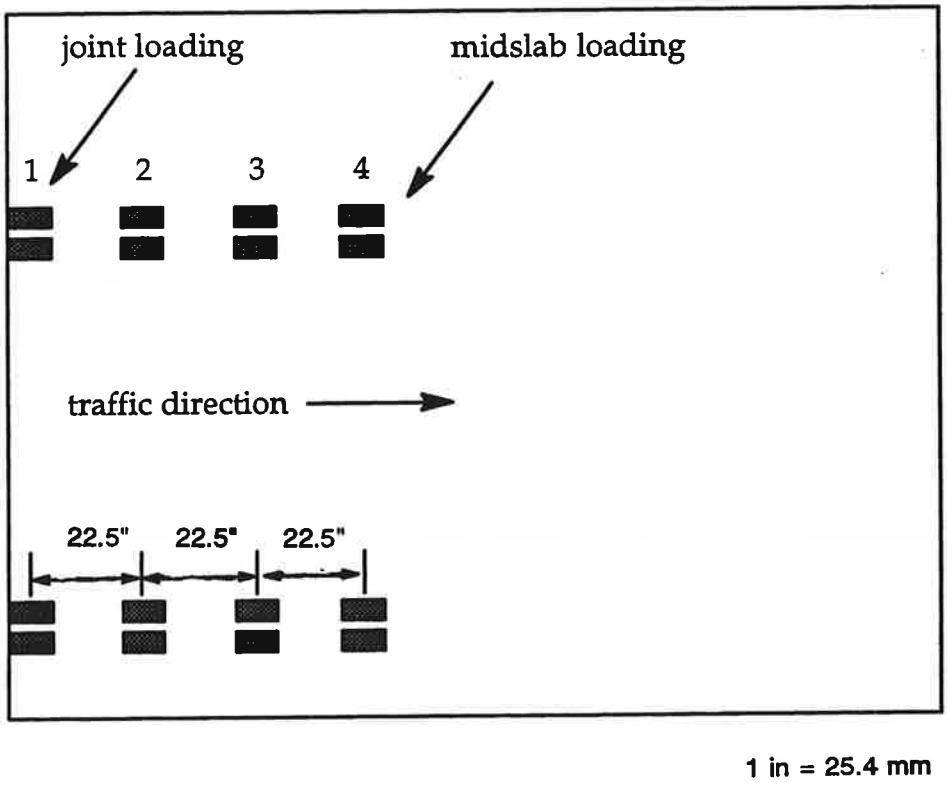

Figure D-33. Load positions simulating traffic loading.

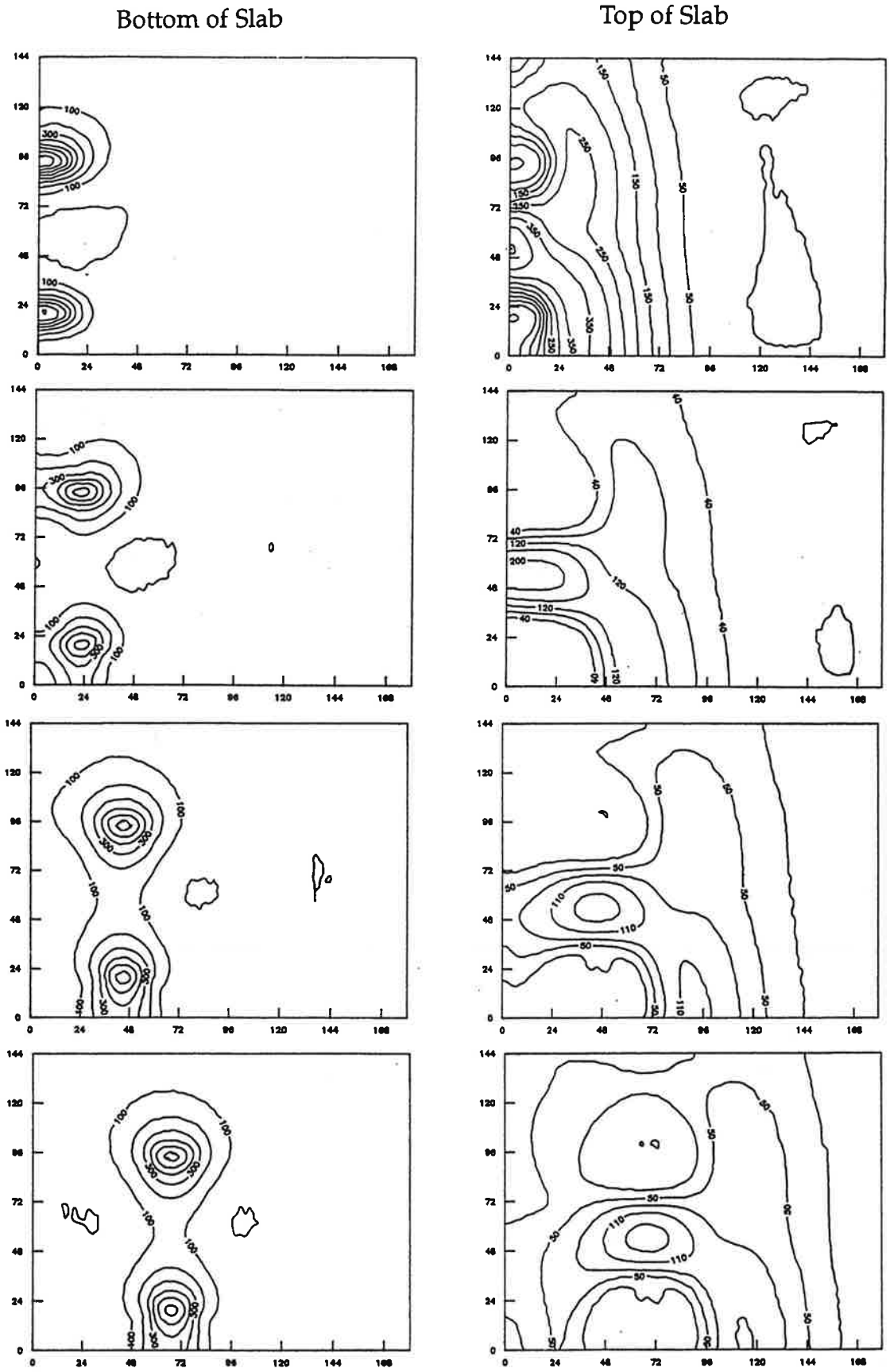

Figure D-34. 3DPAVE stress contours for thin slab for different load positions.

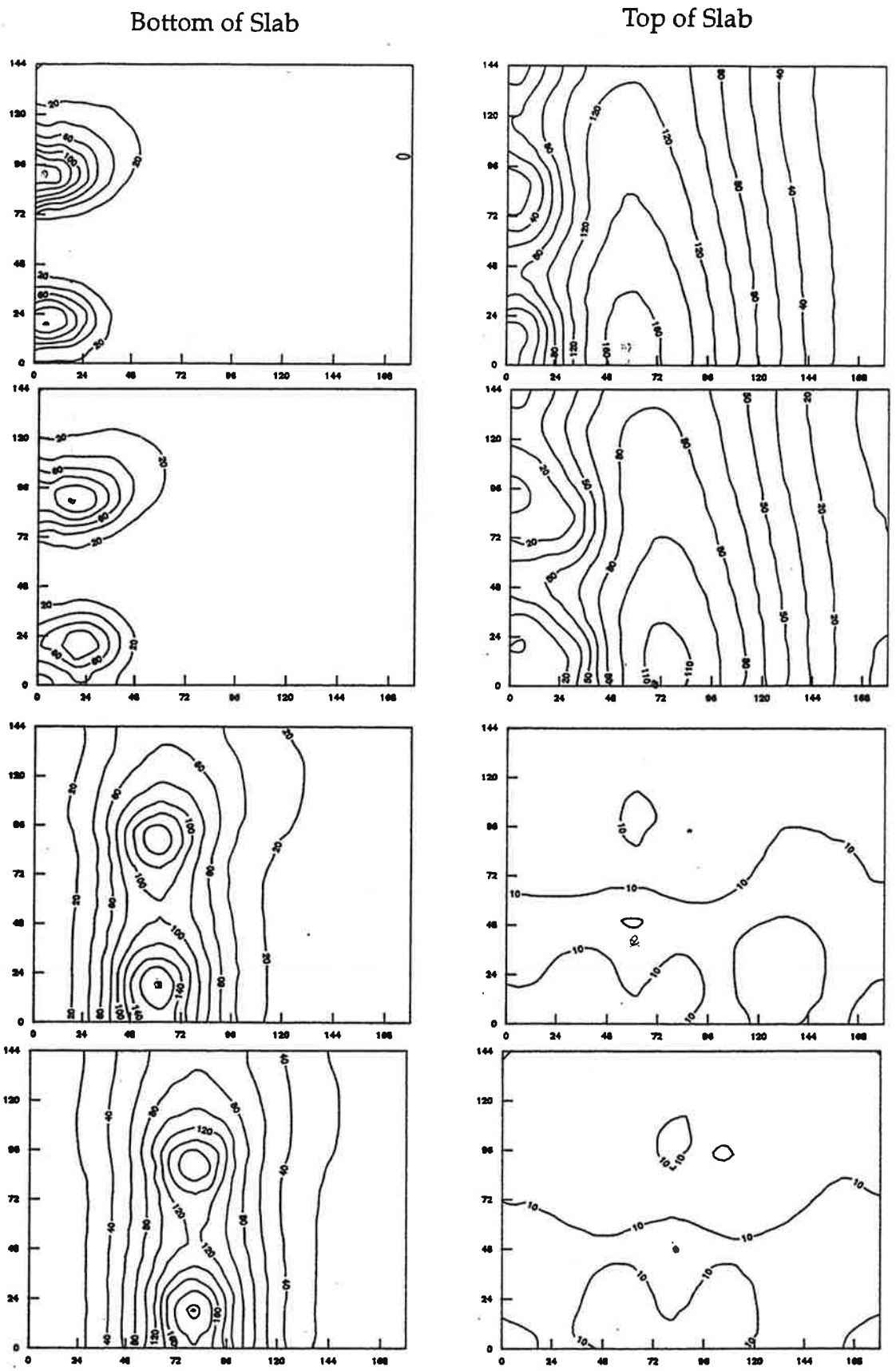

Figure D-35. 3DPAVE stress contours for thick slab for different load positions.

The contours of the principal stresses on the tops and bottoms of slabs not only explain the crack patterns of different slab thicknesses, but also shed some light on whether the cracks initiate from the top or the bottom. In thin slabs, the top stresses are significantly lower than the bottom stresses, so it is likely that the cracks start from the bottom and propagate upward through the slab. In thick slabs, on the other hand, the critical stress at the bottom is only slightly higher than that at the top of the slab. Hence it is possible that the cracks might initiate from either the top or the bottom of the slab. For both thin and thick slabs, however, the critical loading position was along the longitudinal edge midway between the joints.

PCA Tests on Cement-Treated Bases

The Portland Cement Association conducted tests in the 1950s to investigate the responses of pavements with cement-treated base [29]. Many designs were constructed and tested in the laboratory. Among the sections for which data are available, fully bonded sections were selected to be modelled with 3DPAVE because no detailed information was provided in the report for the other sections with various interface treatments.

Comparisons were made for both interior loading and free edge loading conditions. Since edge loading deflections of slabs with bonded bases were only available in "edge with ledge" sections (i.e., the base extended 1 ft [0.3 m] beyond the edge of the slab), a widened base was modelled in 3DPAVE. This feature is impossible to model in a 2-D program because in 2-D analysis, all layers above the foundation must have common horizontal boundaries. A widened base or other difference in horizontal boundaries (e.g., mismatched joints or cracks) is fairly easy to model in 3-D analysis. A widened base is modelled by constructing the two layers with brick elements and then removing a row of brick elements from top layer.

The pavement configuration is shown as Figure D-36. In addition to 3DPAVE, the analysis was also performed with ILLI-SLAB and the Westergaard equations. Figure D-37 shows the deflection comparisons for interior loading. For the 3DPAVE and ILLI-SLAB analyses, the k value used for each section was the value measured by the PCA in plate load tests on the subgrade at that location. For the computation using Westergaard's equation, the k value used was the value measured by the PCA in plate load tests on the cement-treated base at that location. The 3-D model and ILLI-SLAB predict interior deflections very well for the 5-in [127 mm] slab sections on 6-in [152 mm] and 9-in [229 mm] cement-treated base. Some scattered results are observed for 7-in [178 mm] sections (7B6, 7B9). Generally speaking, every analysis method predicted fairly well for interior loading conditions.

For edge loading conditions, the 3-D model results match the measured deflections much better than the other conventional analyses, as shown in Figure D-38. Again, for the 3DPAVE and ILLI-SLAB analyses, the k value used for each section was the value measured by the PCA in plate load tests on the subgrade at that location. For the computation using Westergaard's equation, the k value used was the value measured by the PCA in plate load tests on the cement-treated base at that location. Significant gaps between both the ILLI-SLAB and Westergaard results and the measured test data and 3DPAVE results illustrate the improved capability of the 3-D model. Since Westergaard's solution and ILLI-SLAB are not capable of considering a widened base, they tend to overpredict deflections. With versatile features of geometric modelling, the 3-D model successfully reproduced PCA pavement test results with widened bases.

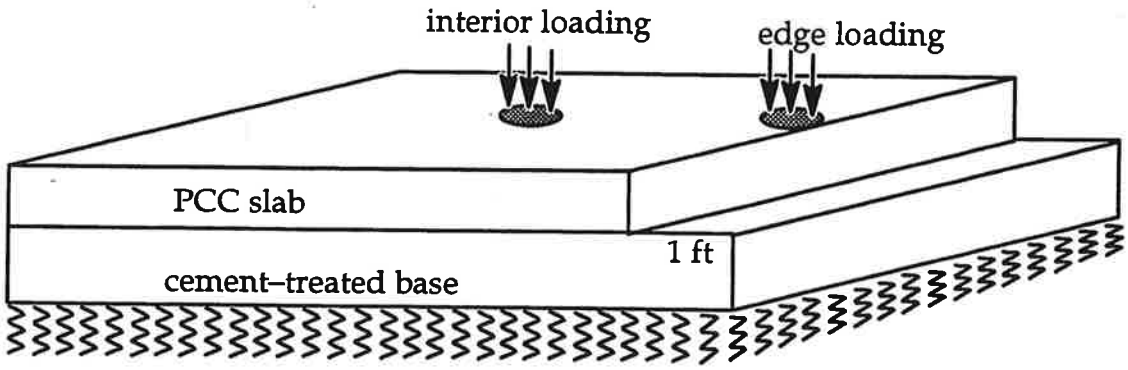

Figure D-36. Configuration of slabs on cement-treated bases in PCA tests.

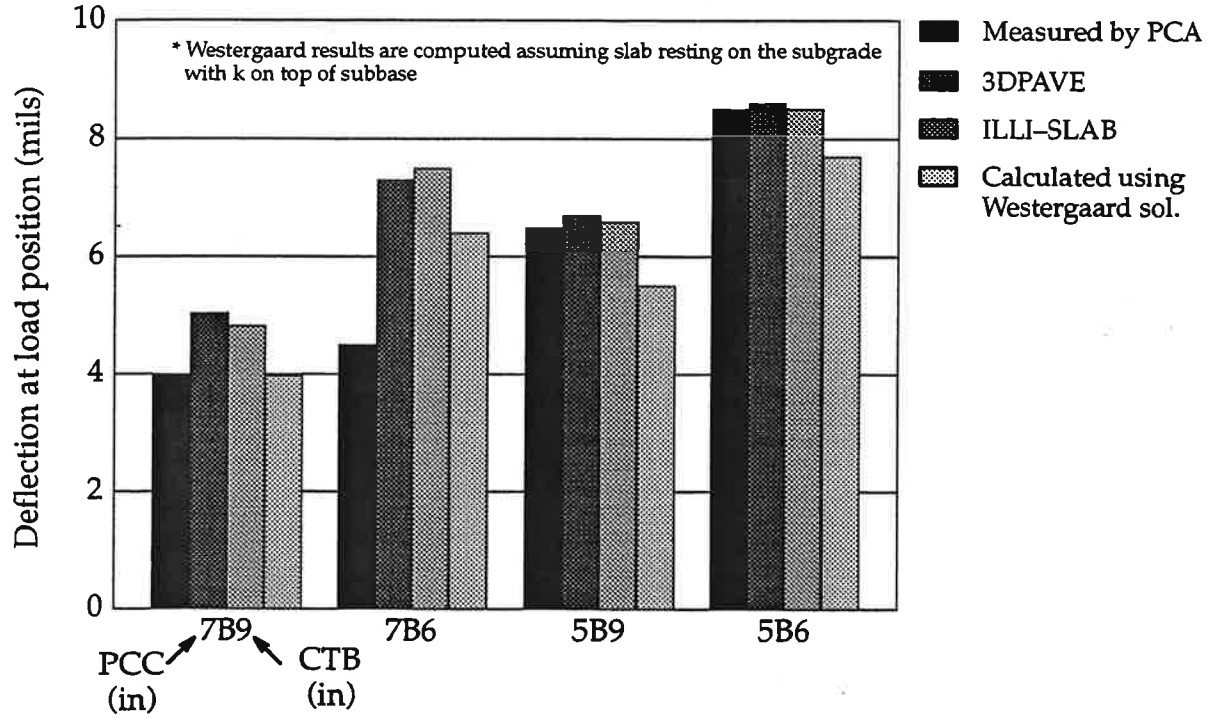

Figure D-37. Comparison of results for interior loading condition.

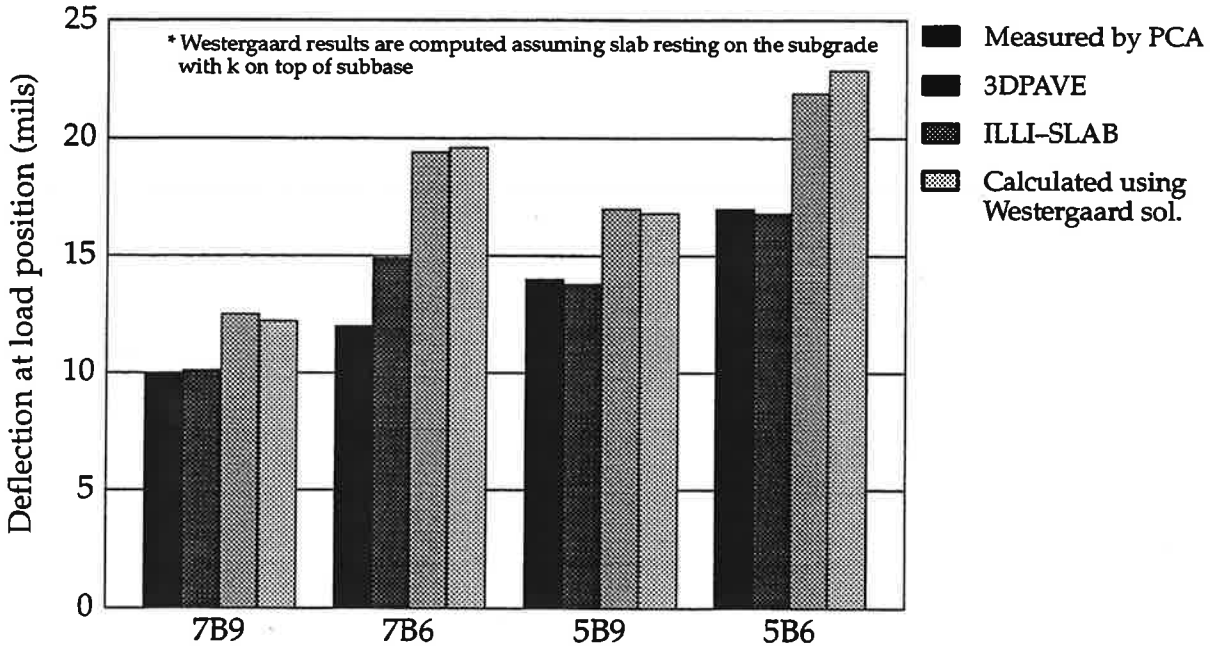

Figure D-38. Comparison of results for edge loading condition.

Arlington Road Test

Data from the Arlington Road Test provide thermal curling stresses computed from measured strains. [49] These field results were compared with 3DPAVE analysis results as well as results obtained using ILLI-SLAB.

The Arlington Road Test slabs were 20 ft [6.1 m] long and 10 ft [3.05 m] wide. Longitudinal edge stresses were computed from measured strains during periods of maximum thermal gradients for several days in 1934. For this comparison, a linear temperature distribution was assumed in the 3-D finite element model and no wheel loading was applied. A summary of data obtained for 6- and 9-in [152 and 229 mm] slabs and the computed finite element edge stress are given in Table D-11 and are plotted in Figure D-39.

As noted in research by Darter and Barenberg [48], the curling stresses computed by the 2-D finite element program are higher than the stresses computed from the measured strains. This is demonstrated in Figure D-39 by the 2-D results all being above the equality line. However, the stresses computed using 3DPAVE not only generally agree with the field stresses, but also are distributed on both sides of the line. These results provide additional evidence that the 3DPAVE model has been properly built to handle temperature curling and demonstrates its predictive capability.

Table D-11. Measured and computed stress due to curling (without applied load) Arlington Road Test.

[1 °F = 0.55°F, 1 psi = 6.89 kPa]

6 in. Slab

Thermal Gradient (°F)	Measured stress (psi)	3–D computed stress (psi)
18	220	243
14	186	187
21	195	280
18	209	243
20	252	268
20	320	268
19	266	255

9 in. Slab

Thermal Gradient (°F)	Measured stress (psi)	3–D computed stress (psi)	2–D computed stress (psi)
25	191	272	276
30	298	306	338
26	306	280	317
33	302	318	368
31	329	311	358
25	213	272	286

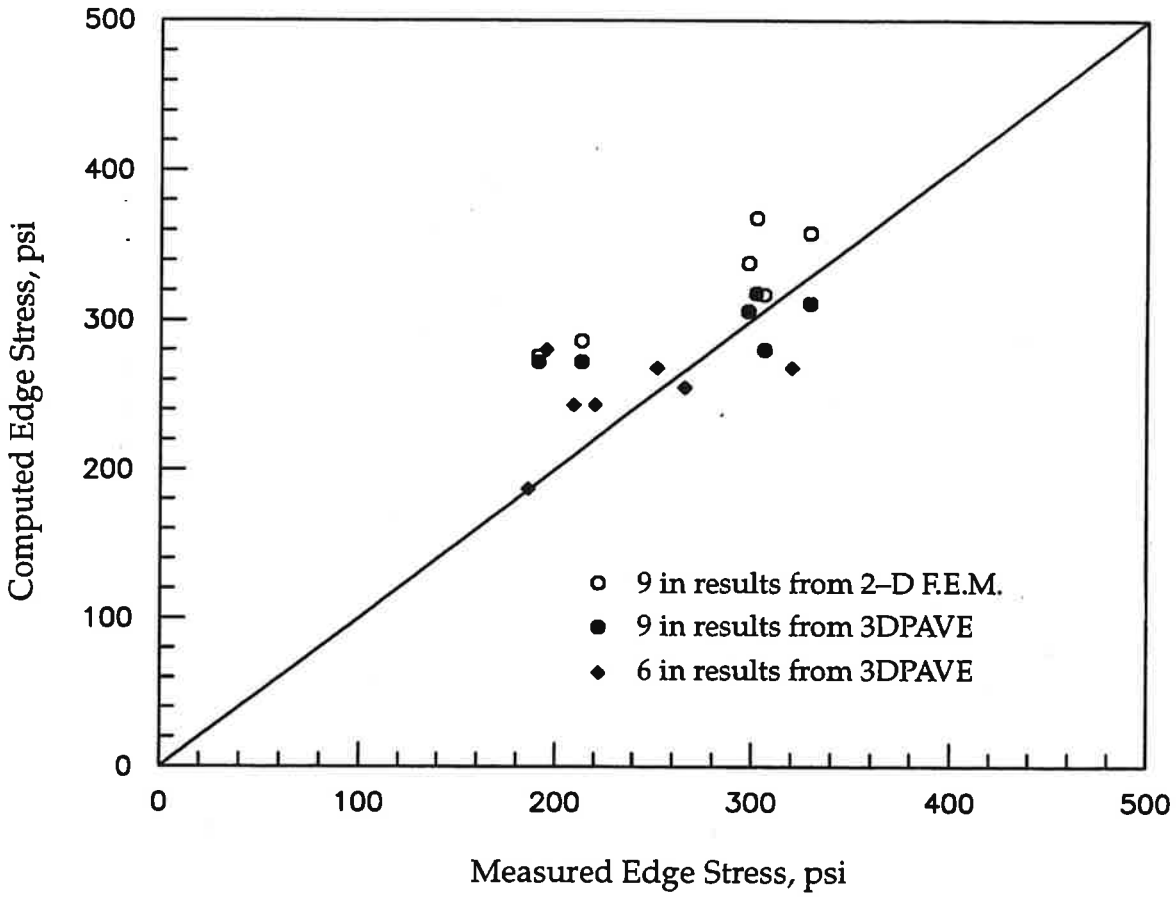

$E = 5 \times 10^6$ psi [34,450 MPa], $\mu = 0.15$,
$k = 200$ psi/in [54 kPa/mm],
$\alpha = 5 \times 10^{-6}$ 1/°F [9×10^{-6} /°C],
$\gamma = 0.083$ lb/in^3 [272 kN/m^3] (PCC slab)

$\frac{\text{computed}}{\text{measured}}$	Max.	Min.	Avg.
2–D F.E.M. (9 in)	1.46	1.04	1.21
3DPAVE (9 in)	1.42	0.92	1.11
3DPAVE (6 in)	1.44	0.83	1.08

Figure D-39. Comparison of measured and computed edge stress due to curling, Arlington Road Test.

REFERENCES FOR APPENDIX D

1. Selvadurai, A.P.S., Elastic Analysis of Soil-Foundation Interaction, Elsevier Scientific Publishing Company, 1979.

2. Zimmermann, H., Calculation of the Upper Surface Construction of Railway Tracks, Ernst and Korn Verlag, Berlin, 1888 (in German).

3. Hertz, H., "On the Equilibrium of Floating Elastic Plates," Weidemann's Annalen der Physik und Chemie, Vol. 22, 1884 (in German).

4. Schleicher, F., Kreisplatten auf Elastischer Unterlage, Julius Springer, Berlin, 1926 (in German).

5. Hetényi, M., Beams on Elastic Foundations, University of Michigan Press, Ann Arbor, Michigan, 1946.

6. Westergaard, H. M., "Stresses in Concrete Pavements Computed by Theoretical Analysis," Public Roads, Vol. 7, No. 2, April 1926.

7. Vesic, A. S., "Slabs on Elastic Subgrade and Winkler's Hypothesis," Proceedings of Eighth International Conference on Soil Mechanics and Foundation Engineering, Moscow, 1973.

8. Hogg, A. H. A., "Equilibrium of a Thin Plate, Symmetrically Loaded, Resting on an Elastic Foundation of Infinite Depth," Philosophical Magazine and Journal of Science, Vol. 25, 1938.

9. Holl, D. L., "Thin Plates on Elastic Foundation," Proceedings of Fifth International Congress on Applied Mechanics, Cambridge, Massachusetts, 1938.

10. Losberg, A., Structurally Reinforced Concrete Pavements, Doktorsavhandlingar Vid Chalmers Tekniska Högskola, Göteborg, Sweden, 1960.

11. Hayashi, K., "Theory of Beams on Elastic Foundation," Journal of Spinger, Berlin, 1921.

12. Terzaghi, K., "Evaluation of Coefficients of Subgrade Reaction," Geotechnique, Vol. 5, No. 4, December, 1955.

13. Engesser, F., "The Theory of Site Foundations," Zantralblatt der Bauverwaltung, 1893.

14. Bergström, Sven G., Ernst Fromén and Sven Linderholm, "Investigation of Wheel Load Stresses in Concrete Pavements," Proceedings, No. 13, Swedish Cement and Concrete Research Institute at the Royal Institute of Technology, Stockholm, 1949.

15. Timoshenko, S. and J. N. Goodier, Theory of Elasticity, McGraw-Hill, 1951.

16. Ioannides, A. M., "Analysis of Slabs-On-Grade for a Variety of Loading and Support Conditions," Ph.D. thesis, University of Illinois at Urbana-Champaign, 1984.

17. Highway Research Board, "The AASHO Road Test, Report 5, Pavement Research," Special Report 61E, 1962.

18. Siddharthan, R., G. M. Norris, and J. A. Epps, "Use of FWD Data for Pavement Material Characterization and Performance," Journal of Transportation Engineering, ASCE, Vol. 117, No. 6, Nov/Dec., 1991.

19. McCavitt, N., M. R. Yates, and M. C. Forde, "Dynamic Stiffness Analysis of Concrete Pavement Slabs, "Journal of Transportation Engineering, ASCE, Vol. 110, No. 4, 1984.

20. Mamlouk, M. S. and T. G. Davies, "Elasto-Dynamic Analysis of Pavement Deflections," Journal of Transportation Engineering, ASCE, Vol. 110, No. 6, 1984.

21. Shebaaly, B., T. G. Davis, and M. S. Mamlouk, "Dynamic Analysis of Falling Weight Deflectometer," Journal of Transportation Engineering, ASCE, Vol. 111, No. 6, 1985.

22. Richart, F. E., R. D. Woods and J. R. Hall, Jr., Vibrations of Soils and Foundations, Prentice-Hall, Inc., New Jersey, 1970.

23. Lambe, T. W. and R. V. Whitman, Soil Mechanics, John Wiley & Sons, Inc., 1969.

24. Jerath, S. and M. M. Shibani, "Dynamic Modulus for Reinforced Concrete Beams," Journal of Structure Engineering, Vol. 110, No. 6, 1984.

25. Casagrande, A. and W. L. Shannon, "Stress Deformation and Strength Characteristics of Soils under Dynamic Loads," Proceedings of Second International Conference on Soil Mechanics and Foundation Engineering, Vol. V, 1948.

26. Seed, H. B. and R. Lungren, "Investigation of the Effect of Transient Loading on the Strength and Deformation Characteristics of Saturated Sands," Proceedings, ASTM, Vol. 54, 1954.

27. Vlasov, V. Z. and N. N. Leont'ev, Beams, Plates and Shell on Elastic Foundations, Israel Program for Scientific Translations, Jerusalem, 1966.

28. Scott, R. F., Foundation Analysis, Prentice-Hall, Inc., 1981.

29. Childs, L. D., "Tests of Concrete Pavement Slabs on Cement-Treated Subbases," Highway Research Record, No. 60, Highway Research Board, Washington, D.C. 1964.

30. Huang, Y. H., Pavement Analysis and Design, Prentice Hall, 1993.

31. Tabatabaie-Raissi, A. M., "Structural Analysis of Concrete Pavement Joints," Ph.D. Thesis, University of Illinois at Urbana-Champaign, 1977.

32. Ioannides, A. M., Khazanovich L. and J. L. Becque, "Structural Evaluation of Base Layers in Concrete Pavement Systems," Transportation Research Record 1370, Transportation Research Board, 1992.

33. Terzaghi, K., "Evaluations of Coefficients of Subgrade Reaction," Geotechnique, Vol. 5, 1955.

34. Cheung, Y. K. and O. C. Zienkiewicz, "Plate and Tanks on Elastic Foundations - An Application of Finite Element Method," International Journal of Solids and Structures, Vol. 1, 1965.

35. A. C. Ugural, Stresses in Plates and Shells, McGraw-Hill Book Company, 1981.

36. Tabatabaie, A. M., E. J. Barenberg, and R. E. Smith, "Longitudinal Joint Systems in Slip-Formed Rigid Pavements, Volume II - Analysis of Load Transfer Systems for Concrete Pavements," U.S. Department of Transportation, Report No. FAA-RD-79-4, II, 1979.

37. Ioannides, A. M. and J. P. Donnelly, "Three-Dimensional Analysis of Slab on Stress-Dependent Foundation," Transportation Research Record 1196, Transportation Research Board, 1988.

38. Zaghloul, S. M and T. D. White, "Use of a Three-Dimensional, Dynamic, Nonlinear Analysis to Develop Load Equivalency Factors for Composite Pavements," presented at Transportation Research 73rd Annual Meeting, Washington, D.C., 1994.

39. Mallela, J. and K. P. George, "Three-Dimensional Response Model for Rigid Pavements," presented at Transportation Research 73rd Annual Meeting, Washington, D.C., 1994.

40. ABAQUS Users Manual, Version 5.2, Hibbitt, Karlsson and Sorensen, Inc., 1993.

41. Cook, R.D., D.S. Malkus and M.E. Plesha, Concepts and Applications of Finite Element Analysis, Third Edition, McGraw-Hill.

42. Zienkiewicz, O. C., The Finite Element Method in Engineering Science, McGraw-Hill, 1971.

43. Timoshenko, S., and S. Woinowsky-Krieger, Theory of Plates and Shells, Second Edition, McGraw-Hill, 1959.

44. Ioannides, A. M. and G. T. Korovesis, "Aggregate Interlock: A Pure-Shear Load Transfer Mechanism," Transportation Research Record 1286, 1990.

45. Kuo, C. M., "Three-Dimensional Finite Element Model for Analysis of Concrete Pavement Support," Ph.D. thesis, University of Illinois at Urbana-Champaign, 1994.

46. "The AASHO Road Test, Report 3, Traffic Operations and Pavement Maintenance," Special Report 61C, Highway Research Board, Appendix A, 1962.

47. Langsner, G., Talbot S. H., and Wallace J. L., "Use of Road Test Findings by AASHO Design Committee," The AASHO Road Test, Proceedings of a Conference Held May 16-18, 1962, St. Louis, Mo., Highway Research Board, Special Report 73.

48. Darter, M. I. and E. J. Barenberg, "Design of Zero-Maintenance Plain Jointed Concrete Pavement," Volume 1, Report No. FHWA-RD-77-111, 1977.

49. Teller, L. W. and E. C. Sutherland, "The Structural Design of Concrete Pavements, Part 2 -- Observed Effects of Variations in Temperature and Moisture on the Size, Shape, and Stress Resistance of Concrete Pavement Slabs," Public Roads, Vol. 16, No. 9, 1935.

APPENDIX E

IMPROVED CONSIDERATION OF SUPPORT IN AASHTO METHODOLOGY

A comprehensive evaluation of the AASHO Road Test and the subsequent development of the concrete pavement design models revealed several major deficiencies related to pavement support. A major effort was required to incorporate improved consideration of concrete pavement support into the AASHTO Design Guide. The concept of "support" is far broader than simply determining a more appropriate k value. Support for a concrete pavement includes at least the following:

- **Stiffness** of underlying layers (resistance to deflection under load),
- **Uniformity** of support along the pavement (localized settlements and heaves) and seasonal variation of support,
- **Base course effect** including friction, stiffness and thickness,
- **Drainability** of the pavement structure and subgrade,
- **Erosion** of the base or subgrade (causing loss of support over time at edges and corners and also joint faulting), and
- **Temperature curling and moisture warping** of the concrete slab (at construction, daily and seasonally).

Appendix E describes an improved methodology for considering support in concrete pavement design using the AASHTO design procedure. Incorporating improved support concepts in the AASHTO design procedure required a detailed examination of the original development of the concrete pavement design equation and its subsequent modifications.

EXISTING AASHTO DESIGN MODEL FOR CONCRETE PAVEMENTS

The existing AASHTO concrete pavement design procedure has evolved from the results of the AASHO Road Test plus various extensions and additions over the past 30 years. Some serious deficiencies were identified with regard to the way that pavement support is considered.

AASHO Road Test Concrete Pavements

The specific design details of the concrete pavements tested at the Road Test are very important because the resulting performance models reflect these conditions. [2]

Slab type and thickness: Two types of concrete pavements were constructed: jointed plain concrete pavements (JPCP) and jointed reinforced concrete pavements (JRCP). Thicknesses ranged from 2.5 to 12.5 in [63.5 to 317.5 mm].

Joint spacing: 15 ft [4.6 m] for JPCP and 40 ft [12.2 m] for JRCP.

Concrete flexural strength: 690 psi [4.75 MPa], third-point loading, 28 days (790 psi [5.44 MPa] at one year).

Concrete modulus of elasticity: 4,200,000 psi [28940 MPa], static, 28 days (5,250,000 psi [36200 MPa] static and 6,250,000 psi [43100 MPa] dynamic at one year).

Concrete thermal coefficient of expansion: 4.6 to 5.6 x $10^{-6}/^{o}F$ [8.2 to 10.1 x $10^{-6}/^{o}C$].

Concrete moisture shrinkage: Length of lab specimens decreased with moisture loss at a rate as high as 355 x 10^{-6} in/in per 1 percent decrease in moisture content. A decrease in length of 229 * 10^{-6} in/in associated with a decrease of 50 percent in the relative humidity of the air surrounding the specimens.

Joint load transfer design: All transverse joints were dowelled with diameters of approximately one eighth the slab thickness. Dowels were spaced at 12 in [305 mm].

Shoulders: Untreated dense-graded aggregate plus a paved shoulder experiment (which showed no effect on performance).

Reinforcement for JRCP: Welded wire fabric placed 2 in [51 mm] from surface.

Dense-graded untreated granular base material: Sand and gravel with very low permeability (7×10^{-6} to 4×10^{-3} ft/min [2.1×10^{-6} to 1.2×10^{-3} m/min]). A few sections were constructed directly on subgrade soil, but the performance model was based on the performance of the sections with granular base.

Subgrade soil: Silty-clay (A-6), CBR of approximately 3 percent, resilient modulus of 3,000 psi [20.7 MPa] at 1 to 2 percent wet of optimum moisture content and deviator stress of 6 psi [41 kPa]. The elastic k value in spring averaged approximately 86 psi/in [23 kPa/mm] on the soil embankment, and varied from 63 to 105 psi/in [17 to 28 kPa/mm] within the main loops.

Subdrainage: "Free water collected under the slab during rains and did not drain laterally through the subbase material in the shoulder to the side ditches at a rate sufficient to prevent pumping." [2]

Traffic loads: Single axles from 2,000 to 30,000 lbf [8.9 to 133.5 kN] and tandem axles from 24,000 to 48,000 lbf [107 to 214 kN].

AASHO Road Test Concrete Pavement Performance

Traffic loadings were applied over the two-year test period. Visible distress and roughness were recorded over this time period.

Extensive pumping and erosion of the sand-gravel base occurred causing loss of support beneath the corners and edges of the slab. The amount of material pumped onto the shoulder was so measured in a cubic foot container. A "pumping index" (PI) was computed in cubic inches per inch along the pavement. The PI ranged from 0 to over 200 depending on slab thickness and axle loading.

> "By removing the concrete from a few failed sections and sampling the underlying material, it was observed that subbase material had apparently been removed by erosive action of water moving across the top of the subbase, and that the remaining subbase material was relatively undisturbed ... Inasmuch as the great majority of the sections which failed pumped severely prior to failure, many of these sections would have survived the two years of traffic had the subbase material been stabilized effectively to resist erosion by water." [2]

Slab cracking occurred on the thinner sections within each loop. Thinner slabs (i.e., 2.5 to 5 in [63.5 to 127 mm]) developed mostly longitudinal cracks in the wheel paths. Thicker slabs developed transverse cracks that initiated mostly in the middle one third of the 15 ft [4.6 m] slabs. Almost none of the 11 and 12.5 in [279 and 317.5 mm] JPCP slabs cracked during the two-year, nor under an additional 14 years of I-80 traffic.

No faulting of the dowelled transverse joints occurred during the two-year period. Some occurred later in the 8-in [203 mm] slabs (which had 1-in-diameter [25 mm] dowels) and 9.5 in [241 mm] slabs under I-80 traffic.

No joint spalling occurred during the two-year period. Some occurred later on I-80 due to "D" cracking.

Original Empirical Concrete Pavement Performance Model

At the end of the two-year traffic period, the performance data were analyzed and various prediction models were developed. Two key prediction models were as follows:

- **EMPIRICAL MAIN LOOP MODEL:** An empirical model for log W (number of axle load applications in lane) as a function of slab thickness, loss of serviceability, axle type and axle weight, based on data from the main trafficked loops. [2]

$$\log W = \log R + \frac{G}{F} \tag{E-1}$$

where W = axle load applications

$$\log R = 5.85 + 7.35 \log (D + 1) - 4.62 \log (L1 + L2) + 3.28 \log L2 \tag{E-2}$$

$$F = 1.00 + \frac{3.63\ (L1 + L2)^{5.2}}{(D + 1)^{8.46}\ L2^{3.52}} \tag{E-3}$$

$$G = \log \left(\frac{P1 - P2}{P1 - 1.5} \right) \tag{E-4}$$

D = concrete slab thickness, in

L1 = load on a single or tandem axle, kips

L2 = axle code, 1 for single axle, 2 for tandem axle

P1 = initial serviceability index

P2 = terminal serviceability index

This empirical performance model depends completely and totally on the design, climate, subgrade, age, and traffic conditions at the Road Test site.

- **MECHANISTIC-EMPIRICAL MODEL:** A mechanistic-empirical model for log W as a function of the ratio of concrete flexural strength to tensile stress in the slab. This model was used to "extend" or incorporate theory into the empirical model (Equation E-1) so that other design features such as concrete modulus of elasticity, concrete strength, and subgrade k value could be included. [2]

Extension of Original Model for Use in Design in 1961

Equation E-1 is useful only in designing pavements located in the area of the Road Test, and JPCP and JRCP having the same design features as the Road Test pavements, such as concrete strength, joint load transfer, joint spacing, granular shoulders, untreated dense-graded base, and welded wire reinforcement. Also, it is only applicable for that climate, and similar traffic characteristics (including tire pressure and lateral spacing in the lane). Thus, the question became one of how could be extended to be used for other sites with different joint designs, materials, subgrades, climates, and traffic loadings.

An innovative extension of Equation E-1 was accomplished by the AASHO Road Test staff as described by Langsner, Huff and Liddle. [1] A mechanistic-empirical relationship between log W and the logarithm of the ratio of concrete strength to slab stress was developed. A plot of log W versus log S'_c/σ revealed a linear relationship that was modelled as follows:

$$\log W' = A + B \log \frac{S'_c}{\sigma} \qquad \text{(E-5)}$$

where W′ = number of axle loads to terminal serviceability index P2

(Note that W′ was computed from Equation E-1 for the regression)

A = a regression constant

B = slope of log W versus log S'_c/σ curve

S'_c = mean 28-day flexural strength, third-point load (690 psi [4.75 MPa])

σ = slab stress computed from Spangler's equation for free corners:

$$\sigma = \frac{J\,P}{D^2}\left[1 - \left(\frac{a_1}{\ell}\right)\right] \qquad \text{(E-6)}$$

J = load transfer coefficient (set equal to 3.2 for AASHO dowelled joints)

P = wheel load, lbf

a_1 = distance from corner of slab to center of load, in

= a $\sqrt{2}$ (a_1 set equal to 10 in [254 mm] for Road Test conditions)

a = radius of a circle equivalent to the tire contact area, in

$$\ell = \sqrt[4]{\frac{Z\,D^3}{12\,(1 - \mu^2)}} \qquad \text{(E-7)}$$

$$Z = \frac{E_c}{k} \qquad \text{(E-8)}$$

E_c = Modulus of elasticity of concrete, psi

k = modulus of subgrade reaction, psi/in

μ = Poisson's ratio for concrete (0.20 measured for Road Test concrete)

The original plot for log W′ versus log S'_c/σ is shown in Figure E-1. Three lines are shown for terminal serviceability indices (P2) of 1.5, 2.0, and 2.5. Spangler's

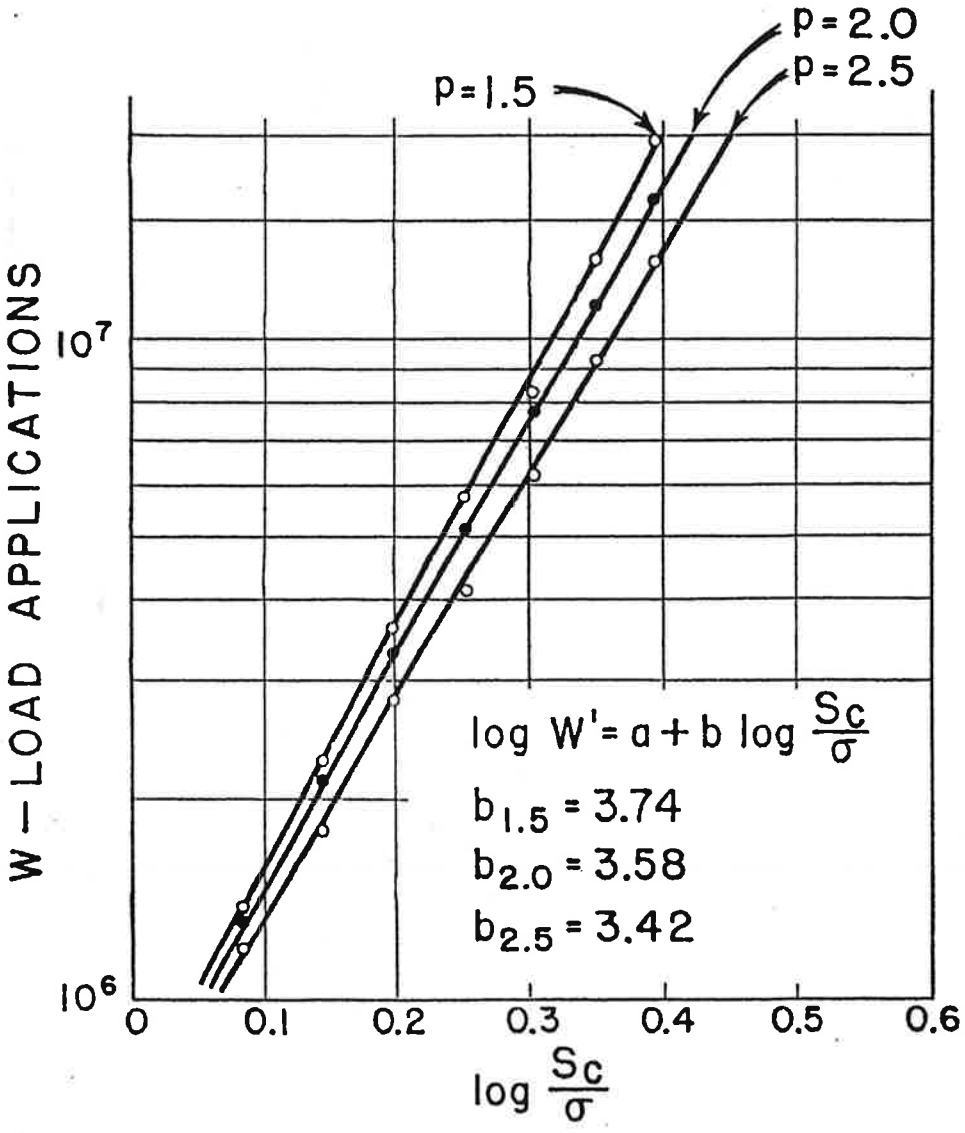

Figure E-1. Original 1961 plot of "extension" to the rigid pavement design equation. [1]

equation was used even though it was derived for a free, undowelled corner. All transverse joints were dowelled at the Road Test. Stresses computed from Spangler's free corner equation were about three times the magnitude of those measured for the protected corner position at the Road Test.

Slab strain measurements were conducted both on the main loops and on Loop 1 which helped to identify the load location that caused the highest stress. The results showed that the maximum slab stress was parallel to and near the longitudinal slab edge as the axle load traversed the length of a slab in the wheel path. Slab stresses (computed from measured strains) were lowest when the axle load was right at the transverse joint. Further discussion on this topic is given later in this Appendix and in Appendix D. Spangler's free corner equation was used apparently because of its simplicity and because it correlated well with the actual stress (even though it predicts a much higher stress than the measured stress).

The next step was to derive an equation for B as a function of P2, the terminal serviceability:

$$B = 4.22 - 0.32\ P2 \tag{E-9}$$

Thus, Equation E-5 can be written:

$$\log W' = A + (4.22 - 0.32\ P2) \log \frac{S'_c}{\sigma} \tag{E-10}$$

Equations E-1 and E-9 were then combined into the "extended" AASHTO design equation for concrete pavements by differentiating Equation E-9:

$$\partial \log W' = B\ \partial \left(\log \frac{S'_c}{\sigma} \right) \tag{E-11}$$

The difference in load applications between a pavement with AASHO Road Test design features described by S'_c/σ and one with different design features described by $(S'_c)'/\sigma'$ is then given by the following equation:

$$\log W' - \log W = B\left[\frac{(S'_c)'}{\sigma'} - \frac{S'_c}{\sigma}\right] \qquad \text{(E-12)}$$

or

$$\log W' - \log W = (4.22 - 0.32\ P2)\left[\frac{(S'_c)'}{\sigma'} - \frac{S'_c}{\sigma}\right] \qquad \text{(E-13)}$$

W' = number of axle load applications required to reach a given terminal serviceability P2 for a pavement similar to the Road Test pavement but with different physical properties as described by $(S'_c)'/\sigma'$

W = number of load applications required to reach a given terminal serviceability P2 for a Road Test pavement described by S'_c/σ (Equation E-1 is used to compute log W)

$(S'_c)'/\sigma'$ = strength/stress ratio for pavement with properties different than the AASHO Road Test pavement properties

S'_c/σ = strength/stress ratio for AASHO Road Test pavements

The following assumptions were made or are inherent in this derivation:

1. The variation in load applications (W) required to reach a certain S'_c/σ level for variable loads is properly evaluated by the Road Test equations and is adequately expressed by the use of equivalence factors to express all loads in terms of 18,000 lbf [80 kN] single-axle loads.

2. Any change in S'_c/σ due to variations in physical constants (such as E, k, D, and S'_c) will have the same effect as varying slab thickness, and this relationship is defined by Equation E-5.

3. Thermal and moisture gradients existed in the Road Test slabs and their effects are represented in Equation E-13; however, the effect of a different climate with different thermal and moisture gradients is not considered in the extension of the equation. Thus, the effects of different design features, such as joint spacing, a stiff base, or interaction of a stiffer subgrade (k value) and temperature and moisture gradients, are not considered at all.

4. Faulting did not occur during the AASHO Road Test because the transverse joints were well dowelled, even though extensive pumping and erosion occurred. The extended Equation E-13 does not include consideration of faulting's potential effect on loss of serviceability. The J factor relates only to corner stresses that lead to cracking, not joint faulting.

The final "extended" 1961 AASHTO design model was obtained after entering the regression and physical constants for an 18-kip single axle load (L1 = 18, L2 = 1):

$$\log W_{18}' = 7.35 \log (D + 1) - 0.06 + \frac{G}{F'} + \log \frac{\left[\frac{(S'_c)'}{\sigma'}\right]}{\left[\frac{S'_c}{\sigma}\right]} \qquad \text{(E-14)}$$

The following design inputs were assumed for the AASHO Road Test pavements:

E_c = 4,200,000 psi [28940 MPa] (mean 28-day, static test)

S'_c = 690 psi [4.75 MPa] (mean 28-day strength, third-point loading)

k = 60 psi/in [16 kPa/mm] (springtime gross k value test, top of granular subbase, 30-in-diameter [762 mm] plate)

The gross k value of 60 psi/in [16 kPa/mm] was measured in the springtime, thus, it is the lowest value during the year. The gross k value includes considerable permanent deformation of the soil. The elastic k values (load divided by elastic deformation only) measured at the AASHO Road Test exceeded the gross k values by an average ratio of 1.77. The mean springtime gross k value of 60 psi/in [16 kPa/mm] represents measurements made on top of the aggregate base, not on the subgrade soil. The mean springtime gross k value of the subgrade was 49 psi/in [13 kPa/mm]).

The final 1961 equation was obtained by substituting values for σ and σ' into Equation E-14:

$$\log W_{18}' = 7.35 \log (D + 1) - 0.06 + \frac{G}{F'} + \log \frac{\left[\frac{(S'_c)'}{\sigma'}\right]}{\left[\frac{S'_c}{\sigma}\right]} \qquad \text{(E-15)}$$

where:

$$G = \log\left(\frac{P1 - P2}{P1 - 1.5}\right) \qquad \text{(E-16)}$$

$$F' = 1.00 + \frac{1.624 * 10^7}{(D + 1)^{8.46}} \qquad \text{(E-17)}$$

P1 and P2 = initial and terminal serviceability index of design pavement

D = concrete slab thickness of design pavement, in

$(S'_c)'$ = flexural strength of concrete, psi (third-point loading, 28 days)

S'_c = 690 psi [4.75 MPa] (mean AASHO Road Test value)

σ = corner stress computed from Equation E-6

using mean AASHO Road Test conditions:

k = 60 psi/in [16 kPa/mm]

E_c = 4,200,000 psi [28940 MPa]

μ = 0.20

J = 3.2

a_1 = 10 in [254 mm]

P = 9,000 lbf [40 kN]

σ' = corner stress computed from Equation E-6 using design pavement inputs for k, E_c, μ, J, a_1, P

Additions to the 1961 Extended Model Through 1993 Related to Support

There have been several additions to Equation E-15 over the years that are related to pavement support. The way in which these additions were made has resulted in serious deficiencies in the current rigid pavement design model.

Composite k value. The k value input defined in 1961 was the gross k value of 60 psi/in [16 kPa/mm] which was actually a typical value in the spring of the year, on top of the granular base layer. In the 1972 version, an alternate graphical procedure was added whereby the k value on top of the base course (called a composite k) could be determined if the resilient modulus and thickness of the base were known, along with the k value or resilient modulus of the subgrade. In 1986, the composite k value approach using elastic layer theory became the standard method. Thus, the effect of the base layer on slab thickness design was accounted for through the composite k value of the foundation. The concept of a composite (top of the base) k value is inappropriate and unrealistic, as described in Appendix A.

Loss of support (LS). A procedure was added whereby the composite k value was reduced depending on the amount of erosion that was expected beneath the concrete slab. With only a moderate amount of erosion, the resulting k value is reduced tremendously. For example, a composite k value of 300 psi/in [81 kPa/mm] would be reduced as shown for different LS values:

LS	Reduced k value	
0	300 psi/in	[81 kPa/mm]
1	100	[27]
2	31	[8.4]
3	13	[3.5]

The LS value is a function of the area of loss of support beneath the transverse joint. This additional consideration of loss of support is unnecessary because the original AASHO Road Test model already inherently includes a large amount of loss of support caused by erosion of the dense-graded base course during the Road Test as previously described. Photographs exist of persons shoving yard sticks under the pavement slab into the voids. Adding another adjustment for even more loss of support would result in much greater slab thickness designs than the AASHO Road Test performance results would predict are needed.

Effective k value over seasons. A procedure to compute a seasonally adjusted k value was added in 1986. The seasonally adjusted k value was called the "effective k value." However, the gross k value built into the 1961 design equation was that measured in the springtime, not the seasonally adjusted "effective k value."

Figure E-2 shows plots of typical elastic k values on top of the base over the two-year period measured on Loop 1 (both flexible and rigid pavement sections). The elastic k value on the subgrade or embankment varies from 60 to nearly 130 psi/in [16 to 35 kPa/mm]. The springtime elastic k values obtained from tests conducted on the main loops ranged from 63 to 105 psi/in [17 to 28 kPa/mm].

Thus, the 1986 revision should have included a basic revision to the concrete pavement extended equation to incorporate a seasonally adjusted effective k value, instead of the low springtime value of 60 psi/in [16 kPa/mm] used in 1961. The use of an seasonally weighted effective k value in the 1986 procedure is not really appropriate until this is accomplished.

Drainage coefficient, C_d. According to the Guide, this factor depends on the percent time that the subgrade approaches saturation and the drainage time for the base course. It is not clear what the C_d is intended to adjust. The Road Test pavements obviously had very poor subdrainage, as evidenced by the extensive

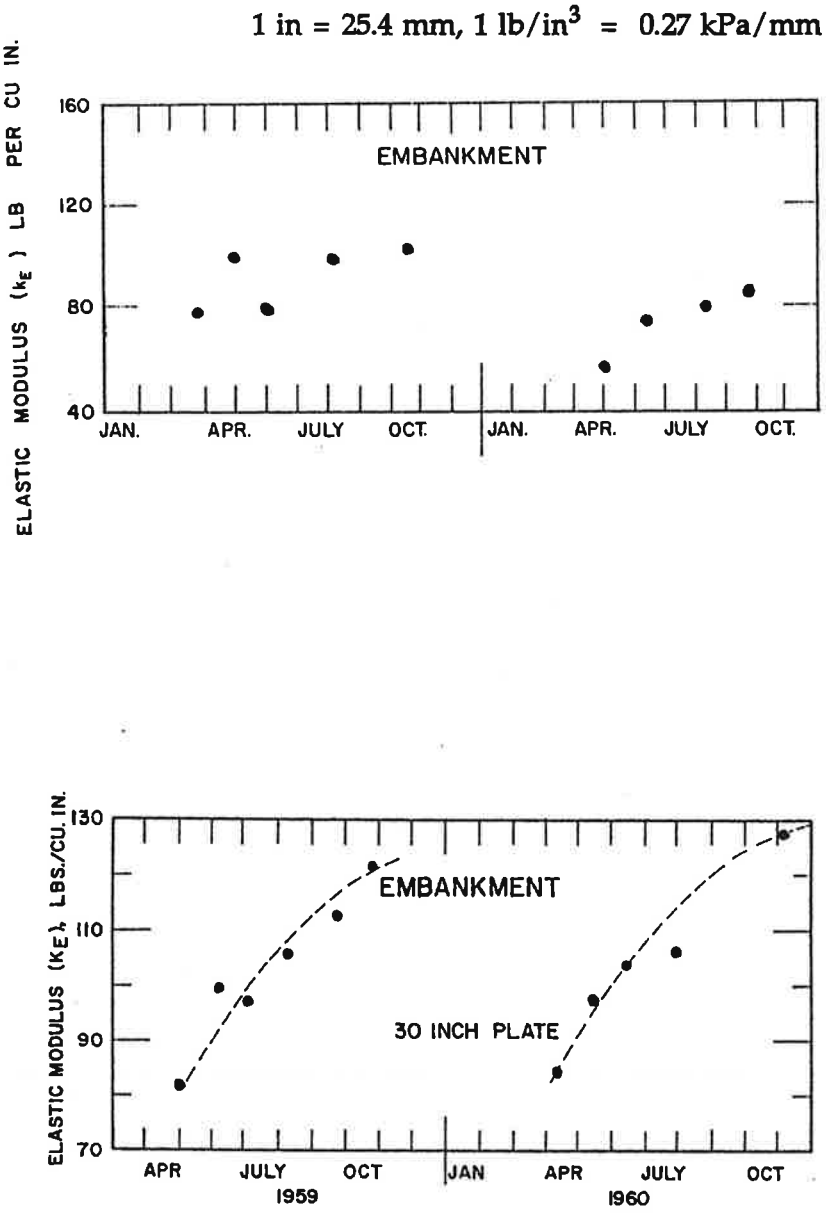

Figure E-2. Seasonal variation in elastic k value at the AASHO Road Test, Loop 1. [2]

erosion, pumping, and loss of support that occurred. This poor subdrainage and loss of support is built into the design equation. Thus, the 1986 version of the Guide not only added an unnecessary loss of support factor that results in an increased slab thickness, but also added a drainage factor that when applied results in a further increase in slab thickness.

A pavement with better subdrainage than the AASHO Road Test pavements had may also have improved support over time and may perform better from a cracking standpoint. Presumable, a C_d factor greater than 1.0 reflects this benefit, but the 1986 Guide does not specifically state what the C_d is intended to adjust: cracking, faulting, or some other distress. Because faulting did not occur at the Road Test, the C_d obviously could not be used to improve on faulting.

Joint load transfer factor, J. The reference value of 3.2 for J is a constant from an equation derived by Spangler for stress due to loading at an unprotected (free) corner conditions, based on slab theory and laboratory test results. The corner stresses (computed from measured strains) actually experienced by the AASHO Road Test pavements were linearly correlated to the free corner stress predicted by Spangler's equation. (The actual magnitude of the corner stresses in the dowelled Road Test pavements was about one third of the magnitude predicted for free corner conditions by Spangler's equation.) Thus, by incorporating Spangler's equation into the AASHO design model (that is, calibrating it to the Road Test pavement stresses), the J value of 3.2 was made to represent a protected (dowelled) joint and no tied shoulders, as existed at the Road Test.

A value greater than 3.2 means higher tensile stress at the top of the slab is expected due to corner loading because the joint load transfer is less than dowels would provide. A value less than 3.2 means the joint has better load transfer than dowels would provide, from improved joint load transfer (e.g., CRCP) and/or

perhaps a tied concrete shoulder. It is very important to remember that the J factor is an adjustment for slab stresses that cause corner breaks, and has absolutely nothing to do with joint faulting. No joint faulting existed at the Road Test. One cannot design a reduction or an increase in joint faulting by changing the J factor. This has been a point of major confusion among pavement engineers for years.

It is also important to realize that Spangler's corner equation considers only load stress for a flat corner and does not include thermal or moisture gradients that cause upward curl and warp of the corner. Different climates or construction methods that result in curling or warping magnitudes different than those which occurred at the Road Test are not considered in the AASHTO design model.

Design reliability. This methodology was added in 1986 to provide a consistent way to apply a design safety factor. The overall standard deviation may be reduced if an improved design model for log W is used and its error can be assessed.

DEFICIENCIES IN 1993 AASHTO PROCEDURE RELATED TO PAVEMENT SUPPORT

The following summary is a list of the specific deficiencies that were found to exist in the current version of the AASHTO design procedure for concrete pavements that are related to pavement support.

- The gross k value input assumes a large amount of permanent deformation and does not represent the support that the pavements actually experience during traffic loading. An elastic k value provides a far more realistic match to measured strains. In analysis of AASHO Road Test pavements, the elastic k value was found to roduce a stress in the slab equal to that

computed from measured strains under creep speed axle loading, as shown in Appendix D.

- The lowest gross k value that was measured on top of the base during the spring (60 psi/in [16 kPa/mm]) was incorporated into the AASHTO model in 1961 and has not been changed. The 1986 version provided a procedure to consider seasonal variation in selection of a design k value; however, the design equation was not modified to incorporate the effective k value that existed at the Road Test site. Thus, the current seasonal adjustment procedure is incompatible with the current design model.

- The effect of the base course on performance is not properly considered through the composite "top of the base" k value. This is especially true for stiff treated bases that act as structural layers in reducing stress in the slab. An improved way to model the effect of the base layer on slab stress is needed.

- Substantial loss of support existed for many sections at the AASHO site which led to increased slab cracking and loss of serviceability; thus, the performance data and design equation already incorporate considerable loss of support. Incorporation of an additional loss of support factor results in overdesign. What is needed is a way to consider the benefit of an improved base on performance in terms of cracking and faulting.

- The 1961 extension used Spangler's unprotected corner equation. The critical stress location at the AASHO Road test was along the slab edge for

slabs 6.5 in [165 mm] and greater, and resulted in transverse fatigue cracks initiating at the bottom of the slab. The stresses in the vicinity of the corner were much lower than those at midslab due to the well dowelled joints. Use of Spangler's corner equation with dowelled joints does not model the critical stress and crack initiation location, and thus cannot possibly provide accurate indications of the effect of slab support on cracking, especially when thermal curling and moisture warping are considered.

- The current AASHTO procedure does not provide a methodology to design a pavement with undowelled joints. The J factor only considers tensile stress that controls cracking, not faulting. An undowelled joint requires improved slab support from the base and a more erosion-resistant base material to prevent loss of support over time and premature failure. Thermal curling and moisture warping, which become much more critical to performance with undowelled joints, are not considered in the current AASHTO procedure.

- Joint spacing other than that of the Road Test slabs is not considered at all in the current design procedure. It is known from many other studies that joint spacing has a major effect on slab cracking and faulting. [12, 56] Subgrade and base support interact with joint spacing to affect combined slab stresses from load, temperature and moisture gradients. Thus, slab support is a very important variable in the selection of joint spacing to minimize transverse cracking.

- The original 1961 model reflects the climate of the AASHO Road Test site only. The 1993 version does not include any variable that adjusts for a different climates. Thus, other climates that cause different magnitudes of slab curling or warping cannot be considered. This limitation alone has led to many pavement failures from premature cracking.

- The only distress manifestation considered directly by the design procedure is transverse slab cracking because that is basically the only distress which occurred at the Road Test (other than erosion and loss of support which contributes to slab cracking). Thus, the loss of serviceability was due almost entirely to slab cracking and the subsequent deterioration of those cracks resulting in roughness and loss of serviceability. Some sections had excessive loss of support prior to failure from slab cracking. Cracking is related to slab support, and the Spangler corner equation incorporated into the AASHO design equation is not a realistic model for predicting the cracking that occurred, as noted above.

- Faulting of transverse joints did not occur during the two years of the Road Test because the joints all had dowels; thus, the performance predicted by the design model does not consider the effect of faulting on loss of serviceabilty. The J factor, often thought to control faulting, has nothing to do with joint faulting.

- Although thermal curling and moisture warping of slabs occurred during the two-year Road Test, the effects of these important factors were not considered in any of the extensions. This is important because any design

feature that would increase stresses from either of these stresses cannot be considered in design of that pavement. For example, joint spacing, base stiffness, and subgrade stiffness all affect stresses from thermal curling and moisture gradients through the slab. None of these can be considered in pavement design using the current AASHTO Guide procedure.

Given these major deficiencies, the following sections describe the research and development efforts that led to a recommended improved methodology for better consideration of slab support in the AASHTO design procedure.

IMPROVED AASHTO METHODOLOGY RECOMMENDED

Improved technology exists today that was not available in 1961, including the capabilities of 3D finite element models to compute slab stresses, larger and faster computers, and advanced mechanistic and statistical modeling. This technology was applied to the original AASHO model to develop an extended and improved design model for concrete pavements that more fully considers pavement "support" aspects. Specific improvements in the proposed revision to the AASHTO design procedure include the following:

1. Defining the k value specifically as the value determined on the finished roadbed soil or embankment, upon which the base and slab will eventually be constructed. A composite "top of the base" k value is not valid and is not recommended for design.

2. The k value input recommended is the elastic k value as tested extensively at the AASHO Road Test and similarly at the Arlington test site. The

elastic k value was found to result in slab stresses similar to those produced in the field by axle loads at creep speed (see Appendix D).

3. Seasonal support variations are considered through the determination of an effective yearly elastic k value of the embankment/subgrade (Appendix H). A procedure was developed to determine the effective k value for design.

4. The effect of the base course on slab stress due to load and temperature and moisture gradients is directly considered. The base thickness, stiffness, and friction coefficient (between the slab and the base) are direct inputs to the design procedure.

5. Temperature gradients and moisture gradients (as equivalent temperature gradients) are directly considered as inputs to the design procedure.

6. A procedure was developed for checking joint faulting and adjusting joint design if deficient, rather than increasing slab thickness.

7. Joint spacing is directly considered through consideration of its interaction with slab support and effect on combined load and temperature curling stresses.

8. The effects of longitudinal edge load transfer or a widened traffic lane on critical stress reduction are considered directly.

9. Joint load position stresses are considered for dowelled and undowelled joints in slab design.

New Proposed Extended AASHTO Concrete Pavement Design Model

This model was developed using the same approach used in 1961 to extend the original empirical model. The following steps were taken in the development.

1. A mechanistic-empirical relationship between log W and the logarithm of the ratio of concrete strength to slab stress was developed. A plot of log W versus log S'_c/σ revealed a linear relationship that was modelled as follows:

$$\log W' = A + B \log \frac{S'_c}{\sigma_t} \qquad \text{(E-18)}$$

where W′ = number of axle loads to terminal serviceability index P2
(Note that W′ was computed from Equation E-1.)

A = a constant

B = slope of log W′ versus log S'_c/σ_t curve

S'_c = mean 28-day flexural strength, third-point load (690 psi [4.75 MPa])

σ_t = maximum slab stress at the bottom of the slab computed using stress equation developed from 3DPAVE results for a midslab 18-kip [80 kN] single-axle load position, considering both load and temperature curl (see paragraph 3 below for computation of σ_t)

2. The midslab location was chosen because the maximum slab tensile stress occurred at this location for the AASHO Road Test JPCP with dowelled joints. The truck axle load was placed at the midpoint between the joints, with the center of the dual tires located 20 in [508 mm] from the edge of the slab as shown in Figure E-3. Stresses developed when the axle load was located at the dowelled slab

1 in = 25.4 mm, 1 ft = 0.305 m

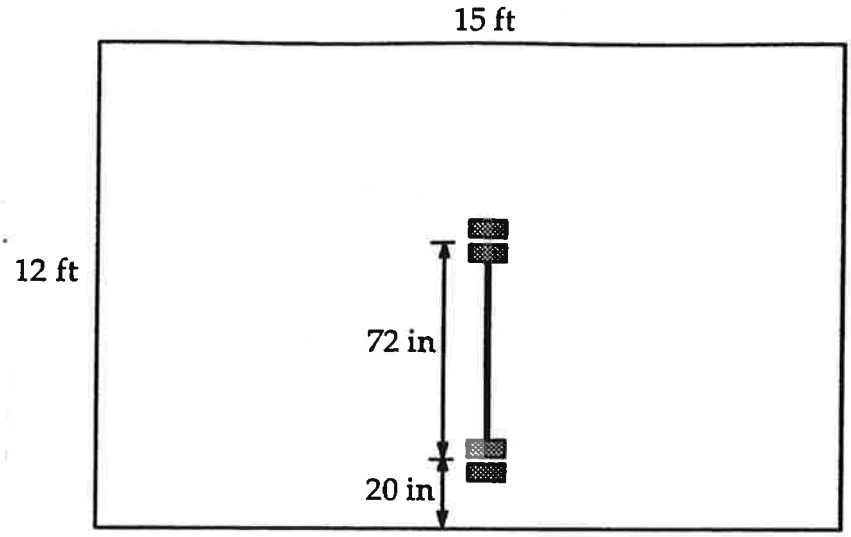

Midslab Loading

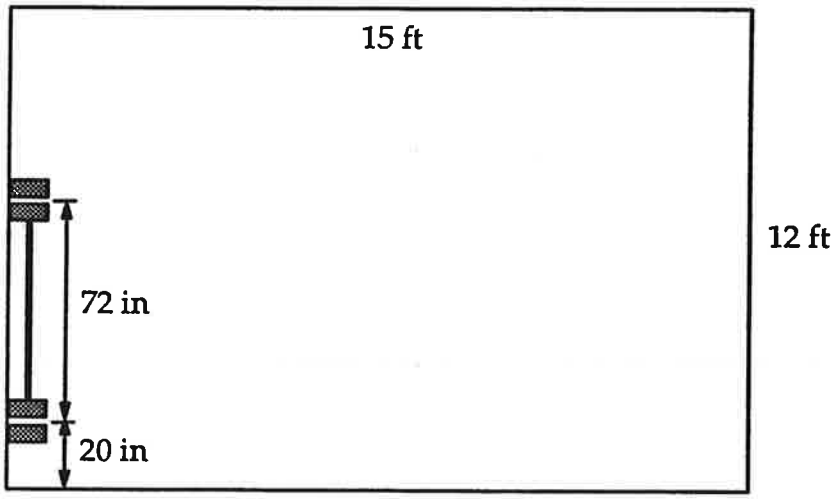

Joint Loading

Tire Print :

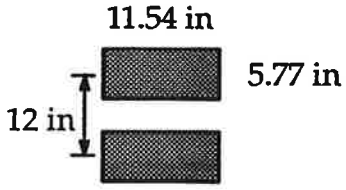

Figure E-3. Midslab and joint loading positions.

corner as shown in Figure E-3 were much lower than those at the midslab location. The maximum stress most often occurred directly beneath the wheel loads for this loading position.

3. The 3DPAVE finite element program produces stresses that accurately reproduce those occurring in the slabs in the field, as shown in Appendix D. Since 3DPAVE cannot be used in actual design, it was necessary to develop a stress model using principles of mechanics and dimensional analysis as well as regression. A large factorial of stress solutions for a wide range of design features was run with 3DPAVE to provide the basic stress data.

The stress model was developed in stages. First a model was developed for stress due to axle load only. Then a model was developed for the ratio of total stress (due to axle load and temperature differential) to load stress. Finally, adjustments for edge support and slab/base friction were derived. The model for load-only stress is as follows (derived for full friction, no slippage, between the concrete slab and the base course):

$$\sigma_l = \frac{18{,}000}{D^2}\left\{4.227 - 2.381\left(\frac{180}{\ell}\right)^{0.2} - 0.0015\left[\frac{E_b\,H_b}{1.4\,k}\right]^{0.5} - 0.155\left[H_b\left(\frac{E_b}{E_c}\right)^{0.75}\right]^{0.5}\right\} \qquad \text{(E-19)}$$

where σ_l = maximum tensile stress in the concrete slab for the midslab load position with an 18-kip [80 kN] single-axle load shown in Figure E-3 with no thermal curling, for conventional 12-ft [3.66 m] lane width

D = concrete slab thickness, in

E_c = modulus of elasticity of concrete slab, psi

E_b = modulus of elasticity of base, psi

H_b = thickness of base, in

$$\ell = \sqrt[4]{\frac{Z\,D^3}{12\,(1-\mu^2)}} \qquad \text{(E-20)}$$

$$Z = \frac{E_c}{k} \qquad \text{(E-21)}$$

k = elastic modulus of subgrade support, psi/in

μ = Poisson's ratio for concrete (0.20 measured for Road Test concrete)

Statistics: R^2 = 93 percent

σ_Y = 24 psi [165 kPa] (standard error of the estimate)

n = 120

The model for the ratio of total stress (load and curl) to load-only stress is as follows:

$$\frac{\sigma_t}{\sigma_l} = 1.0 + b\,TD \qquad \text{(E-22)}$$

where σ_t = total maximum stress from axle load and temperature differential through slab for midslab position, psi

σ_l = maximum tensile stress from axle load only at midslab position, psi

TD = temperature differential (top - bottom) through slab, degrees F

b = slope of relationship between σ_t and σ_l

This equation is illustrated in Figure E-4. The slope, b, depends on design variables such as slab thickness, k value, slab and base moduli, and others. The following model for σ_t was obtained by taking the logarithm of b to linearize the relationship and adding adjustment factors for edge support and slab/base friction.

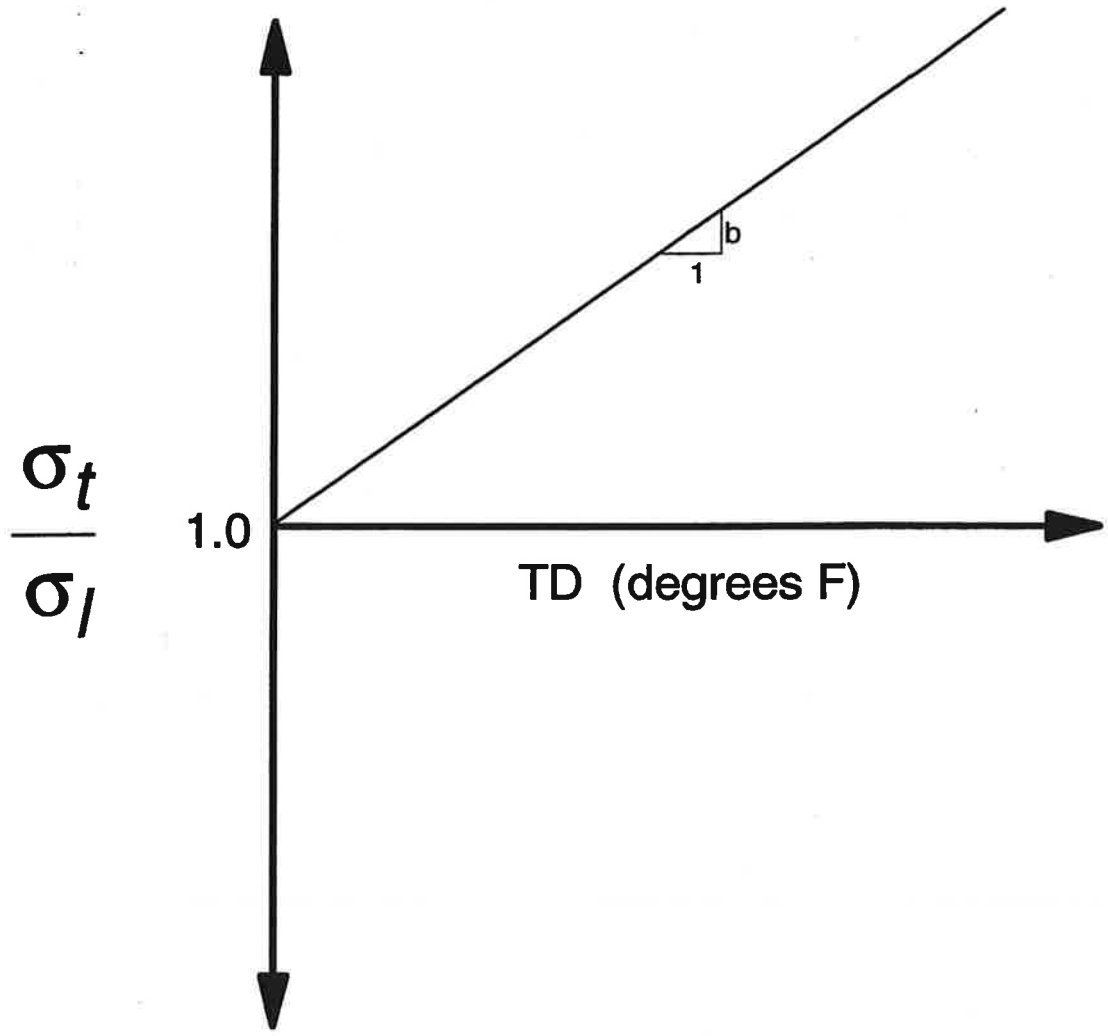

Figure E-4. Illustration of Equation E-22, total stress versus load-only stress.

$$\sigma_t = \sigma_l \, E \, F \left[1.0 + 10^{(\log b)} \, TD \right] \quad \text{(E-23)}$$

where σ_t = maximum total stress due to load and temperature differential

σ_l = maximum stress due to load only

E = edge support adjustment factor (described below)

F = slab/base friction adjustment factor (described below)

$$\log b = -1.944 + 2.279 \frac{D}{\ell} + 0.0917 \frac{L}{\ell} - 433{,}080 \frac{D^2}{k \ell^4} + \left(\frac{0.0614}{\ell} \right) * \left(\frac{E_b H_b^{1.5}}{1.4 k} \right)^{0.5} - 438.642 \frac{D^2}{k \ell^2} - 498{,}240 \frac{D^3 L}{k \ell^6} \quad \text{(E-24)}$$

Statistics for Equation E-23:

R^2 = 92 percent

σ_Y = 39 psi [269 kPa]

n = 168

The stress model given by Equation E-23 fits the data well as indicated by the R^2 and the standard error of the estimate. The model closely reproduces the critical stress, σ_t, from the 3DPAVE program.

This equation without the edge support adjustment factor E is applicable to a free edge longitudinal joint. The edge support adjustment factor was derived for the stress reduction achieved by improved edge support, i.e., a tied concrete shoulder or a widened slab (see paragraph 12).

E = 1.00 for conventional 12-ft-wide [3.66 m] traffic lane

= 0.94 for conventional 12-ft-wide [3.66 m] traffic lane plus tied concrete shoulder

= 0.92 for 2-ft [0.6 m] widened slab with paint stripe at conventional 12-ft [3.66 m] lane width

Equation E-23 was derived for full friction (no slippage) between the concrete slab and the base course. The following adjustment was derived for any value of the friction coefficient between the slab and base (see paragraph 13).

F = ratio between slab stress at a given coefficient of friction (f) between the slab and base and slab stress at full friction (no slippage)

$$F = 1.177 - 4.3*10^{-8}\ D\ E_b - 0.01155542\ D + 6.27*10^{-7}\ E_b - 0.000315\ f \quad \text{(E-25)}$$

where D = slab thickness, inches

E_b = elastic modulus of base, psi

f = friction coefficient between slab and base

Appropriate ranges of elastic modulus and friction coefficient for various base types are given later in this Appendix.

4. A study was conducted to determine the extent to which critical stresses computed from strains measured at the Road Test could be predicted using the 3DPAVE, and specifically what k value was required. A description of this study is

given in Appendix D. The results showed that the 3DPAVE could reproduce the Road Test edge stresses quite well using an elastic k value equal to that measured on the embankment at the Road Test site during the period of time when the strain measurements were taken: for a creep speed of 3 mph [4.8 km/hr], the elastic k value was about 86 psi/in [23 kPa/mm], which is about the same as the value measured in plate load tests during the springtime. It was found, however, that vehicle speed had a very large effect on the strains measured, and thus on the required k value. For higher speeds, the k value required to match Road Test strains increased substantially as described in Appendix D.

5. After observing many results from the 3DPAVE it was decided to try to include the temperature differential into the stress calculation so that these critical stress factors would be directly considered in any extension of the Road Test equation. The effects of joint spacing, base layer stiffness, subgrade stiffness, and climate (temperature conditions) could be considered realistically. A moisture shrinkage gradient was also considered for the joint loading position since it adds to the nighttime (negative) temperature differential.

6. A concrete slab is subject to a constantly changing daytime (positive) and nighttime (negative) temperature differentials between the top and bottom of the slab over a year's time period. The magnitude of the temperature differential at any given time of the day varies with season and geographic location. The question that thus arises is what temperature differential should be used in design? Due to the empirical nature of the AASHTO design procedure, the only way to consider the range of temperature differentials is to compute a single effective temperature differential for a given geographic location which represents the daily and seasonal variation in temperature differentials.

Temperature differential data computed hourly throughout a year using the Climate-Materials-Structural (CMS) model for 14 sites around the United States were obtained from Reference 4. These data were used to develop frequency distributions of daytime and nighttime temperature differences was available for each site for a range of slab thickness from 6 to 14 in [152 to 356 mm]. These frequency distributions were used along with the 3DPAVE model to compute an effective positive temperature differential and an effective negative temperature differential for each site that would give the same Miner's fatigue damage [13] at the midslab loading position as the distributions of positive and negative temperature differentials. For the AASHO Road Test site, for example, the effective positive temperature differential between the top and bottom of the slab was 8.7°F [4.8°C] for a 10-in [254 mm] slab (top warmer than bottom). This means that approximately the same fatigue damage would be obtained using 8.7°F [4.8°C] for every load application as would be obtained using the entire spectrum of temperature differentials for that location.

Values of the effective positive temperature differences for the 14 sites are given in Table E-1 and range from 5.9 to 12.6°F [3.3 to 7.0°C] for a 10-in [254 mm] slab. The effective temperature differentials increase with slab thickness.

Since it is quite time-consuming to compute the effective temperature differentials for other locations, a simple procedure was developed for use in design. Climatic data were obtained for each of the sites and prediction models were developed to estimate the effective positive and negative temperature differentials for a given location from the mean annual wind speed, mean annual temperature, mean annual precipitation, and trial slab thickness. The equation for positive temperature differential is as follows:

Table E-1. Summary of daytime positive effective temperature differentials over year for several sites, based on equivalent fatigue damage.

Location	6-in Slab	10-in Slab	14-in Slab	Annual Wind Speed (mph)	Annual Temperature (°F)	Annual Precipitation (in)
Urbana IL	4.9	8.8	9.4	11.6	50.8	35
Rockford IL	4.8	8.7	10.0	10.3	48.6	31
Cairo IL	5.5	9.8	11.1	12.0	57	48
Lansing MI	3.4	6.2	7.7	10.6	49.8	30
St. Louis MO	5.0	9.0	10.5	9.5	55.9	36
Fargo ND	5.1	8.9	10.5	13.0	41.4	16
Little Rock AR	5.7	10.1	11.2	8.2	60.5	48
Raleigh NC	4.5	8.1	8.5	7.9	58.9	43
Tallahassee FL	5.7	9.6	10.9	7.5	68.3	54
Syracuse NY	3.0	5.9	7.2	9.9	47.8	36
Sacramento CA	6.4	11.1	12.5	8.5	60.8	17
Salem OR	4.2	7.1	8.2	7.3	48.0	60
Pendleton OR	4.3	7.7	9.4	7.7	50.0	20
Las Vegas NV	8.1	12.6	14.9	8.8	65.8	4

Values shown under slab thicknesses are effective temperature differentials from top to bottom of slab, °F. [1°F = 0.55°C, 1 in = 25.4 mm, 1 mph = 1.61 km/hr]

$$effective\ positive\ TD = 0.962 - \frac{52.181}{D} + 0.341\ WIND + 0.184\ TEMP - 0.00836\ PRECIP \quad \text{(E-26)}$$

where effective positive TD = top temperature minus bottom temperature, ^{o}F

D = slab thickness, in

WIND = mean annual wind speed, mph (Figure E-5)

TEMP = mean annual temperature, ^{o}F (Figure E-6)

PRECIP = mean annual precipitation, in (Figure E-7)

Statistics: $R^2 = 0.84$

$\sigma_Y = 1.2^{o}F\ [0.67^{o}C]$

n = 42

Contour maps for the three climatic inputs are provided in Figures E-5, E-6, and E-7, and these data are also easily obtainable from local weather stations or other sources. A similar equation for effective negative temperature differential is presented later in this Appendix.

The above analysis assumes that the concrete slab will be flat when the temperature differential through the slab is zero. Field observations have shown that this is not always the case. For example, in one field study in Florida, a temperature positive temperature differential of $9^{o}F$ was found to be needed to flatten the slab. [5] Thus, the corners and edges were curled upward when the temperature differential through the slab was zero. There are at least two possible causes for this upward curling of the slab in the absence of a temperature gradient [7, 8]:

Construction Curl. A permanent upward curl of the slab edges and corners may occur when paving is done on sunny, hot days. After placement, a large

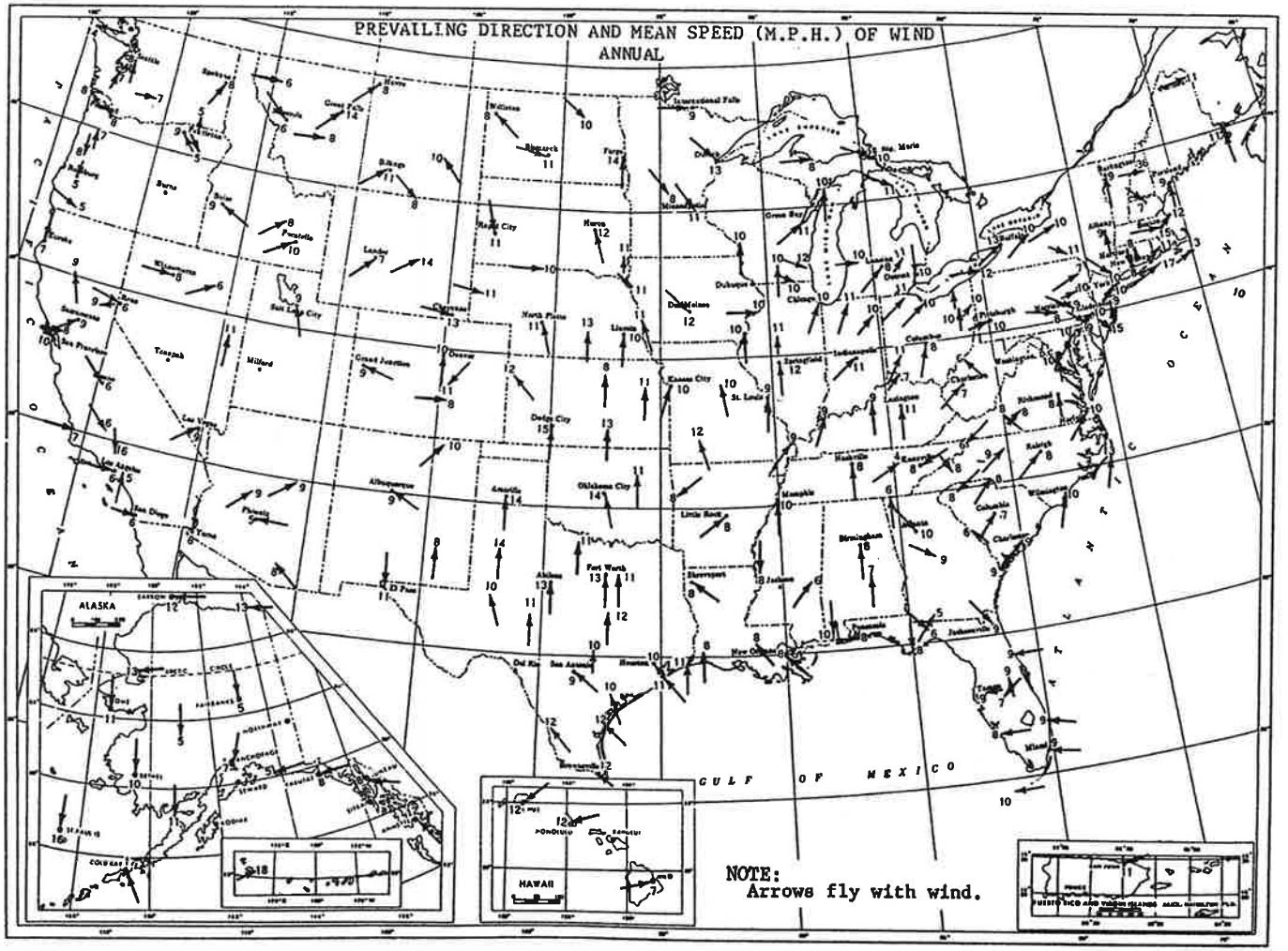

Figure E-5. Mean annual wind speed, mph. [18]

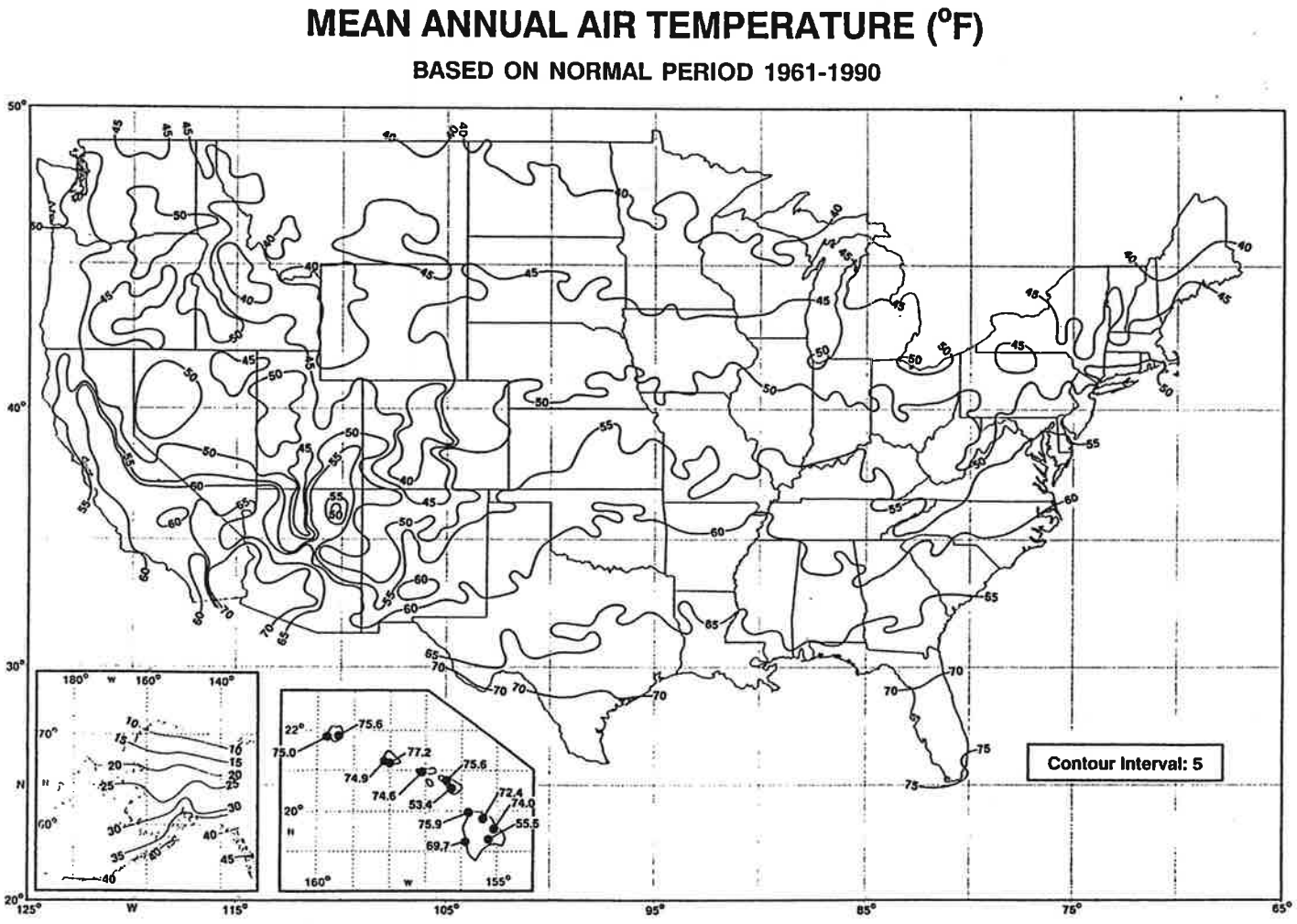

Figure E-6. Mean annual air temperature, °F. [18]

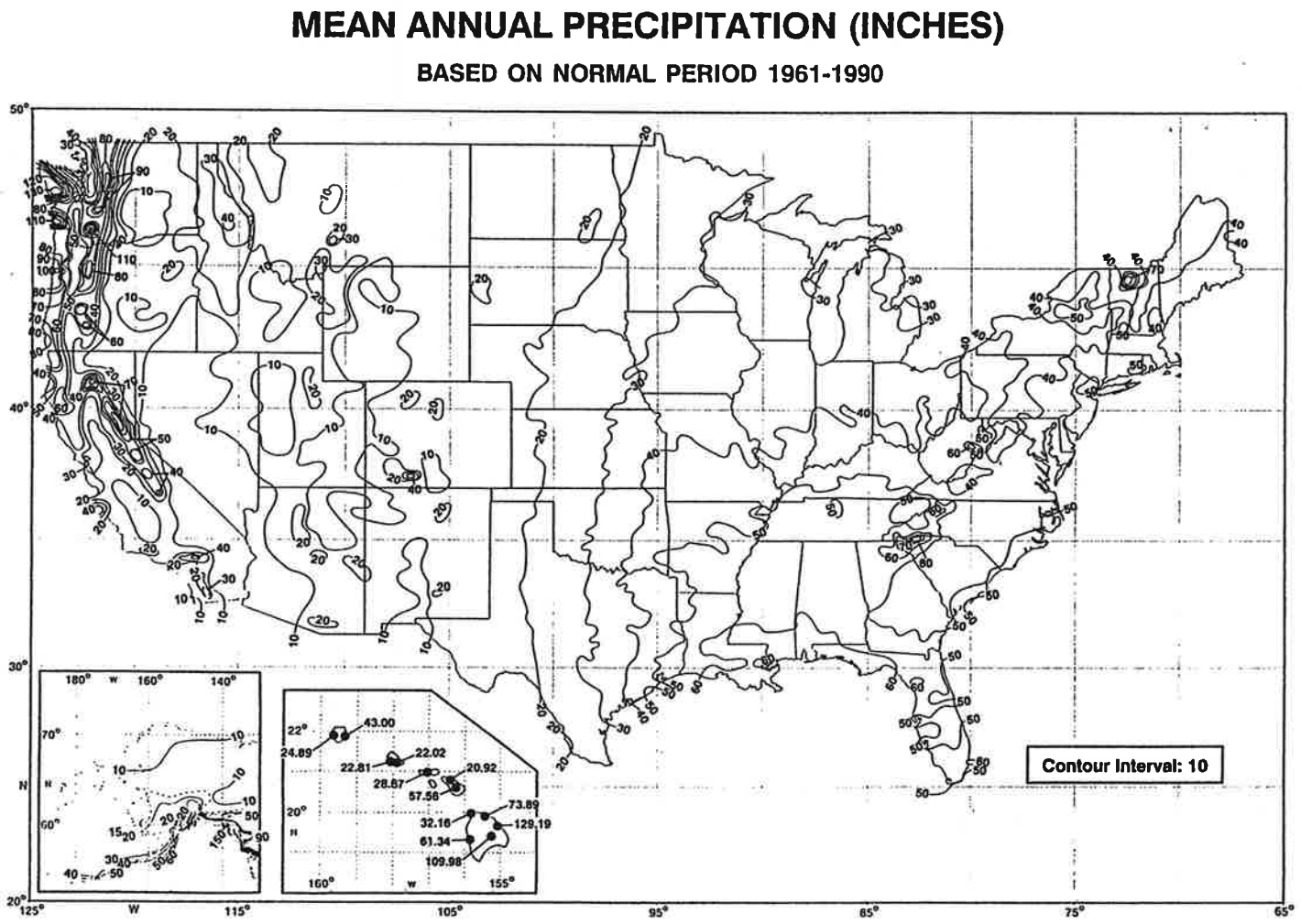

Figure E-7. Mean annual precipitation, in. [18]

temperature differential develops through the slab from a combination of solar radiation and heat of hydration. If the slab solidifies with this large positive temperature differential, when the temperature differential returns to normal daytime and nighttime levels, the slab edges and corners are permanently curled upward. This can be minimized by wet curing of the slab surface. [7] If construction curling occurs, the slab will not be flat when there is a zero temperature differential or zero moisture gradient through the slab. If this occurs, the midslab loading position will not experience the degree of thermal curling stress computed by the above equations, and will thus experience less fatigue damage and cracking.

However, construction curling will produce increased corner stresses under loading, which may increase the likelihood of cracking near the transverse joints. This problem has been well documented in Germany [7] and has also been observed in drier areas of Chile [8]. Since it is not possible to predict this construction-related curling warping to any degree, it is not considered independently in this design procedure. No mention of this phenomenon is made in the AASHO Road Test literature.

Moisture Warp. Seasonal warping up of the slab edges and corners results from shrinkage of the concrete at the top of the slab. This is discussed in paragraph 7 below.

7. The direct consideration of a moisture gradient through the slab was evaluated. Unfortunately, moisture warping of the AASHO Road Test slabs was not mentioned in any of the published literature, although it is very likely to have occurred to some extent. Some data on the shrinkage characteristics of the Road Test concrete was given previously. More recent data from Illinois concrete pavements showed that substantial drying occurs only at the top surface to a depth of less than 2 in [51 mm]. The rest of the slab thickness typically remains at 80 percent saturation

or higher. [9] However, these findings apply to the relatively wet Illinois climate; in other climatic areas the surface of slabs may dry more and thus more upward warping of the slabs may occur. This phenomenon is not considered for the midslab condition, but is considered for the joint load position, as described later in this Appendix.

A plot of log W versus log S'_c/σ_t was developed and is shown in Figure E-8. The log W was computed from Equation E-1 and thus represents AASHO Road Test conditions. Note that the maximum stress, σ_t, at the bottom of the slab is computed for the midslab loading position (Figure E-3) with the effective temperature differential (for the AASHO Road Test site) for slab thickness ranging from 5 to 13 in [127 to 330 mm]. The analysis was conducted for different terminal serviceability indices ranging from 1.5 to 3.5. As was found in 1961, the relationship between log W (from Equation E-1) and log S'_c/σ_t is linear. This linearity within the range of data provides some confidence in extrapolation beyond the limits of the AASHO data.

9. An equation was derived for B (the slope) as a function of P2, the terminal serviceability, as shown in Figure E-9.

$$B = 5.065 - 0.03295\ P2^{2.4} \tag{E-27}$$

An equation for A was also derived but is not used directly.

$$A = 5.102 - 0.00713\ P2^{2.4} \tag{E-28}$$

Thus, Equation E-18 can be written:

$$\log W' = A + B \log \frac{S'_c}{\sigma_t} \tag{E-29}$$

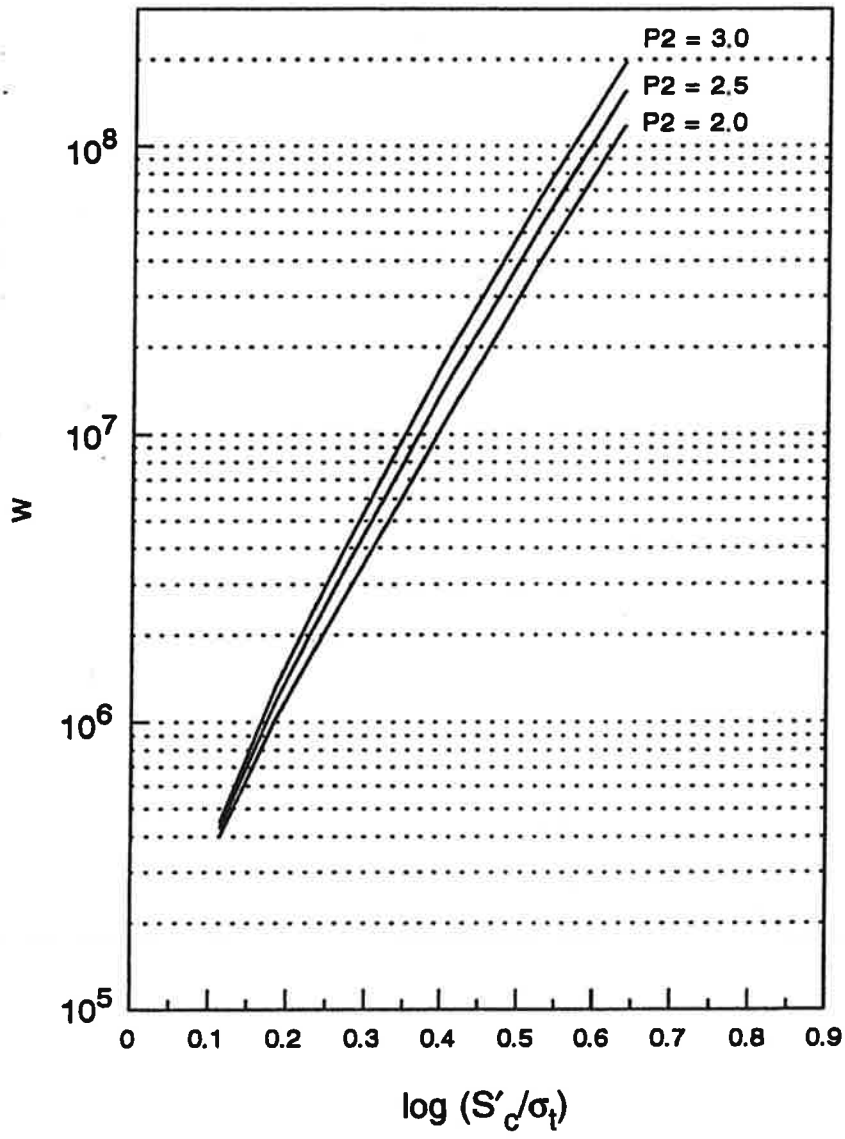

Figure E-8. Relationship of W to log S'_c/σ_t for three terminal serviceability levels for the proposed revised AASHTO extended concrete pavement design model.

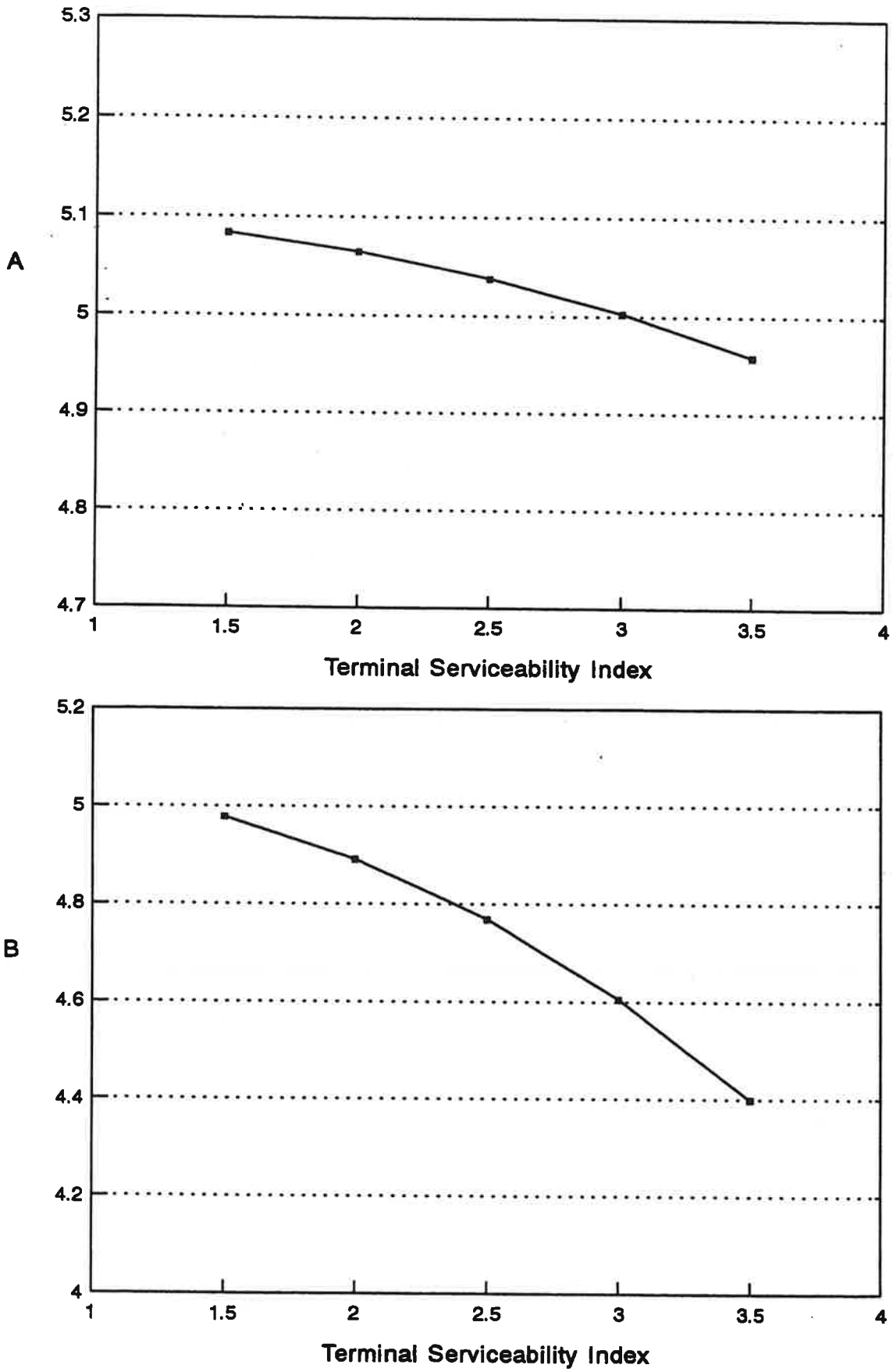

Figure E-9. Relationship between terminal serviceability P2 and log W for proposed revised AASHTO extended concrete pavement design model.

Equation E-29 represents a mechanistic-empirical relationship between the number of axle load applications to a given terminal serviceability and the ratio of concrete flexural strength to maximum tensile stress in the slab under single-axle loading and a positive effective temperature gradient.

10. Equation E-1 and Equation E-29 were then combined into the revised "extended" AASHTO design equation for concrete pavements. Note, while it is possible to use Equation E-29 directly for design purposes, the AASHO Road Test staff chose instead to combine the original empirical Equation E-1 with Equation E-29. Equation E-1 is the original Road Test equation that directly relates log W to D, L1, L2, P1, and P2 for the specific Road Test conditions. It must be remembered that these conditions (i.e., joint spacing, dense-graded aggregate base, subgrade stiffness, gravel shoulders, dowelled joints, etc.) are included indirectly, however. The combination of Equation E-1 and E-29 was done by differentiating Equation E-29.

$$\partial \log W' = B\, \partial \left(\log \frac{S'_c}{\sigma_t} \right) \tag{E-30}$$

The difference in load applications between a pavement with AASHO Road Test design features described by S'_c/σ and one with different design features described by $(S'_c)'/\sigma'$ is then given by the following equation:

$$\log W' - \log W = B \left[\frac{(S'_c)'}{\sigma'_t} - \frac{S'_c}{\sigma_t} \right] \tag{E-31}$$

or

$$\log W' - \log W = \left(5.065 - 0.03295\, P2^{2.4}\right)\left[\frac{(S'_c)'}{\sigma_t'} - \frac{S'_c}{\sigma_t}\right] \qquad \text{(E-32)}$$

where:

W' = number of axle load applications required to reach a given terminal serviceability P2 for a pavement with different physical properties than a Road Test pavement, described by $(S'_c)'/\sigma'$

W = number of load applications required to reach a given terminal serviceability P2 for a Road Test pavement described by S'_c/σ (Equation E-1 is used to compute log W)

$(S'_c)'/\sigma_t'$ = strength/stress ratio for pavement with properties different than the AASHO Road Test pavement properties (note that σ_t includes both load and positive temperature differential curl stresses)

S'_c/σ_t = strength/stress ratio for AASHO Road Test pavements (note that σ_t includes both load and positive temperature differential curl stresses)

The following is presented to further clarify this "extension" of the original AASHO Road Test Equation E-1. Equation E-32 represents a relationship between the number of load applications W', terminal serviceability P2, and strength/stress ratio S'_c/σ_t for AASHO Road Test pavements. Figure E-10 illustrates that B is the slope of the line between any two points. The relationship can be represented by the equation derived from Figure E-10, which of course is the same as Equation E-32.

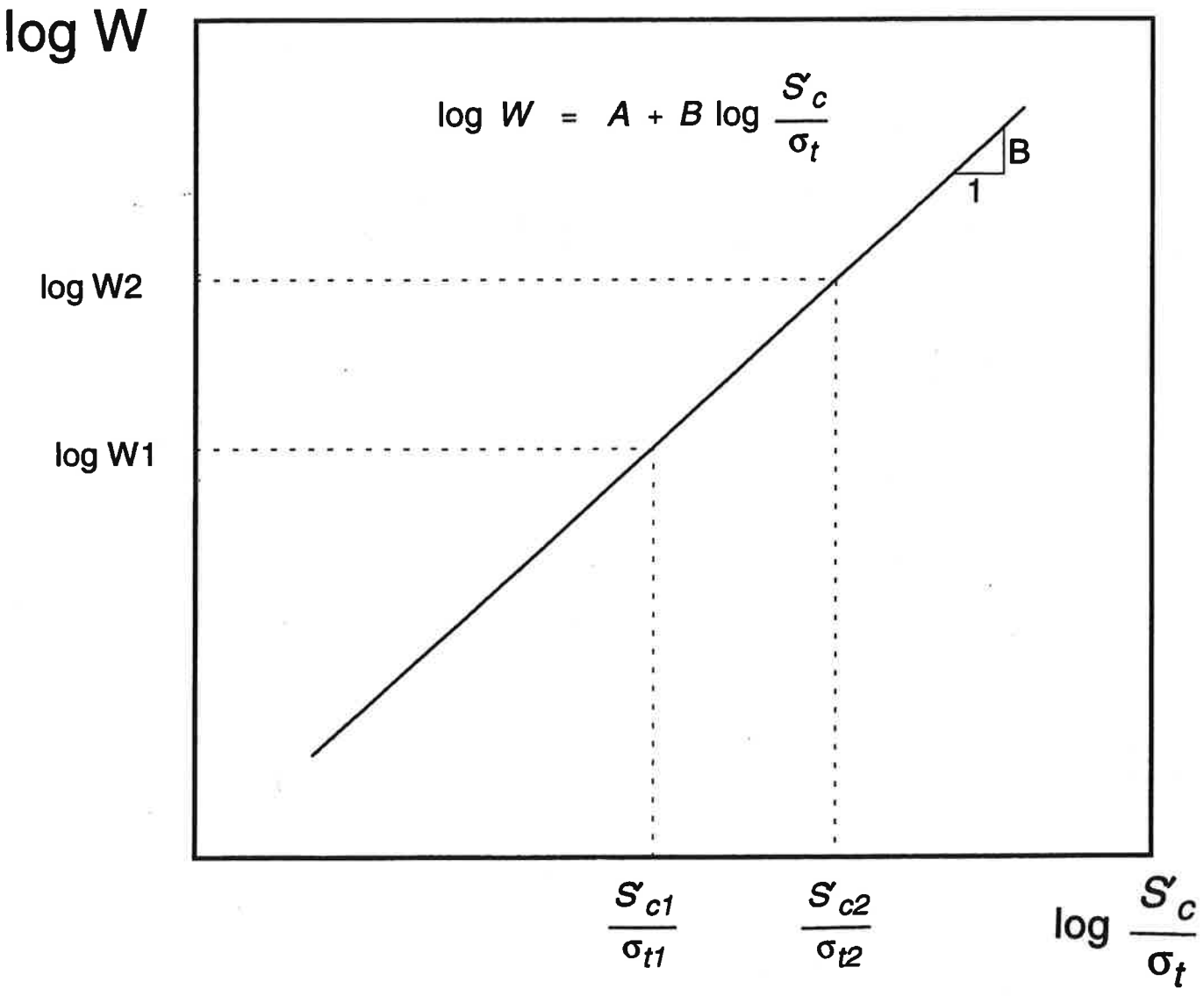

$$B = \frac{\log W_2 - \log W_1}{\log\left(\frac{S'_{c2}}{\sigma_{t2}}\right) - \log\left(\frac{S'_{c1}}{\sigma_{t1}}\right)}$$

$$\log W_2 - \log W_1 = B\left[\log\left(\frac{S'_{c2}}{\sigma_{t2}}\right) - \log\left(\frac{S'_{c1}}{\sigma_{t1}}\right)\right]$$

Figure E-10. Relationship between log W and log S'_c/σ_t.

The only design feature that was varied at the Road Test was slab thickness which provides for a range of $S'_c/\sigma_{t'}$ making the derivation of Figure E-8 possible. To use this relationship in design, the assumption was made that any other variable that changes this strength/stress ratio (such as S'_c itself or anything that changes $\sigma_{t'}$ including k value, joint spacing, temperature differential, etc.) will have the same effect on log W' as a change in slab thickness.

Given the above assumption, Equation E-32 could be directly used for design purposes, or it could be combined with Equation E-1 as was done by the AASHO Road Test staff in 1961 which was called "extending" the AASHO Road Test main empirical relationship. This was accomplished by "assigning" the log W and S'_c/σ_t to the specific design features of the AASHO Road Test. The following definitions help to further clarify the "extension" of the original Equation E-1 empirical model.

log W = Equation E-1 (with AASHO Road Test standard inputs for D, P1, P2, and 18-kip [80 kN] single axle

B = Equation E-27 (a function of P2)

$(S'_c)'$ = mean concrete flexural strength for new pavement design

$\sigma_{t'}$ = Equation E-23 (all inputs for new pavement design)

S'_c = 690 psi [4.75 MPa] (AASHO Road Test mean flexural strength)

σ_t = Equation 23 (AASHO Road Test constants for all inputs: joint spacing, k value, base type and modulus, concrete modulus, etc.

11. The assumptions made or inherent in this derivation are the same as the original model except that the temperature differential through the slab is now directly considered. Of course, the maximum slab stress is computed from the equations developed from the results of the 3DPAVE finite element analyses for the midslab position (Figure E-3).

12. Edge load transfer adjustment. The pavements at the AASHO Road Test had a lane width of 12 ft [3.66 m] and no tied shoulder. Thus, when a design project requires a widened slab or tied concrete shoulder, adjustments must be made to the AASHO design equation to consider the effect of improved edge support. If the slab is more than 12 ft [3.66 m] wide or has a tied concrete shoulder, the critical stress in the slab will be reduced.

A methodology was developed to reduce the critical stress when improved edge support was provided. A range of designs were analyzed with 3DPAVE and the maximum stress computed for the midslab load position, both with and without a positive temperature differential. Table E-2 shows some of the results. The mean ratio of maximum stress with and without a widened slab (2 ft [0.6 m]) was 0.85 for no temperature differential and 0.92 with a temperature differential. Note that this loading position had the center of the dual truck tires an additional 24 in [610 mm] from the free edge of the slab. This assumes that trucks will travel at about the same lateral displacement, as measured from the paint stripe, as they would on a conventional 12-ft-wide slab. This is consistent with the findings of Benekohal, Hall and Miller on the effect of lane widening on lateral distribution of truck wheels. [19] They found that widened slabs had relatively little effect on the mean distance of the truck wheels from the lane edge (paint stripe), and also observed no edge loadings in more than 1,300 observations of truck wheel placements on widened-slab pavement sections.

The mean ratio of maximum stress with and without a tied concrete shoulder (load transfer approximately 74 percent) and a temperature differential was 0.94. Data from various sources showed that the load transfer across the longitudinal lane shoulder joint varies widely, from 30 to 100 percent, depending on the age and design of the tie system. [8, 15] A value of 74 percent was used to represent a typical

Table E-2. Comparison of maximum tensile stresses for conventional lane width (12 ft [3.66 m]), widened slab (2 ft [0.6 m]) and tied concrete shoulder (deflection load transfer 74 percent).

Concrete Pavement					DT=0			DT=5.5 for 7 in, DT=9.0 for 11 in				
Ec	hc	Eb	hb	k	Conventional	Widened Lane	Ratio	Conventional	Widened Lane	Ratio	Tie Shoulder	Ratio
4000000	7	25000	4	100	280	237	0.85	331	291	0.88	299	0.90
4000000	7	25000	6	100	277	235	0.85	328	289	0.88	298	0.91
4000000	7	1000000	4	100	142	121	0.85	212	192	0.90	195	0.92
4000000	7	1000000	6	100	99	87	0.87	177	164	0.93	168	0.95
4000000	7	25000	4	300	218	191	0.87	283	261	0.92	270	0.95
4000000	7	25000	6	300	217	190	0.87	282	260	0.92	268	0.95
4000000	7	1000000	4	300	113	99	0.88	187	175	0.93	179	0.96
4000000	7	1000000	6	300	83	75	0.89	162	154	0.95	156	0.97
4000000	11	25000	4	100	153	128	0.83	195	171	0.88	178	0.91
4000000	11	25000	6	100	153	127	0.83	195	172	0.88	178	0.91
4000000	11	1000000	4	100	98	82	0.84	167	152	0.91	157	0.94
4000000	11	1000000	6	100	78	66	0.84	159	148	0.93	154	0.97
4000000	11	25000	4	300	125	105	0.84	199	185	0.93	189	0.95
4000000	11	25000	6	300	125	106	0.84	199	184	0.93	188	0.94
4000000	11	1000000	4	300	83	70	0.85	168	158	0.94	161	0.96
4000000	11	1000000	6	300	68	58	0.85	160	152	0.95	154	0.96
				Means			0.85			0.92		0.94

DT : Temperature difference from top to bottom of slab,°F

1 in = 25.4 mm, 1 psi = 6.89 kPa, 1°F = 0.55°C

value for deformed tie bars. The following stress reduction multipliers are recommended for design purposes:

Widened traffic lane:	0.92
Tied concrete shoulder:	0.94

While these reductions in stress might not appear to be significant, they do in fact have a significant effect on the number of axle load applications that a pavement can carry (typically a 43 percent increase over a conventional traffic lane or non-tied shoulder) and on design slab thickness (typically a reduction of 0.5 in [13 mm] or more). Of course, these edge support adjustment factors are a simple solution to a very complex problem. A more sophisticated approach would be a comprehensive mechanistic analysis that considers fatigue damage at all points transversely across the slab to locate the critical fatigue point for a given design.

13. Friction Between Concrete Slab And Base. A knowledge of the degree of frictional resistance that develops between the concrete slab and the base course (particularly a treated base with high stiffness) has been considered important for the design of reinforcing steel and for ensuring that weakened-plane joints crack through the slab uniformly. Many horizontal load tests have been conducted over the past fifty years to estimate the coefficient of friction between the slab and base. The coefficient of friction has been used in the computation of tensile restraint stress in the slab and in the reinforcing steel that develops when the temperature is reduced.

Most of the research conducted has been with the objective of reducing the frictional resistance to prevent reflection cracking from the treated base course. However, reflection cracks can be eliminated and uniform cracking of all joints achieved by forming or sawing joints in a cement-treated or lean concrete base course

directly beneath the joints to be placed in the concrete slab. This practice has been standard in Germany for many years [28] and has shown great success, permitting high friction to exist between the slab and base so that erosion is reduced and a monolithic structural slab is achieved. Other European practice (Austria, France, Belgium) has shown that an asphalt-treated interlayer between the slab and treated base will achieve high friction with the slab and prevent reflection cracking. [28] Field studies in Iowa have shown that shear strengths in the range of 87 to 218 psi [600 to 1500 kPa] can develop between an asphalt pavement surface and a concrete overlay. [31]

Other than in Europe, relatively little attention has been paid to the possible benefits of frictional resistance between the slab and the base course for the purpose of reducing bending stresses in the concrete slab from wheel loads. The lack of adequate computational models is one of the main reasons that frictional resistance has not been considered in design. 2-D finite element models can model either full friction or full slip, but cannot analyze a realistic degree of friction somewhere between those two extremes. Another reason that friction is often not considered in design is that magnitude of frictional resistance that commonly exists between a slab and treated base has not been widely understood. Some also feel that the degree of friction may decrease over time, especially at the transverse joints due to erosion.

A summary of friction coefficients between the slab and base course reported in various references over the past fifty years is given in Table E-3. Ioannides and Salsilli have done a comprehensive summary of friction tests and an excellent discussion of friction. [29] The friction coefficients shown in Table E-3 were computed by dividing the applied horizontal force by the weight of the slab. Table E-3 shows that the coefficient of friction of treated bases is very high (typical peak

Table E-3. Summary of measured coefficient of friction between concrete slab and base course from various references and typical ranges of base modulus of elasticity.

Base Type and Typical Modulus of Elasticity Range	Measured Peak Coefficient of Friction (peak) (low-mean-high)	References
Fine-grained soils (E = 3,000-40,000 psi)	0.5---1.3---2.0	21, 22, 24
Sand (E = 10,000-25,000 psi)	0.5---0.8---1.0	21, 24, 30
Aggregate (E = 15,000-45,000 psi)	0.7---1.4---2.0	21, 24, 30
Polyethylene sheeting (on CTB, ATB, LCB, ...)	0.5---0.6---1.0	20, 21, 25, 26, 30
Lime-Stabilized Clay (E = 20,000-70,000 psi)	3.0 to 5.3	22
Cement-Treated Base (gravel) (E = (500 + CS)*1000 CS = compressive strength, psi	8---34---63	25, 26 27
Asphalt-Treated Base (E = 300,000-600,000 psi)	3.7---5.8---10	20, 22, 23
Lean Concrete Base (no curing compound) (E = (500+CS)*1000 CS = compressive strength, psi	> 36	20 27
Lean Concrete Base (single or double wax curing compound) (E = (500+CS) * 1000 CS = compressive strength, psi	3.5 to 4.5	20 27

1 psi = 6.89 kPa

values: lime stabilized soil = 4, asphalt treated aggregate = 6, cement-treated aggregate = 34, and lean concrete = 36 or more) when no attempt is made to reduce friction.

There are actually two different coefficients of friction. The first is the initial peak frictional resistance that develops prior to steady-state sliding, and the second is the steady-state frictional resistance that develops after initial sliding. The peak coefficient of friction ranges from about equal to twice the steady-state coefficient of friction. It seems that the initial peak frictional resistance is more relevant to the friction between layers that develops under moving wheel loads since it occurs rapidly and very small displacements occur. In addition, there is also the weight of the applied load that increases the normal force (slab self-weight plus applied load).

In backcalculation of FWD deflections measured on concrete slabs with underlying treated base layers, the assumption of a frictionless interface between the slab and base often produces an unrealistically high modulus for the concrete slab. The assumption of full friction (no slippage) between layers more often produces a realistic slab and base moduli, although in some cases the moduli may be underestimated using this assumption. Although it is unlikely that full friction between layers occurs, it is certainly true that zero frictional resistance is an unrealistic assumption, especially for treated bases. Even with polyethylene sheeting, coefficients of friction between 0.5 and 1.0 have been measured. The actual degree of frictional resistance for in-service pavements with various base types lies somewhere between the two extremes (full friction and full slip), but how well the friction levels in the field are represented by the lab values that have been reported, and how well the friction level is maintained over the life of the pavement, is not well known.

An adjustment to the full-friction stress to account for the coefficient of friction between the slab and base was developed using the 3DPAVE model. The maximum tensile stress at the bottom of the slab for the midslab load position was computed as previously described (see Appendix D). A range of base course stiffnesses and coefficients of friction were considered. An untreated aggregate base course provides relatively little frictional resistance; however, as the base stiffness increases this resistance increases greatly as shown in Figure E-11. The vertical axis represents the ratio of tensile stress in the slab for the given coefficient of friction divided by the tensile stress in the slab for full friction. The tensile stress in the concrete slab decreases considerably as the base stiffness increases and as the friction coefficient increases. These results were used to develop an equation for the friction adjustment factor, F, as a function of the base stiffness, slab thickness, and the friction coefficient, f, between the base and slab (Equation E-25). For midslab loading, the modulus of the base and the thickness of the concrete slab have a significant effect on the ratio of stress computed with a friction coefficient to stress computed with full friction, as shown in Table E-4 and Figure E-11. For a given slab thickness and base modulus, the stress ratio is not highly sensitive to the friction coefficient, which makes some uncertainty in selecting appropriate friction values tolerable.

The designer can now input both the base stiffness and the friction coefficient for pavement design purposes. Table E-3 can be used as a guide for selecting an appropriate coefficient of friction and base stiffness. Additional research is needed to more clearly determine the coefficients of friction occurring between the slab and base under traffic loadings.

When high friction is desired with a cement-treated or lean concrete base, two alternatives for eliminating reflection cracking are available: (1) form joints in the base, or (2) place a thin asphalt-treated interlayer between the slab and base.

Table E-4. Some results for the friction adjustment factor, F (ratio of σ_t computed wth friction coefficient to σ_t computed with full friction).

Slab Thickness (in)	Base Modulus (psi)	Coefficient of Friction, f	Friction Adjustment Factor, F
8	400,000	35	1.16
10	400,000	35	1.11
13	400,000	35	1.06
8	1,500,000	35	1.48
10	1,500,000	35	1.32
13	1,500,000	35	1.17

f = coefficient of friction between slab and base layer
F = ratio of σ_t at a given coefficient of friction and σ_t at full friction

1 in = 25.4 mm, 1 psi = 6.89 kPa

Another issue that needs to be addressed is the maintenance of the frictional resistance between the slab and base over time. Debonding of the slab and base has been observed in the vicinity of the corners and transverse joint areas in the past due to erosion. However, the midslab position is far less susceptible to erosion than the corners. Several field studies have been conducted in which cores obtained at various slab locations have shown good bond with the base layer. [6] Some have shown debonding, although it is never known whether the debonding occurred prior to or during the coring operation.

Also, some bases disintegrate over time if they do not have adequate resistance to freeze-thaw damage or asphalt stripping. Thus, the materials selection and mix design for the base course requires full consideration of durability aspects.

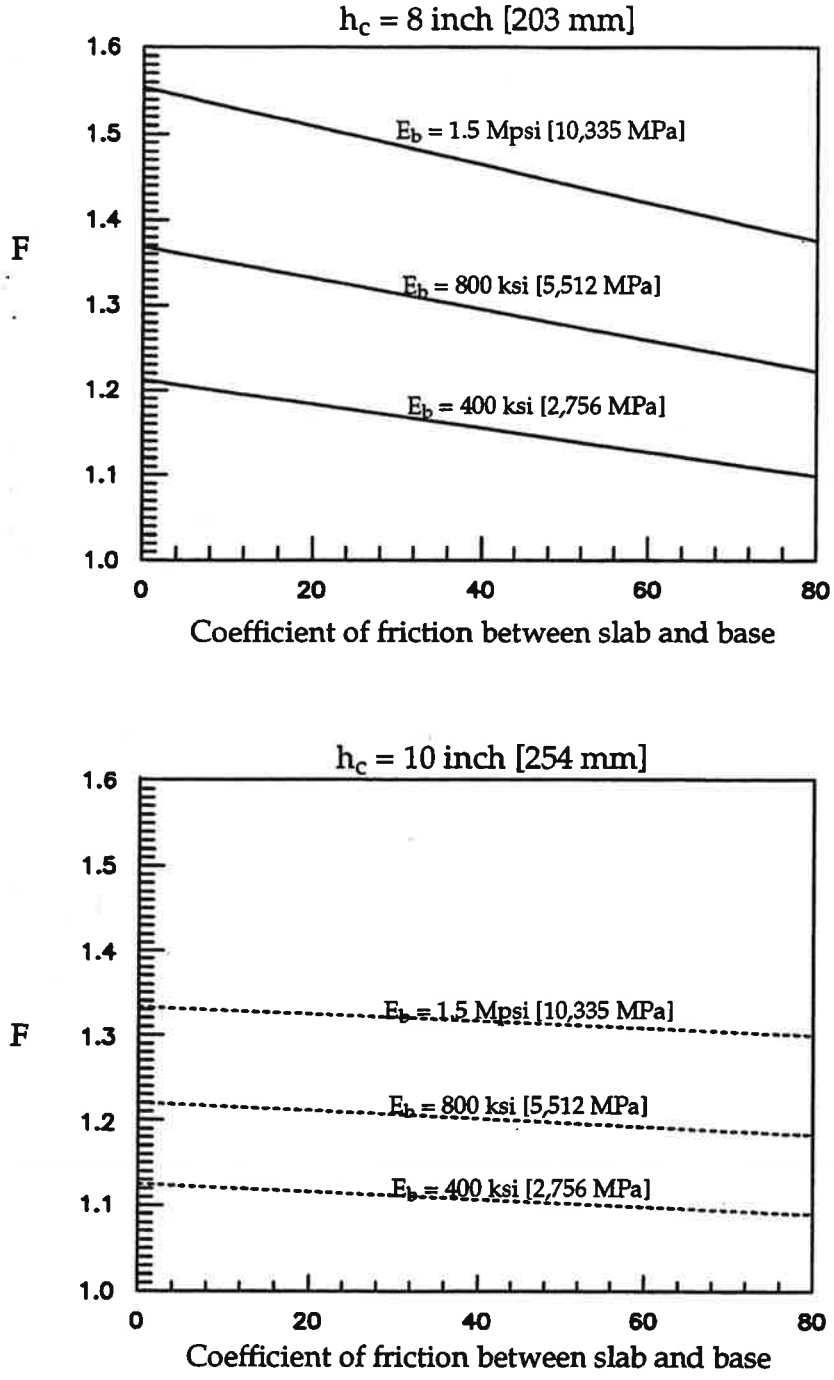

Note: h_b = 5 inch [127 mm] , k = 200 psi/in [54 kPa/mm]
E_c = 4 Mpsi [27,560 MPa] ,
Mid–slab loading with daytime curling DT (°F) [1°F = 0.56°C]

Figure E-11. Effect of slab thickness, base modulus, and friction coefficient on ratio of stress computed with friction coefficient to stress computed with full friction, for midslab loading and daytime temperature gradient.

A mechanistic approach to pavement design could consider the effects of a base course deteriorating over time and frictional resistance possibly declining over time. In order to consider the effects of these phenomena, one must have some reliable models for predicting their development.

The AASHTO design procedure, however, is not an incremental analysis of stress and damage with changing conditions over the life of the pavement. It is, basically, an empirical relationship between initial conditions, effective average conditions (e.g., k value, climatic factors), and predicted performance. In this context, the initial value of friction between the base and slab is believed to be the appropriate input for design. As Figure E-11 shows, the magnitude of friction coefficient selected does not have a large effect on bending stresses due to midslab loading. It must also be remembered that the AASHTO Guide requires that all inputs be mean values, not minimums, because of the way in which reliability is incorporated into the design procedure.

Also, it should be noted that the composite "top of the base" k value concept does not allow for any friction between the "composite" spring foundation and the concrete slab.

14. The proposed "extended" AASHTO design model was obtained as follows:

$$\log W' = 7.35 \log (D + 1) - 0.06 + \frac{G_p}{B'} + \log \left[\frac{\frac{S'_c{}'}{\sigma_{t'}}}{\frac{S'_c}{\sigma_t}} \right] \qquad \text{(E-33)}$$

The following design inputs were assumed for the Road Test pavements:

E_c = 4,200,000 psi [28940 MPa] (mean at 28 days, static test)

k = 110 psi/in [30 kPa/mm] (elastic seasonally adjusted effective k value, top of embankment, 30-in-diameter [762 mm] plate)

Note: The elastic k values for each three-month season used to obtain the effective k value of 110 psi/in [30 kPa/mm] were as follows [2]:

Season	**Elastic k**
Spring	77 psi/in [21 kPa/mm]
Summer	98 [26]
Fall	111 [30]
Winter	60 [16]
Effective k	**110 [30 kPa/mm]**

The effective k value was determined using the procedure given in Appendix H.

S'_c = 690 psi [4.75 MPa] (mean 28-day, third-point loading)

TD = effective temperature differential from top to bottom of slab over a year's time period for the AASHO Road Test site. TD varies with slab thickness, wind speed, precipitation, and temperature according to Equation E-26. TD for the AASHO site is given as follows:

$$\textit{effective positive TD} = 14.06 - \frac{55.29}{D} \qquad \text{(E-34)}$$

The final new concrete pavement log W model for 50 percent reliability was obtained by substituting values for σ_t and σ_t'.

$$\log W' = \log W + \left(5.065 - 0.03295\ P2^{2.4} \right) \left[\log \left(\frac{S'_c{}'}{\sigma_{t'}} \right) - \log \left(\frac{690}{\sigma_t} \right) \right] \qquad \text{(E-35)}$$

where W' = number of 18-kip [80 kN] ESALs estimated for design traffic lane

W = number of 18-kip [80 kN] ESALs computed from Equation E-1

σ_t = stress from Equation E-23 with AASHO Road Test constants

$\sigma_{t'}$ = stress from Eqation E-23 with inputs for new pavement design

This model represents the best-fit relationship between design features and log W. Design reliability can be added with the following model.

$$W_R' = 10^{\left(\log W' + Z\ S_o\right)} \qquad \text{(E-36)}$$

where W_R' = number of 18-kip [80 kN] ESALs at design reliability level R

Z = standard deviate from normal distribution table for a given level of reliability (e.g., Z = 1.28 for R = 90 percent)

S_o = overall standard deviation of traffic and performance

FIELD VERIFICATION OF NEW MODELS

Data were obtained from various databases, including the original two-year AASHO Road Test [2], the extended AASHO Road Test [12], and the RPPR database developed for the FHWA by Smith, et al. [6] This database provides performance data from sections with various base types, subgrades, climates and designs.

First, data from several JPCP sections from the two-year AASHO Road Test were obtained from loops 4, 5 and 6 for slabs thicknesses of 5, 6.5, 8 and 9.5 in [127,

165, 203, and 241 mm]. The number of 18-kip [80 kN] ESALs (log W) were predicted from the initial serviceability (P1) to a terminal serviceability of either P2 = 2.5 or whatever P2 was recorded at the end of the test traffic. The actual number of ESALs were computed from the traffic data on each section. The results shown in Figure E-12 indicate a reasonable prediction of log W.

Next, data for AASHO test sections left under traffic on I-80 from 1962 to 1974 were used to predict the performance of the sections using the new model. The number of ESALs were predicted from an initial serviceability to the serviceability level in 1974. The actual number of ESALs were computed by the Illinois DOT using truck volume and weight data from I-80.

The results for these JPCP are shown in Table E-5. The terminal serviceability value must be adjusted if there is significant faulting of the transverse joints, which occurred on the 8 and 9.5 in [203 and 241 mm] slabs over this time period. Since any equation derived using AASHO Road Test data does not include joint faulting, the life predictions must be adjusted if a pavement actually shows significant faulting since faulting has a major effect on rideability and thus the serviceability index.

Adjustments for faulting were made and are shown in Table E-5. elationships between joint faulting and IRI and serviceability rating and IRI were used. [10] First, the mean faulting was converted to an IRI (considering only faulting). Then the IRI was converted to a serviceability rating. This serviceability rating would occur if only that amount of faulting existed. The difference between this level of serviceability and the measured serviceability level is from other causes.

The prediction of ESALs for a given loss of serviceability appears reasonable except for the thickest slabs.

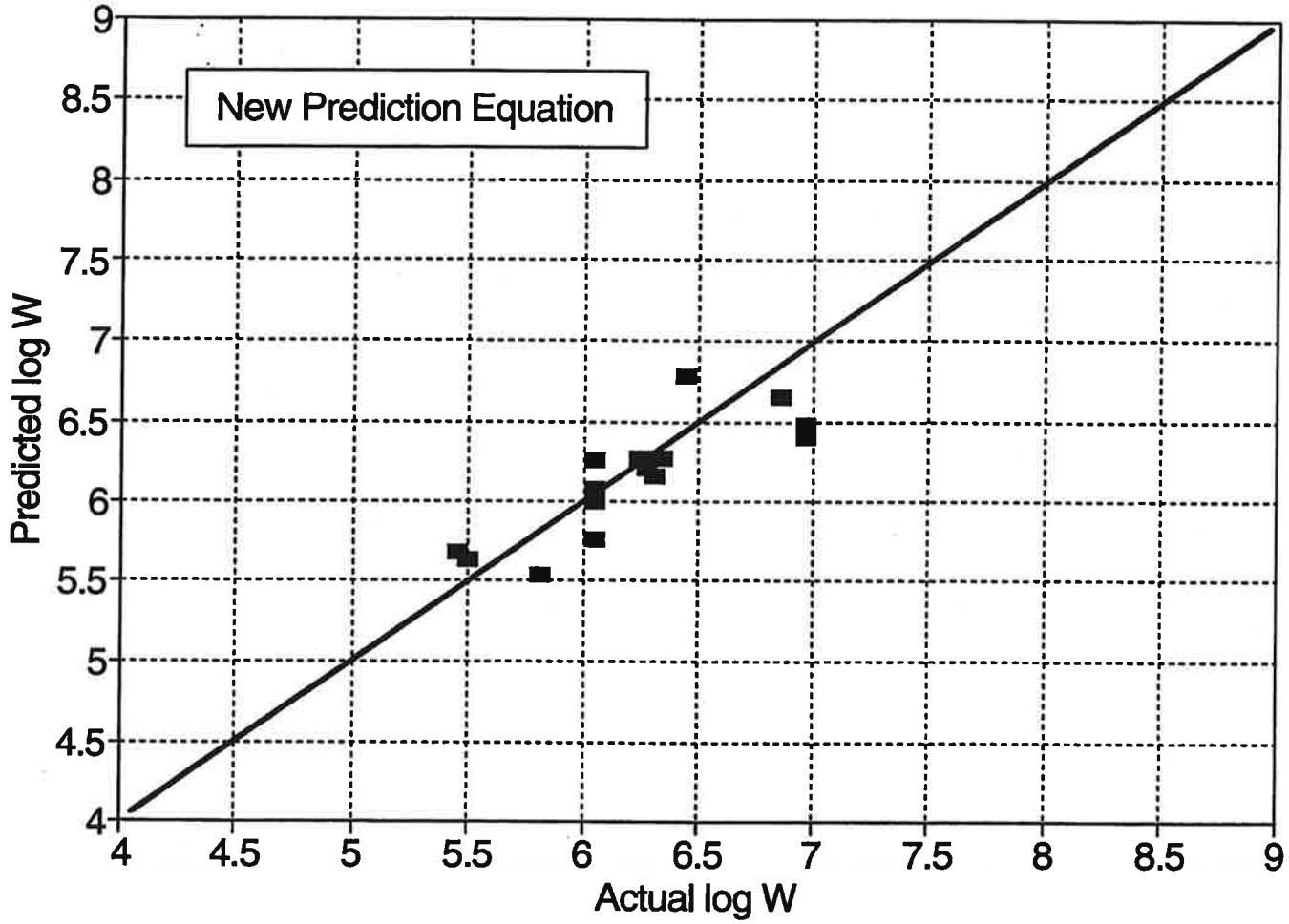

Figure E-12. Predicted versus actual log W for test sections from the two-year AASHO Road Test using the proposed revised concrete pavement design model.

Table E-5. Predicted versus actual ESALs for seven groups of JPCP sections from the extended AASHO Road Test (1958-1974).

ID Location	AASHO I-80	AASHO I-80	AASHO I-80	AASHO I-80	AASHO I-80	AASHO I-80	AASHO I-80
D, in	8	9.5	9.5	9.5	11	11	12.5
S'_c, psi	690	690	690	690	690	690	690
E_c, M psi	4.2	4.2	4.2	4.2	4.2	4.2	4.2
Jt Spacing (ft)	15 Dowel	15 Dowel	15 Dowel	15 Dowel	15 Dowel	15 Dowel	15 Dowel
Base type	Agg.	Agg.	Agg.	Agg.	Agg.	Agg.	Agg.
E_b, psi	25,000	25,000	25,000	25,000	25,000	25,000	25,000
H_b, in	6	6	6	6	6	6	6
k value, psi/in	110	110	110	110	110	110	110
TD, °F	7.2	8.1	8.1	8.1	9.0	9.0	9.6
Measured P2	1.7	2.8	3.1	3.2	3.1	3.4	3.6
Faulting, in	0.25	0.05	0.07	0.08	0.03	0.05	0.03
P2 without Faulting	3.4	2.9	3.4	3.6	3.1	3.5	3.6
Actual ESALs, millions	11.2	11.3	13.8	17.8	14.1	18.9	19.5
Predicted ESALs, millions	4.3	17.1	12.5	9.7	40.2	30.3	59.6

1 in = 25.4 mm, 1 ft = 0.305 m, 1 psi = 6.89 kPa, 1 psi/in = 0.27 kPa/mm. 1°F = 0.55°C

The terminal serviceability was adjusted upward if faulting was significant. This was accomplished as follows for the 8-in [203 mm] slab, for example:

Mean transverse joint faulting = 0.25 in [6.35 mm]
Terminal serviceability level (including faulting effect) = 1.7
Total loss in PSI = 4.5 - 1.7 = 2.8
Total loss in PSI = Loss due to faulting + Loss from other causes = 2.8
Loss due to faulting only:
IRI for faulting only (cm/km) = 35.8 * FAULT (mm) = 227 cm/km
PSI for faulting only = $5\ e^{-(0.0026*IRI)} = 2.8$
Loss in PSI caused only by faulting = 4.5 - 2.8 = 1.7
Therefore, loss in PSI from other causes = 2.8 - 1.7 = 1.1
Therefore, terminal PSI with effect of faulting excluded = 4.5 - 1.1 = 3.4

Next, pavement sections from several different states were obtained from the RPPR database [6] and the same computations were made. Table E-6 shows some of these results. Some of the comparisons look reasonable while others are far apart.

A plot of predicted log W versus actual traffic log W for all three sets of data is shown in Figure E-13. Again, a reasonable scatter of data about the 1:1 line is obtained indicating reasonable predictions.

SENSITIVITY OF PROPOSED AASHTO CONCRETE PAVEMENT DESIGN MODEL

A sensitivity analysis was conducted to show the relative effects of the design features, particularly those related to pavement support, on slab thickness and traffic loadings. The results of the sensitivity analysis are given in the main report in Chapter 2.

COMPARISON WITH 1993 AASHTO DESIGN PROCEDURE

A comparison was between the proposed revised design procedure and the existing AASHTO procedure. These results are also given in the main report.

NEW DESIGN TABLES

The new design equations are too complex to put into nomograph form as was done with the original equation in 1961 and later versions. However, the new design equations can easily be solved in a spreadsheet or computer program. Tables E-6 and E-7 are examples of tables which could easily be generated to determine slab thickness requirements for various design inputs. Any agency could prepare similar tables customized to the agency's own design conditions using a spreadsheet or computer program.

Table E-6. Predicted versus actual ESALs for pavement sections from the RPPR database.

ID/ Location	CA 1-3 Tracy, CA	AZ 1-1 Phoenix, AZ	NY 1-6 Catskill, NY	ONT 2 Toronto, ONT
D, in	8.4	9	9	9
S'_c, psi	672	687	600	700
E_c, psi	4,000,000	4,000,000	4,200,000	4,000,000
Joint spacing, ft	12-19 No Dowels	13-17 No Dowels	20 Dowels	12-19 Dowels
Base type	CTB	CTB	Aggregate	CTB
E_b, psi	800,000	800,000	25,000	1,000,000
H_b, in	5.5	6	3	6
k value, psi/in	175	273	275	150
TD, °F	9.2	11.5	5.2	5.3
Measured P2	3.2	3.5	3.9	3.9
Mean faulting, in	0.10	0.08	0.03	0.01
P2 w/o faulting	3.2	3.5	3.9	3.9
Actual ESALs, millions	7.6	3.1	3.1	35.6
Predicted ESALs, millions	3.7	3.1	5.5	19.7

1 in = 25.4 mm, 1 psi = 6.89 kPa, 1 ft = 0.3 m, 1 psi/in = 0.27 kPa/mm, 1°F = 0.55°C

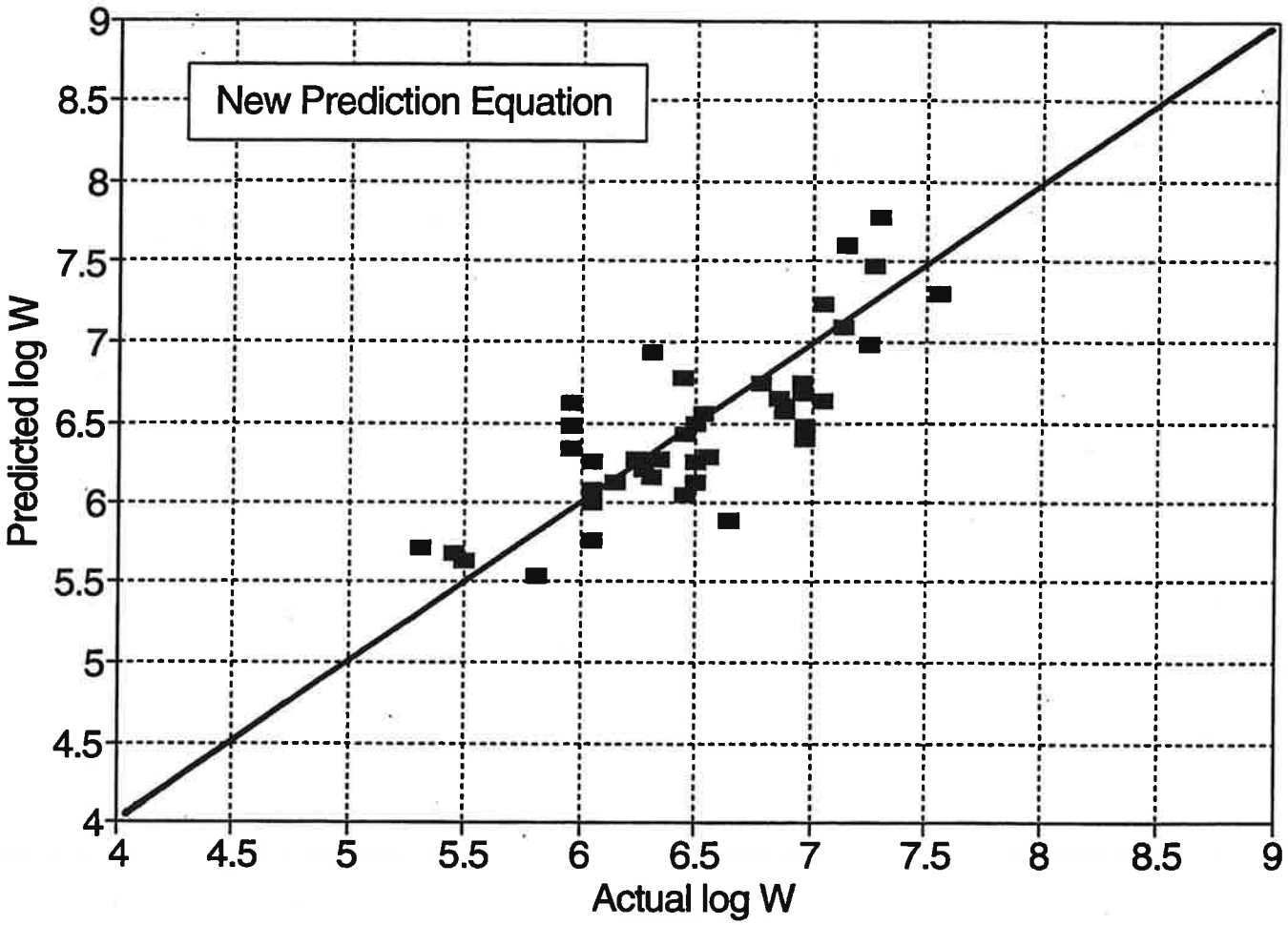

Figure E-13. Predicted versus actual log W for test sections from the 2-year AASHO Road Test, the 14-year extended tests on I-80 and other data from North America using the proposed revised concrete pavement design model.

Table E-7. Slab thickness required for given inputs for untreated aggregate base.

k value psi/in	100	100	100	250	250	250	500	500	500
Design Lane ESAL	S'_c 600 psi	S'_c 700 psi	S'_c 800 psi	S'_c 600 psi	S'_c 700 psi	S'_c 800 psi	S'_c 600 psi	S'_c 700 psi	S'_c 800 psi
1	7.5	6.9	6.4	6.5	6.0*	6.0*	6.0*	6.0*	6.0*
2.5	8.8	8.1	7.5	8.1	7.4	6.8	6.0*	6.0*	6.0*
5	9.8	9.0	8.4	9.5	8.6	7.9	8.6	7.7	6.8
10	10.9	10.0	9.3	10.9	9.9	9.1	10.8	9.7	8.8
20	12.1	11.1	10.3	12.4	11.3	10.4	13.0	11.6	10.5
30	12.8	11.8	10.9	13.5	12.1	11.2	14.4	12.8	11.6
40	13.4	12.3	11.4	14.1	12.8	11.7	15.3	13.6	12.4
50	13.8	12.7	11.8	14.6	13.3	12.2	16.1	14.3	13.0
75	14.7	13.5	12.5	15.7	14.2	13.1	17.6	15.6	14.1
100	15.3	14.1	13	16.5	14.9	13.7	18.7	16.6	15.0

1 in = 25.4 mm, 1 psi/in = 0.27 kPa/mm, 1 psi = 6.89 kPa

* Minimum slab thickness of 6.0 in [152 mm] recommended

ESAL = design lane (millions)

k value = elastic value of subgrade/embankment

P1 - P2 = 2.0

Joint spacing = 15 ft [4.6 m]

Untreated aggregate base: H_b = 6 in [152 mm], E_b = 25,000 psi [172 MPa], f = 1.5

S'_c = mean 28-day, third-point loading

$E_c = 26454 * Sc^{0.77}$

Design reliability = 90 percent (So = 0.39)

Lane width = 12 ft [3.66 m], no tied concrete shoulders

Effective positive DT = 14.06 - (55.29/D) for AASHO Road Test site climate

Table E-8. Slab thickness required for given inputs for treated aggregate base.

k value psi/in	100	100	100	250	250	250	500	500	500
Design Lane ESAL	S'_c 600 psi	S'_c 700 psi	S'_c 800 psi	S'_c 600 psi	S'_c 700 psi	S'_c 800 psi	S'_c 600 psi	S'_c 700 psi	S'_c 800 psi
1	6.2	6.0*	6.0*	6.0*	6.0*	6.0*	6.0*	6.0*	6.0*
2.5	7.9	7.3	6.9	6.0*	6.0*	6.0*	6.0*	6.0*	6.0*
5	8.9	8.3	7.8	8.8	8.1	7.6	8.6**	7.9**	7.4**
10	9.9	9.3	8.8	10.2	9.5	8.9	9.8**	9.1	8.4
20	11.0	10.3	9.7	11.5	10.8	10.1	11.9	11.1	10.3
30	11.6	10.9	10.3	12.3	11.5	10.8	13.0	12.0	11.2
40	12.0	11.3	10.7	12.9	12.0	11.3	13.7	12.7	11.9
50	12.4	11.6	11.0	13.3	12.4	11.7	14.2	13.2	12.4
75	13.0	12.2	11.6	14.1	13.2	12.4	15.2	14.1	13.2
100	13.5	12.7	12.0	14.7	13.7	12.9	15.9	14.8	13.8

1 in = 25.4 mm, 1 psi/in = 0.27 kPa/mm, 1 psi = 6.89 kPa

* Minimum slab thickness of 6.0 in [152 mm] recommended. ** Estimated values.

ESAL = design lane (millions)

k value = elastic value of subgrade/embankment

P1 - P2 = 2.0

Joint spacing = 15 ft [4.6 m]

Treated aggregate base: H_b = 4 in [102 mm], E_b = 800,000 psi [5512 MPa], f = 35

S'_c = mean 28-day, third-point loading

$E_c = 26454 * Sc^{0.77}$

Design reliability = 90 percent (So = 0.39)

Lane width = 12 ft [3.66 m], no tied concrete shoulders

Effective positive DT = 14.06 - (55.29/D) for AASHO Road Test site climate

Note that these tables were developed assuming that there will be no significant joint faulting that would reduce the serviceability level, thereby reducing the number of axle loads that the pavement can carry. A design check for faulting is presented in the next section.

DESIGN OF JOINT LOAD TRANSFER TO CONTROL FAULTING

Because all joints were adequately dowelled at the Road Test, no significant faulting occurred during the two-year test:

> "One joint faulted seriously, but investigation showed that the joint had been accidentally sawed at some distance beyond the end of the dowels intended to protect it. Over the 2-year period of the test there were no other cases of measurable faulting at joints, all of which were dowelled." [2]

If the joints had not been properly dowelled, a large amount of faulting would have occurred. Faulting is one of the most important distresses affecting rideability and serviceability. Therefore, any pavement that faults significantly will have reduced serviceability and carry fewer traffic loads to terminal serviceability. The current (1993) AASHTO design concept is to design for different load transfer levels by selection of the J factor. A higher J factor will result in an increase in slab thickness according to the 1993 AASHTO equation. However, field studies have demonstrated that slab thickness does not affect faulting significantly. [6, 12] Thus, significant faulting must be prevented through good joint load transfer, joint spacing, base design, and subdrainage design, not through increased slab thickness. The following procedure is recommended to determine the adequacy of a proposed joint load transfer design.

STEP 1: The required slab thickness is determined. This requires the selection of several key joint design features, including joint spacing, base stiffness and friction (both a function of base type), and type of load transfer. The check for cracking due to joint loading is conducted as well. The joint design features may be modified if necessary and a redesign made to achieve an acceptable joint design to prevent cracking.

STEP 2: The joint design details required for the joint faulting check include base type, joint spacing, subdrainage presence, and diameter and spacing of dowels, if used.

STEP 3: Mean joint faulting is predicted using the faulting prediction models from Reference 6, given below, and the adequacy of the design to control faulting below an acceptable level is evaluated.

Faulting Model for Doweled Joints [6]:

$$DFAULT = ESAL^{0.5280}\left[0.1204 + 0.04048\left(\frac{BSTRESS}{1000}\right)^{0.3388} + 0.007353\left(\frac{L}{10}\right)^{0.6725} - 0.1492\left(\frac{k}{100}\right)^{0.05911} - 0.01868\,DRAIN - 0.00879\,EDGESUP - 0.00959\,STYPE\right] \quad \text{(E-37)}$$

where DFAULT = mean transverse doweled joint faulting, in

ESAL = cumulative equivalent 18-kip [80 kN] single-axle loads, millions

BSTRESS = maximum concrete bearing stress from closed-form equation, psi:

$$BSTRESS = f_d\, P\, T \left[\frac{K_d\,(2 + BETA * OPENING)}{4\ E_s\ I\ BETA^3} \right] \quad \text{(E-38)}$$

$$BETA = \sqrt[4]{\frac{K_d\ DOWEL}{4\ E_s\ I}} \quad \text{(E-39)}$$

f_d = distribution factor = 2 * 12 / (ℓ + 12)

ℓ = radius of relative stiffness, in

I = moment of inertia of dowel bar cross-section, in^4:

$$I = 0.25\ \pi \left(\frac{DOWEL}{2} \right)^4 \quad \text{(E-40)}$$

P = applied wheel load, set to 9000 lbf [40 kN]

T = percent transferred load, set to 0.45

K_d = modulus of dowel support, set to 1,500,000 psi/in [405 MPa/mm]

BETA = relative stiffness of the dowel-concrete system

DOWEL = dowel diameter, in

E_s = modulus of elasticity of the dowel bar, psi

k = modulus of subgrade reaction, psi/in

OPENING = average transverse joint opening, in:

$$OPENING = 12 * CON * L * \left(\frac{ALPHA * TRANGE}{2 + e} \right) \quad \text{(E-41)}$$

L = average transverse joint spacing, ft

CON = adjustment factor due to base/slab frictional restraint,

= 0.65 if stabilized base

= 0.80 if aggregate base or lean concrete base with bond breaker

ALPHA = PCC thermal expansion coefficient, set to 0.000006/°F [0.000011/°C]

TRANGE = annual temperature range, °F

e = PCC drying shrinkage coefficient, set to 0.00015 strain;

DRAIN = index for drainage condition,

= 0, if no edge subdrain exists

= 1, if edge subdrain exists

EDGESUP = index for edge support

= 0, if no edge support exists

= 1, if edge support exists

STYPE = index for AASHTO subgrade soil classification,

= 0, if A-4 to A-7

= 1, if A-1 to A-3

Faulting Model for Undowelled Joints [6]:

$$UNFAULT = ESAL^{0.25}\left[0.000038 + 0.0183\,(100 * OPENING)^{0.5585} + 0.000619\,(100 * DEFLAMI)^{1.7229} + 0.04\left(\frac{FI}{100}\right)^{1.9840} + 0.00565\,BTERM - 0.0077\,EDGESUP - 0.00263\,STYPE - 0.00891\,DRAIN\right] \quad \text{(E-42)}$$

where UNFAULT = mean transverse undowelled joint faulting, in

$$DEFLAMI = \frac{P\left(1.2 - 0.88 * 1.4142\,\frac{a}{\ell}\right)}{k\,\ell^2} \qquad \text{(E-43)}$$

BTERM = base type factor:

= $10 * [\ ESAL^{0.2076} * (\ 0.04546 + 0.05115 * GB + 0.007279 * CTB$

$+ 0.003183 * ATB - 0.003714 * OGB - 0.006441 * LCB\ )\ ]$

GB = dummy variable for dense-graded aggregate base,

= 1 if aggregate base

= 0 otherwise

CTB = dummy variable for dense-graded, cement-treated base,

= 1 if cement-treated base

= 0 otherwise

ATB = dummy variable for dense-graded, asphalt-treated base,

= 1 if asphalt-treated base

= 0 otherwise

OGB = dummy variable for open-graded aggregate base,

or open-graded asphalt-treated base,

= 1 if open-graded base

= 0 otherwise

LCB = dummy variable for lean concrete base,

= 1 if lean concrete base

= 0 otherwise

FI = freezing index, Fahrenheit degree-days

All other variables are the same as defined before for DFAULT.

Tables E-9, E-10, and E-11 were prepared using Equations E-37 and E-42 to show the faulting predictions for pavements with and without dowel bars. The mean joint faulting is predicted and compared with recommended critical levels. If the predicted faulting is greater than the recommended level, an adjustment to joint design is made. Adjustments include use of dowels, or if dowels already exist, an increase in the diameter, selection of a different base type and permeability, and a decrease in the joint spacing (for undowelled joints). Slab thickness is not adjusted because it has only a minimal effect on joint faulting.

Table E-9. Mean joint faulting predictions for dowelled jointed plain concrete pavement using Equation E-37.

ESALs millions	No Tied Concrete Shoulders			Tied Concrete Shoulders		
	Dow. Dia. 1.00 in	Dow. Dia. 1.25 in	Dow. Dia. 1.50 in	Dow. Dia. 1.00 in	Dow. Dia. 1.25 in	Dow. Dia. 1.50 in
1	0.02	0.01	0.01	0.01	0.00	0.00
2.5	0.03	0.02	0.01	0.02	0.01	0.00
5	0.04	0.03	0.02	0.02	0.01	0.00
10	0.06	0.04	0.02	0.03	0.01	0.00
20	0.09	0.06	0.03	0.05	0.02	0.00
30	0.12	0.07	0.04	0.06	0.02	0.00
40	0.13	0.08	0.05	0.07	0.02	0.00
50	0.15	0.09	0.05	0.08	0.03	0.00
75	0.19	0.12	0.07	0.10	0.03	0.00
100	0.22	0.14	0.08	0.12	0.04	0.00

Values shown in table are mean predicted joint faulting, in [1 in = 25.4 mm]

Joint spacing = 15 ft [4.6 m]
k-value = 100 psi/in [27 kPa/mm]
Base type = not a factor
Slab thickness = 9 in [229 mm]
Subdrains = 1 (yes)
TRANGE = 85°F (July max - January min)
Subgrade = 0 (fine)
S'_c = 700 psi [4.8 MPa]

Table E-10. Mean joint faulting predictions for dowelled jointed reinforced concrete pavement using Equation E-37.

ESALs millions	No Tied Concrete Shoulders			Tied Concrete Shoulders		
	Dow. Dia. 1.00 in	Dow. Dia. 1.25 in	Dow. Dia. 1.50 in	Dow. Dia. 1.00 in	Dow. Dia. 1.25 in	Dow. Dia. 1.50 in
1	0.03	0.02	0.02	0.02	0.01	0.01
2.5	0.05	0.04	0.03	0.04	0.02	0.01
5	0.07	0.05	0.04	0.05	0.03	0.02
10	0.10	0.08	0.06	0.07	0.05	0.03
20	0.15	0.11	0.09	0.11	0.07	0.04
30	0.18	0.14	0.11	0.13	0.09	0.05
40	0.21	0.16	0.13	0.15	0.10	0.06
50	0.24	0.18	0.14	0.17	0.11	0.07
75	0.30	0.23	0.17	0.21	0.14	0.09
100	0.35	0.26	0.20	0.25	0.16	0.10

Values shown in table are mean predicted joint faulting, in [1 in = 25.4 mm]

Joint spacing = 45 ft [13.7 m]
k-value = 100 psi/in [27 kPa/mm]
Base type = not a factor
Slab thickness = 9 in [229 mm]
Subdrains = 1 (yes)
TRANGE = 85°F (July max - January min)
Subgrade = 0 (fine)
S'_c = 700 psi [4.8 MPa]

Table E-11. Mean joint faulting predictions for undowelled jointed plain concrete pavement using Equation E-42.

ESAL million	Aggregate Base		Asphalt-Treated Base		Lean Concrete Base		Open-Graded Base	
	Jt Sp 15 ft	Jt Sp 20 ft	Jt Sp 15 ft	Jt Sp 20 ft	Jt Sp 15 ft	Jt Sp 20 ft	Jt Sp 15 ft	Jt Sp 20 ft
1	0.06	0.07	0.06	0.07	0.06	0.06	0.06	0.06
2.5	0.08	0.09	0.07	0.08	0.07	0.08	0.07	0.08
5	0.10	0.11	0.09	0.10	0.08	0.10	0.09	0.10
10	0.12	0.14	0.11	0.12	0.10	0.12	0.10	0.12
20	0.15	0.17	0.13	0.15	0.12	0.14	0.12	0.14
30	0.17	0.19	0.15	0.17	0.14	0.16	0.14	0.16
40	0.18	0.20	0.16	0.18	0.15	0.17	0.15	0.17
50	0.19	0.21	0.17	0.19	0.16	0.18	0.16	0.18
75	0.21	0.24	0.19	0.21	0.18	0.20	0.18	0.20
100	0.23	0.26	0.21	0.23	0.19	0.21	0.19	0.22

Values shown in table are mean predicted joint faulting, in [1 in = 25.4 mm]

Joint spacing = 15 or 20 ft [4.6 or 6.1 m]
Slab thickness = 9 in [229 mm] Subgrade = 0 (fine)
k-value = 100 psi/in [27 kPa/mm] Subdrains = 1 (yes) S'_c = 700 psi [4.8 MPa]
Edge support = 1 (yes) TRANGE = 85°F (July max - January min)
Freezing Index = 600 F degree-days

Critical faulting levels for design purposes are suggested as shown in Table E-12. Of course, each agency should select levels that fit its particular needs. These critical levels were derived from extensive field data from Reference 12. The mean faulting was computed for pavements with a serviceability of 3.0 or less. For example, based upon data from many short-jointed JPCP sections, a mean joint faulting of 0.12 in [3 mm] corresponded to a serviceability index of 3.0 or less. [12] For long-jointed JRCP the mean faulting level was 0.26 in [6.6 mm]. [12] The recommended critical levels for design were selected as fifty percent of these values.

Table E-12. Recommended critical joint faulting levels for design.

Joint Spacing	Critical Joint Faulting
Less than 25 ft	0.06 in
Greater than 25 ft	0.13 in

1 ft = 0.305 m, 1 in = 25.4 mm

The slab design may need adjustment after the joint design is completed, especially if the joint spacing is reduced or the base type is changed to reduce expected faulting.

Example joint design check. A JPCP is located in a cold climate, similar to the Chicago, Illinois area. The pavement has a 15-ft [4.6 m] joint spacing, untreated aggregate base, and no dowel bars. Assuming the pavement was designed for 5 million ESALs, a slab thickness of about 9 in [229 mm] is required using the proposed revised AASHTO design procedure.

Checking the joint faulting design with Table E-11 shows that the mean predicted faulting is 0.10 in [2.5 mm]. This faulting is greater than the 0.06 in [1.5 mm] limit recommended in Table E-12, thus the joint design is inadequate.

One possible design modification would be to specify 1.25-in-diameter [32 mm] dowels. Table E-9 shows that with 1.25-in [32 mm] dowels the mean predicted faulting is 0.03 in [0.8 mm], which is below the 0.06 in [1.5 mm] limit, thus this design is acceptable.

Another possible design modification would be to specify a lean concrete base course with no dowel bars. The mean predicted faulting for this design is 0.08 in [2 mm], still above the recommended limit. Of course, other design modifications could be analyzed.

DESIGN OF THE BASE COURSE

The base course is considered a structural layer in the proposed revision to the AASHTO design procedure, as opposed to the current AASHTO procedure in which the base is consider a part of the foundation and thus affects the k value input. In the proposed revision to the design procedure, a coefficient of friction between the slab and base is also an input. An equation was developed, using the results of many 3DPAVE runs, for slab stress due to midslab loading assuming full friction (i.e., a "bonded" interface). The stress in the slab due to a degree of friction less than full friction is computed by multiplying the full friction stress by an adjustment factor which is a function of the slab thickness, base modulus, and friction coefficient. The equation for the friction adjustment factor was also developed using the results of a factorial of 3DPAVE runs.

Ranges of values for friction coefficients for a variety of base types and interface treatments were given in Table E-3, summarized from the available literature. Most of the available data on slab/base interface friction comes from laboratory tests in which small-scale concrete slabs are constructed on bases and pushed horizontally with a measured force. The vertical force in such tests is

generally only the weight of the slab. How well such tests represent field conditions, in which full-scale slabs also bend under the weight of applied loads, is not clear. It is also not clear at this time how much the friction coefficient of various bases and interface treatments change over time and how a coefficient that best represents the typical value over the service life of the pavement should be selected. The addition of a friction coefficient as an explicit input to the slab thickness design process is believed to be a significant improvement to the AASHTO design procedure and a significant need in any mechanistic design procedure. However, long-term field performance studies data are essential to better establish how slab/base interface friction over the life of the pavement should be characterized.

Friction between the slab and base affects the amount of erosion between the layers also. A high degree of friction will greatly reduce or eliminate erosion between the slab and the base. Reasonable friction of the slab to almost any type of base course can be achieved without extraordinary means. To avoid reflection cracking in a slab due to high friction with a cement-treated or lean concrete base, transverse and longitudinal joints should be cut in the base to a depth of approximately one fourth of the thickness of the base prior to slab placement. Joints are not needed in asphalt-treated bases.

The friction between the slab and base is also an input to the calculation of stress due to joint (corner) loading. A check on this stress is included in the proposed revision to the design procedure to identify situations in which the corner loading position might control the design. This is described in the next section.

The effect of the base is directly considered in joint design as well as the slab thickness design. If the initial joint design and base features are not adequate to control faulting below a design value, revisions must be made to the load transfer system and/or the base and subdrainage.

The design procedure allows for a range of coefficient of friction inputs so that the designer can use a low value if measures are taken to reduce friction, such as polyethylene sheeting.

For the corner position, maintenance of high friction is believed to be more tenuous and may decline over time. Analyses conducted with the 3DPAVE shows that the coefficient of friction has a significant effect on the critical stress for joint loading position. This is illustrated in Figure E-14.

The effect of a widened base layer where the base extends beyond the edge of the concrete slab was also studied using 3DPAVE. The maximum tensile stresses were computed for the midslab load position both with and without a widened base of 12 inches [305 mm]. The results are summarized in Table E-13. They show that with a treated base (modulus over 200,000 psi [1378 MPa] and no temperature differential in the slab, the stress ratio (with widened base versus without widened base) ranges from 0.91 to 0.97. When there is a positive temperature differential of 21°F [11.7°C] the ratio ranges from 0.98 to 1.00. These results suggest that when the a temperature differential is present, the benefit of a widened stiff base is diminished. Therefore, no adjustment for a widened base has been proposed.

DESIGN CHECK FOR CRITICAL JOINT LOAD POSITION STRESSES

The proposed revised design procedure uses the midslab loading position shown in Figure E-3 because this was the critical position (maximum stress) at the AASHO Road Test. This occurred because all of the transverse joints were well dowelled and thus had good load transfer. Strain measurements from Loop 1 showed that the maximum stress in the slab under vibratory loading occurred "along the pavement edge with the center of the outer loaded area at the distance of 1 ft from the edge and 4 to 6 ft from the nearest transverse joint." [11] This maximum

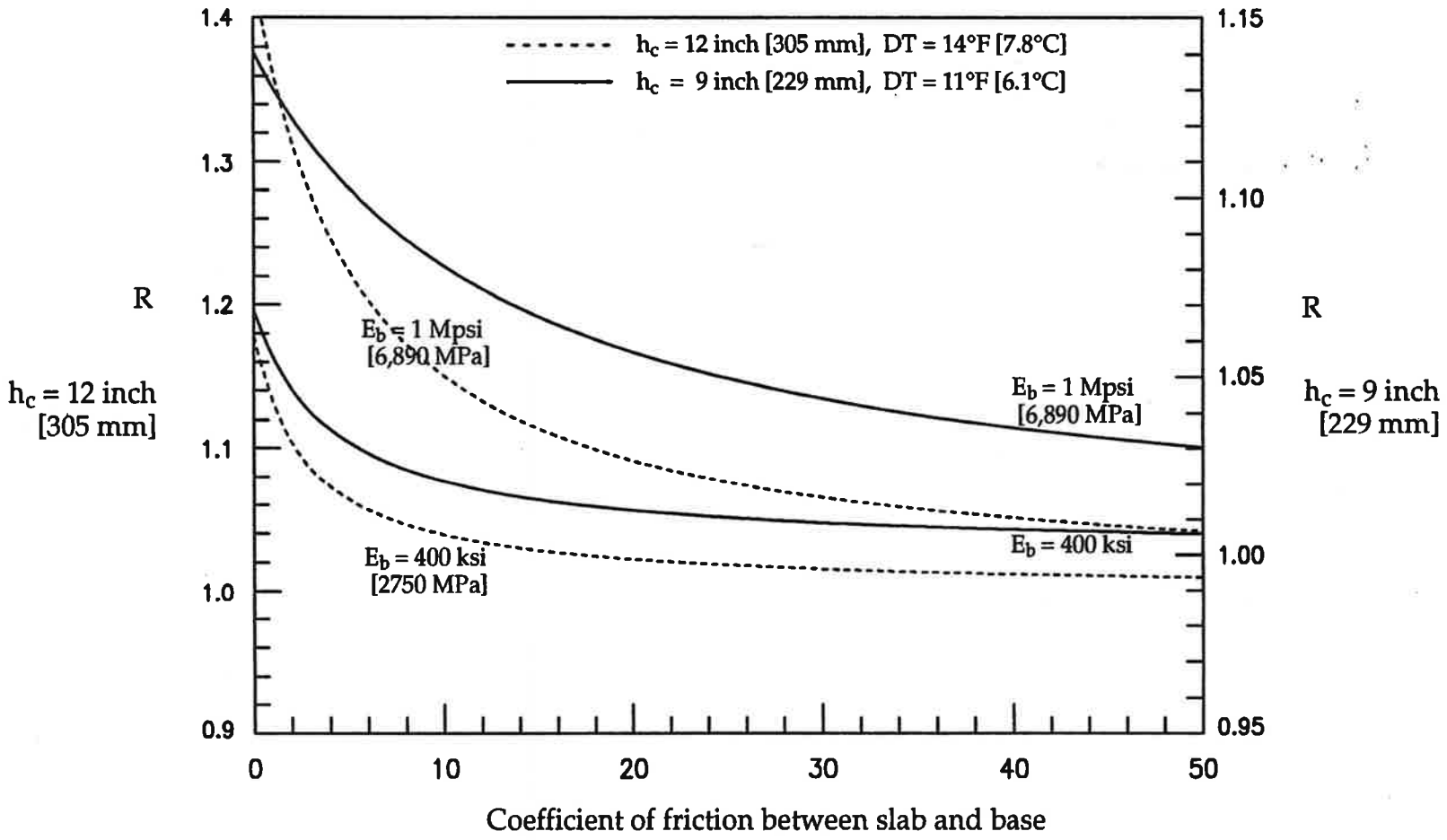

Note : $R = \sigma_f / \sigma_{full\ friction}$
h_b = 5 inch [127 mm] , k = 200 psi/in [54 kPa/mm],
Joint loading with nighttime curling DT

Figure E-14. **Effect of slab thickness, base modulus, and friction coefficient on ratio of stress computed with friction coefficient to stress computed with full friction, for joint loading and nighttime temperature gradient.**

Table E-13. Effect of base widening on critical stress in slab for midslab loading position using 3DPAVE.

WIDENED BASE

Epcc=4M	Hc = 7 in	DT = 0			
k	Ebase	hbase	Conventional	Widened base	wb/b
100	25000	4.0	279	273	0.98
100	25000	8.0	273	262	0.96
100	200000	4.0	239	226	0.95
100	200000	8.0	190	176	0.93
100	1000000	4.0	142	130	0.92
100	1000000	8.0	72	65	0.91
200	25000	4.0	238	233	0.98
200	25000	8.0	235	227	0.96
200	200000	4.0	204	195	0.95
200	200000	8.0	167	156	0.93
200	1000000	4.0	123	114	0.93
200	1000000	8.0	67	61	0.91
500	25000	4.0	196	193	0.98
500	25000	8.0	196	191	0.98
500	200000	4.0	167	162	0.97
500	200000	8.0	141	134	0.95
500	1000000	4.0	102	96	0.94
500	1000000	8.0	60	56	0.93

Epcc=4M	Hc = 7 in	DT = 21			
k	Ebase	hbase	Conventional	Widened base	wb/b
100	25000	4.0	472	463	0.98
100	25000	8.0	464	463	1.00
100	200000	4.0	428	424	0.99
100	200000	8.0	383	372	0.97
100	1000000	4.0	325	311.7	0.00
100	1000000	8.0	271	267	0.99
200	25000	4.0	470	471	1.00
200	25000	8.0	464	463	1.00
200	200000	4.0	430	426	0.99
200	200000	8.0	387	378	0.98
200	1000000	4.0	332	326	0.98
200	1000000	8.0	275	274	1.00
500	25000	4.0	459	459	1.00
500	25000	8.0	454	455	1.00
500	200000	4.0	427	426	1.00
500	200000	8.0	388	389	1.00
500	1000000	4.0	338	340	1.01
500	1000000	8.0	282	283	1.00

Epcc=4M	Hc = 13	DT = 0			
k	Ebase	hbase	Conventional	Widened base	wb/b
100	25000	4.0	118	117	0.99
100	25000	8.0	118	116	0.98
100	200000	4.0	109	106	0.97
100	200000	8.0	98	94	0.96
100	1000000	4.0	81	77	0.95
100	1000000	8.0	55	51	0.93
200	25000	4.0	107	106	0.99
200	25000	8.0	108	106	0.98
200	200000	4.0	99	97	0.97
200	200000	8.0	91	87	0.95
200	1000000	4.0	75	71	0.94
200	1000000	8.0	53	49	0.92
500	25000	4.0	90	89	0.99
500	25000	8.0	92	90	0.98
500	200000	4.0	83	81	0.97
500	200000	8.0	78	74	0.95
500	1000000	4.0	64	60	0.94
500	1000000	8.0	47	44	0.93

Epcc=4M	Hc = 13	DT = 39			
k	Ebase	hbase	Conventional	Widened base	wb/w
100	25000	4.0	241	248	1.03
100	25000	8.0	242	252	1.04
100	200000	4.0	240	250	1.04
100	200000	8.0	254	262	1.03
100	1000000	4.0	234	235	1.00
100	1000000	8.0	272	269	0.99
200	25000	4.0	306	315	1.03
200	25000	8.0	304	315	1.04
200	200000	4.0	301	314	1.04
200	200000	8.0	304	316	1.04
200	1000000	4.0	280	284	1.01
200	1000000	8.0	295	294	1.00
500	25000	4.0	415	417	1.01
500	25000	8.0	405	410	1.01
500	200000	4.0	408	413	1.01
500	200000	8.0	395	403	1.02
500	1000000	4.0	365	369	1.01
500	1000000	8.0	346	348	1.00

stress approximately matched the stresses computed from strains measured at the slab edge for midslab loading from truck axles moving at 30 mph [48 km/hr] [2]:

> "For a constant axle weight and slab thickness, it was estimated that the maximum compressive stress at the (top) edge due to edge loading exceeded, in absolute value, the maximum tensile stress due to corner loading by 51 to 112 percent. The exact percentage depended on the thickness of the slab."[2]

Similar results were also obtained with 3DPAVE for the dowelled AASHO pavements. For dowelled load transfer and typical positive and negative temperature differentials as existed at the AASHO Road Test site, the maximum stress is much greater for the midslab loading position. That is why corner breaks are almost never observed for properly dowelled joints, as many field studies have shown. [6, 12]

However, cracks often do occur near the joints in pavements with no mechanical load transfer such as dowels. Under certain design and climatic conditions, truck axle loadings near the transverse joint may produce even higher tensile stresses at the top of the slab than the tensile stresses produced at the bottom of the slab by midslab loading, as illustrated in Figure E-15. These high tensile stresses in the corner region could result in the development of corner breaks, diagonal cracks, or even transverse cracks several feet from the joint. This mechanism has been well analyzed and described by Poblete et al. for undowelled JPCP in Chile. [8, 14] With good load transfer, these stresses decrease significantly.

Given these findings and concerns, a design check for the joint loading position with negative equivalent temperature differentials was developed. The joint loading position shown in Figure E-15 requires a different analysis due to the additive effects of the following contributors to slab stresses.

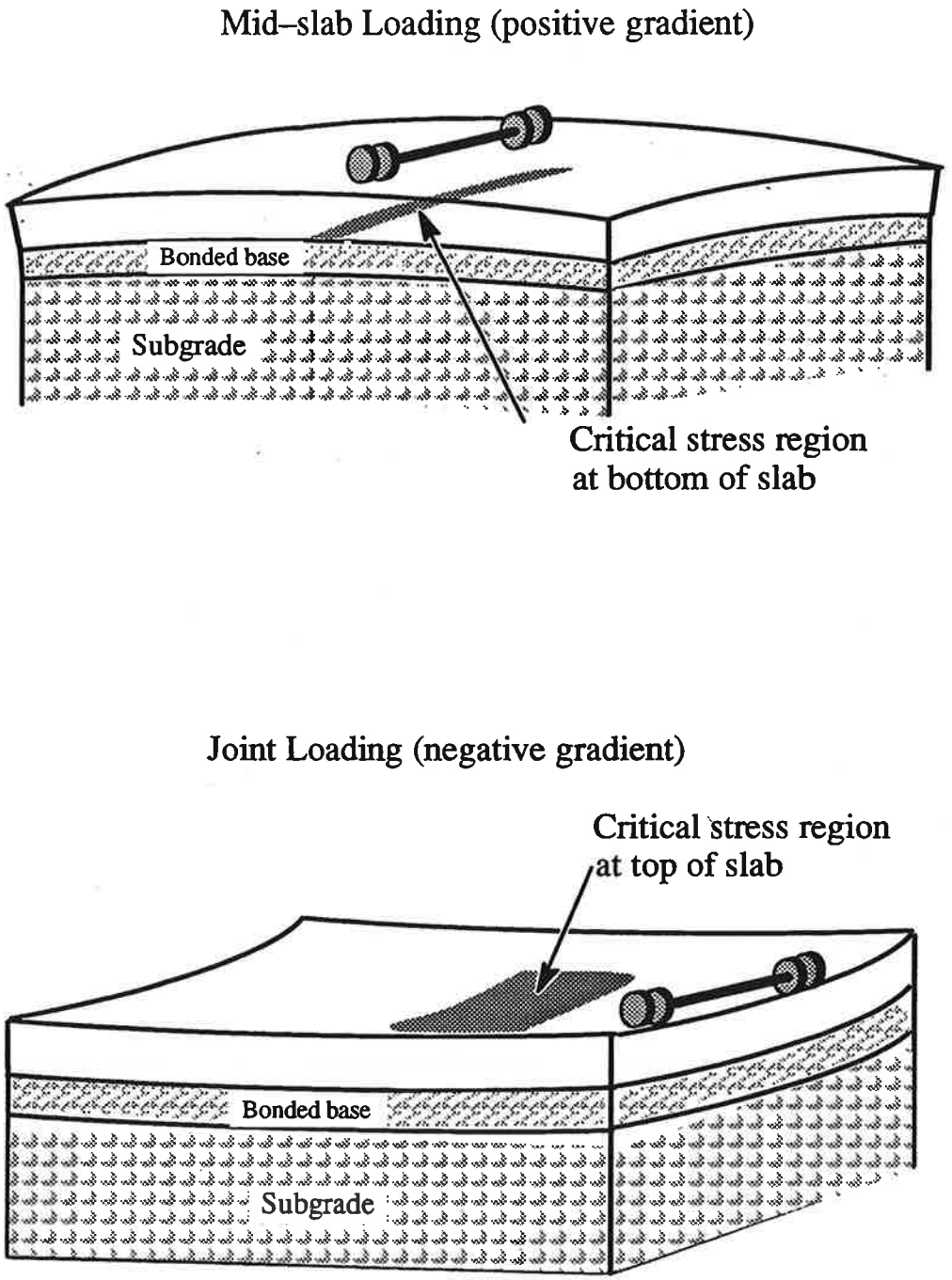

Figure E-15. **Critical location of maximum tensile stresses for the midslab load position and joint load position.**

- **AXLE LOAD STRESS:** When the axle load is near the transverse joint a tensile stress occurs at the top of the slab.

- **NEGATIVE TEMPERATURE DIFFERENTIAL STRESS:** Negative (nighttime) temperature differentials cause corners to curl upward, creating a tensile stress at the slab surface. An effective negative temperature differential stress was computed for each climatic site using a procedure similar to that used for the daytime positive temperature differentials. The results are shown in Table E-14. These data were used to develop the following predictive model for the effective negative temperature differential:

$$effective\ negative\ TD = -18.14 + \frac{52.01}{D} + 0.394\ WIND + 0.07\ TEMP + 0.00407\ PRECIP \quad \text{(E-44)}$$

where effective negative TD = top temperature minus bottom temperature, ^{o}F

D = slab thickness, in

WIND = mean annual wind speed, mph (Figure E-5)

TEMP = mean annual temperature, ^{o}F (Figure E-6)

PRECIP = mean annual precipitation, in (Figure E-7)

Statistics: $R^2 = 0.95$

$\sigma_Y = 0.6^{o}F\ [0.33^{o}C]$

n = 42

- **CONSTRUCTION CURLING STRESS:** Upward curling of corners occurs shortly after concrete slab placement if a high positive temperature differential through the slab is present as the concrete sets. [7, 8] This positive differential occurs particularly on sunny days when conventional curing procedures are

Table E-14. Summary of nighttime negative effective temperature differentials over year for several sites based on equivalent fatigue damage.

Location	6-in Slab	10-in Slab	14-in Slab	Annual Wind Speed (mph)	Annual Temperature (°F)	Annual Precipitation (in)
Urbana IL	-1.7	-5.5	-6.6	11.6	50.8	35
Rockford IL	-2.1	-5.9	-7.1	10.3	48.6	31
Cairo IL	-1.6	-5.4	-6.4	12.0	57	48
Lansing MI	-1.2	-5.0	-6.0	10.6	49.8	30
St. Louis MO	-1.6	-5.4	-6.4	9.5	55.9	36
Fargo ND	-3.5	-7.3	-8.6	13.0	41.4	16
Little Rock AR	-1.8	-5.6	-6.6	8.2	60.5	48
Raleigh NC	-1.1	-4.9	-5.8	7.9	58.9	43
Tallahassee FL	-1.1	-4.9	-5.8	7.5	68.3	54
Syracuse NY	-0.9	-4.7	-5.6	9.9	47.8	36
Sacramento CA	-2.1	-5.9	-7.1	8.5	60.8	17
Salem OR	-0.9	-4.7	-5.7	7.3	48	60
Pendleton OR	-1.3	-5.1	-6.0	7.7	50	20
Las Vegas NV	-2.8	-6.6	-7.8	8.8	65.8	4

Values shown in table are effective negative temperature differential from top to bottom of slab, °F. [1°F = 0.55°C, 1 in = 25.4 mm, 1 mph = 1.61 km/hr]

used. This temperature differential has not been measured extensively in the past and its magnitude is not well known at the present time. [7, 8] This is defined as the temperature differential that would be required to produce a flat slab (note that this is before any moisture shrinkage occurred at the top of the slab).

- **MOISTURE GRADIENT STRESS:** Moisture shrinkage warping of the top of the slab occurs over time. [5, 7, 8, 9] The stress induced by this type of warping can be determined by representing the moisture warping by an equivalent temperature gradient (see Appendix C).

Applied loads and the three climatic factors described above can lead to large tensile stresses at the top of the slab near the joint. Combined stresses from negative temperature differentials and from load can be estimated using 3DPAVE.

Note that the AASHO performance models have built into them an effective negative temperature differential, a moisture shrinkage and construction temperature differential which existed during their construction and over the two year period at the Road Test site. The negative temperature differential can be estimated but the other gradients were apparently not measured and are unknown. The slab stress design check included herein is accomplished by comparing the midslab stress (critical at the AASHO Road Test where the joints were dowelled) with that stress obtained for an undowelled joint loading condition. If the undowelled joint loading stress is greater, then corner breaks, diagonal cracks and even transverse cracks may initiate at the top of the slab first.

Many jointed plain concrete pavements without dowel bars or other mechanical load transfer devices have been constructed in the United States and

other countries. These pavements are often built in warm dry climates (e.g., the Western U.S., Chile, Spain) where the potential for construction curling and moisture shrinkage warping is greater. When the joints are open in cooler weather, the degree of load transfer at the joints provided by aggregate interlock is very low. There is no design check in the current AASHTO design procedure to evaluate this type of design and severe climatic conditions.

Analyses were conducted using 3DPAVE of pavement sections with no load transfer, loaded at the joint position. The maximum stress in the slab due to load and temperature differential was computed and plotted as shown in Figure E-16 for a range of design features. The results showed that under conditions of extreme negative temperature differential and poor load transfer, the tensile stresses due to joint loading can equal or exceed stresses due to midslab loading.

The following procedure was developed to check for critical stress for the joint loading position for pavements that do not have mechanical load transfer devices equivalent to dowel bars. Pavements that have adequate load transfer devices such as properly sized and spaced dowels would not show significantly high stress at the joint.

1. Design the pavement assuming that the midslab loading position is critical.

2. Compute the midslab stress for the required slab thickness using the site's effective positive temperature differential using Equation E-26 and an 18,000-lbf [80 Kn] single-axle load.

3. Estimate a total "equivalent" negative temperature differential from the following sources.

$1^{o}F = 0.55^{o}C$, 1 psi = 6.89 kPa, 1 in = 25.4 mm,
1 lbf = 4.45 N, 1 psi/in = 0.27 kPa/mm

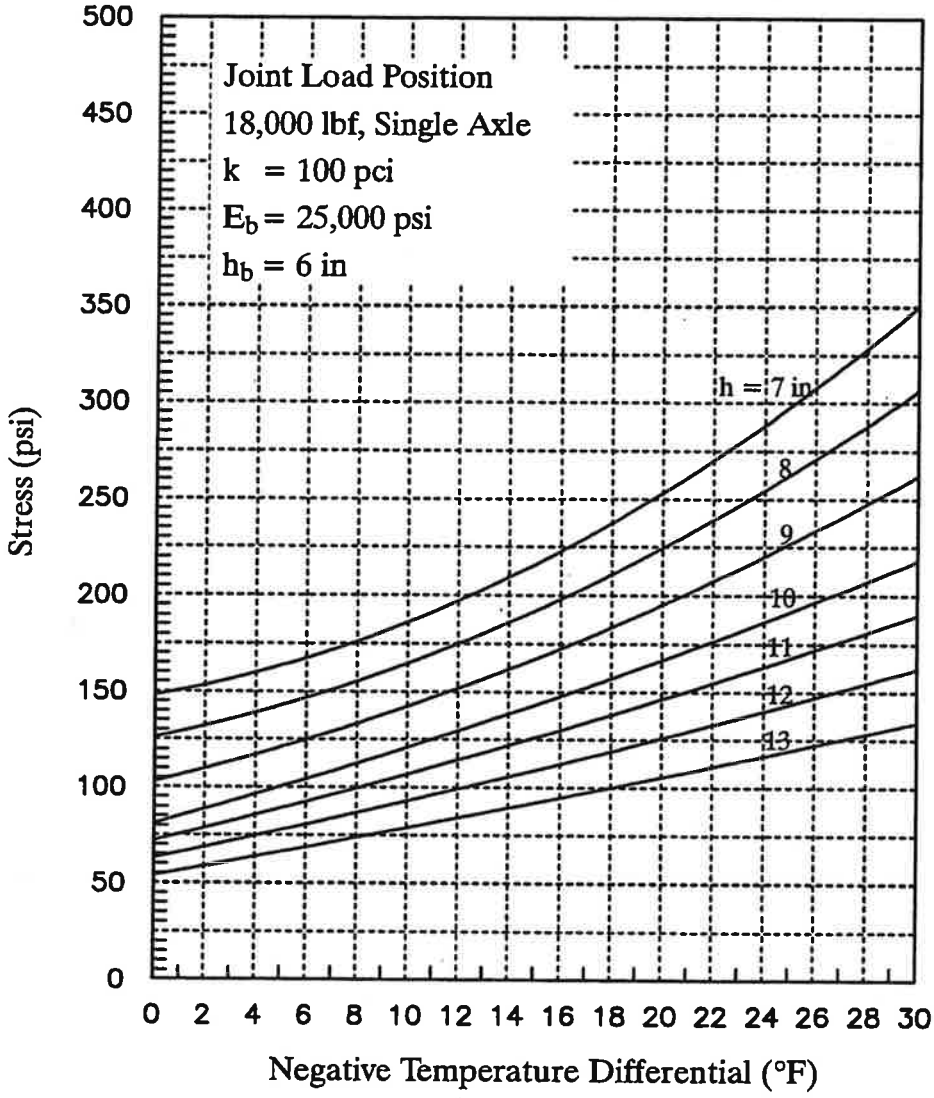

Figure E-16a. Maximum tensile stress on top of slab for joint loading position versus a negative temperature differential through the slab for specific design conditions (aggregate base, soft subgrade).

1°F = 0.55°C, 1 psi = 6.89 kPa, 1 in = 25.4 mm,
1 lbf = 4.45 N, 1 psi/in = 0.27 kPa/mm

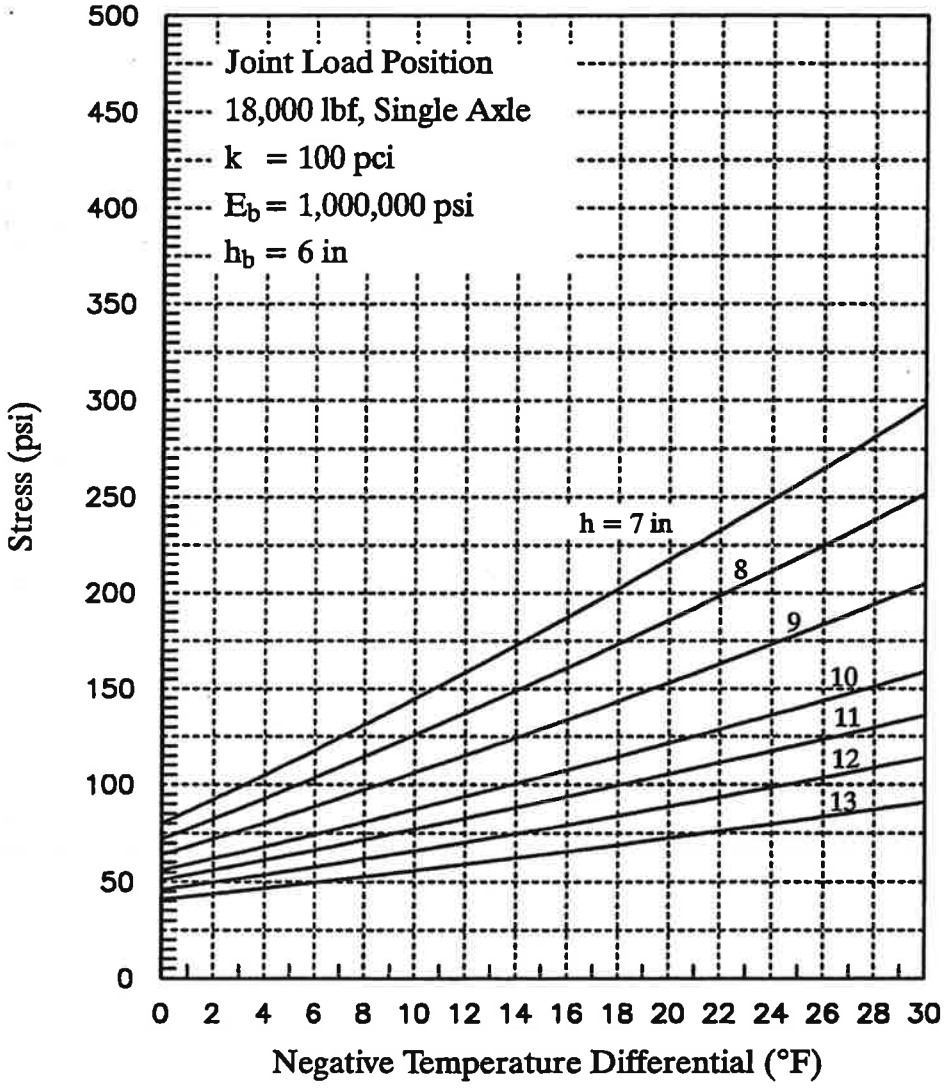

Figure E-16b. Maximum tensile stress on top of slab for joint loading position versus a negative temperature differential through the slab for specific design conditions (treated base, soft subgrade).

1°F = 0.55°C, 1 psi = 6.89 kPa, 1 in = 25.4 mm,
1 lbf = 4.45 N, 1 psi/in = 0.27 kPa/mm

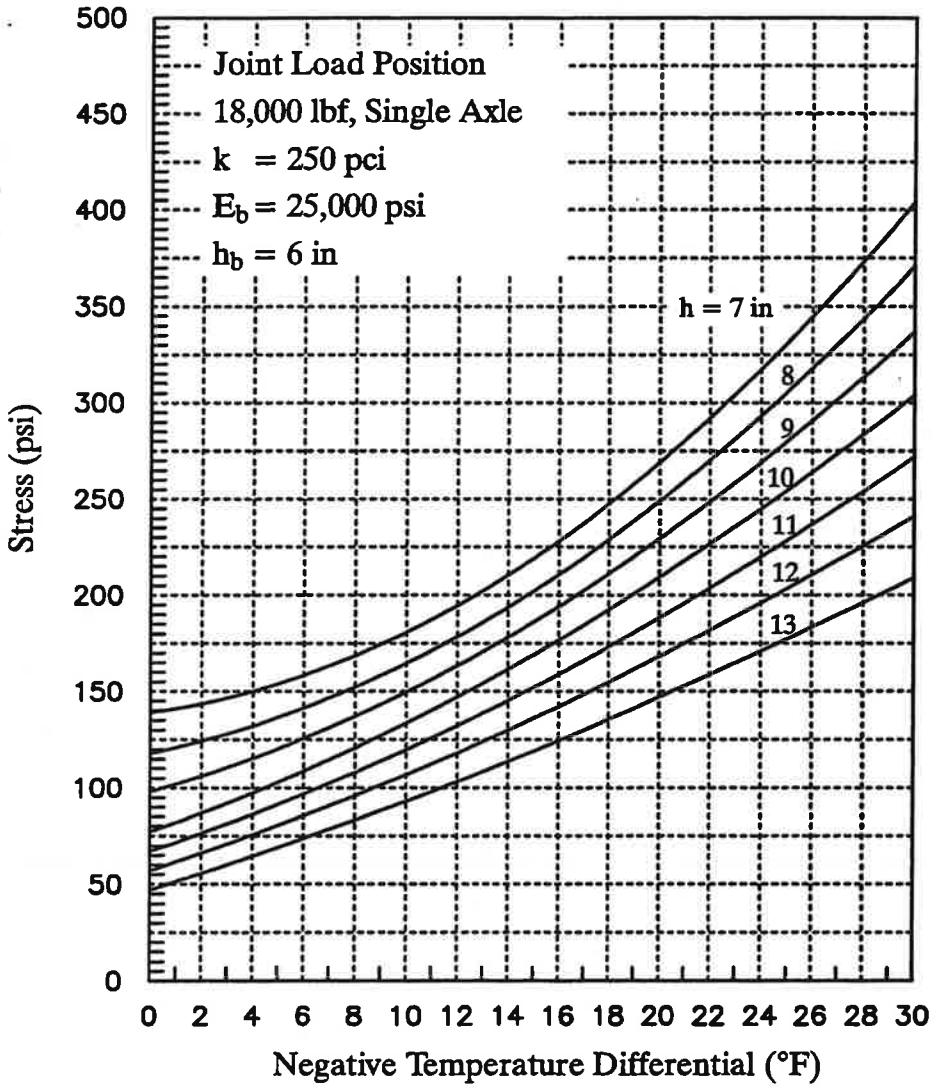

Figure E-16c. Maximum tensile stress on top of slab for joint loading position versus a negative temperature differential through the slab for specific design conditions (aggregate base, medium subgrade).

1°F = 0.55°C, 1 psi = 6.89 kPa, 1 in = 25.4 mm,
1 lbf = 4.45 N, 1 psi/in = 0.27 kPa/mm

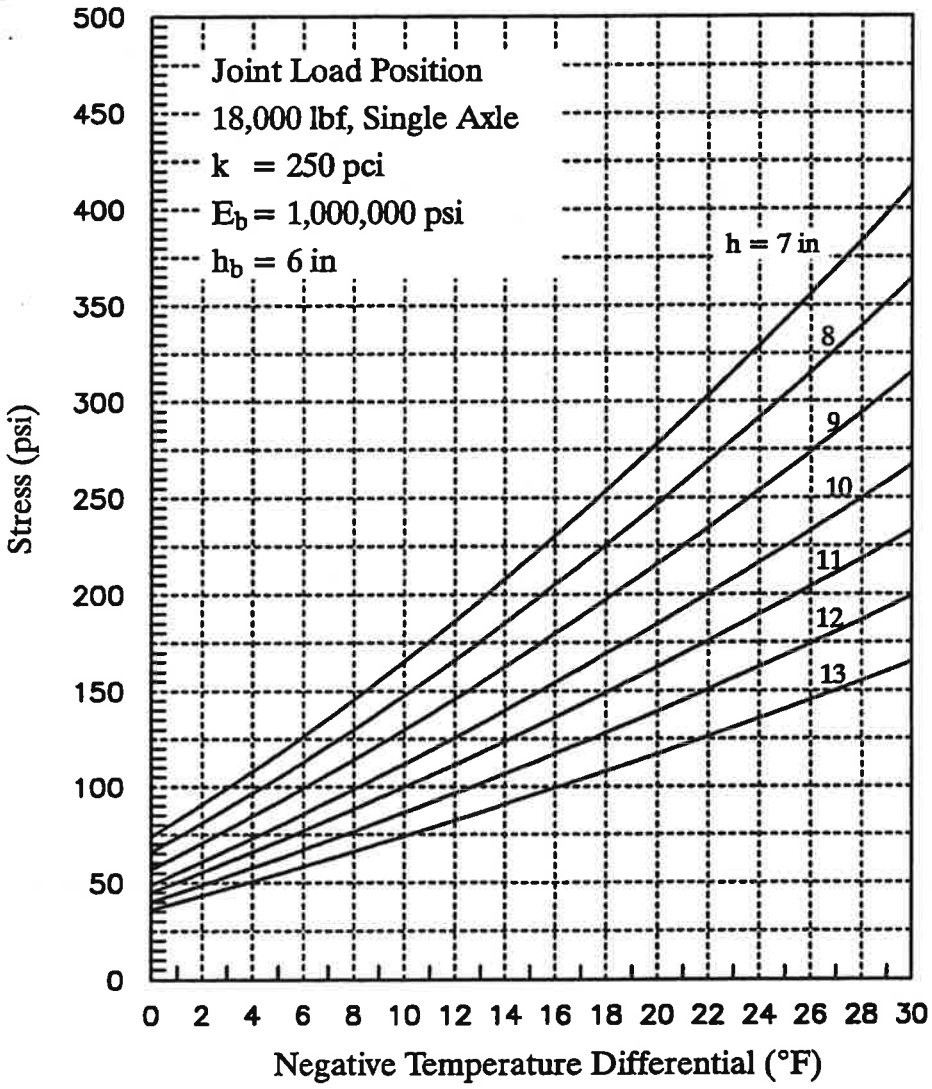

Figure E-16d. Maximum tensile stress on top of slab for joint loading position versus a negative temperature differential through the slab for specific design conditions (treated base, medium subgrade).

1°F = 0.55°C, 1 psi = 6.89 kPa, 1 in = 25.4 mm,
1 lbf = 4.45 N, 1 psi/in = 0.27 kPa/mm

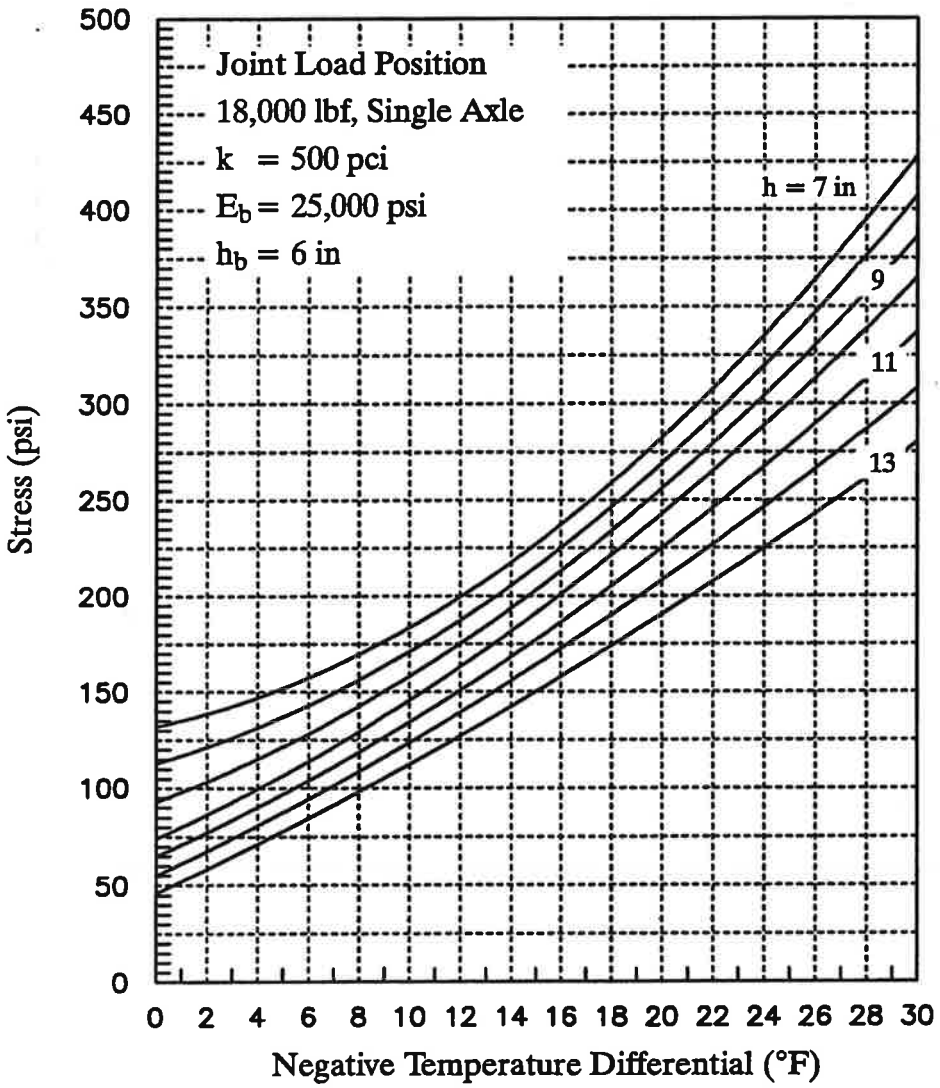

Figure E-16e. Maximum tensile stress on top of slab for joint loading position versus a negative temperature differential through the slab for specific design conditions (aggregate base, stiff subgrade).

1°F = 0.55°C, 1 psi = 6.89 kPa, 1 in = 25.4 mm,
1 lbf = 4.45 N, 1 psi/in = 0.27 kPa/mm

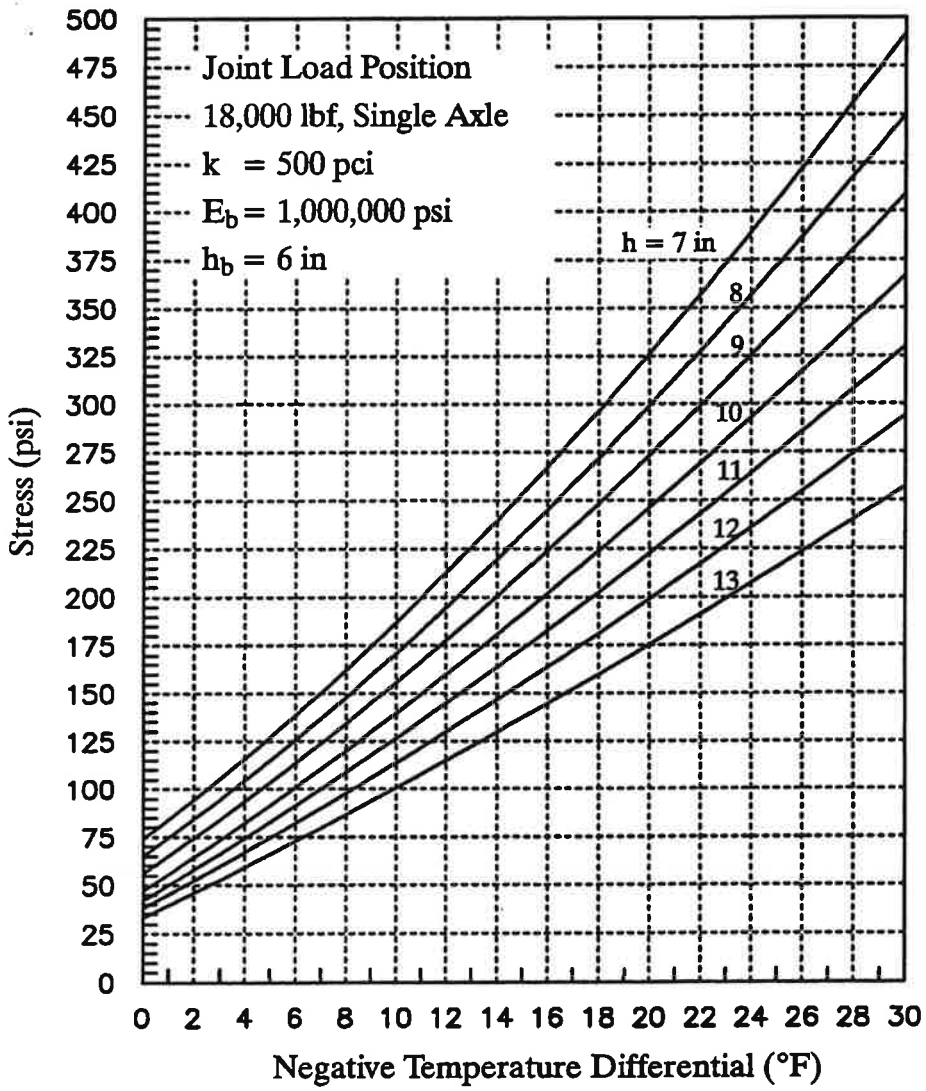

Figure E-16f. Maximum tensile stress on top of slab for joint loading position versus a negative temperature differential through the slab for specific design conditions (treated base, stiff subgrade).

(a) NIGHTTIME TEMPERATURE DIFFERENTIAL: From Equation E-44.

(b) COMBINED MOISTURE GRADIENT AND CONSTRUCTION TEMPERATURE DIFFERENTIAL: These two factors cannot be separated at this time; however, their combined effect can be thought of as the positive temperature differential required to bring the slab into a flat position. An approximate equivalent negative temperature differential is recommended that is related to the general climate of the site, assuming that conventional curing procedures are used (i.e., curing compound, no wet cure).

Wet climatic zone: 0 to 2.0°F per inch of slab thickness (Thornthwaite Moisture Index > 0)

Dry climatic zone: 1.0 to 3.0°F per inch of slab thickness (Thornthwaite Moisture Index < 0)

If wet curing conditions or night construction are used, these values may be reduced significantly.

4. Use Figure E-16 to estimate the critical stress at the top of the slab from load and negative temperature differential. Two different base types (untreated aggregate and treated aggregate) and three levels of subgrade support were used to develop Figure E-16 so that the designer can estimate through interpolation the approximate critical stress in the slab.
5. Adjust the stress from Figure E-16 from full slab/base friction to an appropriate friction level using Figure E-14. Possible friction coefficients are given in Table E-3.
6. Compare the midslab load position stress at the bottom of the slab and the joint loading position stress at the top of the slab. If the joint load position

produces a higher stress, then strong consideration should be given to a redesign of the joints.

Design features that provide a strong defense against critical joint loading stresses are the use of properly sized and spaced dowels and to a lesser degree, a widened slab (i.e., slab paved wider than 12 ft [3.7 m] but traffic lane striped 12 ft [3.7 m] wide) or a tied concrete shoulder. The other effect that good load transfer has on performance is that corner deflections are reduced. High differential deflections at the corner can lead to erosion and loss of support, resulting in even greater stresses under corner loading.

DESIGN OF DIFFERENT TYPES OF CONCRETE PAVEMENT

The current AASHTO Design Guide does not distinguish between JPCP, JRCP and CRCP as far as thickness design is concerned. The proposed revision to the AASHTO procedure applies specifically to JPCP with relatively short joint spacing. Required slab thickness for JRCP and CRCP may be different; however, in keeping with current AASHTO philosophy this thickness should also be adequate for JRCP and CRCP.

SUMMARY COMPARISON OF EXISTING AASHTO DESIGN PROCEDURE AND PROPOSED REVISED PROCEDURE WITH IMPROVED SUPPORT CONSIDERATIONS

Table E-15 summarizes the key differences between the way in which design features related to pavement support are handled in the existing AASHTO procedure and the NCHRP Project 1-30 recommendations.

Table E-15. Summary of comparison between existing and proposed revised design considerations.

Design Feature	Existing AASHTO Procedure	NCHRP 1-30 Proposed Revision
Subgrade Support	Gross k value required, lowest springtime value incorporated into equation, NOT seasonally adjusted k value. Effect of subgrade stiffness not considered in thermal curling stresses in slab.	Elastic k value of subgrade, seasonal adjustment if needed. Subgrade stiffness directly considered in slab design for load and thermal curling stresses. Brings climate into design process. Ability to estimate k value for variety of soils and bedrock.
Base Course	Considered only through a composite (top-of-base) k value. Base stiffness and friction are not considered in load or curling stresses in slab.	Direct consideration of base as structural layer (thickness, stiffness and friction). Effect of base on both load and thermal curling stresses.
Joint Spacing	Built-in 15 ft [4.6 m] JPCP. Built-in 40 ft [12.2 m] JRCP. Not considered otherwise.	Direct consideration of joint spacing effect on load and curl stresses. Brings climate into design process.
Climatic Effects	AASHO site climate built into design model. Only adjustment is through seasonal composite k value. Other climates (temperature differentials) not considered.	Seasonal variation of subgrade elastic k value possible through effective k procedure. Effective temperature differentials can be determined for climates different than AASHO site.
Seasonal Variation in Support	Seasonal adjustment is possible using effective k value method, but adjustment is inconsistent with lowest springtime gross k value built into model.	Seasonally adjusted AASHO site effective k value built into design model. Seasonal adjustment possible for other locations.
Loss of Support	Substantial loss of support built into existing model. Additional reduction of k value for loss of support is overdesign.	Substantial loss of support built into model from AASHO site, no further adjustment needed.
Joint Faulting	Not considered at all in current procedure. Mistakenly thought to be considered through J factor, which results in increased slab thickness, not improved joint design or reduced faulting.	Faulting checked after slab thickness design completed. If joint design is inadequate, joint design and/or base changes allowed, but not slab thickness increase.
Joint Load Transfer	Dowelled joints built into existing model. J factor attempts to adjust corner stress for more or less load transfer. No way to consider curling or warping of corners, especially for undowelled joints.	Effect of joint load transfer on corner load, curl and moisture gradient stresses for undowelled joints is checked directly.
Widened Slab, Tied Shoulders	Inadequate stress adjustment through J factor.	Direct adjustment of critical stress through consideration of longitudinal load transfer.

REFERENCES FOR APPENDIX E

1. Langsner, G., T. S. Huff, and W. J. Liddle, "Use of Road Test Findings by AASHO Design Committee," Special Report 73, Highway Research Board, 1962.

2. Highway Research Board, "The AASHO Road Test Report 5, Pavement Research," Special Report 61E, 1962.

3. American Association of State Highway and Transportation Officials, Guide for Design of Pavement Structures, Washington, D.C., 1993.

4. Thompson, M. R. and E. J. Barenberg, "Calibrated Mechanistic Structural Analysis Procedures For Pavements Phase 2," Final Report, NCHRP Project 1-26, Transportation Research Board, 1992.

5. Armaghani, J. M, T. J. Larsen, and L. L. Smith, "Temperature Response of Concrete Pavements," Transportation Research Record 1121, Transportation Research Board, 1987.

6. Smith, K. D., et al., "Performance of Jointed Concrete Pavements, Volume IV - Appendix A," Report No. FHWA-RD-89-139, Federal Highway Administration, 1990.

7. Eisenmann, J. and G. Leykauf, "Effect of Paving Temperatures on Pavement Performance," Proceedings of the Second International Workshop on the Design and the Evaluation of Concrete Pavements, Siguenza, Spain, October 1990.

8. Poblete, M., A. Garcia, J. David, P. Ceza, and R. Espinosa, "Moisture Effects on the Behaviour of PCC Pavements," Proceedings of the Second International Workshop on the Design and the Evaluation of Concrete Pavements, Siguenza, Spain, October 1990.

9. Janssen, D. J., "Moisture in Portland Cement Concrete," Transportation Research Record 1121, Transportation Research Board, 1987.

10. Al-Omari, B. and M. I. Darter, "Effect of Pavement Deterioration Types on IRI and Rehabilitation," University of Illinois at Urbana-Champaign and Illinois Department of Transportation, 1993.

11. Hudson, W. R. and F. H. Scrivner, "AASHO Road Test Principal Relationships -- Performance with Stress, Rigid Pavements," Proceedings of the Saint Louis Conference, Special Report 73, Highway Research Board, 1962.

12. Darter, M. I., J. M. Becker, M. B. Snyder, and R. E. Smith, "Portland Cement Concrete Pavement Evaluation System -- COPES," NCHRP Report No. 277, Transportation Research Board, 1985.

13. Miner, M. A., "Cumulative Damage in Fatigue," Transactions, American Society of Mechanical Engineers, Vol. 67, 1945.

14. Poblete, M., R. Salsilli, R. Valenzuela, A. Bull, and P. Spratz, "Field Evaluation of Thermal Deformations in Undowelled PCC Pavement Slabs," Transportation Research Record 1207, Transportation Research Board, 1989.

15. Sawan, J. S., M. I. Darter, and B. J. Dempsey, "Structural Analysis and Design of PCC Shoulders," Report No. FHWA/RD-81/122, Federal Highway Administration, 1982.

16. Thornthwaite, C. W., "An Approach Towards a Rational Classification of Climate," Geographical Review, Volume 38, 1948.

17. Darter, M. I., "Design of Zero-Maintenance Plain Jointed Concrete Pavement, Vol. I - Development of Design Procedures," Report FHWA-RD-77-111, Federal Highway Administration, 1977.

18. National Oceanic and Atmospheric Administration, "Climatic Atlas of the United States," U.S. Department of Commerce, Washington, D.C., 1983.

19. Benekohal, R. F., K. T. Hall, and H. Miller, "Effect of Lane Widening of Lateral Distribution of Truck Wheels," Transportation Research Record 1286, Transportation Research Board, Washington, D.C., 1990.

20. Gulden, W., and W. Bailey, "Field Tests on Materials That Reduce the Restraint Stress Between Concrete Pavement and Base Courses," unpublished report, Georgia Department of Transportation (date unknown).

21. Timms, A. G., "Evaluating Subgrade Friction-Reducing Mediums for Rigid Pavements," Highway Research Record 60, Highway Research Board, 1964.

22. Wesevich, J. W., B. F. McCullough, and N. H. Burns, "Stabilized Subbase Friction Study for Concrete Pavements," Research Report 459-1, University of Texas at Austin, 1987.

23. Wimsatt, A. J., B. F. McCullough, and N. H. Burns, "Methods of Analyzing and Factors Influencing Frictional Effects of Subbases," Research Report 459-2F, University of Texas at Austin, 1987.

24. Goldbeck, A. T., "Friction Tests of Concrete on Various Subbases," Public Roads, Vol. 5, No. 5, July, 1924.

25. Eisenmann, J., D. Birmann, and G. Leykauf, "Research Results on the Bond Between Cement Treated Subbases and Concrete Slabs," International Seminar on Drainage and Erodibility at the Concrete Slab-Subbase-Shoulder Interfaces, Paris, France, March 1983.

26. Portland Cement Association, "Methods for Reducing Friction between Concrete Slabs and Cement Treated Subbases," unpublished report for FHWA, Cement and Concrete Research Institute, September, 1971.

27. Thompson, M. R., "A Proposed Thickness Design Procedure for High Strength Stabilized Base Pavements," Civil Engineering Studies, Transportation Engineering Series No. 48, University of Illinois at Urbana-Champaign, May, 1988.

28. Darter, M. I., et al., "Report on the 1992 U.S. Tour of European Concrete Highways," FHWA-SA-93-012, Federal Highway Administration, 1993.

29. Ioannides, A. M. and R. A. Salsilli, "Interlayer and Subgrade Friction: A Brief Review of the State-of-the-Art," draft report prepared for Federal Highway Administration, University of Illinois, 1988.

30. Stott, J. P., "Tests on Materials for Ue in Sliding Layers Under Concrete Road Slabs," Civil Engineering and Public Works Review, Vol. 56, No. 663, October, November and December, 1961.

31. Grove, J. D., G. K. Harris, and B. J. Skinner, "Bond Contribution to Whitetopping Performance on Low Volume Roads," presented at 72nd Annual Meeting of the Transportation Research Board, Washington, D.C., January 1993.

APPENDIX F

RECOMMENDED REVISION TO AASHTO GUIDE, PART II, SECTION 3.2 RIGID PAVEMENT DESIGN AND SECTION 3.3 RIGID PAVEMENT JOINT DESIGN

This Appendix has been prepared for possible inclusion into the next version of the AASHTO Design Guide. It contains the recommendations from this study for improving the consideration of support in the AASHTO Design Guide.

3.2 RIGID PAVEMENT DESIGN

This section describes the design for Portland cement concrete pavements, including plain jointed (JCP), jointed reinforced (JRCP), and continuously reinforced (CRCP). As in the design for flexible pavements, it is assumed that these pavements will carry traffic levels in excess of 50,000 18-kip [80 kN] ESAL over the performance period. Examples of use of this rigid pavement design procedure are presented in Appendix G.

Design of Different Types of Concrete Pavement. This guide does not distinguish between JPCP, JRCP and CRCP as far as thickness design is concerned. The thickness and joint design procedures apply specifically to JPCP with relatively short joint spacing. However, JRCP is expected to crack at regular intervals, relieving the curling and shrinkage stresses. Required slab thickness for JPCP should also be adequate for JRCP and CRCP.

Load Transfer at Joints. The AASHTO design procedure is based on the AASHO Road Test pavement performance algorithm that was extended to include additional design features. Inherent in the use of the AASHTO procedure is the use of dowels at transverse joints. Joint faulting was not a distress manifestation at the

Road Test due to the adequacy of the dowel design. A faulting design check is provided for dowelled joints, to ensure that the dowels are sized properly. If a significant faulting problem is expected, an increase in dowel diameter may be warranted.

If the designer wishes to consider undowelled joints, a design check for faulting is provided. If the faulting check indicates inadequate load transfer, design modifications such as the use of dowels or changes in base type, drainage, and joint spacing may be made.

In addition, if the designer wishes to consider undowelled joints, a design check is also made for critical stresses due to axle loads applied near the transverse joint, along with a negative thermal gradient, creating a corner loading situation that would lead to premature cracking. If this check shows a potential problem, design modifications such as the use of dowels, increased slab thickness, or changes in base type may be made.

3.2.1 Develop Effective Modulus of Subgrade Reaction (k value)

The modulus of subgrade reaction (k value) is defined as that measured or estimated on top of the finished roadbed soil or embankment upon which the base course and/or concrete slab will eventually be constructed. The k value represents the subgrade (and embankment, if present); it does not represent the base course. The base course is considered a structural layer of the pavement along with the concrete slab, and thus its thickness and modulus are important design inputs to determining the required slab thickness in Section 3.2.2.

K value input defined. The elastic k value on top of the subgrade or embankment is the required design input. The gross k value incorporated in previous versions of this Guide represents not only elastic deformation of the

subgrade under a loading plate but also substantial permanent deformation. Only the elastic component of this deformation is considered representative of the response of the subgrade to traffic loads on the pavement. The elastic k value test was the main subgrade test conducted extensively at the AASHO Road Test. When the elastic k value was used in structural analysis of the AASHO Road Test pavements, it was found that slab stresses computed with a 3D finite element model were approximately equal to those measured in the field under full-scale truck axle loadings at creep speed, providing further justification for use of the elastic k value in design.

Elastic k value test. Several methods are provided for estimating the elastic k value of the subgrade for a pavement design project. The first category of methods is the **correlation methods** category. Guidelines are presented for selecting an appropriate k value based on soil classification, moisture level, density, California Bearing Ratio (CBR), Hveem Stabilometer data (R-value), or Dynamic Cone Penetrometer (DCP) data. These correlation methods are anticipated to be used routinely for design. K values obtained from correlation methods may need to be adjusted for embankment above the subgrade or a shallow rigid layer beneath the subgrade.

The second category of methods for k value is the **deflection testing and backcalculation methods** category. These methods are suitable for determining k value for design of overlays of existing pavements, or for design of a reconstructed pavements on existing alignments, or for design of similar pavements in the same general location on the same type of subgrade. An agency may also use backcalculation methods to develop correlations between nondestructive deflection testing results and subgrade types and properties. Cut and fill sections are likely to yield different k values. No embankment or rigid layer adjustment is required for

backcalculated k values if these characteristics are similar for the pavement being tested and the pavement being designed, but backcalculated dynamic k values do need to be reduced by a factor of approximately two to estimate a static elastic k value for use in design.

The third category of methods for k value is the **plate testing methods** category. The most direct method is of determining k is by repetitive or nonrepetitive plate loading tests (AASHTO T 221 or T 222, ASTM D 1195 or D1196) on a prepared section of the subgrade or embankment. These are the most direct methods of determining the elastic k value of the soil, but because these tests are costly and time-consuming, it is not anticipated that they will be conducted routinely. AASHTO T 221 and T 222 specify that if the pavement is to be built on an embankment, the plate bearing tests should be conducted on a test embankment.

The AASHTO Design procedure requires the mean k value, not the lowest value measured or some other conservative value.

Loss of support. Substantial loss of support existed for many sections at the AASHO Road Test, which led to increased slab cracking and loss of serviceability. Therefore, the performance data and design equation already includes considerable loss of support. Incorporation of an additional loss of support factor results in two separate adjustments which is not appropriate. Therefore, no additional adjustment for loss of support is applied.

Steps required to determine design effective k value.

Step 1. Select subgrade k value for each season. A season is defined as a period of time within a year, such as three months (i.e., spring, summer, fall, winter). There

are several ways to measure or estimate the subgrade elastic k value. Procedures are provided for the following methods.

K Values and Correlations for Cohesive Soils (A-4 through A-7)

The characteristics of the various classes of cohesive soils are summarized below:

A-4: Nonplastic or slightly plastic silts, may have some coarse material.
Comparable Unified classes: ML, OL
Typical dry density range: 90 to 125 lb/ft^3 [14300 to 19900 N/m^3]
Typical CBR range: 4 to 15

A-5: Poorly graded silts, usually micaceous or diatomaceous, may be highly elastic.
Comparable Unified class: MH
Typical dry density range: 80 to 100 lb/ft^3 [12700 to 15900 N/m^3]
Typical CBR range: 4 to 8

A-6: Plastic clays, sometimes with moderate coarse fraction, usually exhibit high volume change from wet to dry states.
Comparable Unified class: CL
Typical dry density range: 100 to 125 lb/ft^3 [15900 to 19900 N/m^3]
Typical CBR range: 5 to 15

A-7-5: Elastic clays, moderate plasticity index. May be highly elastic, may undergo considerable volume change.
Comparable Unified class: CL, OL
Typical dry density range: 90 to 125 lb/ft^3 [14300 to 19900 N/m^3]
Typical CBR range: 4 to 15

A-7-6: Elastic clays, high plasticity index. May be highly elastic, may undergo extremely high volume changes.
Comparable Unified class: CH, OH
Typical dry density range: 80 to 110 lb/ft^3 [12700 to 17500 N/m^3]
Typical CBR range: 3 to 5

The bearing capacity of these cohesive soils is strongly influenced by their degree of saturation (S_r, percent), which is a function of water content (w, percent), dry density (γ, lb/ft^3), and specific gravity (G_s):

$$S_r = \frac{w}{\left(\frac{62.4}{\gamma}\right) - \left(\frac{1}{G_s}\right)} \qquad \text{(F-1)}$$

Recommended k values for each fine-grained soil type as a function of degree of saturation are are shown in Figure F-1. Each line represents the midrange of reasonable values for k. For any given soil type and degree of saturation, the range of reasonable values is about ± 40 psi/in [11 kPa/mm]. So, for example, an A-6 soil might be expected to exhibit k values between about 180 and 260 psi/in [49 and 70 kPa/mm] at 50 percent saturation, and k values between about 45 and 115 [12 and 31 kPa/mm] at 100 percent saturation.

Two different types of materials can be classified as A-4: predominantly silty materials (at least 75 percent passing the #200 sieve, possibly organic), and also mixtures of silt, sand, and gravel (up to 64 percent retained on #200 sieve). The former may have a density between about 90 and 105 lb/ft^3 [14300 and 16700 N/m^3], and a CBR between about 4 and 8. The latter may have a density between about 100 and 125 lb/ft^3 [15900 and 19900 N/m^3], and a CBR between about 5 and 15. The line labelled A-4 in Figure 16 is more representative of the former group. If the material in question is A-4, but possesses the properties of the stronger subset of materials in the A-4 class, a higher k value at any given degree of saturation (for example, along the line labelled A-7-6 in Figure F-1) is appropriate.

K Values and Correlations for Cohesionless Soils (A-1 and A-3)

The characteristics of the various cohesionless soils are summarized below:

A-1-a: Predominantly stone fragments and gravel, with or without binder.
Comparable Unified classes: GW, GP
Typical dry density range:
125 to 140 lb/ft^3 [19900 to 22200 N/m^3] if well graded,
120 to 130 lb/ft^3 [19100 to 20700 N/m^3] if poorly graded
Typical CBR range: 60 to 80 if well graded, 35 to 60 if poorly graded

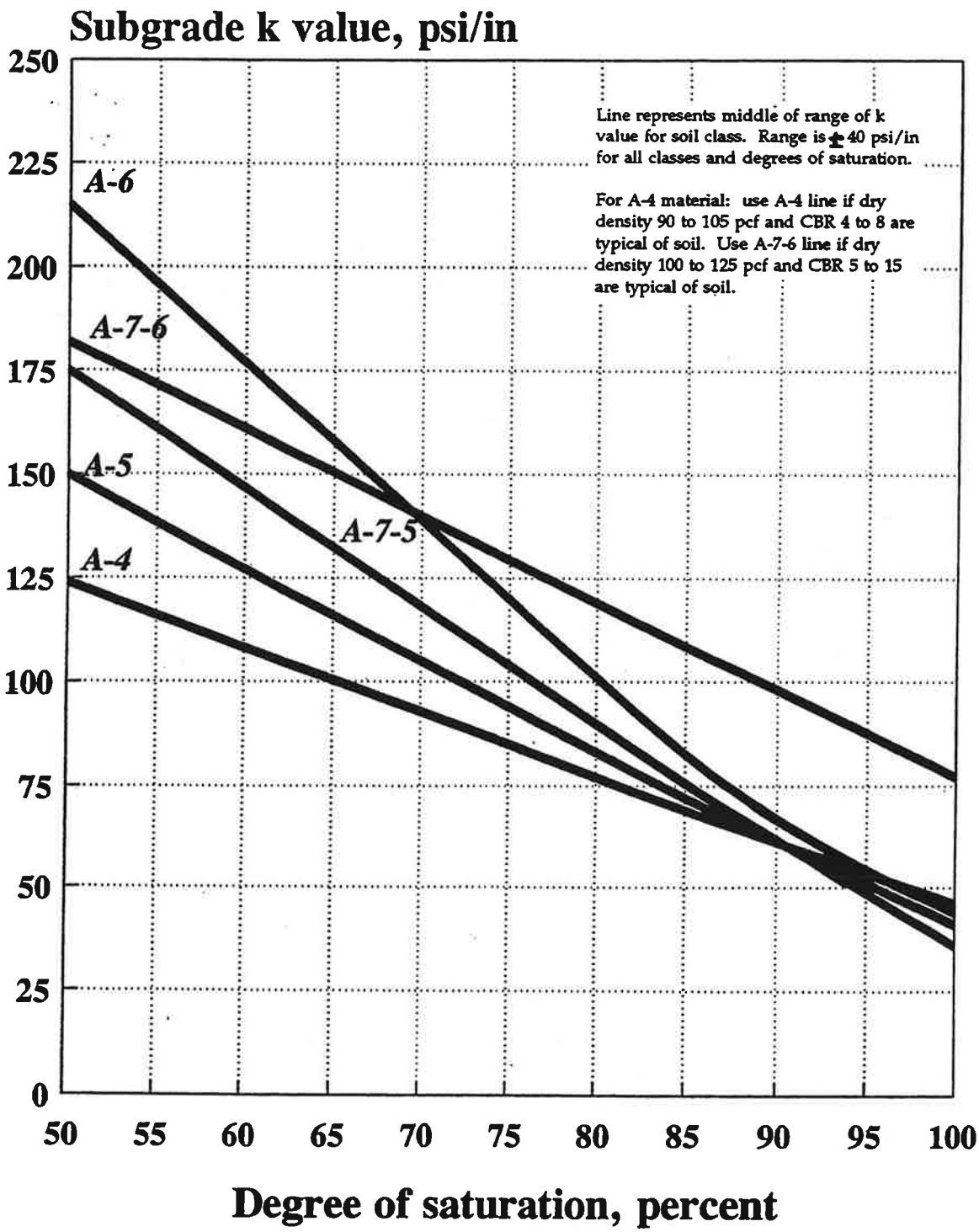

Figure F-1. k values versus degree of saturation for cohesive soils.

A-1-b: Predominantly coarse sand with or without binder.
Comparable Unified class: SW
Typical dry density range: 110 to 130 lb/ft^3 [17500 to 20700 N/m^3]
Typical CBR range: 20 to 40

A-3: Fine beach or desert sand without fines. Also alluvial mix of poorly graded fine sand and small amounts of coarse sand and gravel.
Comparable Unified class: SP
Typical dry density range: 105 to 120 lb/ft^3 [16700 to 19100 N/m^3]
Typical CBR range: 15 to 25

The bearing capacity of cohesionless materials is primarily a funtion of their dry density, and is fairly insensitive to moisture variation. Recommended k value ranges for A-1 and A-3 soils are given in Table F-1.

Table F-1. Recommended k value ranges for A-1 and A-3 soils.

Soil Class	k Range (psi/in)	Dry Density Range (lb/ft^3)
A-1-a, well graded	300 - 450	125 - 140
A-1-a, poorly graded	300 - 400	120 - 130
A-1-b	200 - 400	110 - 130
A-3	150 - 300	105 - 120

1 psi/in = 0.27 kPa/mm, 1 lb/ft^3 = 159 N/m^3

K Values and Correlations for A-2 Soils

Soils in the A-2 class are all granular materials falling between A-1 and A-3. Some of their properties are described below:

A-2-4 and A-2-5: Gravel and coarse sand with fines content in excess of A-1 limits, and fine sand with fines content in excess of A-3 limits. The fraction passing the #40 sieve behaves like nonplastic (A-4 and A-5) clays and silts.

Gravelly A-2-4 and A-2-5 (silty gravel or silty sandy gravel):

Comparable Unified class: GM
Typical dry density range:
130 to 145 lb/ft^3 [20700 to 23100 N/m^3]
Typical CBR range: 40 to 80

Sandy A-2-4 and A-2-5 (silty sand or silty gravelly sand):

Comparable Unified class: SM
Typical dry density range:
120 to 135 lb/ft^3 [19100 to 21500 N/m^3]
Typical CBR range: 20 to 40

A-2-6 and A-2-7: Gravel and coarse sand with fines content in excess of A-1 limits, and fine sand with fines content in excess of A-3 limits. The fraction passing the #40 sieve behaves like plastic (A-6 and A-7) clays and silts.

Gravelly A-2-6 and A-2-7 (clayey gravel or clayey sandy gravel):

Comparable Unified class: GC
Typical dry density range:
120 to 140 lb/ft^3 [19100 to 22300 N/m^3]
Typical CBR range: 20 to 40

Sandy A-2-6 and A-2-7 (clayey sand or clayey gravelly sand):

Comparable Unified class: SC
Typical dry density range:
105 to 130 lb/ft^3 [16700 to 20700 N/m^3]
Typical CBR range: 10 to 20

Although it is difficult to predict the behavior of such a wide variety of materials, the available data indicates that in terms of bearing capacity, A-2 materials behave similarly to cohesionless materials of comparable density. Recommended k value ranges for A-2 soils are given in Table F-2.

Table F-2. Recommended k value ranges for A-2 soils.

Soil Class	k Range (psi/in)	Dry Density Range (lb/ft^3)
A-2-4, gravelly	300 - 500	130 - 145
A-2-5, gravelly	300 - 500	130 - 145
A-2-4, sandy	300 - 400	120 - 135
A-2-5, sandy	300 - 400	120 - 135
A-2-6, gravelly	200 - 450	120 - 140
A-2-7, gravelly	200 - 450	120 - 140
A-2-6, sandy	150 - 350	105 - 130
A-2-7 sandy	150 - 350	105 - 130

Correlation of K Value to Other Tests

The following correlations are also available for estimating k value from other types of soil test data:

California Bearing Ratio: Figure F-2 illustrates the approximate range of k values which might be expected for a soil with a given California Bearing Ratio.

R-Value: Figure F-3 illustrates the general relationship between k value and R-value.

Dynamic Cone Penetrometer. Figure F-4 illustrates the range of k values which might be expected for a soil with a given penetration rate (inches per blow) measured with a Dynamic Cone Penetrometer. This is a rapid hand-held testing device which can be used to quickly test dozens of locations along an alignment. The DCP can also penetrate AC surfaces and surface treatments to test the foundation below.

Assignment of k values to seasons. Among the factors which should be considered in selecting seasonal k values are the seasonal movement of the water table, seasonal precipitation levels, winter frost depths, number of freeze-thaw cycles, and the extent to which the subgrade will be protected from frost by embankment material.

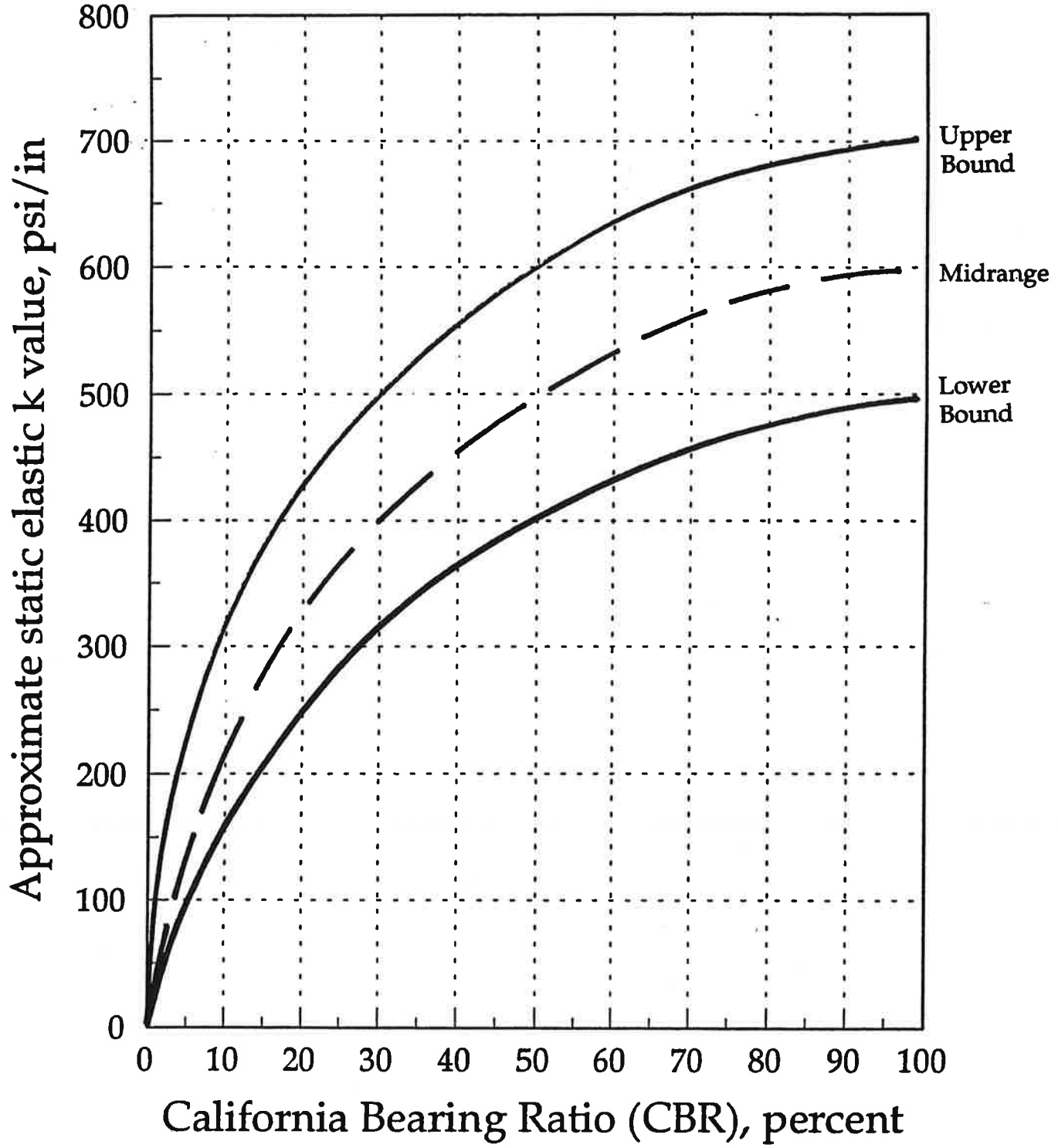

Figure F-2. Approximate relationship of k value range to CBR.

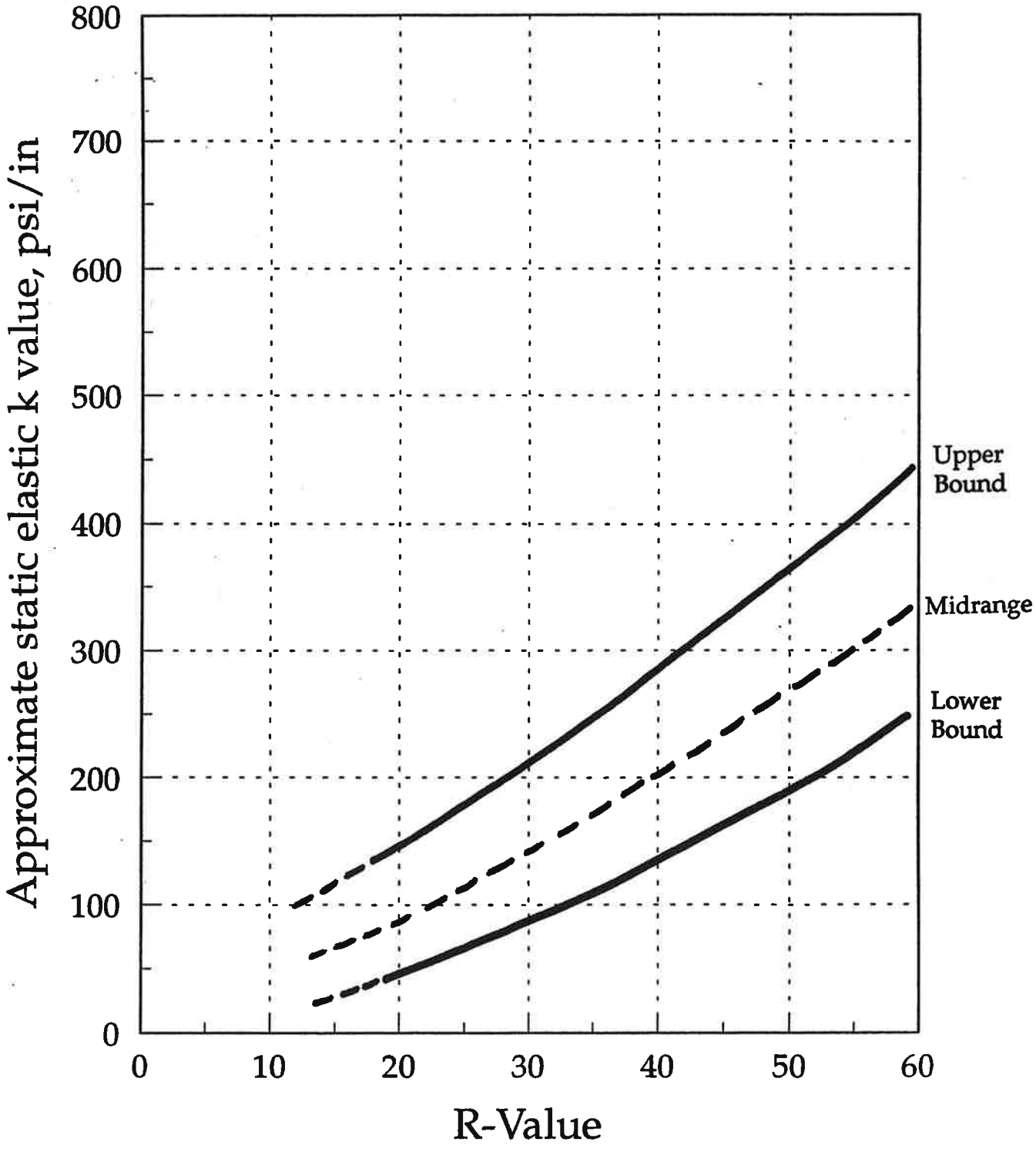

Figure F-3. Approximate relationship of k value range to R-value.

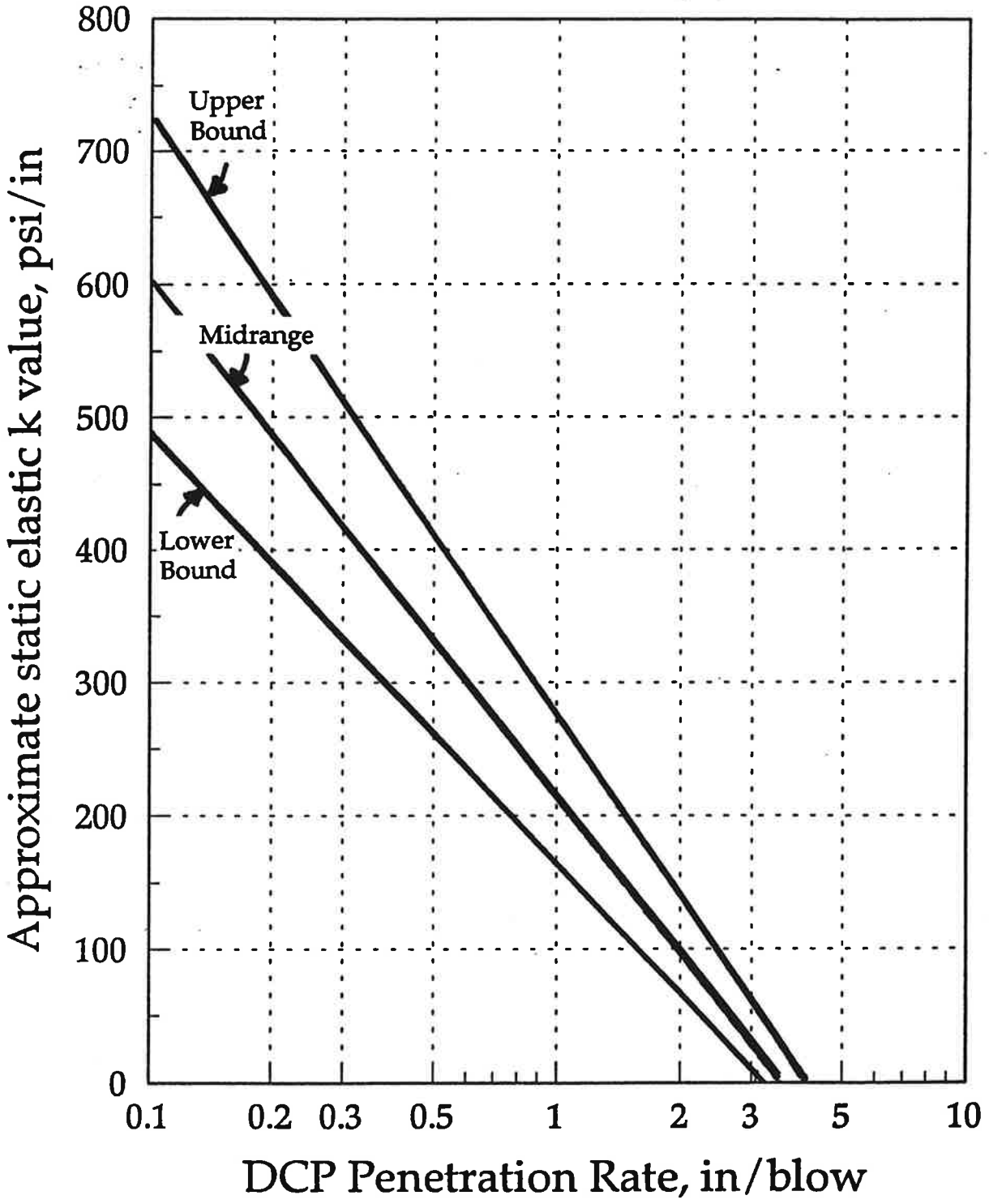

Figure F-4. Approximate relationship of k value range to DCP penetration rate.

A "frozen" k may not be appropriate for winter, even in a cold climate, if the frost will not reach and remain in a substantial thickness of the subgrade throughout the winter. If it is anticipated that a substantial depth (e.g., a few feet) of the subgrade will be frozen, a k value of 500 psi/in [135 kPa/mm] would be an appropriate "frozen" k.

The seasonal variation in degree of saturation is difficult to predict, but in locations where a water table is constantly present at a depth of less than about 10 ft [3 m], it is reasonable to expect that fine-grained subgrades will remain at least 70 and 90 percent saturated, and may be completely saturated for substantial periods in the spring. County soil reports can provide data on the position of the high water table (i.e., the typical depth to the water table at the time of the year that it is at its highest). Unfortunately, county soil reports do not provide data on the variation in depth to the water table throughout the year.

Deflection Testing and Backcalculation Methods

Equations for backcalculation of concrete elastic moduli and subgrade k values for concrete and composite pavements are provided in this section. This solution method is based on deflection of an infinite slab, and produces a dynamic elastic k value, which should be reduced by a factor of two to estimate a static elastic k value for design. These methods are suitable for determining k value for design of overlays of existing pavements, or for design of a reconstructed pavements on existing alignments, or for design of similar pavements in the same general location on the same type of subgrade. An agency may also use backcalculation methods to develop correlations between nondestructive deflection testing results and subgrade types and properties.

Measure slab deflection basins along the project at an interval sufficient to adequately assess conditions. Intervals of 100 to 1000 feet [30 to 300 m] are typical. Measure deflections with sensors located at 0, 12, 24 and 36 inches [0, 305, 610, and 915 mm] from the center of load. Measure deflections in the outer wheel path. A heavy-load deflection device (e.g., Falling Weight Deflectometer) and a load magnitude of 9,000 lbf [40 kN] are recommended. ASTM D 4694 and D 4695 provide additional guidance on deflection testing.

The AREA of each deflection basin is computed by the following equation. AREA will typically range from 29 to 32 for sound concrete.

$$AREA = 6 * \left[1 + 2\left(\frac{d_{12}}{d_0} \right) + 2\left(\frac{d_{24}}{d_0} \right) + \left(\frac{d_{36}}{d_0} \right) \right] \quad \text{(F-2)}$$

where d_0 = deflection in center of loading plate, inches

d_i = deflections at 12, 24 and 36 inches from plate center, inches

Dynamic elastic k value. For each slab tested, determine the dynamic elastic k value from Figure F-5. Enter Figure F-5 with d_0 and AREA to determine the effective dynamic k-value beneath each slab for a circular load radius of 5.9 inches [150 mm] and magnitude of 9,000 lbf [40 kN]. For loads within 2,000 lbf [9 kN] more or less, deflections may be scaled linearly to 9,000-lbf [40 kN] deflections. Compute the mean dynamic k value of the slabs tested in the uniform section. Do not use any k values that appear to be significantly out of line with the rest of the data.

Static elastic k value. Divide the mean dynamic elastic k value by two to estimate the static elastic k value for use in design.

Seasonal variation in backcalculated k values. The design k value determined from backcalculation as described above represents the k value for the season in which the deflection testing was conducted. An agency may wish to conduct deflection testing on selected projects in different seasons of the year to assess the seasonal variation in backcalculate k values for different types of subgrades.

Backcalculated k value for existing composite pavement. The procedure described above may be applied to backcalculating k values from deflections measured on existing composite (AC-overlaid PCC) pavements, if the AREA and the k value are calculated with a maximum deflection d_0 which has been corrected for compression in the AC surface. This correction depends on the thickness of the AC, the elastic modulus

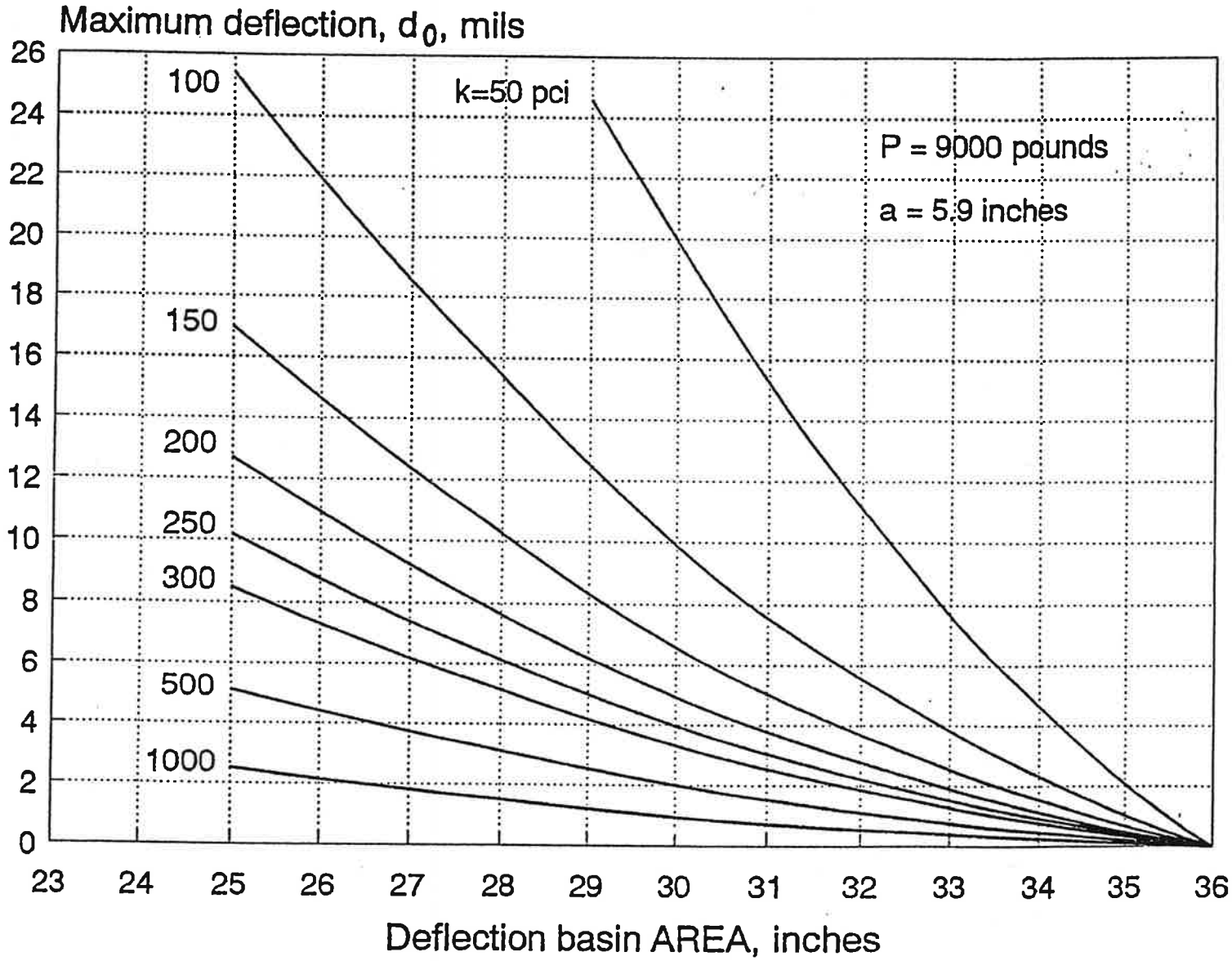

Figure F-5. Dynamic elastic k value determination from d_0 and AREA.

of the AC, and whether the AC and PCC layers are bonded or unbonded (as determined from examination of cores). The AC elastic modulus is a function of temperature, and should be determined for each deflection basin as a function of the AC mix temperature at the time of testing. The relationship between AC elastic modulus and temperature for a given AC mix may be established as a function of mix properties from an equation developed by the Asphalt Institute, or from diametral resilient modulus tests on cores in accordance with ASTM D 4123. Detailed guidance on deflection testing and backcalculation for AC-overlaid PCC pavements is provided in Part III, Section 5.7.

Plate Bearing Test Methods

The subgrade or embankment k value may be determined from either of two types of plate bearing tests: repetitive static plate loading (AASHTO T 221, ASTM D 1195) or nonrepetitive static plate loading (AASHTO T 222, ASTM D 1196). These test methods were developed for a variety of purposes, and do not provide explicit guidance on the determination of the required k value input to the design procedure described in this Guide.

For the purpose of concrete pavement design, the recommended subgrade input parameter is the static elastic k value. This may be determined from either a repetitive or nonrepetitive test on the prepared subgrade or on a prepared test embankment.

In a repetitive test, the elastic k value is determined from the ratio of load to elastic deformation (the recoverable portion of the total deformation measured). In a nonrepetitive test, the load-deformation ratio at a deformation of 0.05 in [1.25 mm] is considered to represent the elastic k value, according to extensive research by the Corps of Engineers. Note also that a **30-in-diameter [762 mm] plate** should be used to determine the elastic static k value for use in design. Smaller-diameter plates will yield substantially higher k values which are not appropriate for use in this design procedure.

Step 2. Determine seasonally adjusted effective k value. The effective k value is obtained by combining the seasonal k values into a single "effective" value for use in

concrete pavement design. The effective k value is essentially a weighted average based on fatigue damage. The effective k value results in the same fatigue damage over the entire year that is caused by the seasonally varying k value. Appendix H provides details on the derivation of the seasonal adjustment procedure.

The rigid pavement design equation includes an effective seasonally adjusted elastic k value of 110 psi/in [30 kPa/mm] for the AASHO Road Test site. Therefore, the design of a new pavement requires the determination of a seasonally adjusted k value when significant changes in support are anticipated over the year.

This calculation requires the selection of the following tentative design features and parameters: slab thickness D, concrete elastic modulus E_c, base elastic modulus E_b and friction coefficient f (both depending on base type), base thickness H_b, design temperature differential TD (for a given climatic region as a function of trial slab thickness D), and joint spacing L. These tentative selections need only be approximate as a difference in any of them will not affect the effective k value results very much.

Table F-3 may be used to determine the effective k value. The k values for each season are entered. The W_{18} corresponding to each k value is computed from Equation H-1 in Appendix H. The relative damage for each season is computed as $1/W_{18}$. The mean damage is computed by dividing the total damage by the number of seasons. The W_{18} required to produce this mean damage is the inverse of the mean damage. The k value corresponding to this W_{18} is then determined using Equation H-1 in Appendix H.

Step 3. Adjustment to k value for fill thickness and rigid layer. A nomograph is provided in Figure F-6 for adjustment of the seasonally adjusted effective subgrade k value if (a) fill material will be placed above the natural subgrade, and/or (b) a rigid layer (e.g., bedrock or hardpan clay) is present at a depth of 10 ft [3 m] or less beneath the existing subgrade surface. Note that the rigid layer adjustment should only be applied if the subgrade k was determined on the basis of soil type or similar correlations. If the k value was determined from nondestructive deflection testing or from plate bearing tests, the effect of a rigid layer, if present at a depth of less than 10 ft [3 m], is already represented in the k value obtained.

Table F-3. Determination of effective subgrade k value for a specific project site and design features.

Seasons (3 months)	k value (psi/in)	W_{18} (millions)*	Relative Damage ($1 / W_{18}$)
Spring			
Summer			
Fall			
Winter			
		Mean Damage	
		W_{18}	million
		Effective k value	psi/in

*The W_{18} is computed from Equation H-1 in Appendix H using approximate inputs. It is the mean predicted pavement life for a given loss in serviceability.

1 psi/in = 0.27 kPa/mm

EXAMPLE:

Seasons (3 months)	k value (psi/in)	W_{18} (millions)*	Relative Damage ($1 / W_{18}$)
Spring	77	12.75	0.0784
Summer	98	13.15	0.0760
Fall	111	13.37	0.0748
Winter	168	14.20	0.0704
		Mean Damage	0.0749
		W_{18}	13.35 million
		Effective k value	110 psi/in

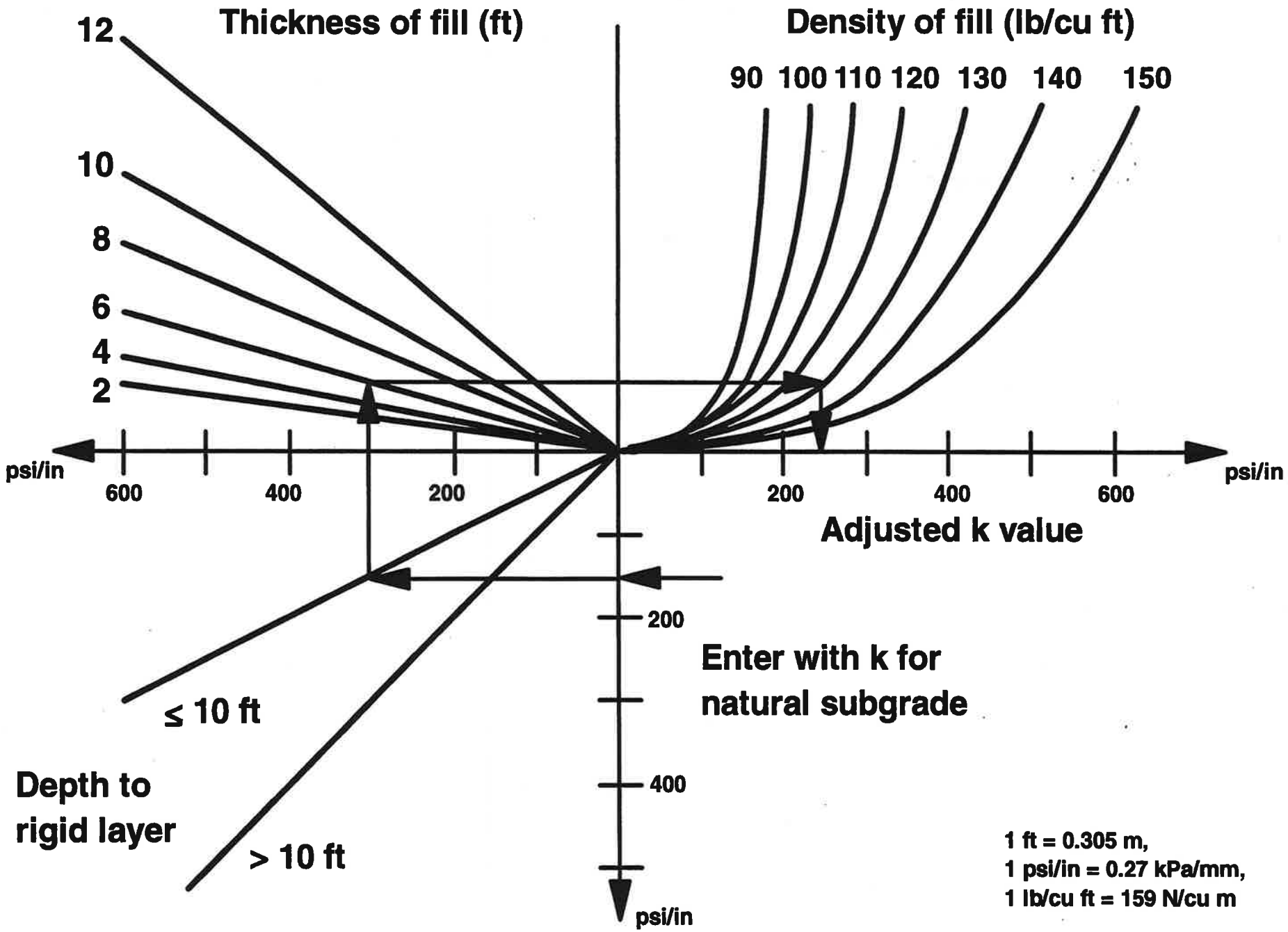

Figure F-6. Adjustment to k for fill and/or rigid layer.

3.2.2 Determine Required Slab Thickness

Slab thickness is determined using the midslab load position shown in Figure F-7 because for dowelled pavements this position produces the critical tensile stress in the concrete slab. Most cracks initiate along the edge of the slab as a result of this loading. This slab thickness becomes the final design thickness if the transverse joints are dowelled. If the joints are not dowelled, a design check is made to see if the joint loading position causes a more critical stress at the top of the slab. Also, a design check is made for joint faulting adequacy as described in Section 3.3.

Determine Required Inputs. The following inputs must be selected or obtained.

(1) effective (seasonally adjusted) elastic k value of the subgrade, psi/in (Section 3.2.1)
(2) the estimated future traffic, W_{18} (Section 2.1.2), for the performance period in the design lane,
(3) the design reliability, R (Section 2.1.3),
(4) the overall standard deviation, S_o (Section 2.1.3)
(5) design serviceability loss, $PSI = P_1 - P_2$ (Section 2.2.1)
(6) concrete modulus of rupture, S'_c (Section 2.3.4)
(7) concrete elastic modulus, E_c (Section 2.3.3)
(8) joint spacing, L (Section 3.3.2)
(9) base modulus, E_b (Section 2.3.3)
(10) slab/base friction coefficient,
(11) base thickness, H_b
(12) effective positive temperature differential through concrete slab, TD
(13) lane edge support condition
    (a) conventional lane width (12 ft [3.7 m]) with free edge
    (b) conventional lane width (12 ft [3.7 m]) with tied concrete shoulder
    (c) wide traffic lane (i.e., 14 ft [4.3 m]) with paint stripe at conventional width (12 ft [3.7 m])

1 in = 25.4 mm, 1 ft = 0.305 m

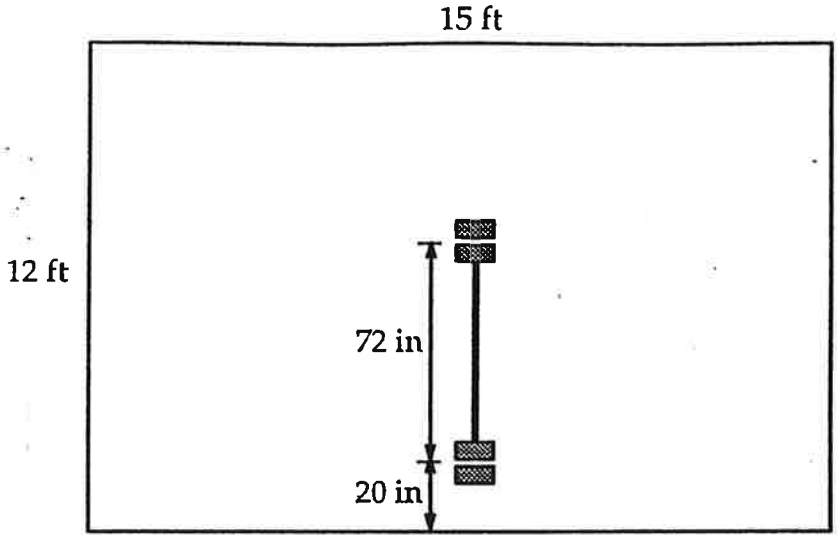

Midslab Loading

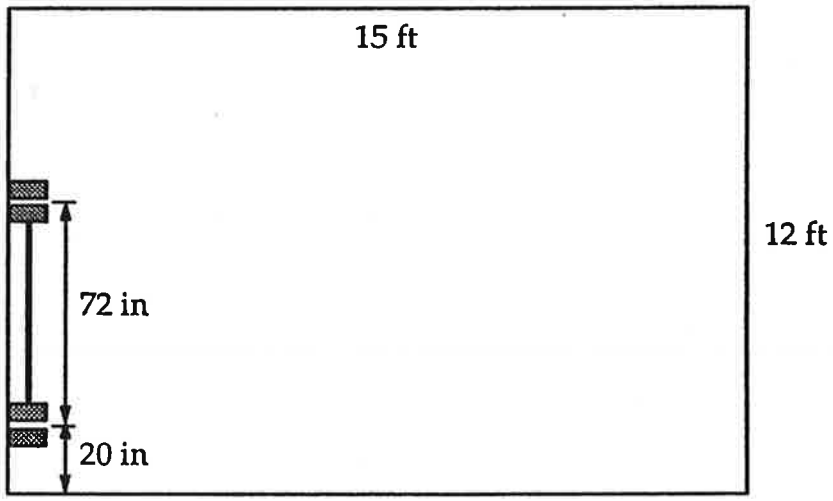

Joint Loading

Tire Print :

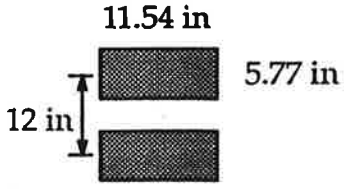

Figure F-7. Midslab and joint loading positions defined.

Design Equations for Rigid Pavement. The rigid pavement design equation for 50 percent reliability is given below:

$$\log W' = \log W + \left(5.065 - 0.03295\ P2^{2.4} \right) \left[\log \left(\frac{(S'_c)'}{\sigma_{t'}} \right) - \log \left(\frac{690}{\sigma_t} \right) \right] \quad \text{(F-3)}$$

where W′ = number of 18-kip [80 kN] ESALs estimated for design traffic lane

W = number of 18-kip [80 kN] ESALs computed from Equation F-4 below:

$$\log W = \log R + \frac{G}{F} \quad \text{(F-4)}$$

$$\log R = 5.85 + 7.35 \log (D + 1) - 4.62 \log (L1 + L2) + 3.28 \log L2 \quad \text{(F-5)}$$

$$F = 1.00 + \frac{3.63\ (L1 + L2)^{5.2}}{(D + 1)^{8.46}\ L2^{3.52}} \quad \text{(F-6)}$$

$$G = \log \left(\frac{P1 - P2}{P1 - 1.5} \right) \quad \text{(F-7)}$$

D = concrete slab thickness, in

L1 = load on a single or tandem axle, kips

L2 = axle code, 1 for single axle, 2 for tandem axle

P1 = initial serviceability index

P2 = terminal serviceability index

$(S'_c)'$ = mean 28-day, third-point loading flexural strength, psi (690 psi for AASHO Road Test)

σ_t = midslab tensile stress due to load and temperature from Equation F-8 with AASHO Road Test constants

$\sigma_{t'}$ = midslab tensile stress due to load and temperature from Equation F-8 with inputs for new pavement design

$$\sigma_t = \sigma_l \, E \, F \left[1.0 + 10^{(\log b)\, TD} \right] \quad \text{(F-8)}$$

σ_l = midslab tensile stress due to load only

$$\sigma_l = \frac{18{,}000}{D^2} \left\{ 4.227 - 2.381 \left(\frac{180}{\ell} \right)^{0.2} - 0.0015 \left[\frac{E_b \, H_b}{1.4 \, k} \right]^{0.5} - 0.155 \left[H_b \left(\frac{E_b}{E_c} \right)^{0.75} \right]^{0.5} \right\} \quad \text{(F-9)}$$

E_c = modulus of elasticity of concrete slab, psi
(4,200,000 psi [28940 MPa] for AASHO Road Test)

E_b = modulus of elasticity of base, psi
(25,000 psi [172 MPa] for AASHO Road Test)

H_b = thickness of base, in (6 in [152 mm] for AASHO Road Test)

$$\ell = \sqrt[4]{\frac{Z \, D^3}{12 \, (1 - \mu^2)}} \quad \text{(F-10)}$$

$$Z = \frac{E_c}{k} \quad \text{(F-11)}$$

k = effective elastic modulus of subgrade support, psi/in
(110 psi/in for AASHO Road Test)

μ = Poisson's ratio for concrete (0.20 for AASHO Road Test)

E = edge support adjustment factor (1.00 for AASHO Road Test)
= 1.00 for conventional 12-ft-wide [3.66 m] traffic lane
= 0.94 for conventional 12-ft-wide [3.66 m] traffic lane plus tied concrete shoulder
= 0.92 for 2-ft [0.6 m] widened slab with paint stripe at conventional 12-ft [3.66 m] lane width

F = ratio between slab stress at a given coefficient of friction (f) between the slab and base and slab stress at full friction

f = friction coefficient between slab and base (see Table F-4)

$$F = 1.177 - 4.3*10^{-8}\ D\ E_b - 0.01155542\ D + 6.27*10^{-7}\ E_b - 0.000315\ f \quad \text{(F-12)}$$

$$\log b = -1.944 + 2.279\ \frac{D}{\ell} + 0.0917\ \frac{L}{\ell} - 433{,}080\ \frac{D^2}{k\ \ell^4} + \left(\frac{0.0614}{\ell}\right) * \left(\frac{E_b\ H_b{}^{1.5}}{1.4\ k}\right)^{0.5} - 438.642\ \frac{D^2}{k\ \ell^2} - 498{,}240\ \frac{D^3\ L}{k\ \ell^6}$$

L = joint spacing, inches (180 in [4572 mm] for AASHO Road Test)

TD = effective positive temperature differential, top temperature minus bottom temperature, °F

$$\textit{effective positive TD} = 0.962 - \frac{52.181}{D} + 0.341\ \textit{WIND} + 0.184\ \textit{TEMP} - 0.00836\ \textit{PRECIP} \quad \text{(F-14)}$$

D = slab thickness, in

WIND = mean annual wind speed, mph (Figure F-8)

TEMP = mean annual temperature, °F (Figure F-9)

PRECIP = mean annual precipitation, in (Figure F-10)

Contour maps for the three climatic inputs are provided in Figures F-8, F-9, and F-10, and these data are also easily obtainable from local weather stations or other sources.

Required Slab Thickness. The rigid pavement design equations given above may be used to determine the required slab thickness for the design traffic. The design equations are too complex to put into nomograph form. However, the new design equations can easily be solved in a spreadsheet or programmed into a

Table F-4. Summary of measured coefficient of friction between concrete slab and base course from various references and typical ranges of base modulus of elasticity.

Base Type and Typical Modulus of Elasticity Range	Measured Peak Coefficient of Friction (low-mean-high)
Fine-grained soils (E = 3,000-40,000 psi)	0.5---1.3---2.0
Sand (E = 10,000-25,000 psi)	0.5---0.8---1.0
Aggregate (E = 15,000-45,000 psi)	0.7---1.4---2.0
Polyethylene sheeting (on CTB, ATB, LCB, ...)	0.5---0.6---1.0
Lime-Stabilized Clay (E = 20,000-70,000 psi)	3.0 to 5.3
Cement-Treated Base (gravel) [E = (500 + CS) * 1000] CS = compressive strength, psi	8---34---63
Asphalt-Treated Base (E = 300,000-600,000 psi)	3.7---5.8---10
Lean Concrete Base (no curing compound) [E = (500 + CS) * 1000] CS = compressive strength, psi	> 36
Lean Concrete Base (single or double wax curing compound) [E = (500 + CS) * 1000] CS = compressive strength, psi	3.5 to 4.5

1 psi = 6.89 kPa

Figure F-8. Mean annual wind speed, mph.

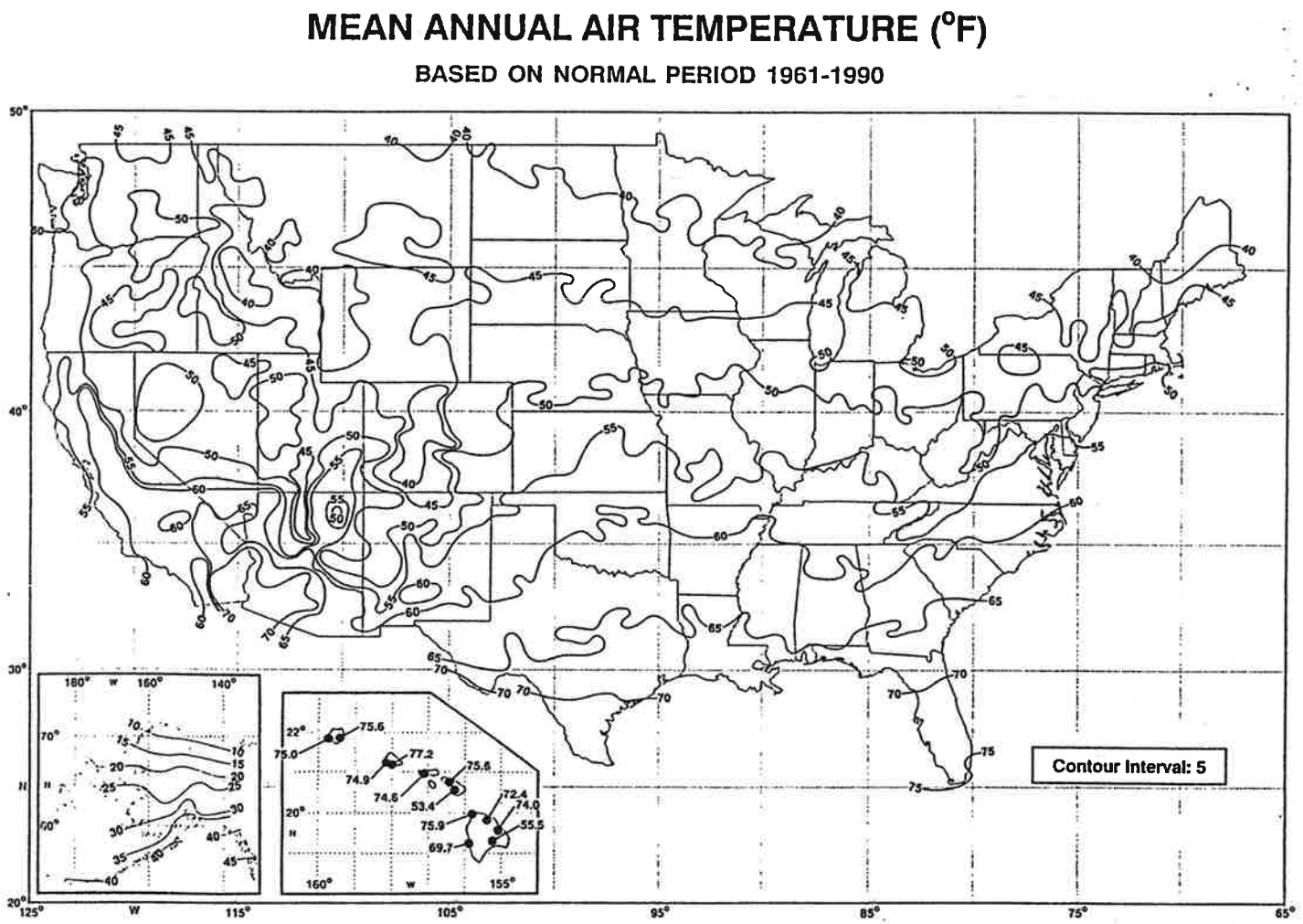

Figure F-9. Mean annual air temperature, °F.

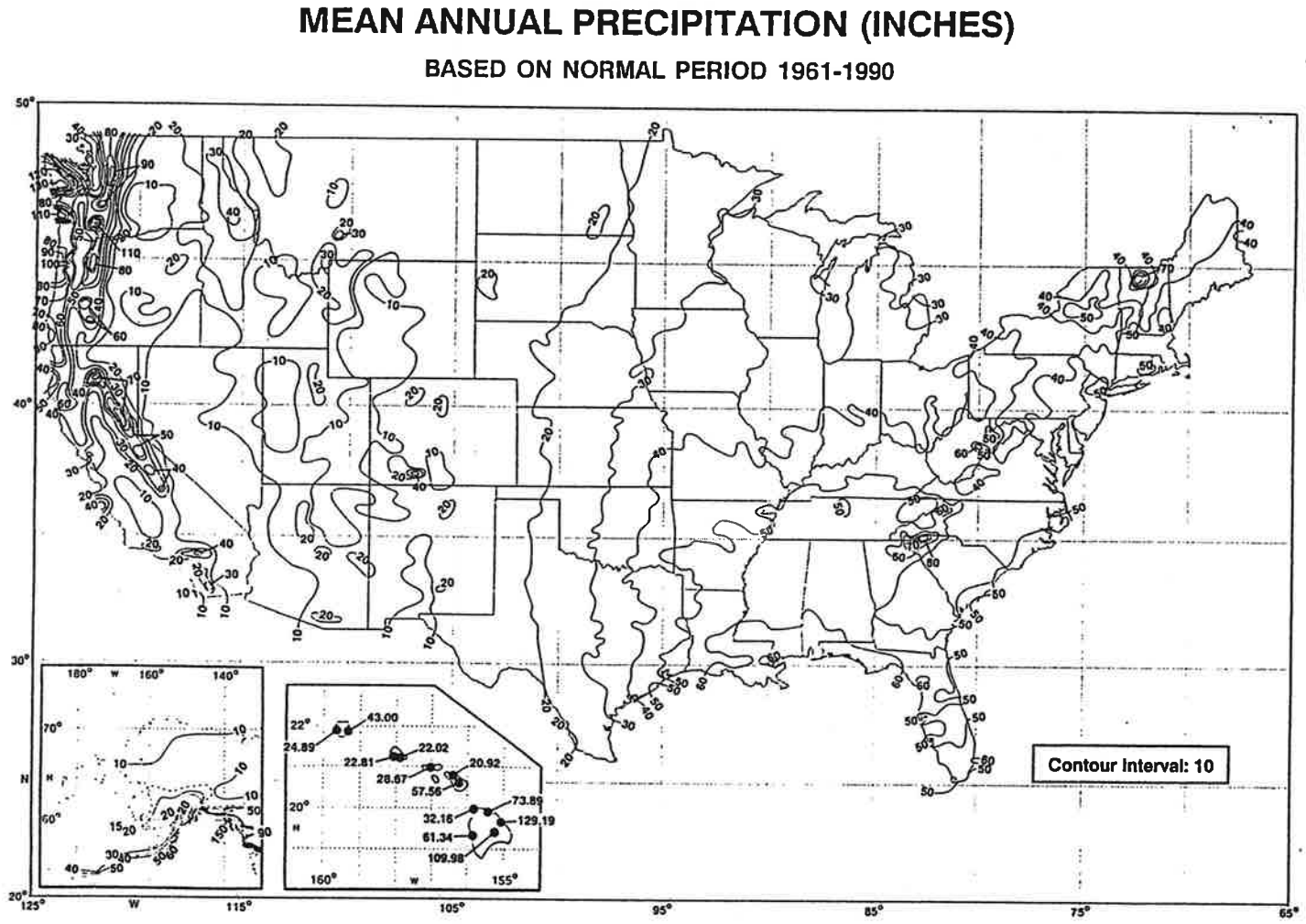

Figure F-10. Mean annual precipitation, in.

software package. In addition, it was determined that for a given set of design inputs, a plot of log W_{18} vs D (slab thickness) is a straight line relationship. The relationship can be modelled as:

$$D = A_0 + A_1 \log_{10} W_{18\,R} \qquad \text{(F-14)}$$

where D = required slab thickness, in

A_0 and A_1 = regression constants dependent on other design features

W_{18R} = design 18-kip [80 kN] ESALs for the specified level of design reliability R

The W_{18R} for any level of design reliability and overall standard deviation is computed as follows:

$$W_{18R} = 10^{(\log W_{18} + Z S_o)} \qquad \text{(F-15)}$$

where W_{18R} = design 18-kip [80 kN] ESALs for the specified level of design reliability R

W_{18} = estimated 18-kip [80 kN] ESALs over the design period in the design lane

Z = standard deviate from normal distribution table for given level of reliability (e.g., 1.28 for R = 90 percent)

S_o = overall standard deviation

The required slab thickness D was computed over a range of W_{18R} using the rigid pavement design equations, and the regression constants A_0 and A_1 were computed for all combinations of design conditions. Table F-5 provides these constants for a wide range of design conditions.

Table F-5. A_0 and A_1 constants for model $D = A_0 + A_1 \log W$, for P2 = 2.5, conventional 12-ft lane.

Base Modulus (psi)	Joint Spacing (in)	Concrete S'c (psi)	Temp Diff (oF)	k = 100		k = 250		k = 500	
				A0	A1	A0	A1	A0	A1
25,000	144	600	5	-16.555	3.711	-21.202	4.264	-31.660	5.556
25,000	144	600	7	-16.552	3.698	-21.663	4.343	-33.857	5.910
25,000	144	600	9	-17.032	3.754	-22.497	4.474	-36.137	6.275
25,000	144	600	11	-17.031	3.744	-22.672	4.510	-37.885	6.567
25,000	144	600	13	-17.030	3.734	-23.357	4.618	-39.508	6.839
25,000	144	700	5	-15.974	3.499	-20.819	4.062	-28.981	5.046
25,000	144	700	7	-15.921	3.482	-20.460	4.043	-30.312	5.281
25,000	144	700	9	-16.430	3.545	-21.078	4.144	-33.082	5.696
25,000	144	700	11	-16.386	3.531	-21.048	4.153	-34.124	5.888
25,000	144	700	13	-16.348	3.519	-21.536	4.234	-34.916	6.042
25,000	144	800	5	-15.161	3.281	-19.620	3.789	-27.213	4.688
25,000	144	800	7	-15.065	3.261	-20.154	3.880	-28.621	4.930
25,000	144	800	9	-14.978	3.243	-20.631	3.962	-29.888	5.148
25,000	144	800	11	-14.901	3.227	-21.058	4.035	-30.355	5.258
25,000	144	800	13	-14.829	3.213	-21.445	4.102	-30.603	5.335
25,000	192	600	5	-16.668	3.748	-21.362	4.321	-33.261	5.828
25,000	192	600	7	-16.699	3.746	-21.879	4.420	-35.910	6.270
25,000	192	600	9	-16.732	3.745	-22.808	4.576	-38.080	6.646
25,000	192	600	11	-16.759	3.744	-22.923	4.613	-40.082	6.998
25,000	192	600	13	-16.789	3.744	-23.644	4.736	-41.249	7.229
25,000	192	700	5	-16.034	3.529	-20.221	4.031	-29.518	5.182
25,000	192	700	7	-16.002	3.522	-20.453	4.092	-32.560	5.662
25,000	192	700	9	-15.973	3.516	-21.102	4.210	-33.491	5.866
25,000	192	700	11	-15.947	3.511	-21.668	4.314	-34.320	6.050
25,000	192	700	13	-15.924	3.506	-21.740	4.346	-34.816	6.183
25,000	192	800	5	-15.183	3.306	-19.887	3.866	-27.819	4.838
25,000	192	800	7	-15.097	3.295	-20.464	3.977	-28.697	5.034
25,000	192	800	9	-15.021	3.285	-20.970	4.075	-30.129	5.290
25,000	192	800	11	-14.953	3.276	-19.846	3.958	-30.559	5.416
25,000	192	800	13	-14.892	3.268	-20.187	4.029	-30.743	5.502
25,000	240	600	5	-16.186	3.702	-21.469	4.376	-34.979	6.130
25,000	240	600	7	-16.248	3.712	-21.964	4.486	-37.708	6.615
25,000	240	600	9	-16.308	3.722	-22.923	4.660	-39.917	7.028
25,000	240	600	11	-16.357	3.730	-23.737	4.811	-40.901	7.266
25,000	240	600	13	-16.402	3.737	-23.536	4.811	-42.624	7.603
25,000	240	700	5	-16.072	3.559	-20.116	4.061	-31.731	5.547
25,000	240	700	7	-15.488	3.483	-20.894	4.214	-32.777	5.801
25,000	240	700	9	-15.470	3.486	-21.137	4.288	-33.409	5.990
25,000	240	700	11	-15.452	3.487	-21.173	4.329	-33.859	6.144
25,000	240	700	13	-15.436	3.489	-21.597	4.422	-34.089	6.259
25,000	240	800	5	-15.172	3.331	-20.088	3.942	-27.776	4.916
25,000	240	800	7	-15.085	3.327	-19.248	3.885	-29.183	5.204
25,000	240	800	9	-15.011	3.325	-19.666	3.984	-29.293	5.316
25,000	240	800	11	-14.942	3.322	-19.497	3.997	-29.355	5.410
25,000	240	800	13	-14.884	3.320	-19.781	4.070	-29.261	5.471

Table F-5. A_0 and A_1 constants for model $D = A_0 + A_1 \log W$, for P2 = 2.5, conventional 12-ft lane (continued).

Base Modulus (psi)	Joint Spacing (in)	Concrete S'c (psi)	Temp Diff (oF)	k = 100		k = 250		k = 500	
				A0	A1	A0	A1	A0	A1
500,000	144	600	5	-16.437	3.498	-23.558	4.386	-33.563	5.598
500,000	144	600	7	-16.058	3.463	-22.963	4.364	-33.446	5.694
500,000	144	600	9	-15.750	3.436	-22.659	4.371	-32.745	5.699
500,000	144	600	11	-15.496	3.414	-22.356	4.371	-36.888	6.311
500,000	144	600	13	-15.281	3.396	-22.230	4.391	-34.923	6.132
500,000	144	700	5	-15.750	3.298	-21.145	3.965	-32.605	5.344
500,000	144	700	7	-14.886	3.206	-21.468	4.055	-30.287	5.160
500,000	144	700	9	-14.506	3.172	-20.946	4.034	-29.717	5.175
500,000	144	700	11	-14.199	3.145	-20.655	4.036	-32.327	5.576
500,000	144	700	13	-13.944	3.123	-20.476	4.047	-30.627	5.428
500,000	144	800	5	-14.841	3.093	-20.018	3.726	-27.592	4.624
500,000	144	800	7	-14.367	3.051	-19.528	3.714	-28.475	4.822
500,000	144	800	9	-13.996	3.019	-19.437	3.745	-27.407	4.771
500,000	144	800	11	-13.111	2.921	-19.026	3.730	-29.159	5.053
500,000	144	800	13	-12.836	2.898	-18.769	3.730	-27.768	4.943
500,000	192	600	5	-16.160	3.491	-22.995	4.366	-33.301	5.646
500,000	192	600	7	-15.735	3.459	-22.370	4.352	-32.861	5.723
500,000	192	600	9	-15.398	3.435	-22.018	4.364	-36.080	6.247
500,000	192	600	11	-14.854	3.379	-21.714	4.374	-34.625	6.163
500,000	192	600	13	-14.623	3.364	-24.924	4.837	-34.793	6.281
500,000	192	700	5	-14.990	3.233	-21.410	4.050	-30.238	5.138
500,000	192	700	7	-14.462	3.191	-20.566	4.009	-29.039	5.110
500,000	192	700	9	-14.058	3.160	-19.958	3.986	-30.516	5.396
500,000	192	700	11	-13.740	3.138	-19.672	3.997	-29.136	5.312
500,000	192	700	13	-13.479	3.120	-20.184	4.102	-28.428	5.299
500,000	192	800	5	-14.428	3.072	-19.294	3.691	-28.220	4.784
500,000	192	800	7	-13.388	2.968	-18.947	3.709	-26.456	4.680
500,000	192	800	9	-12.946	2.934	-18.399	3.694	-27.105	4.854
500,000	192	800	11	-12.603	2.909	-18.081	3.700	-25.895	4.785
500,000	192	800	13	-12.326	2.890	-18.053	3.735	-27.608	5.070
500,000	240	600	5	-15.840	3.482	-22.429	4.350	-32.949	5.694
500,000	240	600	7	-15.107	3.416	-21.784	4.348	-36.616	6.318
500,000	240	600	9	-14.734	3.395	-21.325	4.357	-33.870	6.102
500,000	240	600	11	-14.438	3.379	-22.813	4.611	-33.369	6.158
500,000	240	600	13	-13.916	3.328	-21.875	4.542	-36.436	6.672
500,000	240	700	5	-14.566	3.213	-20.478	3.992	-28.956	5.074
500,000	240	700	7	-13.995	3.174	-19.584	3.957	-29.849	5.326
500,000	240	700	9	-13.573	3.148	-20.308	4.114	-28.167	5.236
500,000	240	700	11	-13.245	3.130	-19.111	4.018	-30.326	5.625
500,000	240	700	13	-12.983	3.117	-18.446	3.980	-28.948	5.541
500,000	240	800	5	-13.482	2.988	-18.803	3.689	-26.067	4.615
500,000	240	800	7	-12.861	2.945	-17.936	3.657	-26.007	4.739
500,000	240	800	9	-12.408	2.916	-17.822	3.706	-24.504	4.660
500,000	240	800	11	-12.064	2.897	-16.948	3.648	-24.765	4.786
500,000	240	800	13	-11.794	2.883	-16.313	3.611	-23.789	4.742

Table F-5. A_0 and A_1 constants for model $D = A_0 + A_1 \log W$, for P2 = 2.5, conventional 12-ft lane (continued).

Base Modulus (psi)	Joint Spacing (in)	Concrete S'c (psi)	Temp Diff (oF)	k = 100		k = 250		k = 500	
				A0	A1	A0	A1	A0	A1
1,000,000	144	600	5	-16.868	3.452	-23.074	4.251	-29.476	5.023
1,000,000	144	600	7	-15.710	3.336	-20.953	4.053	-32.996	5.569
1,000,000	144	600	9	-14.930	3.263	-19.903	3.976	-29.456	5.232
1,000,000	144	600	11	-14.923	3.282	-20.749	4.128	-27.156	5.025
1,000,000	144	600	13	-14.170	3.206	-19.835	4.055	-31.121	5.605
1,000,000	144	700	5	-15.980	3.251	-22.247	4.050	-28.188	4.760
1,000,000	144	700	7	-14.711	3.124	-19.667	3.796	-29.825	5.063
1,000,000	144	700	9	-13.887	3.046	-21.496	4.072	-25.809	4.661
1,000,000	144	700	11	-13.520	3.022	-18.750	3.777	-24.586	4.586
1,000,000	144	700	13	-12.864	2.958	-17.848	3.703	-26.418	4.880
1,000,000	144	800	5	-14.828	3.032	-21.681	3.898	-27.158	4.545
1,000,000	144	800	7	-13.857	2.943	-18.592	3.580	-28.810	4.846
1,000,000	144	800	9	-13.013	2.865	-19.221	3.707	-24.272	4.376
1,000,000	144	800	11	-12.414	2.812	-17.360	3.520	-22.732	4.257
1,000,000	144	800	13	-11.834	2.759	-16.522	3.453	-23.394	4.396
1,000,000	192	600	5	-15.975	3.374	-21.364	4.093	-27.649	4.878
1,000,000	192	600	7	-14.866	3.272	-19.699	3.962	-29.784	5.275
1,000,000	192	600	9	-14.551	3.262	-20.073	4.071	-26.995	5.036
1,000,000	192	600	11	-13.693	3.180	-18.979	3.989	-28.997	5.386
1,000,000	192	600	13	-13.099	3.127	-18.240	3.942	-27.235	5.246
1,000,000	192	700	5	-14.926	3.155	-19.863	3.813	-25.718	4.543
1,000,000	192	700	7	-13.760	3.048	-20.180	3.925	-25.223	4.601
1,000,000	192	700	9	-13.117	2.999	-17.875	3.701	-27.832	5.033
1,000,000	192	700	11	-12.357	2.930	-16.891	3.630	-24.104	4.649
1,000,000	192	700	13	-11.818	2.885	-16.245	3.593	-23.103	4.600
1,000,000	192	800	5	-14.027	2.970	-18.623	3.581	-24.087	4.259
1,000,000	192	800	7	-12.840	2.861	-18.187	3.599	-23.255	4.272
1,000,000	192	800	9	-12.014	2.791	-16.367	3.433	-23.347	4.375
1,000,000	192	800	11	-11.320	2.731	-15.486	3.373	-21.419	4.218
1,000,000	192	800	13	-10.821	2.691	-15.728	3.445	-22.681	4.445
1,000,000	240	600	5	-15.147	3.306	-20.046	3.986	-31.091	5.386
1,000,000	240	600	7	-14.533	3.273	-20.020	4.071	-27.169	5.054
1,000,000	240	600	9	-13.419	3.169	-18.455	3.948	-29.660	5.509
1,000,000	240	600	11	-12.698	3.109	-17.485	3.886	-27.870	5.395
1,000,000	240	600	13	-12.171	3.069	-18.835	4.118	-30.166	5.800
1,000,000	240	700	5	-13.983	3.075	-18.300	3.680	-26.125	4.679
1,000,000	240	700	7	-13.011	3.000	-17.510	3.667	-27.426	4.989
1,000,000	240	700	9	-12.034	2.915	-16.236	3.578	-23.144	4.567
1,000,000	240	700	11	-11.384	2.865	-16.588	3.682	-24.211	4.803
1,000,000	240	700	13	-10.908	2.831	-15.366	3.576	-22.157	4.623
1,000,000	240	800	5	-13.012	2.883	-18.860	3.672	-23.534	4.283
1,000,000	240	800	7	-11.853	2.785	-15.855	3.384	-22.292	4.260
1,000,000	240	800	9	-10.969	2.713	-15.977	3.466	-20.205	4.109
1,000,000	240	800	11	-10.373	2.670	-14.402	3.326	-20.113	4.186
1,000,000	240	800	13	-9.936	2.642	-13.599	3.272	-18.759	4.088

Example Determination of Required Slab Thickness. The following design inputs must be determined (note that an approximate estimate for D must be made):

(1) effective subgrade k value, k = 100 psi/in [27 kPa/mm]
(2) estimated future traffic, W_{18} = 20 million
(3) design reliability, R = 90 percent
(4) overall standard deviation, S_o = 0.39
(5) design serviceability loss, PSI = P_1 - P_2 = 4.5 - 2.5 = 2.0
(6) mean concrete modulus of rupture, S'_c = 700 psi [4820 kPa]
(7) mean concrete elastic modulus, $E_c = 26454\ S'^{0.77}_c$ = 4,100,000 psi [28249 MPa]
(8) joint spacing, L = 16 ft = 192 in [4877 mm]
(9) base modulus, E_b = 1,000,000 psi (treated base)
(10) slab/base friction coefficient, f = 35
(11) base thickness, H_b = 5 in
(12) effective positive temperature differential through slab, TD:
    Annual wind speed = 10 mph [16 km/hr]
    Annual temperature = 53°F [29°C]
    Annual precipitation = 40 in [1016 mm]
    Effective positive TD = 9°F [5°C] (from Equation F-13)
(13) lane edge support condition: conventional lane width (12 ft [3.66 m]), free edge
(14) initial estimate of slab thickness = 11 in [279 mm]

The design traffic for a 90 percent level of reliability and an overall standard deviation of 0.39 is computed as follows:

$$W_R = 10^{(\log W + Z\ So)} = 10^{(\log 20{,}000{,}000 + 1.28 * 0.39)} = 63 \text{ million}$$

The rigid pavement design equations presented may be used to obtain the required slab thickness of 10.4 in [264 mm] for a design reliability of 90 percent.

Similarly, Table F-5 may be used to determine the A_0 and A_1 constants to predict the required slab thickness for a design reliability of 90 percent:

$$D_{90} = A_0 + A_1 \log W = -12.357 + 2.930 * \log (63{,}000{,}000) = 10.5 \text{ in } [267 \text{ mm}]$$

These thicknesses are close to the initial estimate of 11 in [279 mm]. If the required thickness differed by an inch or more, the above calculations would be repeated, beginning with a new effective temperature differential for the new trial slab thickness. The A_0 and A_1 constants may be linearly interpolated from Table F-5 as necessary for other temperature differential values.

An agency could prepare its own design tables such as those shown in Tables F-6 and F-7 that fit the agency's design conditions using a spreadsheet or software program.

Design Check For Joint Load Position Cracking. This check is not necessary if dowels are to be used at the transverse joints. Dowels reduce the stresses at the joint to levels much lower than those at the midslab load position. Field surveys show that cracks do not occur near adequately dowelled joints.

If dowels are not used at the transverse joints, a check must be made to ensure that stresses created at the top of the slab when the axle load is at the joint are not excessive. Under certain design and climatic conditions, truck axle loadings near a undowelled transverse joint may produce even higher tensile stresses at the top of the slab than the stresses produced at the bottom of the slab by midslab loading. These repeated high tensile stresses could result in the development of corner breaks, diagonal cracks, or even transverse cracks away from the joint that initiate at the top of the slab.

Table F-6. Example slab thickness required for given inputs for untreated aggregate base, conventional width traffic lane with no tied concrete shoulders for Midwestern location.

k value psi/in	100	100	100	250	250	250	500	500	500
Design Lane ESAL	S'_c 600 psi	S'_c 700 psi	S'_c 800 psi	S'_c 600 psi	S'_c 700 psi	S'_c 800 psi	S'_c 600 psi	S'_c 700 psi	S'_c 800 psi
1	7.5	6.9	6.4	6.5	6.0*	6.0*	6.0*	6.0*	6.0*
2.5	8.8	8.1	7.5	8.1	7.4	6.8	6.0*	6.0*	6.0*
5	9.8	9.0	8.4	9.5	8.6	7.9	8.6	7.7	6.8
10	10.9	10.0	9.3	10.9	9.9	9.1	10.8	9.7	8.8
20	12.1	11.1	10.3	12.4	11.3	10.4	13.0	11.6	10.5
30	12.8	11.8	10.9	13.5	12.1	11.2	14.4	12.8	11.6
40	13.4	12.3	11.4	14.1	12.8	11.7	15.3	13.6	12.4
50	13.8	12.7	11.8	14.6	13.3	12.2	16.1	14.3	13.0
75	14.7	13.5	12.5	15.7	14.2	13.1	17.6	15.6	14.1
100	15.3	14.1	13	16.5	14.9	13.7	18.7	16.6	15.0

1 in = 25.4 mm, 1 psi/in = 0.27 kPa/mm, 1 psi = 6.89 kPa

* Minimum slab thickness of 6.0 in [152 mm] recommended

ESAL = design lane (millions)

k value = elastic value of subgrade/embankment

P1 - P2 = 2.0

Joint spacing = 15 ft [4.6 m]

Untreated aggregate base: H_b = 6 in [152 mm], E_b = 25,000 psi [172 MPa], f = 1.5

S'_c = mean 28-day, third-point loading

$E_c = 26454 * Sc^{0.77}$

Design reliability = 90 percent (So = 0.39)

Lane width = 12 ft [3.66 m], no tied concrete shoulders

Effective positive DT = varies with slab thickness for a given climate

Table F-7. Slab thickness required for given inputs for treated aggregate base.

k value psi/in	100	100	100	250	250	250	500	500	500
Design Lane ESAL	S'_c 600 psi	S'_c 700 psi	S'_c 800 psi	S'_c 600 psi	S'_c 700 psi	S'_c 800 psi	S'_c 600 psi	S'_c 700 psi	S'_c 800 psi
1	6.2	6.0*	6.0*	6.0*	6.0*	6.0*	6.0*	6.0*	6.0*
2.5	7.9	7.3	6.9	6.0*	6.0*	6.0*	6.0*	6.0*	6.0*
5	8.9	8.3	7.8	8.8	8.1	7.6	8.6**	7.9**	7.4**
10	9.9	9.3	8.8	10.2	9.5	8.9	9.8**	9.1	8.4
20	11.0	10.3	9.7	11.5	10.8	10.1	11.9	11.1	10.3
30	11.6	10.9	10.3	12.3	11.5	10.8	13.0	12.0	11.2
40	12.0	11.3	10.7	12.9	12.0	11.3	13.7	12.7	11.9
50	12.4	11.6	11.0	13.3	12.4	11.7	14.2	13.2	12.4
75	13.0	12.2	11.6	14.1	13.2	12.4	15.2	14.1	13.2
100	13.5	12.7	12.0	14.7	13.7	12.9	15.9	14.8	13.8

1 in = 25.4 mm, 1 psi/in = 0.27 kPa/mm, 1 psi = 6.89 kPa

* Minimum slab thickness of 6.0 in [152 mm] recommended. ** Estimated values.

ESAL = design lane (millions)

k value = elastic value of subgrade/embankment

P1 - P2 = 2.0

Joint spacing = 15 ft [4.6 m]

Treated aggregate base: H_b = 4 in [102 mm], E_b = 800,000 psi [5512 MPa], f = 35

S'_c = mean 28-day, third-point loading

$E_c = 26454 * Sc^{0.77}$

Design reliability = 90 percent (So = 0.39)

Lane width = 12 ft [3.66 m], no tied concrete shoulders

Effective positive DT = varies with slab thickness for a given climate

A design check for the joint loading position with negative equivalent temperature differentials is provided in this section. There are four load and climatic conditions that could potentially contribute to this maximum stress for the joint loading position.

Axle load stress: When the axle load is near the transverse joint a tensile stress occurs at the top of the slab.

Negative temperature differential stress: Negative (nighttime) temperature differentials cause corners to curl upward, creating a tensile stress at the slab surface. An equation for effective negative temperature differential stress is provided below:

$$\textit{effective negative TD} = -18.14 + \frac{52.01}{D} + 0.394\ \textit{WIND} + 0.07\ \textit{TEMP} + 0.00407\ \textit{PRECIP} \quad \text{(F-16)}$$

where effective negative TD = top temperature minus bottom temperature, ^{o}F

D = slab thickness, in

WIND = mean annual wind speed, mph (Figure F-8)

TEMP = mean annual temperature, ^{o}F (Figure F-9)

PRECIP = mean annual precipitation, in (Figure F-10)

Construction curling stress: Upward curling of corners occurs shortly after concrete slab placement if a high positive temperature differential through the slab is present as the concrete sets. This positive differential occurs particularly on sunny days when conventional curing procedures are used. This temperature differential has not been measured extensively in the past

and its magnitude is not well known at the present time. This is defined as the temperature differential that would be required to produce a flat slab (exclusive of moisture warping).

Moisture gradient stress: Moisture shrinkage warping of the top of the slab occurs over time. The stress induced by this type of warping can be determined by representing the moisture warping by an equivalent temperature gradient.

It is difficult to quantify construction curling stress and moisture gradient stress separately. However, their combined effect can be thought of as the positive temperature differential required to bring the slab into a flat position in the absence of an actual temperature differential through the slab. An approximate equivalent temperature differential may be assumed that is related to the general climate of the site and to conventional curing procedures (i.e., curing compound, no wet cure):

Wet climate zone (Annual precipitation $\geq$ 30 in [762 mm], or Thornthwaite Moisture Index > 0): 0 to 2°F per inch [0 to 0.044°C per mm] of slab thickness.

Dry climate zone (Annual precipitation < 30 in [762 mm], or Thornthwaite Moisture Index < 0): 1 to 3°F per inch [0.02 to 0.066°C per mm] of slab thickness.

If wet curing conditions or night construction are used, these values may be reduced significantly.

The following procedure was developed to check for critical stress for the joint loading position for pavements that do not include mechanical load transfer devices equivalent to dowel bars.

STEP 1: Design pavement according to Section 3.2.2 (Required Slab Thickness) assuming that the midslab loading position is critical. (Note that the effect of slab/base friction is included in the required slab thickness obtained.)

STEP 2: Compute the midslab stress for the required slab thickness and the site's effective positive temperature differential, using the stress equations provided in Section 3.2.2 for an 18,000-lbf [80 kN] single-axle load, or using Figures F-11 and F-12. Two different base types (untreated aggregate and treated aggregate) and three levels of subgrade support are shown in Figure F-11 so that the designer can estimate through interpolation the approximate full friction stress in the slab. The full friction stress from Figure F-11 is multiplied by the friction adjustment factor from Figure F-12 to obtain the proper midslab stress.

STEP 3: Estimate a total "equivalent" negative temperature differential from the following sources.

(a) Effective negative temperature differential: From Equation F-16.

(b) Combined moisture gradient and construction temperature differential:

Wet climate zone (Annual precipitation $\geq$ 30 in [762 mm], or Thornthwaite Moisture Index > 0): 0 to 2°F per inch [0 to 0.044°C per mm] of slab thickness.

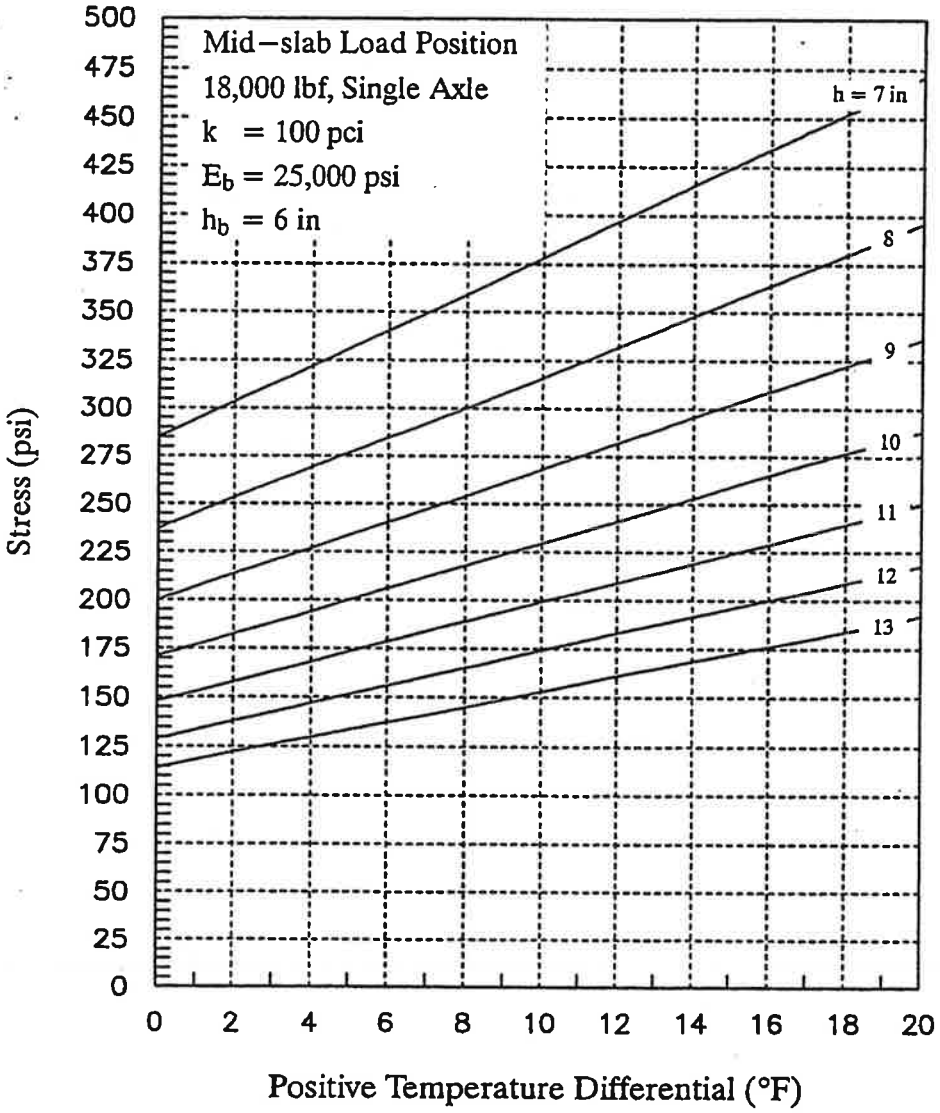

Figure F-11a. Maximum tensile stress at bottom of slab for midslab loading position versus a positive temperature differential through the slab for specific design conditions (aggregate base, soft subgrade).

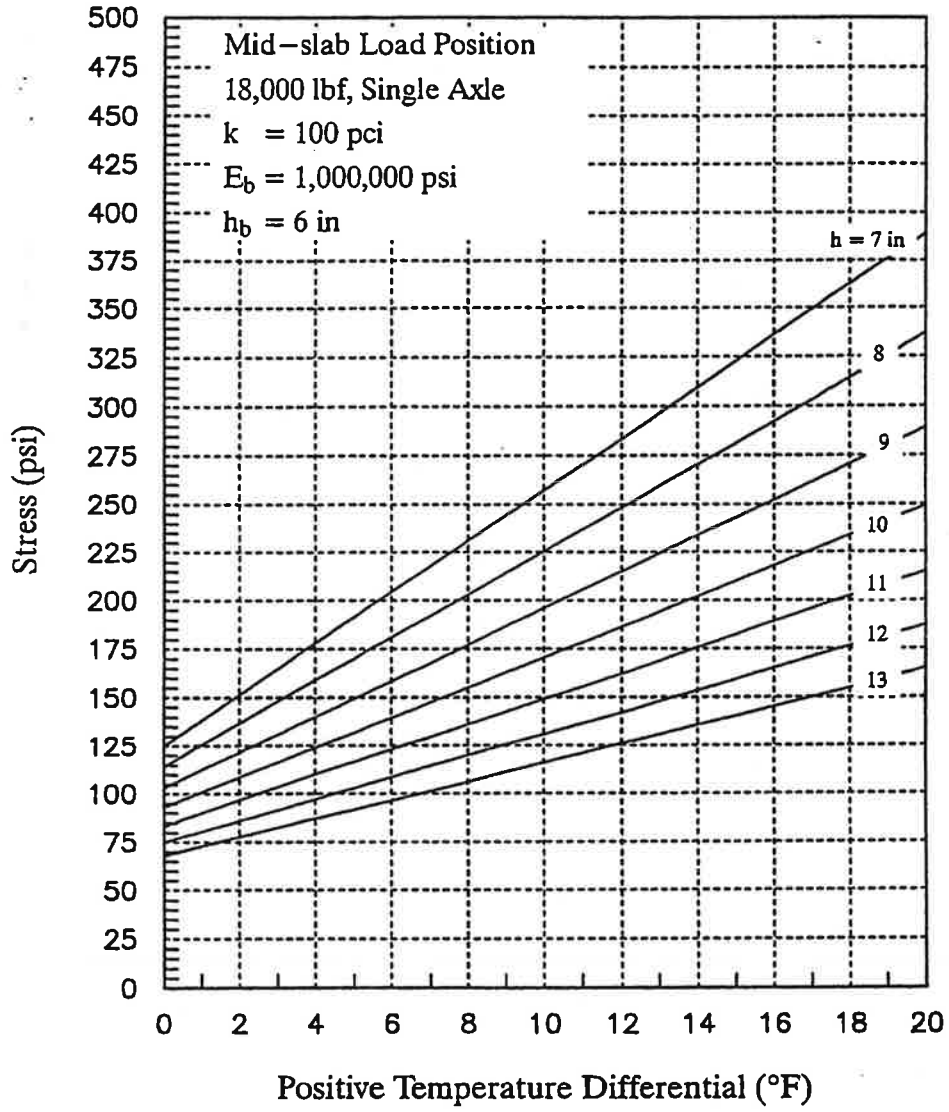

Figure F-11b. Maximum tensile stress at bottom of slab for midslab loading position versus a positive temperature differential through the slab for specific design conditions (treated base, soft subgrade).

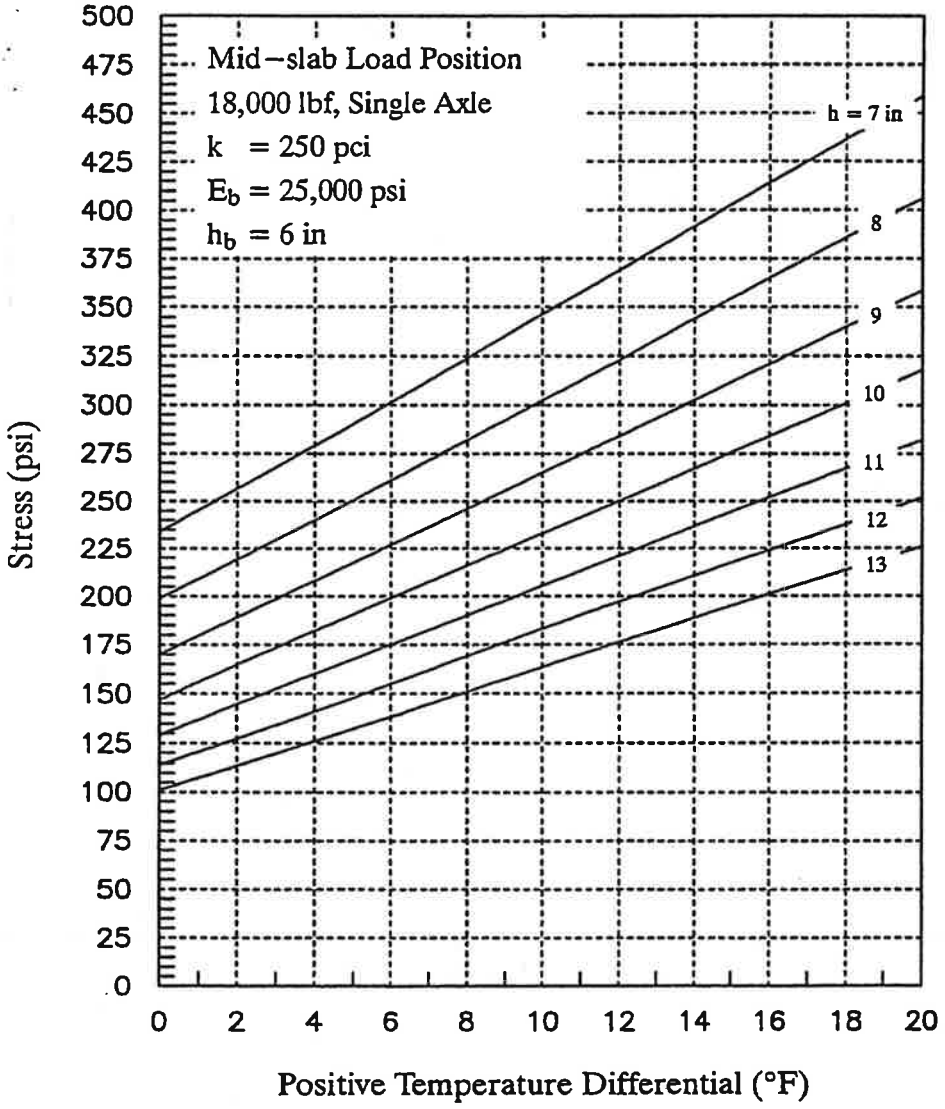

Figure F-11c. Maximum tensile stress at bottom of slab for midslab loading position versus a positive temperature differential through the slab for specific design conditions (aggregate base, medium subgrade).

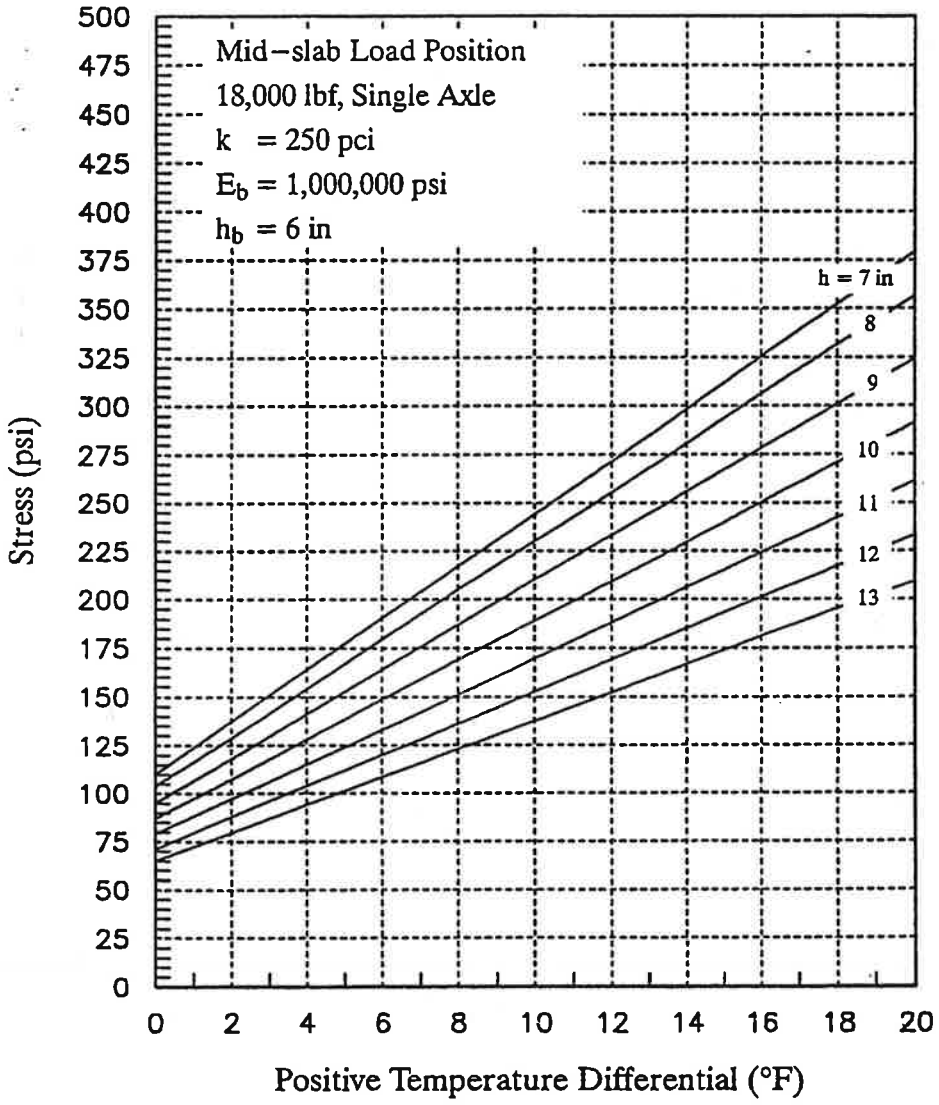

Figure F-11d. Maximum tensile stress at bottom of slab for midslab loading position versus a positive temperature differential through the slab for specific design conditions (treated base, medium subgrade).

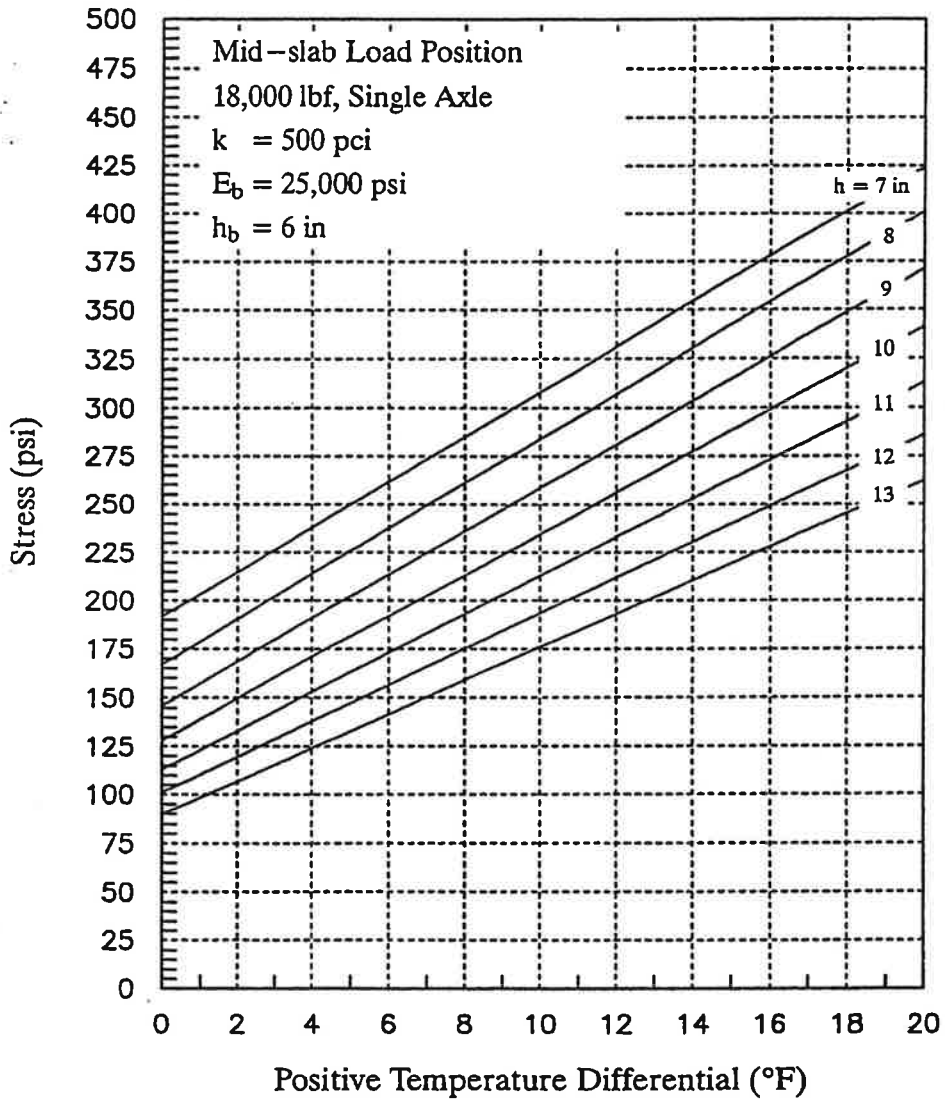

Figure F-11e. Maximum tensile stress at bottom of slab for midslab loading position versus a positive temperature differential through the slab for specific design conditions (aggregate base, stiff subgrade).

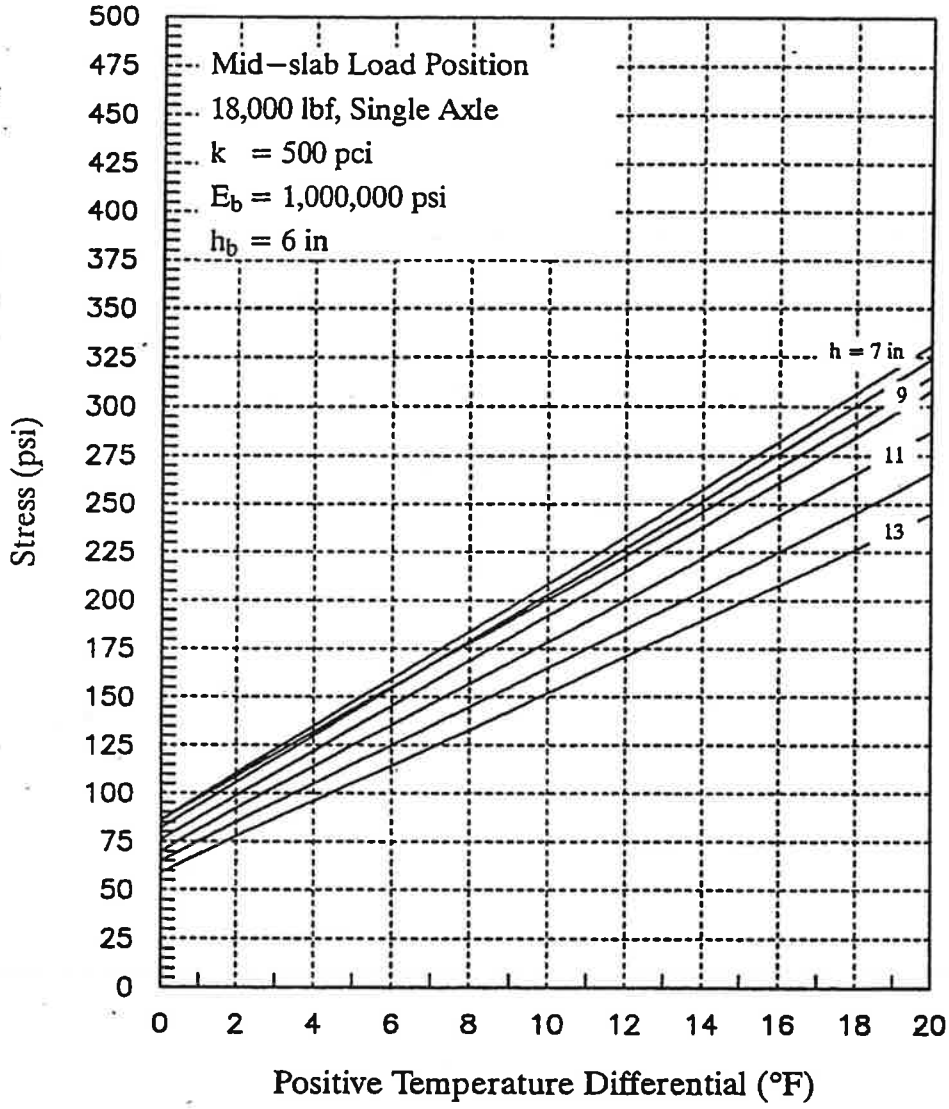

Figure F-11f. Maximum tensile stress at bottom of slab for midslab loading position versus a positive temperature differential through the slab for specific design conditions (treated base, stiff subgrade).

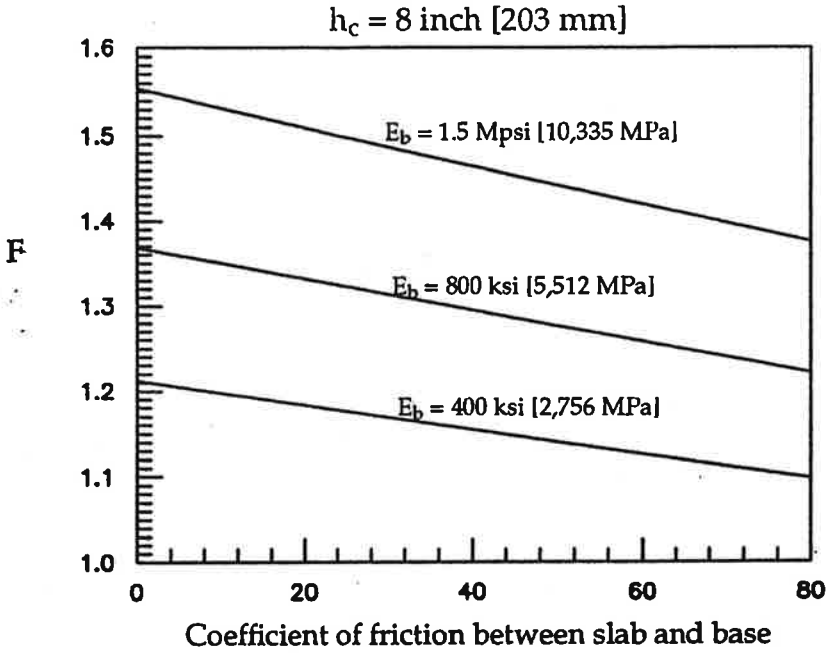

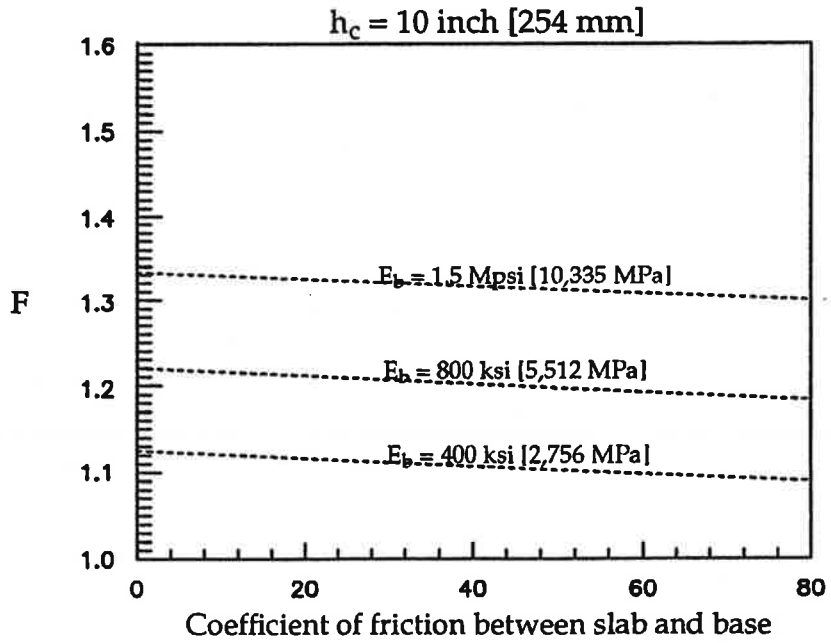

Note: h_b = 5 inch [127 mm] , k = 200 psi/in [54 kPa/mm]
E_c = 4 Mpsi [27,560 MPa] ,
Mid–slab loading with daytime curling DT (°F) [1°F = 0.56°C]

Figure F-12. Friction adjustment factor for stress at bottom of slab for midslab loading.

Dry climate zone (Annual precipitation < 30 in [762 mm], or Thornthwaite Moisture Index < 0): 1 to 3°F per inch [0.02 to 0.066°C per mm] of slab thickness.

STEP 4: Use Figures F-13 and F-14 to estimate the critical stress at the top of the slab from joint loading and negative temperature differential. Two different base types (untreated aggregate and treated aggregate) and three levels of subgrade support are shown in Figure F-13 so that the designer can estimate through interpolation the approximate full friction stress in the slab. The full friction stress from Figure F-13 is multiplied by the friction adjustment factor from Figure F-14 to obtain the proper joint load stress.

STEP 5: Compare the midslab load position stress at the bottom of the slab and the joint loading position stress at the top of the slab. If the joint load position produces an equal or higher stress, then strong consideration should be given to a redesign of the joints (e.g., dowel bars, shorter joint spacing, base type).

<u>Example Design Check for Joint Load Position Cracking.</u> Assume the same pavement defined previously:

(1) effective subgrade k value, k = 100 psi/in [27 kPa/mm]
(2) estimated future traffic, W_{18} = 20 million
(3) design reliability, R = 90 percent
(4) overall standard deviation, S_0 = 0.39

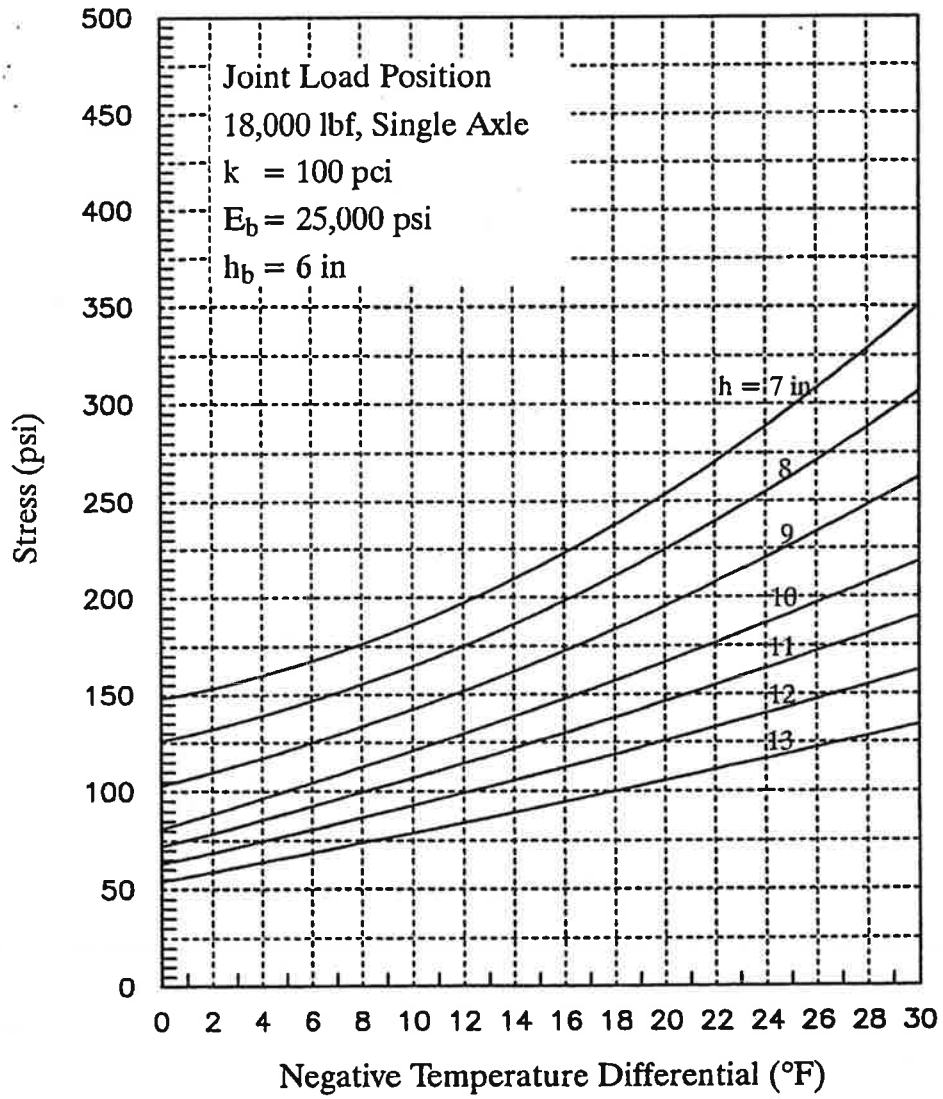

Figure F-13a. Maximum tensile stress at top of slab for joint loading position versus a negative temperature differential through the slab for specific design conditions (aggregate base, soft subgrade).

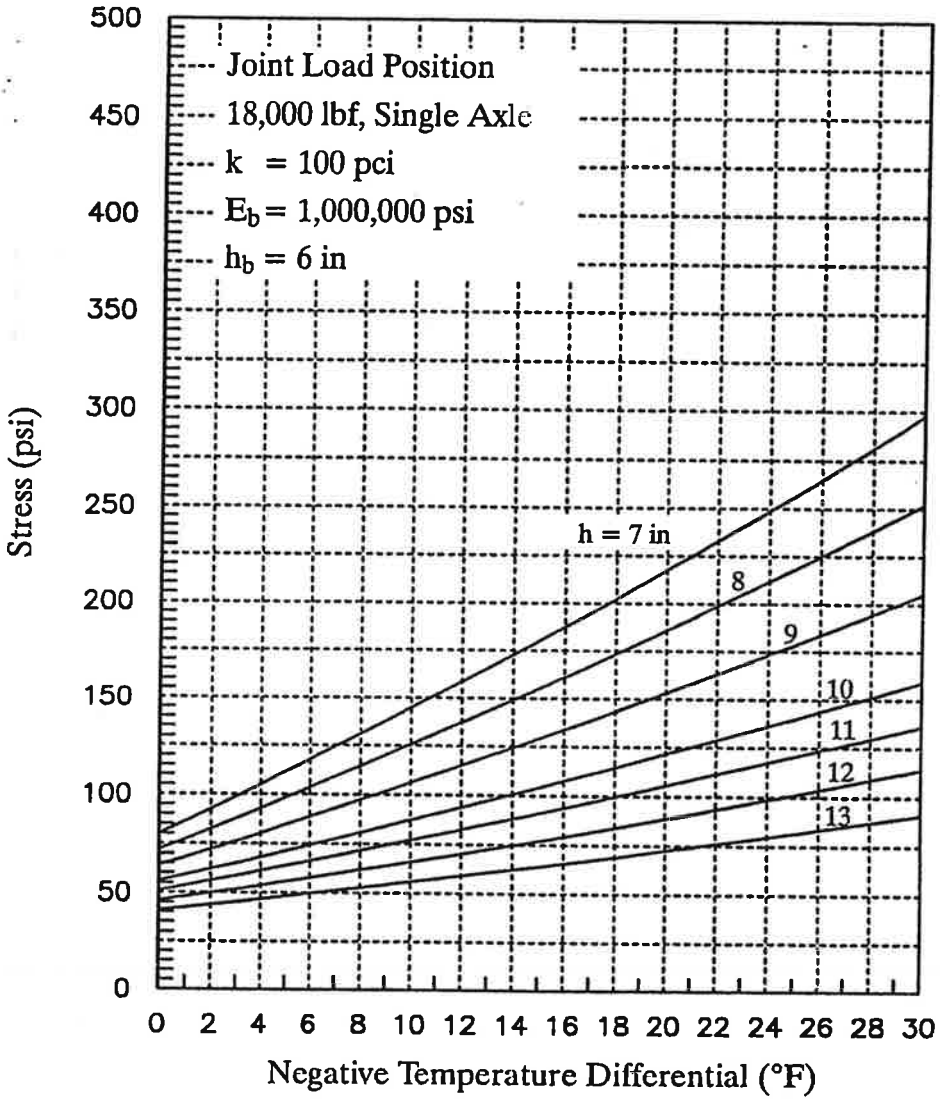

Figure F-13b. Maximum tensile stress at top of slab for joint loading position versus a negative temperature differential through the slab for specific design conditions (treated base, soft subgrade).

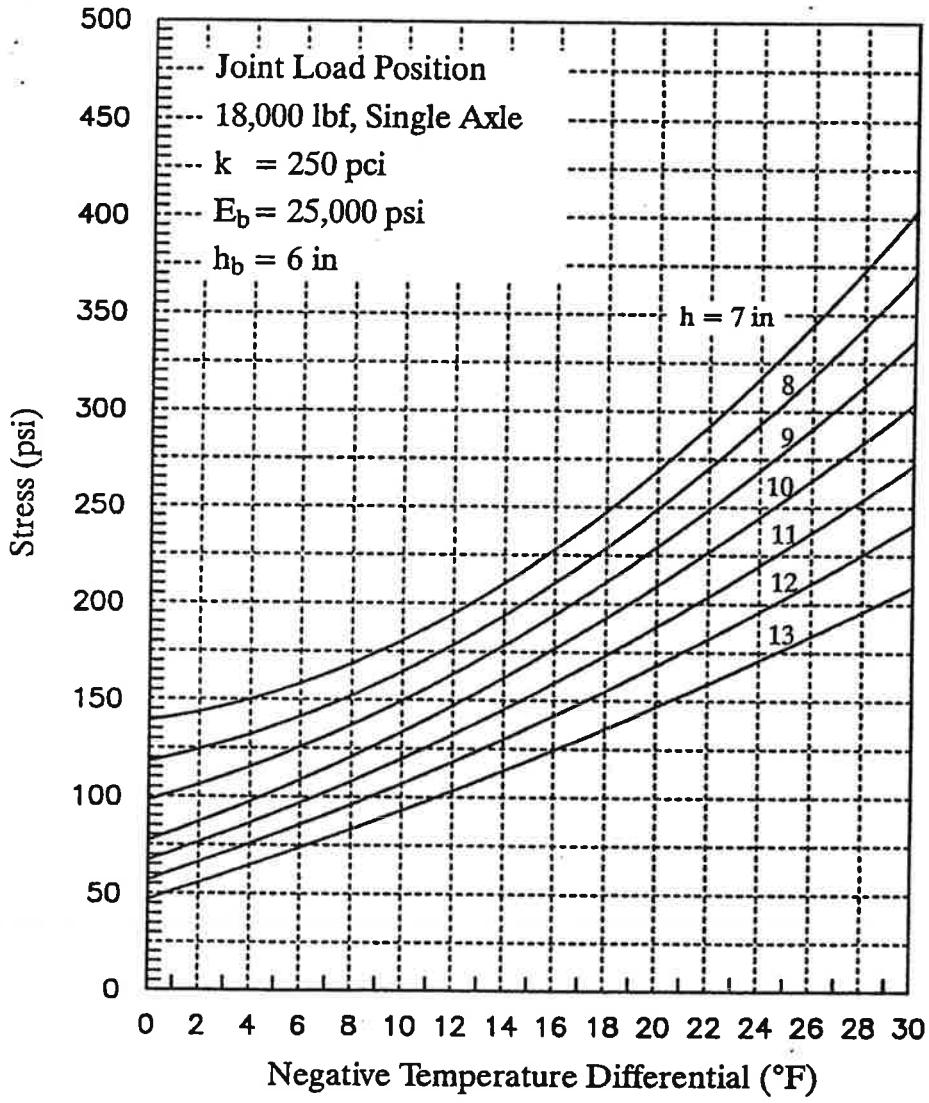

Figure F-13c. Maximum tensile stress at top of slab for joint loading position versus a negative temperature differential through the slab for specific design conditions (aggregate base, medium subgrade).

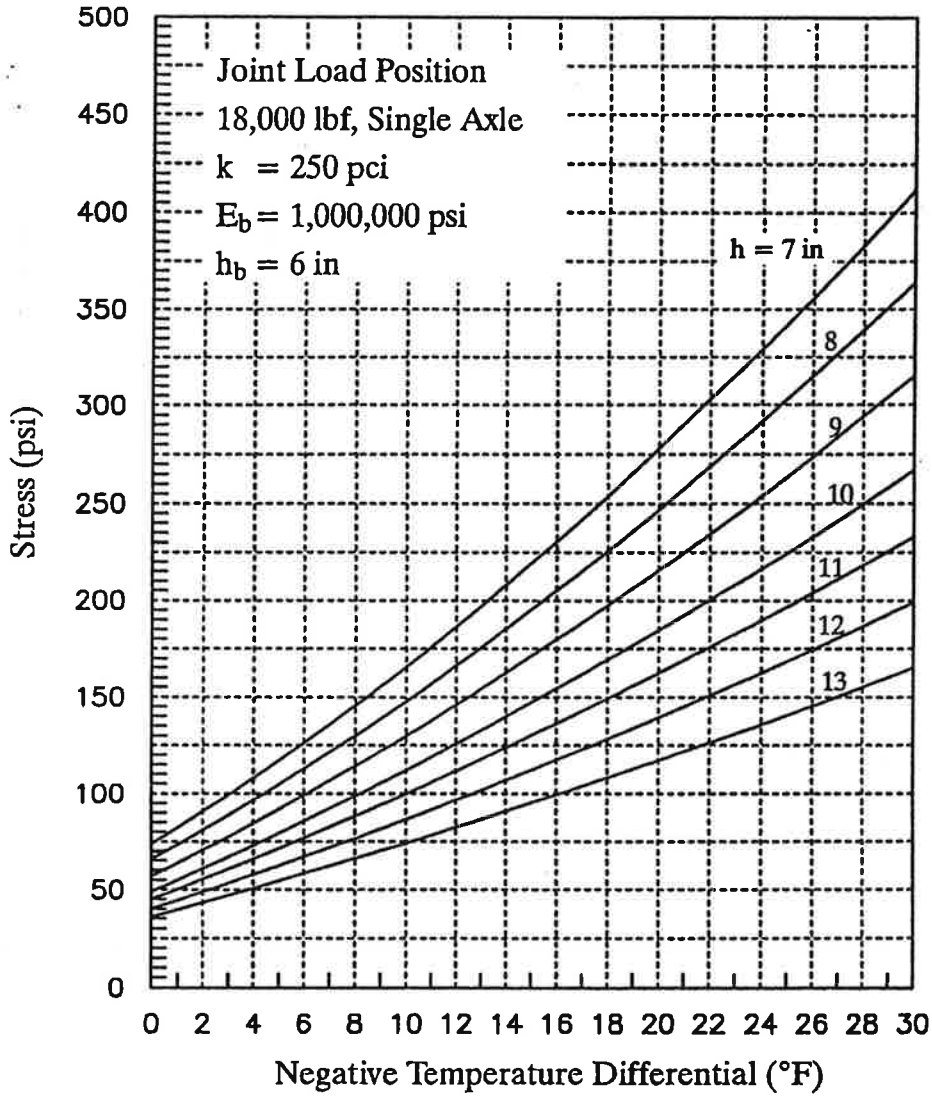

Figure F-13d. Maximum tensile stress at top of slab for joint loading position versus a negative temperature differential through the slab for specific design conditions (treated base, medium subgrade).

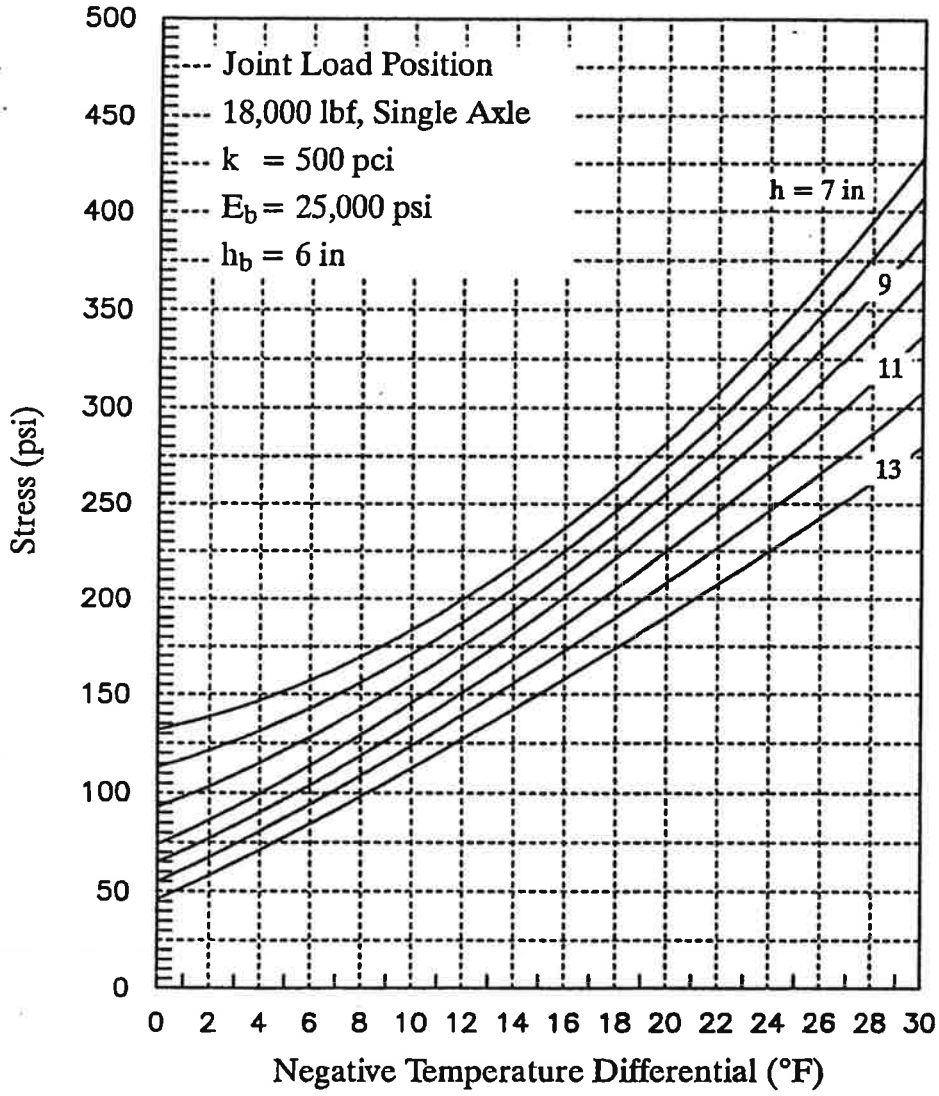

Figure F-13e. Maximum tensile stress at top of slab for joint loading position versus a negative temperature differential through the slab for specific design conditions (aggregate base, stiff subgrade).

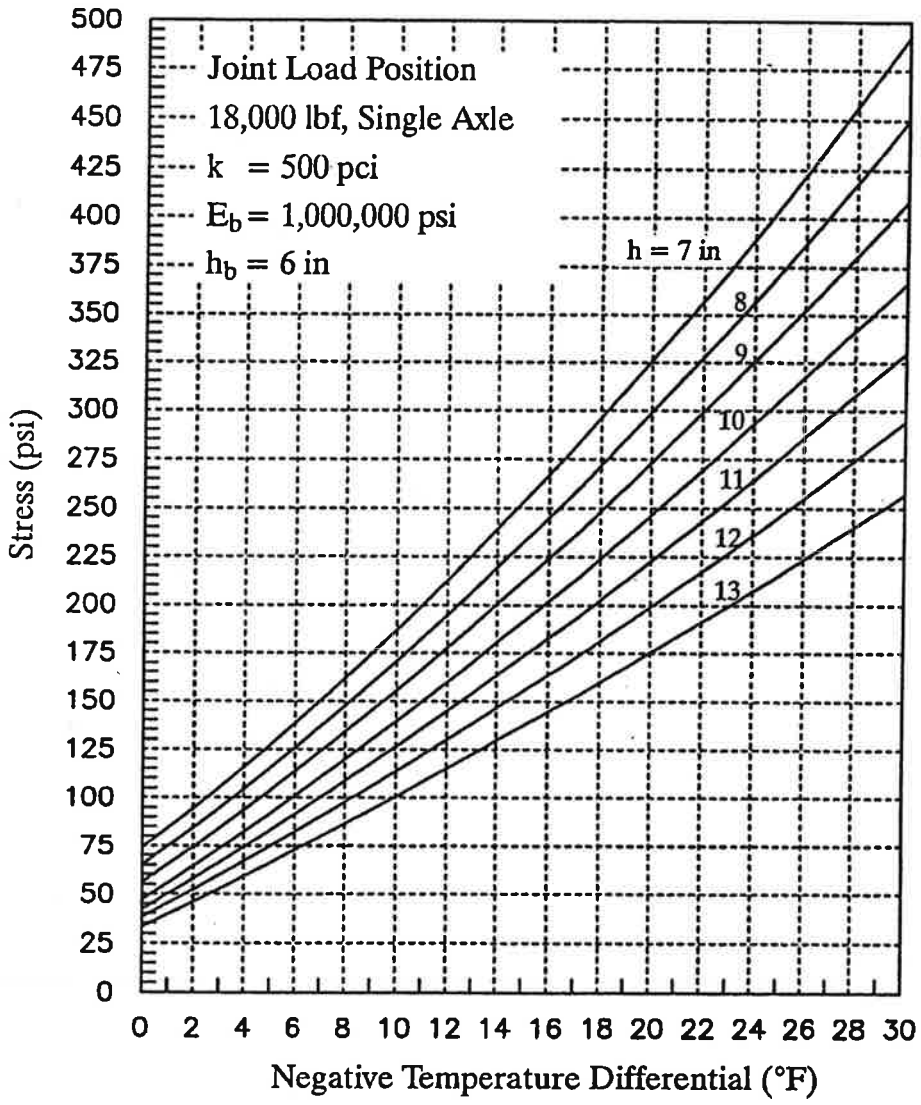

Figure F-13f. Maximum tensile stress at top of slab for joint loading position versus a negative temperature differential through the slab for specific design conditions (treated base, stiff subgrade).

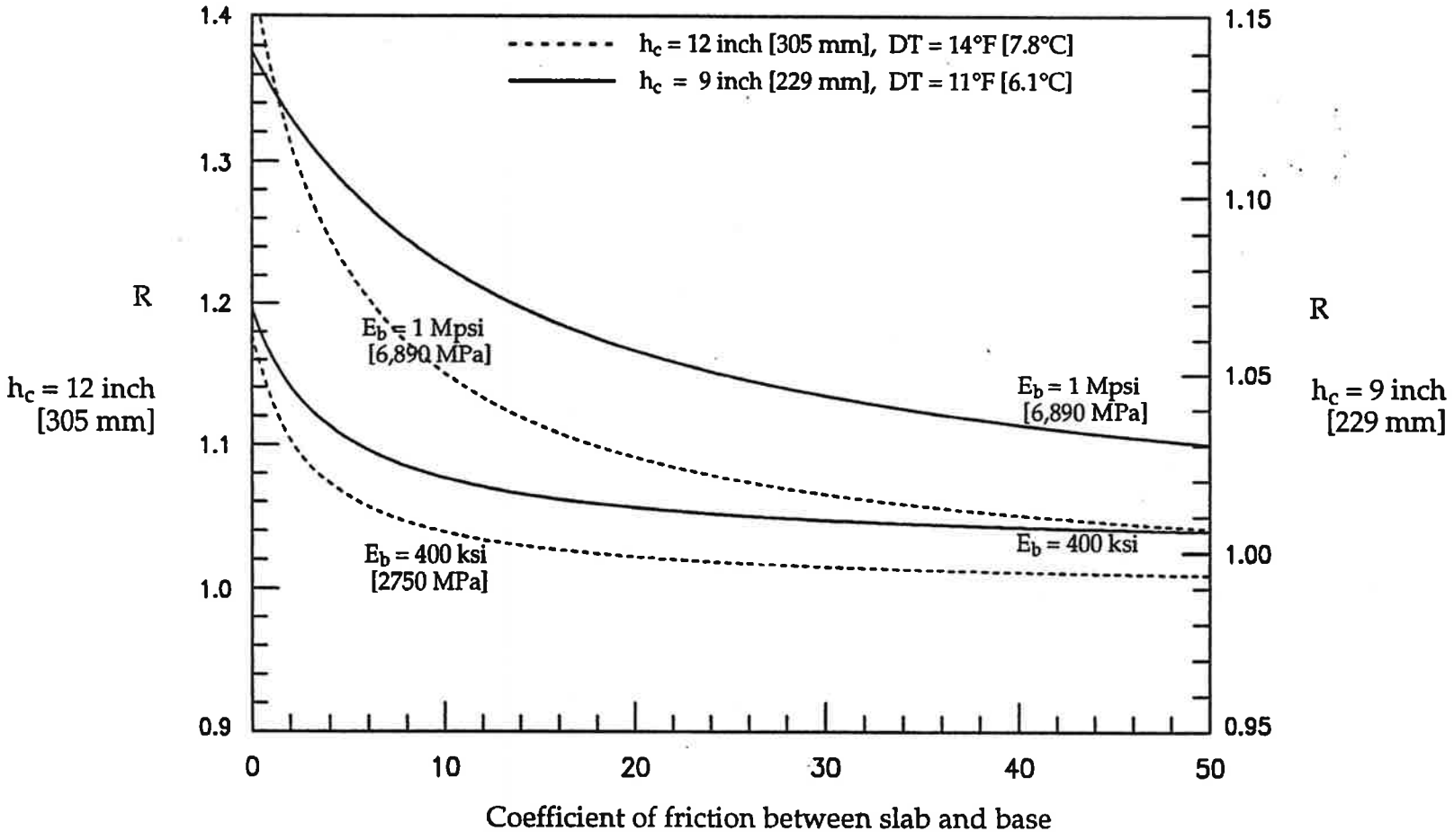

Note : $R = \sigma_f / \sigma_{full\ friction}$
h_b = 5 inch [127 mm] , k = 200 psi/in [54 kPa/mm],
Joint loading with nighttime curling DT

Figure F-14. Friction adjustment factor for stress at top of slab for joint loading.

(5) design serviceability loss, PSI = $P_1 - P_2 = 4.5 - 2.5 = 2.0$

(6) mean concrete modulus of rupture, S'_c= 700 psi [4820 kPa]

(7) mean concrete elastic modulus, $E_c = 26454\ Sc^{0.77}$ = 4,100,000 psi [28249 MPa]

(8) joint spacing, L = 16 ft = 192 in [4877 mm]

(9) base modulus, E_b = 1,000,000 psi (treated base)

(10) slab/base friction coefficient, f = 35

(11) base thickness, H_b = 5 in

(12) effective temperature differentials through concrete slab, TD

Annual wind speed = 10 mph [16 km/hr]

Annual temperature = 53°F [29°C]

Annual precipitation = 40 in [1016 mm]

Effective positive TD = + 8.9.0°F [4.9°C] (from Equation F-13)

Effective negative TD = - 5.3°F [2.9°C] (from Equation F-16)

(13) lane edge support condition: conventional lane width (12 ft [3.66 m]), free edge

(14) Slab thickness required for midslab loading = 10.4 in [279 mm]

The tensile stress at the bottom of the slab due to midslab load and positive curling is 199 psi [1371 kPa] from the equations given in Section 3.2.2.

The negative effective temperature gradient is -5.3°F [2.9°C]. The combined negative construction and moisture shrinkage is assumed for this example to be the maximum for a wet climate, -2°F per inch [0.044°C per mm] of slab thickness, or -22°F [-12°C]. Thus, the total negative temperature differential is about -27°F [15°C]. Using Figure F-13, the full friction tensile stress at the top of the slab due to joint load and negative curling of 140 psi [965 kPa], which when multiplied by the joint friction factor of 1.08 obtained from Figure F-14 yields a joint stress of 151 psi [1040 kPa]. The joint load position results in a lower stress than the midslab load position, so it is not necessary to modify the joint design based on slab cracking.

Design features that provides strong defense against critical joint load stresses are the use of properly sized and spaced dowels and to a lesser degree a widened slab (i.e., slab paved wider than 12 ft [3.66 m] but traffic lane striped 12 ft [3.66 m] wide) or tied concrete shoulder. The other effect that good load transfer has on performance is that corner deflections are reduced. High differential deflections can lead to erosion and loss of support, resulting in even greater stresses under corner loading.

3.2.3 Stage Construction (no change)

3.2.4 Roadbed Swelling and Frost Heave (no change)

3.3 RIGID PAVEMENT JOINT DESIGN

This section covers the design considerations for the different types of joints in portland cement concrete pavements. These criteria are applicable to the design of joints in both jointed and continuous pavements. A joint faulting check is made after the required slab thickness is determined in Section 3.2.2.

3.3.1 Joint Types (no change)

3.3.2 Joint Geometry And Load Transfer

The joint geometry is considered in terms of the spacing, load transfer and general layout.

Joint Spacing. In general, the spacing of both transverse and longitudinal contraction joints depends on local conditions of materials and environment, whereas expansion and construction joints are primarily dependent on layout and construction capabilities. For contraction joints, the spacing to prevent intermediate cracking decreases as the thermal coefficient, positive temperature gradient, or base frictional resistance increases; and the spacing increases as the concrete tensile strength increases. Spacing is also related to the slab thickness and the joint sealant capabilities.

The determination of a required slab thickness includes an input for joint spacing. As joint spacing increases, stresses due to thermal curling and moisture warping increase. For JPCP and JRCP, the following is recommendations are made.

JPCP (short-jointed plain concrete): Transverse cracking must be controlled. Increased joint spacing requires increased slab thickness, especially for stiffer bases and subgrades. The joint spacing interacts with slab thickness, base stiffness, subgrade stiffness (k value) and also with the effective temperature gradient which is location dependent. Thus, there are tradeoffs between all of these variables that should be considered when selecting a design joint spacing.

JRCP (long-jointed reinforced concrete): Transverse cracking is an expected occurrence and the steel reinforcement is provided to hold the cracks tight. For JRCP the designer should input a joint (crack) spacing of 15 ft [4.6 m] for thickness design purposes.

Local performance data are valuable for helping to establish a joint spacing that will control cracking. Local experience must be tempered since a change in any of several concrete properties or construction methods (e.g., a change in coarse aggregate type), may have a significant impact on the concrete thermal coefficient and consequently, the acceptable joint spacing. As a rough guide, the joint spacing (in feet) for plain concrete pavements should not exceed twice the slab thickness (in inches).

For example, the maximum joint spacing for an 8-in [203 mm] slab is 16 ft [4.9 m]. For treated bases and stiff subgrades, this general guide may produce too long a joint spacing. Also, as a general guideline, the ratio of slab width to length should not exceed 1.25.

The use of expansion joints is generally minimized on a project due to cost, complexity, and performance problems. They are used at structures where pavement types change (e.g., CRCP to jointed), with prestressed pavements, and at intersections.

The spacing between construction joints is generally dictated by field placement and equipment capabilities. Longitudinal construction joints should be

placed at lane edges to maximize pavement smoothness and minimize load transfer problems. Transverse construction joints occur at the end of a day's placement or in connection with equipment breakdowns.

Joint Load Transfer. A check of the adequacy of the joint load transfer system is conducted. Because all joints were adequately dowelled at the Road Test, no significant faulting occurred during the two years. If the joints had not been properly dowelled, a large amount of faulting would have occurred which would have greatly changed the rigid pavement design equations.

Faulting is one of the most important distresses affecting rideability and serviceability. Therefore, any pavement that faults significantly will have reduced serviceability and carry fewer traffic loads to terminal serviceability. Thus, joints must be prevented from significant faulting through good joint load transfer and spacing design, base design, subdrainage design, not slab thickness increases.

The following procedure is used to determine the adequacy of the proposed joint load transfer.

STEP 1: The required slab thickness is determined. This requires the selection of several key joint design features, including joint spacing, base stiffness and friction (both a function of base type), and type of load transfer. The check for cracking due to joint loading is conducted as well. The joint design features may be modified if necessary and a redesign made to achieve an acceptable joint design to prevent cracking.

STEP 2: The joint design details required for the joint faulting check include base type, joint spacing, subdrainage presence, and diameter and spacing of dowels, if used.

STEP 3: Mean joint faulting is predicted using the faulting prediction models given below.

Faulting Model for Doweled Joints:

$$DFAULT = ESAL^{0.5280}\left[0.1204 + 0.04048\left(\frac{BSTRESS}{1000}\right)^{0.3388} + 0.007353\left(\frac{L}{10}\right)^{0.6725} - 0.1492\left(\frac{k}{100}\right)^{0.05911} - 0.01868\ DRAIN - 0.00879\ EDGESUP - 0.00959\ STYPE\right] \quad \text{(F-17)}$$

where DFAULT = mean transverse doweled joint faulting, in

ESAL = cumulative equivalent 18-kip [80 kN] single-axle loads, millions

BSTRESS = maximum concrete bearing stress from closed-form equation, psi:

$$BSTRESS = f_d\ P\ T\left[\frac{K_d\,(2 + BETA * OPENING)}{4\ E_s\ I\ BETA^3}\right] \quad \text{(F-18)}$$

$$BETA = \sqrt[4]{\frac{K_d\ DOWEL}{4\ E_s\ I}} \quad \text{(F-19)}$$

f_d = distribution factor = 2 * 12 / (ℓ + 12)

ℓ = radius of relative stiffness, in

I = moment of inertia of dowel bar cross-section, in^4:

$$I = 0.25\ \pi\left(\frac{DOWEL}{2}\right)^4 \quad \text{(F-20)}$$

P = applied wheel load, set to 9000 lbf [40 kN]

T = percent transferred load, set to 0.45

K_d = modulus of dowel support, set to 1,500,000 psi/in [405 MPa/mm]

BETA = relative stiffness of the dowel-concrete system

DOWEL = dowel diameter, in

E_s = modulus of elasticity of the dowel bar, psi

k = modulus of subgrade reaction, psi/in

OPENING = average transverse joint opening, in:

$$OPENING = 12 * CON * L * \left(\frac{ALPHA * TRANGE}{2 + e} \right) \qquad \text{(F-21)}$$

L = average transverse joint spacing, ft

CON = adjustment factor due to base/slab frictional restraint,

= 0.65 if stabilized base

= 0.80 if aggregate base or lean concrete base with bond breaker

ALPHA = PCC thermal expansion coefficient, set to 0.000006/^{o}F [0.000011/^{o}C]

TRANGE = annual temperature range, ^{o}F

e = PCC drying shrinkage coefficient, set to 0.00015 strain;

DRAIN = index for drainage condition,

= 0, if no edge subdrain exists

= 1, if edge subdrain exists

EDGESUP = index for edge support

= 0, if no edge support exists

= 1, if edge support exists

STYPE = index for AASHTO subgrade soil classification,

= 0, if A-4 to A-7

= 1, if A-1 to A-3

Faulting Model for Undowelled Joints:

$$UNFAULT = ESAL^{0.25} \left[0.000038 + 0.0183 \left(100 * OPENING\right)^{0.5585} + 0.000619 \left(100 * DEFLAMI\right)^{1.7229} + 0.04 \left(\frac{FI}{100}\right)^{1.9840} + 0.00565\ BTERM - 0.0077\ EDGESUP - 0.00263\ STYPE - 0.00891\ DRAIN \right] \quad \text{(F-22)}$$

where UNFAULT = mean transverse undowelled joint faulting, in

$$DEFLAMI = \frac{P\left(1.2 - 0.88 * 1.4142\ \frac{a}{\ell}\right)}{k\ \ell^2} \quad \text{(F-23)}$$

BTERM = base type factor:

= $10 * [\ ESAL^{0.2076} * (\ 0.04546 + 0.05115 * GB + 0.007279 * CTB + 0.003183 * ATB - 0.003714 * OGB - 0.006441 * LCB\ )\ ]$

GB = dummy variable for dense-graded aggregate base,
= 1 if aggregate base
= 0 otherwise

CTB = dummy variable for dense-graded, cement-treated base,
= 1 if cement-treated base
= 0 otherwise

ATB = dummy variable for dense-graded, asphalt-treated base,
= 1 if asphalt-treated base
= 0 otherwise

OGB = dummy variable for open-graded aggregate base,
or open-graded asphalt-treated base,
= 1 if open-graded base
= 0 otherwise

LCB = dummy variable for lean concrete base,
= 1 if lean concrete base
= 0 otherwise
FI = freezing index, Fahrenheit degree-days

All other variables are the same as defined before for DFAULT.

Tables F-8, F-9, and F-10 were prepared using Equations F-17 and F-22 to show the faulting predictions for pavements with and without dowel bars. The mean joint faulting is predicted and compared with recommended critical levels. If the predicted faulting is greater than the recommended level, an adjustment to joint design is made. Adjustments include use of dowels, or if dowels already exist, an increase in the diameter, selection of a different base type and permeability, and a decrease in the joint spacing (for undowelled joints). Slab thickness is not adjusted because it has only a minimal effect on joint faulting.

STEP 4: The predicted mean joint faulting is compared with the recommended maximum critical levels given in Table F-11. Of course, each agency should select levels that fit its particular needs. These critical levels were derived from extensive field data. The mean faulting was computed for pavements with a serviceability of 3.0 or less. For example, based upon data from many short-jointed JPCP sections, a mean joint faulting of 0.12 in [3 mm] corresponded to a serviceability index of 3.0 or less. For long-jointed JRCP the mean faulting level was 0.26 in [6.6 mm]. The recommended critical levels for design were selected as fifty percent of these values.

Table F-8. Mean joint faulting predictions for dowelled jointed plain concrete pavement using Equation F-17.

ESALs millions	No Tied Concrete Shoulders			Tied Concrete Shoulders		
	Dow. Dia. 1.00 in	Dow. Dia. 1.25 in	Dow. Dia. 1.50 in	Dow. Dia. 1.00 in	Dow. Dia. 1.25 in	Dow. Dia. 1.50 in
1	0.02	0.01	0.01	0.01	0.00	0.00
2.5	0.03	0.02	0.01	0.02	0.01	0.00
5	0.04	0.03	0.02	0.02	0.01	0.00
10	0.06	0.04	0.02	0.03	0.01	0.00
20	0.09	0.06	0.03	0.05	0.02	0.00
30	0.12	0.07	0.04	0.06	0.02	0.00
40	0.13	0.08	0.05	0.07	0.02	0.00
50	0.15	0.09	0.05	0.08	0.03	0.00
75	0.19	0.12	0.07	0.10	0.03	0.00
100	0.22	0.14	0.08	0.12	0.04	0.00

Values shown in table are mean predicted joint faulting, in [1 in = 25.4 mm]

Joint spacing = 15 ft [4.6 m]
k-value = 100 psi/in [27 kPa/mm]
Base type = not a factor
Slab thickness = 9 in [229 mm]
Subdrains = 1 (yes)
TRANGE = 85°F (July max - January min)
Subgrade = 0 (fine)
S'_c = 700 psi [4.8 MPa]

Table F-9. Mean joint faulting predictions for dowelled jointed reinforced concrete pavement using Equation F-17.

ESALs millions	No Tied Concrete Shoulders			Tied Concrete Shoulders		
	Dow. Dia. 1.00 in	Dow. Dia. 1.25 in	Dow. Dia. 1.50 in	Dow. Dia. 1.00 in	Dow. Dia. 1.25 in	Dow. Dia. 1.50 in
1	0.03	0.02	0.02	0.02	0.01	0.01
2.5	0.05	0.04	0.03	0.04	0.02	0.01
5	0.07	0.05	0.04	0.05	0.03	0.02
10	0.10	0.08	0.06	0.07	0.05	0.03
20	0.15	0.11	0.09	0.11	0.07	0.04
30	0.18	0.14	0.11	0.13	0.09	0.05
40	0.21	0.16	0.13	0.15	0.10	0.06
50	0.24	0.18	0.14	0.17	0.11	0.07
75	0.30	0.23	0.17	0.21	0.14	0.09
100	0.35	0.26	0.20	0.25	0.16	0.10

Values shown in table are mean predicted joint faulting, in [1 in = 25.4 mm]

Joint spacing = 45 ft [13.7 m]
k-value = 100 psi/in [27 kPa/mm]
Base type = not a factor
Slab thickness = 9 in [229 mm]
Subdrains = 1 (yes)
TRANGE = 85°F (July max - January min)
Subgrade = 0 (fine)
S'_c = 700 psi [4.8 MPa]

Table F-10. Mean joint faulting predictions for undowelled jointed plain concrete pavement using Equation F-22.

ESAL million	Aggregate Base		Asphalt-Treated Base		Lean Concrete Base		Open-Graded Base	
	Jt Sp 15 ft	Jt Sp 20 ft	Jt Sp 15 ft	Jt Sp 20 ft	Jt Sp 15 ft	Jt Sp 20 ft	Jt Sp 15 ft	Jt Sp 20 ft
1	0.06	0.07	0.06	0.07	0.06	0.06	0.06	0.06
2.5	0.08	0.09	0.07	0.08	0.07	0.08	0.07	0.08
5	0.10	0.11	0.09	0.10	0.08	0.10	0.09	0.10
10	0.12	0.14	0.11	0.12	0.10	0.12	0.10	0.12
20	0.15	0.17	0.13	0.15	0.12	0.14	0.12	0.14
30	0.17	0.19	0.15	0.17	0.14	0.16	0.14	0.16
40	0.18	0.20	0.16	0.18	0.15	0.17	0.15	0.17
50	0.19	0.21	0.17	0.19	0.16	0.18	0.16	0.18
75	0.21	0.24	0.19	0.21	0.18	0.20	0.18	0.20
100	0.23	0.26	0.21	0.23	0.19	0.21	0.19	0.22

Values shown in table are mean predicted joint faulting, in [1 in = 25.4 mm]

Joint spacing = 15 or 20 ft [4.6 or 6.1 m]
Slab thickness = 9 in [229 mm] Subgrade = 0 (fine)
k-value = 100 psi/in [27 kPa/mm] Subdrains = 1 (yes) S'_c = 700 psi [4.8 MPa]
Edge support = 1 (yes) TRANGE = 85°F (July max - January min)
Freezing Index = 600 F degree-days

Table F-11. Recommended critical joint faulting levels for design.

Joint Spacing	Critical Joint Faulting
Less than 25 ft	0.06 in
Greater than 25 ft	0.13 in

1 ft = 0.305 m, 1 in = 25.4 mm

The slab design may need adjustment after the joint design is completed, especially if the joint spacing is reduced or the base type is changed to reduce expected faulting.

Example Check for Joint Faulting. Assume the same pavement defined in the previous example. The pavement has a 16-ft [4.9 m] joint spacing, treated base, subdrains, and no dowel bars. A Freezing Index of 500 and an annual temperature range of 85°F [47°C] are also assumed for the location. A slab thickness of 10.4 in [264 mm] was obtained for a design traffic of 20 million ESALs and 90 percent reliability. The mean predicted joint faulting of 0.13 in [3.3 mm] exceeds the recommended limit of 0.06 in [1.5 mm], and thus the joint design is inadequate.

One possible design modification would be to specify 1.25-in-diameter [32 mm] dowels. The mean predicted joint faulting would then be 0.05 in [1.27 mm], which would be acceptable.

Joint Layout. (no change)

Joint Dimensions. (no change)

3.3.3 Joint Sealant Dimensions (no change)

APPENDIX G

RIGID PAVEMENT DESIGN EXAMPLE

(PROPOSED REVISION TO AASHTO GUIDE APPENDIX I)

A jointed concrete pavement is to be designed to carry 10 million ESALs and the pavement is located in the southeastern United States.

GENERAL DESIGN INPUTS

Design reliability = 90 percent

Overall standard deviation S_o = 0.39

Design traffic = 10 million ESALs in the design lane

P1 - P2 = 4.5 - 2.5 = 2.0

Concrete flexural strength, mean 28-day, third-point loading, S'_c = 700 psi [4820 kPa]

Concrete elastic modulus, E_c = 4,100,000 psi [28249 MPa]

Subgrade soil type: silty-clay

k value = elastic value of subgrade/embankment = 100 psi/in [27 kPa/mm]

Subdrains = 1 (yes)

Climate: WIND = mean annual wind speed = 7.9 mph [12.7 km/hr]

TEMP = annual temperature = 58.9°F [32.7]

PREC = annual precipitation = 43 in [1092]

Effective positive temperature differential:

Slab thickness	Temperature Differential
9 in [229 mm]	8.3°F [4.6°C]
10 in [254 mm]	8.9°F [4.9°C]
11 in [279 mm]	9.4°F [5.2°C]

Freezing Index = 0 °F-days below freezing

Temperature Range = 50°F [27.7°C] (maximum July - minimum January)

DESIGN ALTERNATIVE A

Undowelled joints

Untreated aggregate base, 6 in [152 mm], E_b = 25,000 psi [172 MPa], friction f = 1.5

Joint spacing = 15 ft [4.6 m]

Conventional lane width = 12 ft [3.7 m]

AC shoulders

Slab Thickness Design

Assuming an effective temperature differential of about 9°F [5°C], a required slab thickness of 10.2 in [259 mm] is obtained for design ESALs of 10 million, at a design reliability level of 90 percent.

Joint Faulting Check

The initial design has undowelled joints with a 15-ft [4.6 m] joint spacing. The estimated mean faulting for this design is 0.09 in [2.3 mm]. This value exceeds the recommended limit of 0.06 in [1.5 mm]. Therefore, a joint design modification (e.g., dowels, shorter joint spacing, different base type, tied shoulder) is required to control faulting.

Joint Load Position Stress Check

The joint load position check is required since the pavement is undowelled. The total negative temperature differential is estimated from the climatic data as -5.6°F [-3°C] (use -6°F [-3.3°C]).

Combined moisture gradient and construction differential: - 10°F [-5.5°C] (wet climatic zone, conventional concrete cure).
Total negative equivalent temperature differential = -16°F [8.9°F]

The critical stress for joint loading is determined to be about 145 psi [999 kPa] for a slab thickness of 10.2 in [259 mm]. This joint loading stress is compared to that obtained for the midslab location with a positive temperature differential of 9°F [5°C], which is found to be 233 psi [1605 kPa]. Therefore, the midslab load design is adequate to control stresses at the joint loading position. A total negative temperature differential of about -30°F [-17°C] would be required to produce a stress greater than 233 psi [1605 kPa].

DESIGN ALTERNATIVE B

Undowelled joints
Permeable asphalt-treated aggregate base, 6 in [152 mm], E_b = 100,000 psi [689 MPa], friction f = 6
Joint spacing = 15 ft [4.6 m]
Widened slab width = 14 ft [4.3 m] (with AC shoulders)

Slab Thickness Design

Assuming an effective positive temperature differential of about 9°F [5°C], a a required slab thickness of 9.4 in [239 mm] is obtained. Note that a stress reduction factor of 0.92 for the widened slab was used in the calculation.

Joint Faulting Check

The mean faulting estimated for this design is 0.06 in [1.5 mm] which just equals the recommended limit. Therefore the joint design is acceptable.

Joint Load Position Stress Check

The joint load position check is required since the pavement is undowelled. The total negative temperature differential is the same as estimated for Alternative A, -16°F [8.9°C].

The critical stress for joint loading is determined to be 165 psi [1137 kPa] for a slab thickness of 9.4 in [239 mm]. This stress is compared to that obtained for the midslab location with a positive temperature differential of 9°F, which is found to be 234 psi [1612 kPa]. Therefore, the midslab load design is adequate to control stresses at the joint loading position.

DESIGN ALTERNATIVE C

Dowelled joints, 1.25-in [32 mm] diameter

Untreated aggregate base, 6 in [152 mm], E_b = 25,000 psi [172 MPa], friction f = 1.5

Joint spacing = 17 ft [5.2 m]

Conventional lane width = 12 ft [3.7 m]

Tied concrete shoulder

Slab Thickness Design

Assuming an effective temperature differential of about 9°F [5°C], the required slab thickness is 9.9 in [251 mm]. Note that a stress reduction factor of 0.94 for a tied concrete shoulder was used in the calculation.

Joint Faulting Check

The estimated mean faulting for this design is 0.01 in [0.25 mm] which is well below the 0.06 in [1.5 mm] recommended limit.

Joint Load Position Stress Check

The joint load position check is not required since the pavement is dowelled and the joint load position stress will be well below the midslab stress.

APPENDIX H

DEVELOPMENT OF EFFECTIVE ROADBED SOIL K VALUE

(Recommended Revisions to AASHTO Guide Appendix HH)

EFFECTIVE MODULUS OF SUBGRADE REACTION (k value)

This section describes the development of the effective modulus of subgrade reaction, or effective k value, used to consider seasonal variation of foundation support for rigid pavement design. A season is defined as a period of time within a year, such as three months. The basic steps behind this approach are as follows:

STEP 1: Compute the relative damage associated with specific support (k values) for each season. The rigid pavement performance equation is as follows.

$$\log W' = \log W + \left(5.065 - 0.03295\ P2^{2.4} \right) \left[\log \left(\frac{\left(S'_c \right)'}{\sigma_{t'}} \right) - \log \left(\frac{690}{\sigma_t} \right) \right] \qquad \text{(H-1)}$$

where W′ = number of 18-kip [80 kN] ESALs estimated for design traffic lane

W = number of 18-kip [80 kN] ESALs computed from Equation H-2:

$$\log W = \log R + \frac{G}{F} \qquad \text{(H-2)}$$

$$\log R = 5.85 + 7.35 \log (D + 1) - 4.62 \log (L1 + L2) + 3.28 \log L2 \qquad \text{(H-3)}$$

$$F = 1.00 + \frac{3.63\ (L1 + L2)^{5.2}}{(D + 1)^{8.46}\ L2^{3.52}} \qquad \text{(H-4)}$$

D = concrete slab thickness, in

$$G = \log\left(\frac{P1 - P2}{P1 - 1.5}\right) \qquad \text{(H-5)}$$

L1 = load on a single or tandem axle, kips

L2 = axle code, 1 for single axle, 2 for tandem axle

P1 = initial serviceability index

P2 = terminal serviceability index

$(S'_c)'$ = mean 28-day, third-point loading flexural strength, psi

(690 psi for AASHO Road Test)

σ_t = midslab tensile stress due to load and temperature from Equation F-8 with AASHO Road Test constants

$\sigma_{t'}$ = midslab tensile stress due to load and temperature from Equation F-8 with inputs for new pavement design

$$\sigma_t = \sigma_l \, E \, F \left[1.0 + 10^{(\log b)\, TD} \right] \qquad \text{(H-6)}$$

σ_l = midslab tensile stress due to load only

$$\sigma_l = \frac{18{,}000}{D^2}\left\{ 4.227 - 2.381\left(\frac{180}{\ell}\right)^{0.2} - 0.0015\left[\frac{E_b\, H_b}{1.4\, k}\right]^{0.5} - 0.155\left[H_b\left(\frac{E_b}{E_c}\right)^{0.75}\right]^{0.5} \right\} \qquad \text{(H-7)}$$

E_c = modulus of elasticity of concrete slab, psi

(4,200,000 psi [28940 MPa] for AASHO Road Test)

E_b = modulus of elasticity of base, psi

(25,000 psi [172 MPa] for AASHO Road Test)

H_b = thickness of base, in

(6 in [152 mm] for AASHO Road Test)

$$\ell = \sqrt[4]{\frac{Z\,D^3}{12\,(1-\mu^2)}} \qquad \text{(H-8)}$$

$$Z = \frac{E_c}{k} \qquad \text{(H-9)}$$

k = effective elastic modulus of subgrade support, psi/in
(110 psi/in for AASHO Road Test)

μ = Poisson's ratio for concrete
(0.20 for AASHO Road Test)

E = edge support adjustment factor
(1.00 for AASHO Road Test)
= 1.00 for conventional 12-ft-wide [3.66 m] traffic lane
= 0.94 for conventional 12-ft-wide [3.66 m] traffic lane plus tied concrete shoulder
= 0.92 for 2-ft [0.6 m] widened slab with paint stripe at conventional 12-ft [3.66 m] lane width

F = ratio between slab stress at a given coefficient of friction (f) between the slab and base and slab stress at full friction

$$F = 1.177 - 4.3*10^{-8}\,D\,E_b - 0.01155542\,D + 6.27*10^{-7}\,E_b - 0.000315\,f \qquad \text{(H-10)}$$

f = friction coefficient between slab and base (see Table F-4)

$$\log b = -1.944 + 2.279 \frac{D}{\ell} + 0.0917 \frac{L}{\ell} - 433{,}080 \frac{D^2}{k\,\ell^4}$$

$$+ \left(\frac{0.0614}{\ell} \right) * \left(\frac{E_b\, H_b{}^{1.5}}{1.4\, k} \right)^{0.5} - 438.642 \frac{D^2}{k\,\ell^2} - 498{,}240 \frac{D^3\, L}{k\,\ell^6} \qquad \text{(H-11)}$$

L = joint spacing, inches (180 in [4572 mm] for AASHO Road Test)

TD = effective positive temperature differential, top temperature minus bottom temperature, °F

$$\textit{effective positive TD} = 0.962 - \frac{52.181}{D} + 0.341\ \textit{WIND} + 0.184\ \textit{TEMP} - 0.00836\ \textit{PRECIP} \qquad \text{(H-12)}$$

D = slab thickness, in

WIND = mean annual wind speed, mph (Figure F-8)

TEMP = mean annual temperature, °F (Figure F-9)

PRECIP = mean annual precipitation, in (Figure F-10)

Equation H-1 is used to estimate W_{18}, the number of ESALs that a given rigid pavement can carry to a specific terminal serviceability, P2, for any specified k value and other inputs. For example, assume that there are four seasons selected in one year (three months per season) for a given site. Each of the seasons has a different estimated k value, based perhaps on soil properties and degree of saturation, or perhaps on deflection testing in different seasons.

Suppose, for example, the following inputs were used in Equation H-1:

E_c = 4,200,000 psi [28940 MPa]

E_b = 25,000 psi [172 kPa] for aggregate base

H_b = 6 in [152 mm]

D = 9 in [229 mm]

S'_c = 690 psi [4654 kPa]

P1 = 4.5

P2 = 2.5

L = 180 in [4572 mm]

TD = +7.92°F [4.4°C] (for a slab thickness of 9 in [229 mm]

Suppose also that k values of 100, 200, 300, and 400 psi/in [27, 54, 81, and 108 kPa/mm] are estimated for the four seasons of the year. The W_{18} values calculated for this example are shown in Table H-1 below.

Table H-1. Example calculation of effective k value.

Seasons (3 months)	k value (psi/in)	W_{18} (millions)*	Relative Damage ($1 / W_{18}$)
Spring	100	13.18	0.0759
Summer	200	14.60	0.0685
Fall	300	15.71	0.0637
Winter	400	16.72	0.0598
		Mean Damage	0.0670
		W_{18}	14.92 million
		Effective k value	229 psi/in

1 psi/in = 0.27 kPa/mm

STEP 2: Compute the "relative damage" for each season as the inverse of the W_{18} calculated for the season. The damage values calculated for this example are shown in Table H-1 above.

STEP 3: Compute the total relative damage for the year and divide by the number of seasons to obtain the mean damage.

STEP 4: Compute a W_{18} corresponding to the mean damage as the inverse of the mean damage.

STEP 5: Use Equation H-1 to solve for the k value which produces a predicted W_{18} matching the W_{18} obtained in Step 4. This k value is the seasonally adjusted effective k value.

Consider another example for which a different pavement design is considered for the same site:

E_c = 5,000,000 psi

E_b = 500,000 psi [3445 MPa]for treated aggregate base

H_b = 4 in [102 mm]

D = 10 in [254 mm]

S'_c = 750 psi [5168 kPa]

P1 = 4.5

P2 = 3.0

L = 14 ft [4.3 m]

TD = 8.5°F [4.7°C] (for a 10-in [254 mm] slab)

Table H-2. Effective k value calculation for second example.

Seasons (3 months)	k value (psi/in)	W_{18} (millions)*	Relative Damage ($1 / W_{18}$)
Spring	100	32.65	0.0306
Summer	200	27.28	0.0367
Fall	300	25.03	0.0399
Winter	400	23.68	0.0422
		Mean Damage	0.03735
		W_{18}	26.77 million
		Effective k value	217 psi/in

1 psi/in = 0.27 kPa/mm

The effective k value for this example pavement design is not very different than the value obtained for the first example design, even though the design features are very different.

The effective subgrade k value for the AASHO Road Test site was calculated by this procedure, as shown in Table H-3 on the following page. The effective subgrade k value obtained is 110 psi/in [29.7 kPa/mm].

A blank worksheet (Table H-4) is also provided on the following page.

Table H-3. Effective subgrade k value for AASHO Road Test site.

Seasons (3 months)	k value (psi/in)	W_{18} (millions)*	Relative Damage ($1 / W_{18}$)
Spring	77	12.75	0.0784
Summer	98	13.15	0.0760
Fall	111	13.37	0.0748
Winter	168	14.20	0.0704
		Mean Damage	0.0749
		W_{18}	13.35 million
		Effective k value	110 psi/in

1 psi/in = 0.27 kPa/mm

Table H-4. Worksheet for computation of effective subgrade k value.

Seasons (3 months)	k value (psi/in)	W_{18} (millions)*	Relative Damage ($1 / W_{18}$)
Spring			
Summer			
Fall			
Winter			
		Mean Damage	
		W_{18}	million
		Effective k value	psi/in

1 psi/in = 0.27 kPa/mm